Development of *in-vitro* human and rat proximal tubule cell models as a platform for drug transporter and drug-drug interaction studies

Sarah Faye Billington

Thesis submitted for the degree of

Doctor of Philosophy

Institute for Cell and Molecular Biosciences,

Newcastle University, UK

September 2015

Abstract

The kidney plays a key role in the systemic clearance of new molecular entities (NMEs). Approximately 32% of drugs exhibit significant renal elimination. It is estimated that nephrotoxicity accounts for 8 % of pre-clinical and 9% of clincal safety failures in drug development. Current pre-clinical models used to screen NMEs are poor predictors of human nephrotoxicity. The focus of my project is thus to develop predictive *in-vitro* rat and human primary proximal tubule cell models as a platform drug transporter and drug-drug interaction (DDI) studies.

Primary human and rat proximal tubule cells (PTCs) were isolated from renal cortex using a combination of enzymatic digestion and density centrifugation. The isolation procedure was optimised to maximise cell yield and viability. Human and rat PTCs cultured on Transwell® inserts formed confluent monolayers with low paracellular permeability. Quantitative PCR showed mRNA expression of key renal transporters, OAT1, OAT3, OATP4C1, OCT2, BCRP, MATE1, MATE2-K, MDR1, MRP2, URAT1, NaPi-IIa, NaPi-IIc and PiT2, in human PTC monolayers. Orthologs of these transporters were also detected in rat PTC monolayers.

The utility of human and rat PTC monolayers as predictive *in-vitro* models of proximal tubular drug handling were demonstrated using radiolabeled [^{3}H]-tenofovir (TFV). Human and rat PTC monolayers exhibited a cell-to-media ratio greater than 1, which indicated uptake and accumulation of TFV across the basolateral membrane. We also observed a predominant absorptive pathway of TFV. The transporters mediating the transport of TFV were identified using a cocktail of transporter inhibitors. The basolateral uptake of TFV was mediated by OATP4C1 and OAT1. TFV had low affinities for the apical efflux transporters MRP2, MRP4, MDR1 and BCRP. The novel identification of OATP4C1 as a TFV transporter has led Gilead to develop assays for investigating OATP4C1-mediated DDIs, and the FDA to recognise OATP4C1 as a key renal transporter.

The handling of radiolabelled inorganic [^{32}P]-phosphate (P_i) by human and rat PTC monolayers was also investigated. P_i flux measurement revealed a net absorptive pathway of P_i across human and rat PTC monolayers. Uptake of P_i across the apical membrane was sodium dependent, saturable, and inhibited by parathyroid hormone, fibroblast growth-factor 23 and α-klotho. Apical uptake of P_i was also inhibited by TFV in a saturable manner. This suggests that the mechanisim of TFV-induced hypophosphatemia is not via TFV-induced nephrotoxicity, but TFV inhibition of P_i reabsorption. The outcomes of this work have initiated a patient clinical trial. This finding could have a large translational impact, as over 14.9 million HIV-patients are pescribed TFV and TFV-related hypophosphatemia affects 30 % of patients.

The data highlight the importance of developing holistic cell based models of the proximal tubule. The outcomes of this work demonstrate the power of translational science to have an impact on how the pharmaceutical industry operates.

Acknowledgements

I would like express my special appreciation and thanks to my PhD supervisor Dr Colin Brown who has been a tremendous mentor to me. I would like to thank him for his guidance, critique and encouragement throughout the project, which has allowed me to grow as a research scientist. Colin has been supportive of me showcasing my research and networking at international meetings. He has given me the freedom to pursue various extra-curricular projects without objection. His advice on both research as well as my career have been invaluable.

I would like to thank the National Centre for the Replacement, Refinement and Reduction of animals in research (NC3Rs) whom funded my research project and have played an active role in my professional development. I would like to say a special thank you to my colleague Git Chung. The joy, energy and enthusiasm he has for research was contagious and motivational for me. We have had many insightful discussions and he has been very supportive throughout my studies. I also have to thank my internal assessment panel Prof Matthew Wright and Prof Brendan Kenny who have provided constructive criticism and an alternative perspective in our annual meetings. My thanks also go to my commercial collaborators Scievita, Gilead, and Chimerix who have provided me with laboratory consumables.

Thanks are also due to the members of the Epithelial Research Group, past and present, who have contributed immensely to my personal and professional time at Newcastle University. The group has been a source of friendship as well as advice and collaboration. Additionally, I would like to thank the staff at the Comparative Biology Centre led by Christopher Huggins.

A special thanks to my family for all the sacrifices they made on my behalf. Finally, I would like to thank my fiancé, Matthew Hall, for his love, support and patience. He has help me with proofreading, listened to hours of presentation rehearsals and incentivised me with delicious home cooked meals throughout my project.

Table of Contents

List of figures

List of tables

List of abbreviations

[^{32}P]-P_i	[^{32}P]-monosodium phosphate
[^{3}H]-TFV	[Adenine-2,8-^{3}H]-Tenofovir
3Rs	Reduction, refinement, replacement
ABC	ATP-binding cassette superfamily

ANOVA	A one-way analysis of variance test
AP1	Activator protein 1 (transcription factor)
ART	Antiretroviral therapy
ATP	Adenosine triphosphate
AUC	Area under the curve
BCRP	Breast cancer resistance protein
BSA	Bovine serum albumin
CDC	Chenodeoxycholic acid
CIM	Cimetidine
ciPTEC	Human conditionally immortalised proximal tubular epithelial cell line
C_{max}	Maximum serum concentrations
CMFDA	5-chloromethylfluorescein-diacetate
DDI	Drug-drug interaction(s)
dNTP	Deoxyribonucleotide triphosphate
DPM	Disintegrations per minute
DX	Digoxin
E3S	Estrone-3-Sulphate
EDTA	Ethylenediaminetetraacetic acid
EGF	Epidermal growth factor
EMA	European medicines agency
EVOM	Epithelial voltohmmeter
FCS	Foetal calf serum
FDA	Food and drug administration
FGF-23	Fibroblast growth factor 23
FGFR1	FGF receptor 1
G418	Insulin and Geneticin
GA-1000	Gentamycin amphotericin-B
H33342	Bisbenzimide Hoechst 33342
HBSS	Hank's balanced salt solution
HBV	Chronic hepatitis B
HEK293	Human embryonic kidney 293
HEPES	4-(2-hydroxyethyl)-1-piperazineethanesulfonic acid
HEPTEC	Human renal proximal tubule epithelial cell line
HG-DMEM	High glucose Dulbecco's modified eagle medium
HIV	Human immunodeficiency virus
HK-2	Human kidney 2 - proximal tubule epithelial cell line
hr	Hour(s)
ITC	International transporter consortium
J_{A-B}	Transepithelial absorption
J_{B-A}	Transepithelial secretion
Ko143	Ko143 hydrate
LAP	Leucine aminopeptidase
LLC-PK1	Lilly laboratories cell-porcine kidney 1
MATE	Multidrug and toxic compound extrusion transport protein
MDCK	Madin-Darby canine kidney 1
MDR1	Multidrug resistance protein 1
min	Minute(s)
MK-571	5-(3-(2-(7-Chloroquinolin-2-yl)ethenyl)phenyl)-8-

	dimethylcarbamyl-4,6-dithiaoctanoic acid
M-MLV	Moloney murine leukaemia virus
MRP	Multidrug resistance-associated protein
MTS	3-(4,5-dimethyl-2-yl) – 5 – (3-carboxymethoxyphenyl)-2-(4-sulfophenyl)-2H-tetrazolium salt
n	Technical replicates
N	Biological replicates
NME	New molecular entity (or entities)
OA^-	Organic anion
OAT	Organic anion transporter
OATP	Organic anion transporting polypeptide
OC^+	Organic cation
OCT	Organic cation transporter
OK	Opossum kidney 1
PAH	Para-aminohippurate
PBS	Phosphate buffered saline solution
PFA	Trisodium phosphonoformate
P_i	Inorganic phosphate
PMDA	Pharmaceuticals and medical devices agency
PTCs	Proximal and distal tubular and collecting duct epithelial cells
PTH	Parathyroid hormone
PTHR1	Parathyroid hormone receptor 1
qPCR	Quantitative real-time polymerase chain reaction
R^2	Coefficient of determination
REGM	Renal epithelial cell growth medium
rpm	Revolutions per minute
RPMI	Roswell Park memorial institute medium
RPTEC	Immortalised human renal proximal tubule cells
RSV	Rosuvastatin
SEM	Standard error of the mean
SLC	Solute carrier superfamily
SNP	Single nucleotide polymorphism(s)
SP1	Specificity protein 1 (transcription factor)
T3	Triiodothyronine
TDF	Tenofovir disoproxil fumarate
TEER	Transepithelial electrical resisance
TFV	Tenofovir

List of Abstracts

Billington, S., Chung, G., Brown, CDA., (2015) M1022. The use of primary human proximal tubule cells as an *in-vitro* model for the investigation or renal urate transport. AAPS / ITC Joint Transporter Joint Workshop on Drug Transporters in ADME, Baltimore (USA).

Billington, S., Chung, G., Brown, CDA., (2014) R6327. Tenofovir is a substrate of OATP4C1 in human proximal tubule cell monolayers. AAPS Annual Meeting, San Diego (USA).

Billington, S., Chung, G., Brown, CDA., (2014) R6328. Tenofovir inhibits Na^+-dependent phosphate uptake in human proximal tubule cell monolayers. AAPS Annual Meeting, San Diego (USA).

Billington, S., Chung, G., Brown, CDA., (2014) T2286. Marked species difference in the handling of digoxin by primary human and rat proximal tubule cells. AAPS Annual Meeting, San Diego (USA).

Billington, S., Chung, G., Brown, CDA., (2014) Human proximal tubule cell monolayers provide a predictive drug safety platform. NC3Rs / MHRA Human Tissue Workshop, London (UK)

Chung, G., Billington, S., Brown, CDA., (2014) Screening in rat kidney is not an accurate predictor of digoxin handling in human kidney. NC3Rs / MHRA Human Tissue Workshop, London (UK)

Billington, S., Chung, G., Brown, CDA., (2013) The development of an *in-vitro* mouse proximal tubule cell model as a platform for drug transporter and drug-drug interaction studies. International Congress of Physiological Sciences, Birmingham (UK).

Chung, G., Billington, S., Brown, CDA., (2013) Development and characterisation of rat proximal tubule cells. International Congress of Physiological Sciences, Birmingham (UK).

Billington, S., Chung, G., Brown, CDA., (2013) The development of an *in-vitro* mouse proximal tubule cell model as a platform for drug transporter and drug-drug interaction studies. AAPS / ITC Joint Transporter Joint Workshop on Drug Transporters in ADME, Bethesda (USA).

Chung, G., Billington, S., Brown, CDA., (2013) Regulation of drug transporters by HIF-1 in HK-2 human proximal tubule epithelial cells. AAPS / ITC Joint Transporter Joint Workshop on Drug Transporters in ADME, Bethesda (USA).

1. Introduction and literature review

1.1. Improving research and development productivity

Without a dramatic increase in research and development productivity, today's pharmaceutical industry is not sustainable. For every dollar lost in declining product revenues due to patent expirations in 2012, large pharmaceutical companies were only able to replace on average 26 cents with new product revenues (Goodman, 2008). A key aspect of this problem is the decreasing number of NMEs approved by the regulatory bodies such as the European Medicines Agency (EMA) and United States Food and Drug Administration (FDA). With an estimated $50 billion in collective annual research and development spending by the large pharmaceutical companies, the average cost for these companies to bring an NME to market in 2013 was approximately $2.87 billion (Tufts Center for the Study of Drug Development, 2014).

It is estimated that the probability of successful transition from pre-clinical to Phase I, Phase I to Phase II, Phase II to Phase III and Phase III to launch is 59.52%, 35.52%, 61.95% and 90.35%, respectively with an overall success of 11.83% between Phase I and regulatory approval (Tufts Center for the Study of Drug Development, 2014). Miscalculation of drug distribution is a key factor in attrition in drug development; it can result in a lack of efficacy or adverse drug reactions. This is highlighted in Figure 1.1, where the primary causes of NME failure from 2005 to 2010 at AstraZeneca are shown (Cook *et al.*, 2014).

Intracellular drug concentrations are important in the prediction of drug efficacy, toxicity and drug interactions, yet difficult to quantify in humans. Based upon the free drug hypothesis i.e. the free drug concentration is the same on both sides of any biomembrane (Smith *et al.*, 2010) the plasma drug concentrations are typically used as a surrogate measure under the assumption that unbound drug concentrations in the systemic circulation mirror intracellular unbound drug concentrations (Chu *et al.*, 2013). However this assumption is not valid for many

drug molecules which have poor membrane permeability (charged or polar compounds) or are extensively metabolised *in-vivo* (Muller and Milton, 2012).

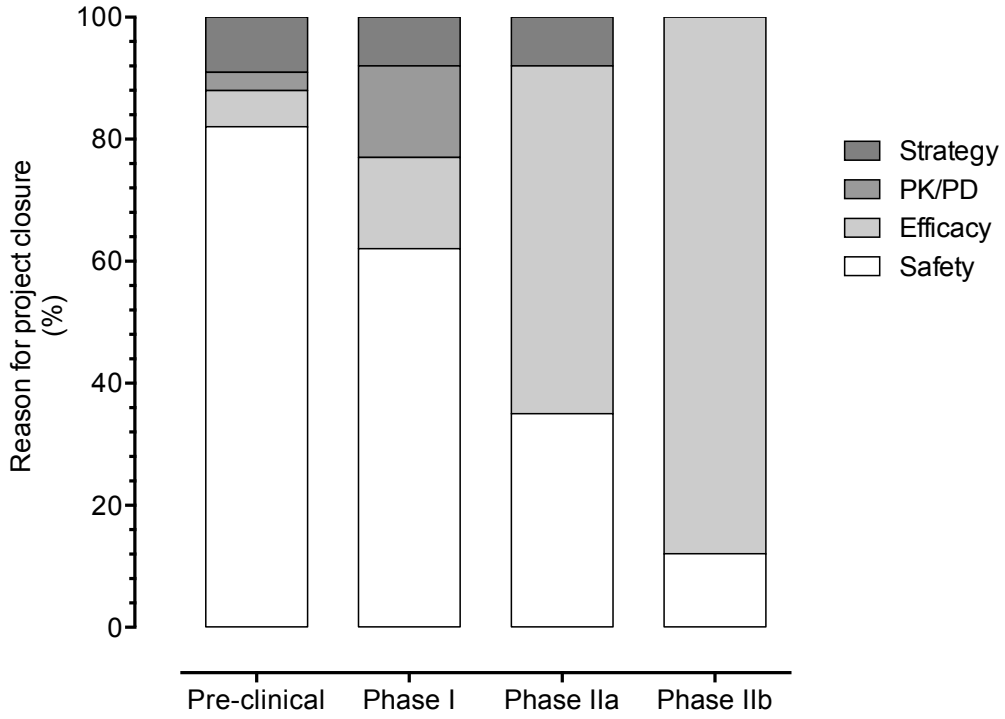

Figure 1.1: The primary reasons for project closures from 2005 to 2010 at AstraZeneca.

Project closures were classified as failing due to safety (toxicology or clinical safety), efficacy (failure to achieve sufficient efficacy), pharmacokinetics/ pharmacodynamics (PK/PD, Bioavailability, formulation, target occupancy) or the strategy (molecular diverse back-up candidate molecules). The pre-clinical phase was defined as the phase from the first good laboratory practice toxicology dose of a candidate drug through to an investigational new drug application or first clinical trial application before first-in-human testing. Phase I was defined as the phase that included the first-in-human trials within a small trial population (<50 patients) and included safety, tolerability and dose-ranging studies. These studies were often conducted in healthy volunteers. Phase II trials were defined as trials that were aimed at evaluating the candidate drug's efficacy in a patient population, leading up to clinical proof of concept. Phase II was subdivided into Phase IIa and Phase IIb. Phase IIa studies were generally smaller (<200 patients) and designed to mainly address early evidence of drug activity, whereas Phase IIb studies included larger numbers of patients (<400 patients) and were designed to demonstrate clinical proof of concept and an understanding of dose response. Information taken from Cook et al., (2004).

Species and inter-individual differences in the pharmacokinetic and toxicokinetic profiles between pre-clinical animals and man result from differential expression of transport proteins and metabolic enzymes (Bleasby *et al.*, 2006; Hilgendorf *et al.*, 2007). Transport proteins in the cellular membrane assist in the passage of specific molecules across the phospholipid bilayer and can thus determine drug disposition. Substances may pass through transport proteins by diffusion or active transport. Metabolic enzymes are responsible for the conversion of lipophilic chemical compounds into more readily excreted hydrophillic products. The rate of drug metabolism therefore determines the duration and intensity of a drug's pharmacological action. Predicting metabolic drug clearance from *in-vitro* studies using physiologically based pharmacokinetic models is well validated, however prediction of transporter mediated drug disposition has been hampered by a lack of critical information on the tissue localisation and expression of transporters in human and animal tissue. Unlike metabolic enzymes, selective inhibitors or antibodies for most drug transporters have not been identified.

With the realisation that screening of drug molecules through animals is poorly predictive of the outcome in man, both the FDA and EMA have endeavoured to promote the development of alternative screening technologies to reduce and replace animal testing in pre-clinical assessments of drug safety and efficacy (Giacomini *et al.*, 2010). One strategy to achieve this would be the development of *in-vitro* cell based screening assays, in which species differences in pharmacokinetics and toxicokinetics are identified before animal studies commence. In terms of the 3Rs (reduction, replacement, refinement), this would effectively reduce the total number of animals entering the mandatory pre-clinical drug safety testing regime by identifying the 54% of compounds with the potential to generate human toxicity at the *in-vitro* screening stage.

Realistic cell based models of drug transport in the liver have been established. The development of human and rat primary sandwich-cultured hepatocytes has given an insight into species differences and the prediction of *in-vitro* to *in-vivo* handling of drug molecules (Xu *et al.*, 2008; Swift *et al.*, 2010). In contrast, the development of similar predictive *in-vitro* methodology to understand the renal handling and metabolism of drug molecules has lagged behind, due to the lack

of a suitable *in-vitro* human or rat proximal tubule experimental model to investigate renal drug transport. In this project, we aim to characterise and validate primary renal proximal tubule models from human and rat kidney as *in-vitro* platform for drug safety studies.

1.2. Renal clearance of xenobiotic compounds

The renal clearance of xenobiotic compounds is a mechanism essential to protecting the body from toxicity. Foreign chemical substances that undergo renal excretion include drug molecules; toxic contaminants found in food; toxins produced by micro-organisms; agrichemicals and heavy metals. The process of renal clearance can be broken down into three key mechanisms, glomerular filtration, tubular secretion and tubular reabsorption.

Each human kidney is composed of approximately 1.2 million functional units called nephrons (Nyengaard and Bendtsen, 1992). Comparatively, each rat kidney contains roughly 30 000 nephrons (Haley and Bulger, 1983). Blood enters each nephron through afferent arterioles, passes through glomerular capillaries then leaves via efferent arterioles. In the glomerular capillaries water, urea, glucose, amino acids and other small molecules pass across the basement membrane of the Bowman's capsule into the nephron due to Starling forces, in a process named ultrafiltration, leaving red blood cells, proteins and other large molecules too large to pass through the capillaries behind. This is a highly efficient process; on average the human kidneys collectively receive 20% of cardiac output (1000 mL of blood per minute) then form around 120 mL of protein free ultrafiltrate per minute (Levey *et al.*, 2006; McArdle *et al.*, 2010). The ultrafiltrate within the nephron then passes through the proximal tubule, the loop of Henle, the distal convoluted tubule and a series of collecting ducts to form urine. During the passage through renal tubules and ducts, solutes and water can be reabsorbed from the ultrafiltrate into the blood of peritubular capillaries. This two-step process is known as tubular reabsorption. Within the first step, solutes are taken up from the tubular lumen into an epithelial cell, by transport proteins, driven predominately by an inwardly directed sodium gradient. Solutes then exit out of the epithelial cells into peritubular capillaries via passive diffusion or transporter-mediated mechanisms.

More importantly, in the context of this project, molecules can also be transported from peritubular capillaries to the renal tubular lumen through proximal tubule epithelial cells in a process named tubular secretion. This two-step process consists of uptake of molecules across the basolateral membrane followed by exit across the apical membrane.

In terms of renal drug clearance, many drug molecules and their metabolites are excreted in urine solely as a consequence of glomerular filtration. If a xenobiotic is freely filtered from the renal glomerular capillaries into the Bowman's capsule and is neither reabsorbed nor secreted, then its clearance rate will equal the glomerular filtration rate. Several techniques can be used to estimate an individual's glomerular filtration rate, the most common method is to collect urine over a timed period to determine the amount of endogenous creatinine removed from the blood over a given time interval.

In addition to clearance by glomerular filtration, some drug molecules (particularly small hydrophilic compounds) also undergo tubular secretion. The rate of renal clearance of these drug metabolites exceeds the rate of filtration by several-fold. For several drug molecules, a combination of glomerular filtration and tubular secretion can result in the total removal of the drug molecule from plasma in a single pass (compared to a glomerular filtration fractional clearance of 20 % in a single pass). Tubular secretion is primarily mediated in the proximal tubule of the nephron, to fulfil this role epithelial cells lining the proximal tubule express a number of drug transport proteins asymmetrically distributed to either the basolateral or apical membrane.

1.3. Drug transporter expression in the proximal tubule

Renal proximal tubular cells carry out specialised directional transport of various endogenous and exogenous molecules. Whilst all transporters expressed in the proximal tubule cells are vital in homeostasis, in the context of drug transport, several families of transporters are paramount. In 2010, the international transporter consortium (ITC) published a review titled; "Membrane transporters in drug development" in which transporters considered to be clinically relevant and should be investigated in drug development were highlighted (Giacomini *et al.*, 2010). In 2012 and 2014 the EMA and Japanese pharmaceuticals and

medical devices agency (PMDA) published similar guidance (European Medicines Agency, 2012; Japanese Ministry of Health Labour and Welfare, 2014). If renal secretion of the NME separately accounts for more than 25 % of drug elimination, renal transporters are considered to be clinically relevant. The renal transporters that should be studied in this instance according to the reviews are summarised in Table 1.1 and discussed in detail in this subchapter. Furthermore, a summary of transporters deemed clinically relevant in drug development by the regulatory authorities at the human and rat renal pharmacological barrier are compared in Figure 1.2.

Transporter	ITC/FDA	EMA	PMDA
OCT1	-	consider	-
OCT2	+	+	+
OAT1	+	+	+
OAT3	+	+	+
MATEs	consider	consider	+
MDR1	+	+	+
BCRP	+	+	+
MRPs	consider	-	-
OATP4C1	consider	-	-

Table 1.1: Renal transporters that the FDA, EMA and PMDA consider to be clinically relevant in drug development.

These transporters play key roles in determining the bioavailability, therapeutic efficacy, and pharmacokinetics of a variety of drug molecules. Information gathered from Giacomini et al., 2010; EMA, 2012; and Japanese Ministry of Health Labour and Welfare, 2014.

The uptake of molecules from circulation across the basolateral membrane of proximal tubular cells is generally mediated by the solute carrier (SLC) transporter superfamily. Many drugs are known substrates of the SLC

superfamily therefore they significantly contribute to the pharmacokinetics and toxicity of drugs. SLC transporters can be grouped into three categories by their transport mechanisms: (i) facilitated diffusion via a concentration gradient (ii) sodium utilisation or hydrogen co-transport, and (iii) substrate exchange (Kusuhara and Sugiyama, 2009). All SLC transporters act independently of adenosine triphosphate (ATP) hydrolysis. The main renal xenobiotic transporters include members of the organic organic anion transport (OAT), organic organic anion transporting polypeptide (OATP), and organic cation transport (OCT) families.

The efflux of molecules across the apical membrane of proximal tubule cells into ultrafiltrate is typically mediated by the ATP-binding cassette (ABC) and SLC transporter superfamilies. The physiological function of ATP binding cassette transporters (ABC transporters) is to protect cells against toxic compounds and metabolites. ABC transporters utilise energy from ATP hydrolysis to efflux substrates by active transport. The main renal efflux transporter families include the multidrug resistance-associated protein (MRP) and multidrug and toxin extrusion (MATE) familes, in addition to multidrug resistance protein 1 (MDR1) and breast cancer resistance protein (BCRP).

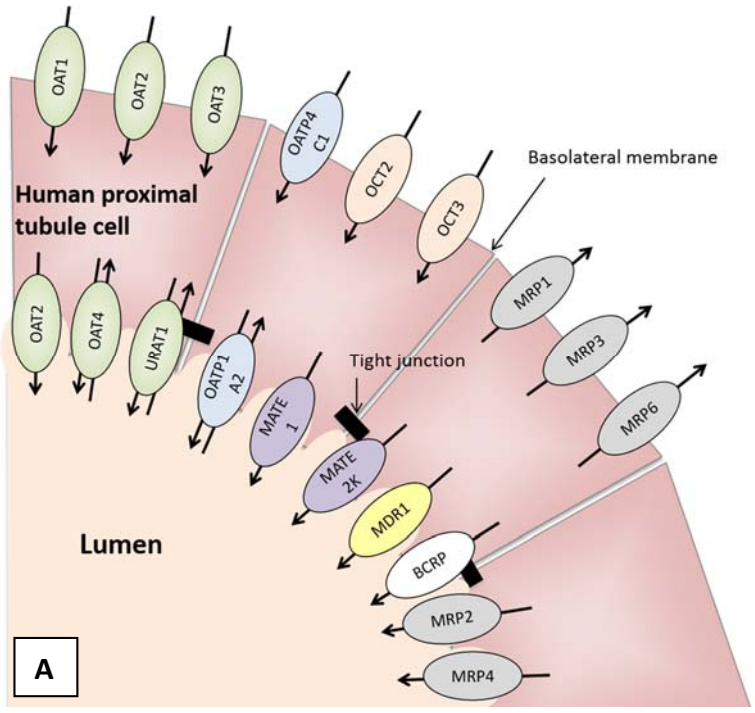

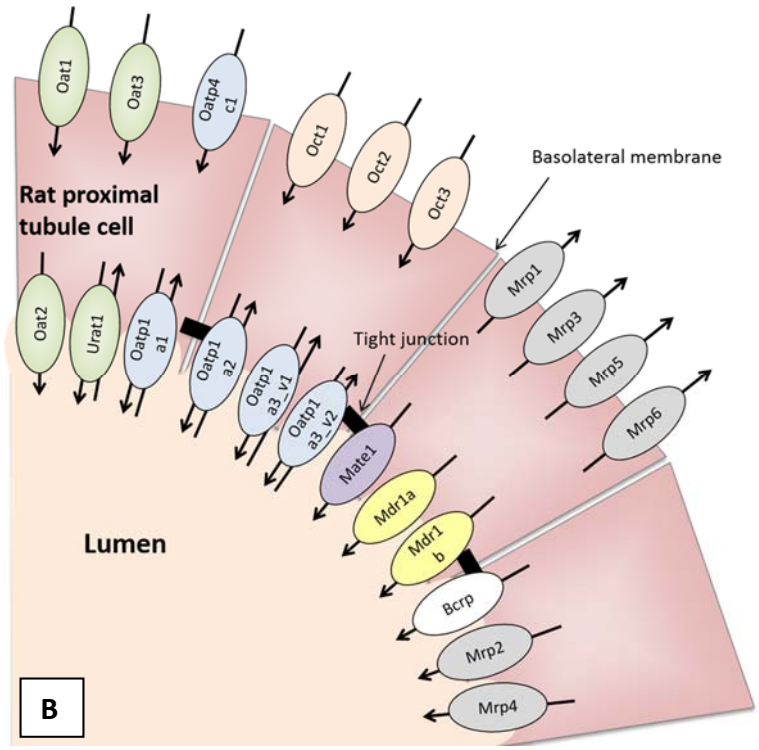

Figure 1.2: Species differences in the expression of transport proteins clinically relevant in drug development.

A wide range of transporters are expressed in human (A) and rat (B) proximal tubule cells to regulate the excretion and reabsorption of endogenous and exogenous organic anions, cations, peptides and nucleosides, thereby influencing the plasma levels of these substances. Renal transporters that the FDA, EMA and PMDA consider to be clinically relevant in drug development include the OATs, OATPs, OCTs, MATEs, MDR1, BCRP and MRPs. Species differences in renal transporter expression are listed. OAT2/Oat2 is present at both the apical and basolateral membrane of human proximal tubule cells, but only the apical membrane in rodents. Apical OAT4 has only been identified in humans and primates. Only one OATP isoform has been characterised at the apical membrane of human proximal tubule cells, OATP1A2. In contrast, rodents are thought to express multiple isoforms including Oatp1a1, Oatp1a2, Oatp1a3_v1 and Oatp1a3_v2. Oct1 has been identified at the basolateral membrane of rodent proximal tubule cells but comparative studies in humans have failed to detect OCT1 in human kidney. MATE2-K appears to be exclusively expressed in the apical membrane of human proximal tubule cells. In humans apical MDR1 is encoded by one gene, whereas rats possess two isoforms Mdr1a and Mdr1b. BCRP is expressed at low levels at the apical membrane of human proximal tubular cells, whilst Bcrp is expressed abundantly in rat kidney. Additionally, Mrp5 is expressed at the basolateral membrane of rat proximal tubular cells but absent from human kidney.

1.3.1. OAT family

The OAT isoforms OAT1/Oat1 (SLC22A6), OAT2/Oat2 (SLC22A7), OAT3/Oat3 (SLC22A8) and URAT1/Urat1 (SLC22A12) are found in both humans and rat proximal tubule cells. OAT4 (SLC22A11) has only been found in humans and primates thus far (VanWert *et al.*, 2010). In both species OAT1/Oat1 and OAT3/Oat3 are localised to the basolateral membrane and mediate the transport of organic anions and anionic drugs (OA^-) from blood into the tubule. OAT2 is present in the basolateral and apical membrane of human proximal tubule cells, but only the apical membrane in rodents (Burckhardt and Burckhardt, 2011; Shen *et al.*, 2015). OAT4 and URAT1/Urat1 are located at the apical membrane.

Oat1 was the first OAT to be cloned within rat kidney in 1997 (Sekine *et al.*, 1997; Sweet *et al.*, 1997). The gene is located on chromosome 11q12.3, and is co-localised with the gene for OAT3 (Eraly *et al.*, 2003). Oat3 was first cloned from rat brain in 1999 (Kusuhara *et al.*, 1999). OATs are 542 to 556 amino acids long with 12 predicted transmembrane spanning domains (Koepsell and Endou, 2004). They function as antiporters; the uptake of extracellular OA^- across the basolateral membrane is driven by the efflux of intracellular α-ketoglutarate (Berkhin and Humphreys, 2001). Thus, OAT1/Oat1 and OAT3/Oat3 are functionally coupled to sodium driven mono- and di-carboxylate transporters that establish and maintain the intracellular extracellular gradients of lactate, nicotinate and α-ketoglutarate.

OAT1/Oat1 and OAT3/Oat3 substrates, listed in Table 1.2, are generally monovalent or divalent anions that are less than 500 Daltons (Giacomini *et al.*, 2010); although OAT3 can also transport some positively charged drugs such as cimetidine (Wright, 2005). Studies of OAT1/Oat1 and OAT3/Oat3 in expression systems such as *Xenopus Laevis* oocytes and transfected cell lines have shown that they have wide overlapping substrate specificities (Rizwan and Burckhardt, 2007). OAT1/Oat1 is primarily known for its high affinity transport of para-aminohippurate (PAH) from renal proximal tubule cells (Hosoyamada *et al.*, 1999). OAT3 can also transport PAH but with slightly lower affinity (Cha *et al.*, 2001). Studies using Oat1 and Oat3 knock out mice have led to identification of endogenous OAT substrates and initial assessments of the influence of each

transporter on the renal handling of selected compounds (Eraly *et al.*, 2006; Vallon *et al.*, 2008). Genetic variants in the OATs have not been associated with clinically significant DDIs or changes in the amino acids transcribed (Shin *et al.*, 2010).

OAT1/Oat1 and OAT3/Oat3 can be the site of DDIs during competition of two or more drugs for the same transporter, particularly for drugs with a narrow therapeutic index. For example, several case studies have reported an increase in serum urate levels during antihypertensive therapy with low-dose diuretics (toasemide and hydrochlorothiazide). The diuretics are substrates of OATs and, by counter exchange, cause increased urate absorption resulting in hyperuricemia. Furthermore, OAT1 and OAT3 can also mediate cell damage by transporting cytotoxic compounds. Probenecid can be used to reduce the nephrotoxic liability of therapeutics by inhibiting transport of potentially nephrotoxic drugs into proximal tubular cells. Cidofovir is toxic in the proximal tubular cells, co-administration with probenecid results in a reduced accumulation of cidofovir in the proximal tubule cells and thus reduced nephrotoxicity (Cundy *et al.*, 1996).

Oat2 expression was first identified in rat liver (Simonson *et al.*, 1994; Sekine *et al.*, 1998). Oat2 was later found to be highly expressed at the mRNA level in rat kidney (Buist *et al.*, 2002; Kobayashi *et al.*, 2005). Evidence for similar renal expression of OAT2 in human kidney was not published until recently (Cheng *et al.,* 2012). OAT2 interacts with a wide range of nucleobases, nucleosides and nucleotides. Three splice variants of OAT2, which result in amino acid changes, have been identified (Emami Riedmaier *et al.*, 2012). The clinical consequences of these are yet to be investigated. OAT2 has been implicated in the renal handling of creatinine; previous evidence suggested that the basolateral organic cation transporter OCT2 served as the primary means of uptake into proximal tubular cells. This theory was challenged when knock out of Oct1/Oct2 expression in mice had no effect creatinine clearance, but the presence of cimetidine and PAH significantly reduced creatinine secretion (Eisner *et al.*, 2010). At physiologically relevant creatinine concentrations, the affinity of creatinine for OAT2 has been shown to be greater than the affinity for OCT2, OCT3, MATE1 and MATE-2K (Lepist *et al.*, 2014; Shen *et al.*, 2015). OAT2

mRNA expression is reported to be 3-fold higher than expression of OCT2 (Cheng *et al.*, 2012). Collectively this suggests that OAT2 plays a major role in the tubular secretion of creatinine.

OAT4 has been linked with drug exit into the ultrafiltrate and the uptake of estrone-3-sulphate (E3S) and urate from ultrafiltrate into the cell. It effluxes OA^- accumulated within the cell by OAT1/Oat1 and OAT3/Oat3 in exchange with extracellular chloride ions. Additionally, urate and E3S are reabsorbed by OAT4 from ultrafiltrate in exchange for dicarboxylate/hydroxyl ions. The gene for OAT4 is located on chromosome 11q13.1 and is co-localised with the gene encoding URAT1 (Eraly et al., 2003). URAT1/urat1 is the major urate reabsorbing transporter in proximal tubular cells and the target of uricosuric drugs. Many genetic variants in SLC22A12 (URAT1) have been associated with hypouricemia (Enomoto et al., 2002; Anzai et al., 2007; Roth et al., 2012).

Substrates of OAT1/Oat1 and OAT3/Oat3	
Endogenous compounds	α-Ketoglutarate
	Prostaglandin E2/F2α
	Cyclic nucleotides
	Folate
	Urate
	Estone-3-Sulphate
	Conjugated hormones
Drugs	
Antibiotic	Benzylpenicillin, Cephaloridine, Tetracycline
ACE inhibitor	Captopril
Antiviral	Acyclovir, Adefovir
Histamine receptor 2 antagonist	Cimetidine, Ranitidine
Anti-inflammatory	Ibuprofen, Diclofenac
Diuretic	Torasemide, Chlorothiazide
Statin	Pravastatin, Fluvastatin
Cytostatic	Methotrexate, Chlorambucil
Uricosuric	Probenecid, Benzbromarone, Losartan

Table 1.2: Substrates of OAT1/Oat1 and OAT3/Oat3 transporters.

1.3.2. OATP family

In human renal proximal tubule cells only two OATP family isoforms have been characterised, basolateral OATP4C1 (SLCO4C1) and apical OATP1A2 (SLCO1A2). In contrast, rodents are thought to express multiple OATP isoforms including basolateral Oatp4c1, and apical Oatp1a1 (SLCO1A1), Oatp1a2, Oatp1a3_v1 (SLCO1A3, previously known as Oat-K1), and Oatp1a3_v2 (SLCO1A3, previously known as Oat-K2) (Hagenbuch B, 2004).

OATPs are located in numerous epithelia throughout the body. They mediate the sodium-independent transport of a diverse range of amphiphilic organic compounds with a molecular weight greater than 350 Daltons (Hagenbuch and Meier, 2003; Roth *et al.*, 2012). The general predicted structure consists of 12

transmembrane spanning domains (Hagenbuch and Gui, 2008). The majority of substrates are OA^-, although some OATPs have been reported to also transport neutral and cationic compounds (Bossuyt *et al.*, 1996). They function as antiporters, the uptake of organic compounds is coupled with the efflux of bicarbonate, glutathione, or glutathione-s-conjugates in an electroneutral exchange (Takeuchi A, 2001; Badagnani I, 2006). The overall direction of transport is dependent upon the local substrate gradients. Examples of OATP4C1 and OATP1A2 substrate are listed in Table 1.3 and Table 1.4.

Oatp4c1 was first cloned from rat kidney in 2004, based upon northern blot analysis it was thought to be kidney-specific (Mikkaichi T, 2004). More recently however, microarrays have suggested that it is also expressed within the liver, however, this has not yet been verified with PCR or protein analysis (Bleasby *et al.*, 2006). The human gene is located on chromosome 5q21 (Hagenbuch B, 2004; Mikkaichi *et al.*, 2004). From rat Oatp4c1 localisation studies it is assumed that human OATP4C1 is also located on the basolateral membrane of proximal tubule cells. Oatp4c1 is reported to possess multiple substrate recognition sites. So far, two distinct recognition sites for E3S and digoxin (DX) have been characterised (Mikkaichi *et al.*, 2004).

Oatp1a2 (SLCO1A2) first cloned within rat liver, is located on human chromosome 12p12 (Kullak-Ublick GA, 1995; Hagenbuch B, 2004). In human and rat proximal tubular cells OATP1A2/Oatp1a2 is expressed at the apical membrane (Lee *et al.*, 2005), where it is thought to be responsible for either the reabsorption from or the secretion of xenobiotics into ultrafiltrate. In the kidney OATP1/Oatp1 expression is stimulated by testosterone and inhibited by oestrogen. As a consequence, kidney Oatp1 is less abundantly expressed in female compared to male rats (Lu *et al.*, 1996; Gotoh *et al.*, 2002). Functional downregulation of OATP1/Oatp1 can occur via serine phosphorylation by extracellular ATP (Glavy *et al.*, 2000). Furthermore, protein kinase C activation in Oatp1a expressing *Xenopus Laevis* oocytes leads to decreased transport of E3S (Guo and Klaassen, 2001). Altered expression levels and polymorphisms of OATP1A2 are associated with disease states and altered drug disposition e.g. imatinib (Yamakawa *et al.*, 2011), and methotrexate (Badagnani *et al.*, 2006). Six nonsynonymous single nucleotide polymorphisms (SNPs) have been

identified (T38C (I13T), A516C (E172D), G559A (A187T), A382T (N128Y), A404T (N135I), and C2003G (T668S)), the allelic frequencies of which appear to be ethnicity-dependent (Lee *et al.*, 2005). A516C and A404T variants have a reduced capacity for mediating the cellular uptake of OATP1A2 substrates such as E3S, whereas G559A and C2003G variants appear to have substrate-dependent changes in transport activity.

Substrates of OATP4C1	
Endogenous compounds	Cyclic nucleotides
	Estrone-3-sulphate
	Thyroid hormones
Drugs	
Cytostatic	Methotrexate
Cardiac glycoside	Ouabain, Digoxin
Antidiabetic	Sitagliptin

Table 1.3: Substrates of OATP4C1/Oatp4c1 transporters.

Substrates of OATP1A2	
Endogenous compounds	Anionic cyclic and linear peptides
	Estrone-3-sulphate
	Thyroid hormones
	Bile acids
	Steroid hormones and conjugates
Drugs	
Antibiotic	Erythromycin, Rifampicin
Antiviral	Ritonavir, Lopinavir
Antihypertensive	Enalapril, Verapamil
Statin	Pravastatin, Rosuvastatin
Anti-inflammatory	Dexamethosone
Narcotic	Naloxone
Antihistamine	Fexofenadine
Cytostatic	Imatinib, Methotrexate
β-blocker	Acebutolol, Atenolol

Table 1.4: Substrates of OATP1A2/Oatp1a2 transporters.

1.3.3. OCT family

The OCT isoforms OCT2/Oct2 (SLC22A2), and OCT3/Oct3 (SLC22A3) are found in both humans and rat proximal tubule cells. Oct1 (SLC22A1) has been identified at the basolateral membrane of rodent proximal tubular cells by northern analysis and RNA *in-situ* hybridisation (Gründemann D, 1994; Karbach *et al.*, 2000). However *in-situ* hybridization studies have failed to detect OCT1 in human kidney. It is reported to be primarily expressed in the liver, indicating a species difference in renal transporter expression (Gorboulev V, 1997; Zhang *et al.*, 1997).

Oct1 was the first OCT isoform to be cloned in 1994 from rat kidney (Gründemann D, 1994). A human orthologue was later cloned in 1997 (Gorboulev *et al.*, 1997). By homology screening, a second member Oct2 was identified in rat kidney (Okuda *et al.*, 1996) and later cloned in human (Gorboulev *et al.*, 1997). OCT3/Oct3 was independently cloned and identified

as the extraneuronal monoamine transporter in 1998 (Grundemann *et al.*, 1998; Kekuda *et al.*, 1998; Wu *et al.*, 1998). OCTs encode proteins that are 542 to 556 amino acids long with 12 predicted transmembrane spanning domains (Koepsell and Endou, 2004). Oct1, OCT2/Oct2, and OCT3/Oct3 located at the basolateral membrane of proximal tubule cells mediate the passive facilitated diffusion of a broad range of structurally diverse organic cations (OC^+s) down their electrochemical gradients (Urakami *et al.*, 1998; Karbach *et al.*, 2000). Therefore transport can occur in either direction and is driven not only by the difference in substrate concentration but also by membrane potential. Due to the negative resting membrane potential of the cell maintained by Na^+/K^+ ATPase, transport is favoured at normal membrane potential (Wright SH and Dantzler WH, 2004). The functional characteristics of these transporters have been studied in expression systems such as *Xenopus Laevis* oocytes and transfected cell lines. They have extensively overlapping substrate specificities. The OC^+s range in size from 60 to 350 Daltons, with at least one positively charged moiety at physiological pH (Jonker and Schinkel, 2004), examples are shown in Table 1.5.

OCT regulation can occur at the transcriptional or protein level. The OCT2/Oct2 promoter region has androgen receptor elements. Activation via steroid hormones increases both OCT2/Oct2 mRNA levels and activity (Shu *et al.*, 2001). Additionally phosphorylation of Oct1 and OCT2/Oct2 by tyrosine kinase and protein kinase A, C and G can alter activity (Roth *et al.*, 2012). Whilst OCT3/Oct3 activity can be altered by both the mitogen activated protein kinase pathway and calcium-calmodulin pathway. Oct1, Oct2, Oct3 knock out mice have been generated with no obvious phenotype (Jonker *et al.*, 2001; Zwart *et al.*, 2001; Jonker *et al.*, 2003). Similarly no polymorphisms in OCTs are associated with pathologies. OCT1 has 18 SNPs that alter amino acids – 6 have reduced transport activity and 1 has increased activity (Kerb *et al.*, 2002). OCT2 has 10 variants with the exception of a premature stop codon, all are functionally active, though substrate selectivity and the ability to transport may be slightly altered (Koepsell *et al.*, 2007). 5 non-synonymous polymorphisms have been identified in OCT3, 3 of which show reduced transport activity (Sakata *et al.*, 2010). In Chinese and Korean populations the OCT2 variant A270S has been associated with a significant reduction in renal clearance of

metformin (Song *et al.*, 2008; Wang *et al.*, 2008). Tubular secretion of creatainine can be inhibited by OCT2 substrates. Therefore, alternative methods should be used to assess golmerular filtration rate in NMEs capable of OCT2 inhibition.

Substrates of OCT2/Oct2 and OCT3/Oct3 transporters	
Endogenous compounds	Creatinine
	Bile acids
	Choline
	Hormones
	Neurotransmitters
	L-Carnitine
	Guanidine
Drugs	
Antidiabetic	Metformin
Antihypertensive	Debrisoquine, Verapamil
Antiviral	Amantadine
Histamine H2 receptor antagonist	Cimetidine, Ranitidine
Antiparkinsonian	Amantadine, Memantine
Antiarrhythmic	Procainamide
β-blocker	Propranolol
Diuretic	Amiloride
Cytostatic	Cisplatin, Oxaliplatin
Nicotinic receptor partial agonist	Varenicline
Antidepressant	Citalopram, Desipramine
Antimalarial	Quinine

Table 1.5: Substrates of OCT2/Oct2 and OCT3/Oct3 transporters.

1.3.4. MATE family

Within mammals there are two MATE proteins, MATE1/Mate1 (SLC47A1) and MATE2 (SLC47A2). MATE1/Mate1 is expressed in both human and rat kidney.

Currently the MATE2 splice variant, MATE2-K, is the only member of the subfamily in which functional transport activity has been demonstrated. MATE2-K appears to be exclusively expressed in the apical membrane of human renal proximal tubular cells, whilst MATE2 is expressed in intracellular vesicles (Komatsu *et al.*, 2011).

MATE1, first cloned within humans is highly expressed on the apical membrane of both rat and human proximal tubular cells (Otsuka *et al.*, 2005; Terada *et al.*, 2006). A paralog of MATE1, MATE-2K was first cloned from human kidney in 2006 (Masuda *et al.*, 2006). The predicted structure is 12 transmembrane domains (He *et al.*, 2010). Both MATEs expressed at the apical membrane of proximal tubular cells appear to function in conjunction with basolateral OCT2 to mediate the excretion of OC^+s from blood into ultrafiltrate (Dresser *et al.*, 2001; Otsuka *et al.*, 2005). Initial characterisation of the transporter when it was first identified within *Vibrio Parahaemolyticus* described MATE1 as a secondary active antiporter (Morita *et al.*, 2000). It couples the movement of toxic OC^+ out of the cell, against the concentration gradient using the energetically favourable inward movement of hydrogen and sodium ions along their electrochemical gradient. Similar to OCTs, substrates of these transporters include structurally diverse low molecular weight OC^+s. In addition select OA^-s such as E3S, acyclovir and gancyclovir are reported to be substrates for MATE1 (Tanihara *et al.*, 2007). Functional characterisation *in-vitro* studies in membrane vesicles and transfected cell lines have revealed an extensive overlapping substrate specificity but different binding affinities. The functional characteristics of these transporters have been studied in expression systems such as *Xenopus Laevis* oocytes and transfected cell lines. They have extensively overlapping substrate specificities (Masuda *et al.*, 2006; Tanihara *et al.*, 2007). Examples of endogenous and exogenous substrates are shown in Table 1.6.

The ubiquitously expressed transcription factors specificity protein 1 (SP1) and activator protein 1 (AP1) are reported to affect MATE1/Mate1 transcription in both human and rat proximal tubule cells (Kajiwara *et al.*, 2007; Ha Choi *et al.*, 2009; Baumann *et al.*, 2010). In MATE1 and MATE2-K 11 and 2 nonsynonymous SNPs have been identified (Chen *et al.*, 2009; Kajiwara *et al.*, 2009; Yonezawa and Inui, 2011). The mutations G64D and V480M in MATE1

and G211V in MATE2-K cause a complete loss of membrane expression. Thus these variants can affect the pharmacokinetics of substrates. The allelic frequency of dysfunctional mutations is less than 5% and homozygous carriers have not been found. Polymorphisms in both the SP1 and AP1 transcription factor binding regions have also been identified (rs72466470, rs2252281), which result in a decreased binding and a reduced transcriptional activity. The frequency of these polymorphisms is 3.7 and 23.1 to 44.5 %, respectively. The MATE genes are also located in the commonly deleted region in Smith-Magenis syndrome, a genomic disorder of chromosome 17p11.2 (Bi *et al.*, 2002; Slager *et al.*, 2003). The disease is a developmental disorder, with major features including mild to moderate intellectual disability, distinctive facial features, sleep disturbances and behavioural problems. The relevance of MATE1 and MATE2-K to the progression of this disorder is under investigation. Experiments in Mate1 knock out mice have identified the role of MATE1 in the pharmacokinetics of many drug molecules. For instance in Mate1 knock out mice, plasma and renal concentrating of metformin increased and urinary excretion decreased, indicating Mate1 plays a role in the tubular secretion of metformin (Tsuda *et al.*, 2009). In heterozygous Mate1 knock out mice the pharmacokinetics of metformin were not significantly different from wild type, suggesting Mate1 is not the rate limiting step in the tubular secretion of metformin (Toyama *et al.*, 2010).

Substrates of MATE1/Mate1 and MATE2-K transporters	
Endogenous compounds	Peptides
	Nucleosides
	Creatinine
	Thiamine
	Guanidine
	Estrone-3-sulphate
Drugs	
Antidiabetic	Metformin
Antibiotic	Cephalexin, Cephradine
Antiviral	Acyclovir, Gancyclovir
Antihistamine	Fexofenadine
Cytostatic	Oxaliplatin, Topotecan
Histamine H2 receptor antagonist	Cimetidine
Antiarrhythmic	Quinidine, Verapamil, Procainamide
Antimalarial	Pyrimethamine

Table 1.6: Substrates of MATE1/Mate1 and MATE2-K transporters.

1.3.5. MDR1

MDR1/Mdr1 (ABCB1) first cloned from human carcinoma cells (Ueda *et al.*, 1987), is highly expressed on the apical membrane of human and rat proximal tubule cells. In humans MDR1 is encoded by one gene, whereas rats possess two isoforms Mdr1a and Mdr1b (Bush JA, 2002).

The function of apically expressed MDR1/Mdr1 is the movement of substrates out of the cell for renal clearance. ATP hydrolysis provides the energy for active transport, enabling the transporter to function against steep concentration gradients. Endogenous and exogenous substrates of human and rat MDR1/Mdr1 have been identified through functional studies in membrane vesicles and transfected cell lines. They transport a broad range of therapeutics, as shown in Table 1.7. Substrates preferentially are neutral or hydrophobic OC^{+} molecules ranging in size from less than 200 to 1900 Daltons. The transporter

consist of 1276 to 1280 amino acids in a tandem duplicated structure, with 12 hydrophobic transmembrane domains (Aller *et al.*, 2009). Containing at least three distinct substrate binding sites within the ligand binding domain and two ATP binding motifs (Shapiro *et al.*, 1999). A high resolution structure of mouse Mdr1 has been described (Aller *et al.*, 2009). Cholesterol stimulates basal ATPase activity (Rothnie *et al.*, 2001; Gayet *et al.*, 2005). It is an endogenous substrate of MDR1 (Garrigues *et al.*, 2002). Furthermore, it has been shown that cholesterol effects the affinity of low molecular weight molecules (350 to 500 Daltons) for MDR1 (Kimura *et al.*, 2007). As a result it has been hypothesised that cholesterol may directly bind or allosterically affect the substrate binding site to help the recognition of smaller substrates. Many inhibitors of MRD1/Mdr1 contain aromatic ring structures, a tertiary or secondary amino group, and have high lipophilicity (Wang *et al.*, 2003). They can be categorised into either high-affinity substrates that bind non-competitively, or efficient inhibitors of ATP hydrolysis.

Protein kinases, chaperones (HSP90), ubiquitin-related enzymes, and transcription factors regulate the expression and function of MDR1. A variety of mitogen-activated protein kinase signalling inhibitors have been shown to reduce expression of MDR1/Mdr1. Some have suggested phosphorylation of serine residues in the linker region of MDR1/Mdr1 is essential for the translocation and function. Several groups have reported conflicting results on the role of the transcription factor, AP1. Some have demonstrated that AP1 downregulates expression (Liu *et al.*, 2008; Bark and Choi, 2010), whereas other have reported that AP1 activates expression (Guo *et al.*, 2008; Chen *et al.*, 2014). Suggesting that dual regulation must occur at the site of the AP1 site of the MDR1 promoter (Katayama *et al.*, 2014). Oestrogen mediates down-regulation of MDR1/Mdr1 expression (Mutoh *et al.*, 2006). A number of microRNAs (miR-27a, miR-451) have been reported to modulate expression of MDR1/Mdr1 (Katayama *et al.*, 2014).

MDR1/Mdr1 is highly polymorphic, over 50 SNPs have been identified in both the coding and noncoding regions of the gene, with significant linkage disequilibrium (Marzolini *et al.*, 2004; Coller *et al.*, 2006). SNPs in exons 26 (C3435T), 21 (G2677T/A), and 12 (C1236T) have been characterised in a

number of ethnic populations. The frequencies of the variant alleles differ in various populations (Marzolini *et al.*, 2004). Expression of G2677T and C3435T are reported to protect Chinese but not Caucasian men from late-onset Parkinson's disease (Lee *et al.*, 2004; Tan *et al.*, 2004; Tan *et al.*, 2005). In addition, G2677T/A is linked with lower plasma concentrations of fexofenadine, a higher risk of cyclosporine A failure in steroid resistant ulcerative colitis, and tacrolimus toxicity (Yamauchi *et al.*, 2002; Yi *et al.*, 2004; Daniel *et al.*, 2007). C3435T is associated with an increased efflux of rhodamine 123, reduced efflux of nelfinavir, and no effect on fexofenadine efflux (Hitzl *et al.*, 2001; Drescher *et al.*, 2002; Fellay *et al.*, 2002). C1236T genotype has been linked to an increased exposure to irinotecan and increased response to temozolomide, cyclosporine A (Zhou *et al.*, 2005; Zhang *et al.*, 2008; Schaich *et al.*, 2009).

Direct clinical evidence of the contribution of MDR1/Mdr1 inhibition or induction to DDIs is limited due to cross specificity of MDR1/Mdr1 substrates with the drug metabolising enzymes CYP3A4. DX is a MDR1/Mdr1 substrate that is not metabolised by cytochrome P450 enzymes (Hinderling and Hartmann, 1991; Lacarelle *et al.*, 1991). Therefore it is commonly used as a model substrate to determine MDR1/Mdr1 transporter activity *in-vivo* (Endres *et al.*, 2006). Co-administration of DX with other MDR1/Mdr1 substrates or inhibitors (such as verapamil, quinidine, itraconazole and ritonavir) can significantly affect the bioavailability and/or systemic clearance (Woodland *et al.*, 1998; Hunt, 2005). DX has a narrow therapeutic window thus increases in plasma concentration can cause digitalis toxicity.

Substrates of MDR1/Mdr1 transporters	
Endogenous compounds	Steroids
	Lipids
	Bilirubin
	Bile Acids
	Guanidine
	Estrone-3-sulphate
	Opioid peptides
Drugs	
Analgesic	Asimadoline
Anticancer	Vinblastine, Paclitaxel, Etoposide
HIV protease inhibitor	Saquinavir, Ritonavir
β-blocker	Talinolol
Histamine H2 receptor antagonist	Cimetidine, Ranitidine
Antigout agent	Colchicine
Antidiarrheal agent	Loperamide
Antiemetic	Domperidone, Ondansetron
Antifungal	Ketoconazole, Itraconazole
Antihistamine	Fexofenadine, Cetirizine
Calcium channel blocker	Verapamil, Diltiazem
Cardiac glycoside	Digoxin
Antiarrhythmic agent	Quinidine, Losartan
Statin	Atorvastatin
Immunosuppressant agent	Cyclosporine A, Tacrolimus
Corticosteroid	Dexamethasone, Hydrocortisone
Antibiotic	Erythromycin, Gramicidin D

Table 1.7: Substrates of MDR1/Mdr1 transporters.

1.3.6. BCRP

BCRP/Bcrp (ABCG2) was first identified within MCF-7/AdrVp breast cancer cells (Doyle LA, 1998). It is primarily expressed in the small intestine, blood brain barrier, liver and placenta. The transporter is also expressed within human proximal tubular cells (Huls *et al.*, 2008); however its expression level is very

low in comparison to the small intestine and liver. Alternatively the transporter is abundantly expressed in rat kidney.

BCRP/Bcrp has a major role in drug disposition and distribution, similar to MDR1. BCRP/Bcrp is an apical efflux transporter that mediates the movement of substrates out of the cell for renal clearance. ATP hydrolysis provides the energy for active transport, enabling the transporter to function against steep concentration gradients. Unlike the other multi-substrate transporters BCRP/Bcrp consists of 655 amino acids and six transmembrane domains (Ni *et al.*, 2010). This implies that the transporter need to dimerise to be functional (Nicolle *et al.*, 2009). A homotetramer structure has been reported in humans (Xu *et al.*, 2004; McDevitt *et al.*, 2006). The transporter possess a very broad substrate specificity that overlaps with MDR1/Mdr1 which increases the barrier function of the efflux transporters.

Table 1.8 lists examples of BCRP/Bcrp endogenous and exogenous substrates. High-speed screening and quantitative structure activity relationship analysis methods suggest that one amine bonded to one carbon of a heterocyclic ring is an important component for drug interaction with BCRP/Bcrp (Saito *et al.*, 2006; Nicolle *et al.*, 2009; Giacomini *et al.*, 2010). Many inhibitors of MRD1/Mdr1 are also inhibitors of BCRP/Bcrp with varying affinity. They can be categorised into either high-affinity substrates that bind non-competitively, or efficient inhibitors of ATP hydrolysis.

BCRP expression can be regulated at the transcriptional and protein level. In humans the predominant promoter is E1B/C that contains multiple SP1 sites, followed by E1A (Bailey-Dell *et al.*, 2001). Transcription factors that bind to cis elements upstream of the BCRP E1B/C promoter with subsequent activation or repression of the promoter include hypoxia-inducible factor 1α, estradiol, progesterone, interleukin-6, aryl hydrocarbon receptor agonists, peroxisome proliferators-activated receptor gamma, zinc finger protein - GLI1, nuclear factor 2, and transforming growth factor-β (Natarajan *et al.*, 2012). Epigenetic regulation of the ABCG2 gene has been reported in renal cancer cell lines. Elevated BCRP levels have been associated with hypomethylation and unmethylation of CpG islands, and histone hyperacetylation of the promoter region (To *et al.*, 2006). BCRP expression can be downregulated by microRNAs

(miR-519c, miR520h, miR328) (Mao and Unadkat, 2015). Serine/threonine-protein kinase 1 phosphorylates BCRP/Bcrp which promotes its dimerisation and trafficking to the plasma membrane (Xie *et al.*, 2008).

More than 80 SNPs of the ABCG2 gene have been identified although few modify transport activity (Mao and Unadkat, 2015). Of these, the V12M and Q141K alleles are found at high frequency in East Asians (30 to 60%) with a low frequency in Caucasian and African-American populations (5 to 10%). The Q141K variant results in a reduced protein expression of BCRP/Bcrp (Vethanayagam *et al.*, 2005). Clinically this allele has been linked with higher plasma levels of BCRP substrate drugs such as topotecan, rosuvastatin, sulfasalazine, gefitinib, atorvastatin and methotrexate (Sparreboom *et al.*, 2005; Cusatis *et al.*, 2006; Urquhart *et al.*, 2008; Warren *et al.*, 2008; Keskitalo *et al.*, 2009) but not of irinotecan, pitavastatin and lamivudine (de Jong *et al.*, 2004; Ieiri *et al.*, 2007; Kim *et al.*, 2007). 2 SNPs result in a premature stop codon (Q126stop, E334stop).

Substrates of BCRP/Bcrp transporters	
Endogenous compounds	Flavonoids
	Porphyrins
	Estrone-3-sulphate
Drugs	
Antibiotic	Anthracycline, Daunorubicin
Anticancer agent	Topotecan, Methotrexate
Nucleoside analogue	Azidothymidine, Lamivudine
Antianxiety	Prazosin
Proton pump inhibitor	Pantoprazole
Statin	Rosuvastatin
Antiarthritis	Sulfasalazine
Histamine H2 receptor antagonist	Cimetidine
Antidiabetic	Glibenclamide

Table 1.8: Substrates of BCRP/ Bcrp transporters.

1.3.7. MRP family

The isoforms MRP1/Mrp1 (ABCC1), MRP2/Mrp2 (ABCC2), MRP3/Mrp3 (ABCC3), MRP4/Mrp4 (ABCC4) and MRP6/Mrp6 (ABCC6) are expressed in both human and rat proximal tubular cells. Additionally rat proximal tubular cells also express Mrp5 (ABCC5). MRPs are unidirectional efflux transporters. MRP2/Mrp2 and MRP4/Mrp4 are located at the apical membrane (Schaub *et al.*, 1997; van Aubel *et al.*, 2002). MRP1/Mrp1, MRP3/Mrp3, Mrp5 and MRP6/Mrp6 are located at the basolateral membrane. Of all the MRPs MRP2/Mrp2 is deemed the most clinically relevant.

MRP1 was the first isoform to be characterised; it was originally identified in a human multi-drug resistant lung carcinoma cell line (Cole *et al.*, 1992). By searching the human genome with an expressed sequence tag of ABCC1 the other isoforms of MRP were identified (Allikmets *et al.*, 1996; Kool *et al.*, 1997). Each of the MRPs contain two ATP-binding cassettes and two core membrane spanning domains each consisting of 6 transmembrane regions (MSD_1 and MSD_2). MRP1/Mrp1, MRP2/Mrp2, MRP3/Mrp3 and MRP6/Mrp6 also contain an additional membrane-spanning domain (MSD_0) containing a further 5

transmembrane regions (Toyoda *et al.*, 2008). It has been shown that this additional transmembrane domain within MRP1 is not required for function of MRP1/Mrp1 nor for localisation to the basolateral plasma membrane (Bakos *et al.*, 1998). However, mutation of Cysteine (7) residue within MSD_0 changes the amino-terminal conformation of MRP1, thereby reducing the maximal transport rate (V_{max}) of leukotriene C4 5 to 7-fold (Yang *et al.*, 2002). Suggesting that MSD_0 may have some function. The energy of ATP hydrolysis is used to actively efflux substrates across either the apical of basolateral. The MRPs again have a broad substrate specificity they act as a defence mechanism effluxing potentially cytotoxic endogenous and exogenous molecules from cells. They are able to transport hydrophobic anionic molecules, and conjugates of glucoronate, sulphate and glutathione. Lipophilic glutathione-s-conjugates are transported predominantly by MRP2/Mrp2 (Konig *et al.*, 1999; König J, 1999), while cyclic nucleotides, uric acid, anticancer agents and antiviral drugs are transported by MRP4/Mrp4 (van Aubel *et al.*, 2002). Examples of MRP substrates are listed in Table 1.9. The development of knock out animal models has led to a better understanding of the role of MRP1 and MRP2 in drug disposition (Endres *et al.*, 2006). The remaining isoforms have not been sufficiently characterised to date.

MRP expression is regulated at the transcriptional and protein level in response to substrate concentrations, oxidative stress, and disease states. Characterisation of the human and rat promoter region of the ABCC2 identified numerous transcription factor binding sites, such as SP1 and AP1. A hormone response element in rat ABCC2 promoter has also been recognised. Many lipophilic compounds are ligands for nuclear receptor hormones (such as farnesoid X receptor, pregnane X receptor, or constitutive androstane receptor). The binding of heterodimers of the retinoid X receptor-α with the ligand-activated nuclear receptor hormones at the hormone response element induces transcription of ABCC2 (Nies and Keppler, 2007). Oxidative stress leads to activation of nuclear factor 2. Once activated this transcription factor binds the antioxidant response element to up-regulate transcription of ABCC1 and ABCC2 (Toyoda *et al.*, 2008). In an *in-vivo* rat model of cholestasis it has been shown that ABCC2 expression in the liver is down regulated whilst expression in the kidney is upregulated (Lee *et al.*, 2001). This adaptation in transporter

expression is thought to limit liver injury and facilitate extrahepatic excretion of bile salts.

More than 200 naturally occurring sequence variants have been identified in the human ABCC2 gene (Nies and Keppler, 2007). Many of these sequence variants are SNPs that do not result in amino acid changes and are thus without functional consequence. Impairment of MRP2 function by polymorphisms (i.e. splice site, premature stop codons, deletion and frame insertion mutations) or chemical inhibitors results in Dubin-Johnson syndrome. An autosomal recessive disorder that causes an increase of conjugated bilirubin in the serum without elevation of liver enzymes (Nies and Keppler, 2007).

Substrates of MRP/Mrp transporters	
Endogenous compounds	Bilirubin
	Leukotrienes
	Bile salts
	S-glutationyl- estradiol
	Cholecystokinin peptide
	E3S
	Conjugates of 17β-estradiol
	Leukotriene
	Cyclic nucleotide
	Urate
	Prostaglandins
	PAH
	Taurocholic acid
	Folic Acid
Drugs	
	Glutathione and glucuronide conjugates
Anticancer	Methotrexate, Etoposide
HIV protease inhibitor	Saquinavir, Ritonavir
Angiotensin II receptor antagonist	Valsartan, Olmesartan
Anitviral	Acyclovir
Diuretic	Frusemide
Antibiotic	Ciprofloxacin, Cefazolin
Antihistamine	Fexofenadine
Analgesic	Paracetamol
Statin	Rosuvastatin, Atorvastatin
Stimulant	Para-methoxy-N-ethylamphetamine

Table 1.9: Substrates of MRP/ Mrp transporters.

1.4. Current proximal tubule cell models

Models of the renal proximal tubule commonly used to measure transport activity in drug development pre-clinical *in-vitro* screening assays include; expression systems, transfected cells, immortalised animal and human renal cell lines, membrane vesicles, cortical renal slices, and primary cells. The advantages and disadvantages of these models are discussed herein. These models are commonly used for mechanistic studies, to determine the rate limiting step in transepithelial transport, and identify transporter based DDIs. In academia radiolabelled or fluorescent substrates are commonly used to measure transporter expression in these expression systems. Alternatively pharmaceutical companies utilise expensive, high-throughput, sensitive liquid chromatography – mass spectrometry techniques.

1.4.1. Expression systems

One of the earliest techniques to determine the function of a transport protein is microinjection of the transport protein cRNA into an expression system such as a *Xenopus Laevis* oocyte (Gurdon *et al.*, 1971). This provides a platform for the study of only the transporter of interest, without the influence of others. The structure, substrates and inhibitors of OCTs and OATs have been elucidated using this technique (Gründemann D, 1994; Okuda *et al.*, 1996; Sekine *et al.*, 1997). A drawback of this model is its lack of physiological relevance due to the absence of other transporters that may influence a molecules distribution. Another disadvantage is that oocytes only provide transient expression of transport proteins. As a result marked variation in expression levels and thus kinetic parameters (such as maximum rate of transport and transporter affinity values) between batches of oocytes have been reported (Walker, 2008). Furthermore, kinetic values derived from oocytes differ from those from mammalian expression systems due to differences in the plasma lipid membrane (Goldin, 1992).

1.4.2. Transfected cell lines

Transporters of interest have also been transfected in to immortalised animal and human cell lines. This is achieved by inserting a vector such as a plasmid

containing the cDNA of the desired transporter. Recombinant transporter that are stably of transiently expressed in various cell lines can be used to characterise drug transporter interactions. Cultured renal cell lines commonly used to study drug transporter interactions include MDCK, LLC-PK1 and HEK293 cells. MDCK have been transfected with OATPs and MDR1 (Takeuchi *et al.*, 2001; Kuteykin-Teplyakov *et al.*, 2010). Cells can be stably transfected to express multiple transporters. A quintuple multi-transporter renal model of creatinine clearance containing OAT2, OCT2, OCT3, MATE1 and MATE2-K is commercially produced by Optivia biotechnology. Transfection of cells with recombinant uptake and efflux transporters endogenously missing enables the study of transcellular transport (Cui *et al.*, 2001; Sasaki *et al.*, 2002). However, transporter expression in these cell lines does not reflect the transporters' physiological expression levels as they are driven by the vector promoters and the cells' translation transcription machinery.

1.4.3. Immortalised animal and human renal cell lines

Immortalised mammalian renal epithelial cell lines commonly used include LLC-PK1 (porcine), MDCK (canine), and OK (opossum) cells. Immortalised human renal cell lines include HK-2, RPTEC, HEPTEC and ciPTEC cells. Immortalised renal epithelial cells inherently express some transport proteins. However, overall expression of renal transporters is low in comparison to primary tissue. For example the LLC-PK1 and HK-2 renal epithelial cell lines express functional MDR1 and have been used to investigate the efflux of prototypic substrates (Ryan *et al.*, 1994; Ohtomo *et al.*, 1996; Tramonti *et al.*, 2001). Advantages of such cells are that they are easy to cultivate in large quantities and have an infinite lifespan. Some, but not all of these cell lines can be grown on Transwell® inserts to form polarised monolayers. This enables measurement of the molecules tubular secretion and reabsorption.

A further limitation is that the cells lose differentiation over time with repeated passages. Often they lack expression of key transporters and fail to maintain brush-border microvilli. The LLC-PKI cells lack expression of the enzyme fructose- 1,6-bisphosphatase, rendering them incapable of gluconeogenesis, which is a key metabolic pathway in proximal nephron cells (Gstraunthaler *et al.*, 1985). In addition, LLC-PKI cells are not responsive to parathyroid hormone and

lack a probenecid-sensitive organic anion transporter (Gstraunthaler *et al.*, 1985; Pfaller and Gstraunthaler, 1998). MDCK cells, on the other hand, do not express type 2 sodium/phosphate transporters, Sodium/glucose cotransporter 1 and 2, or amino acid transporters. HK-2 cells lack expression of OAT1, OAT3 and OCT2 (Jenkinson *et al.*, 2012). ciPTEC cells lack expression of OATs (Jansen *et al.*, 2014). SLC transporter expression is yet to be characterised within RPTEC cells (Aschauer *et al.*, 2013). Additionally, slight variations in culture conditions (i.e. culture medium, passage frequency, passage protocol) between laboratories has been shown to effect transporter expression.

1.4.4. Membrane Vesicles

Basolateral and apical brush border plasma membrane vesicles can be used to study transporter activity. The technique was commonly used in transport studies in the 1970s and 80s but has been effectively superseded by cell transfection. Membrane vesicles have previously been prepared from intact renal tissue and primary, immortalised or transfected cell lines. The approach has provided a wealth of information on the quantitative structure activity relationship and interaction of many substrates and inhibitors with various transporters and provided much of the background to our current understanding of epithelial membrane transporters. Advantages of the methodology are that substrates and inhibitors of a known concentration are directly applied to the cytoplasmic compartment, and gradients can be easily optimised to drive transporter activity. But the procedure provides no molecular knowledge about transporter identity, and is unsuitable for hydrophobic compounds due to the molecule binding to the vesicle membrane or cellular systems. More data is available for apical membrane transporters than basolateral transporters as preparation of basolateral membrane vesicles is technically difficult and has mixed yields of membranes orientated in the outside-out and inside-out configuration, which makes experimental design and data interpretation difficult.

1.4.5. Cortical renal slices

An alternative to immortalised cells which dedifferentiate over time is the use of fresh primary tissue. Isolated cortical renal slices represent the truest anatomical *in-vitro* model of the kidney. 80% of each renal slice is composed of

proximal tubule cells, therefore they have potential to provide good information on renal drug handling (Lohr *et al.*, 1998). Cisplatin was shown to competitively inhibit tetraethylammonium uptake in renal slices in 1984, indicating that it was an OCT2 substrate (Nelson *et al.*, 1984). Cross sections are available from human and animal kidneys which allow direct comparison between species. However, the lumen of the tubules within the slices collapse, which means they provide information only on basolateral uptake, not apical membrane transport nor net direction of movement (Atterwill, 1987). Other drawbacks are they contain a heterogeneous population of cells and discriminating between which cell type can be difficult. They have a short finite lifespan, and a skilled experienced worker for kidney dissection.

1.4.6. Primary proximal tubular cells

The need for a robust *in-vitro* model of drug transport that expresses a full complement of transporters has been highlighted. Primary cells are derived from intact tissue, which, at the time of isolation express the full complement of drug transporters present in the tissue of interest. Proximal tubular cells can be isolated by a wide range of techniques that include enzymatic tissue digestion, differential sieving, gradient density centrifugation and fluorescence-activated cell sorting. Isolated proximal tubular cells in suspension are physiologically relevant intact cell models containing all the relevant transporters (Lohr *et al.*, 1998). However they are only viable for 2-3 hrs, after this functional integrity declines rapidly (Jones *et al.*, 1979). Furthermore during the course of an experiment polarity of the cells is lost, which results in a marked down regulation of transporter expression.

In recent years, proximal tubule cells isolated from intact tissue by collagenase digestion and isopynic centrifugation have been successfully cultured from human and rat kidneys. Cultures are structurally polarised, with numerous microvilli and tight junctions at the apical side, and preserved characteristic features of proximal tubule cells e.g. alkaline phosphatase and γ-glutamyl transferase enzyme activity (Racusen *et al.*, 1997; Kim *et al.*, 2001). Human primary proximal tubule cells also express the OA^- and OC^+ transporters absent from many immortalised proximal tubule cell lines in addition to ABC transporters MDR1 and MRP2 (Lash *et al.*, 2006; Brown *et al.*, 2008). The cells

have shown prototypic transport of endogenous OA^- and OC^+ such as PAH and creatinine and xenobiotics such as rosuvastatin (Lash *et al.*, 2006; Brown *et al.*, 2008; Verhulst *et al.*, 2008). Similarly cultured rat proximal tubule cells have shown sodium dependent uptake of α-methyl-D-glucopyranosine, ergothionine and carnitine suggesting expression of sodium-glucose (SGLT) and OC^+/carnitine (OCTN) transport proteins (Nakanishi *et al.*, 2011). Furthermore, Dr Lawrence H Lash (Wayne State University) has published several studies confirming the suitability of rat and human primary proximal tubular cells cultures as an *in-vitro* models to study nephrotoxicity (Cummings and Lash, 2000; Cummings *et al.*, 2000; Lash *et al.*, 2001; Lash *et al.*, 2003; Lash *et al.*, 2005; Lash *et al.*, 2006). A disadvantage of primary culture is the finite lifespan of cells (approximately 14 days). A further limitation is human tissue availability and the expense of transport from hospitals.

As discussed, a key deficiency in the drug development process is the availability of applicable pre-clinical *in-vitro* models that can be used to predict toxicological and efficacious outcomes in the clinical setting. Many widely used pre-clinical *in-vitro* models of transport in the kidney are based on transfected human or animal cells. These models express a limited number of human renal transporters, and so do not accurately reflect the situation *in-vivo.* Wherein the complex interplay between multiple transporters is key to transepithelial transport. In contrast, cultured primary renal proximal tubule cell monolayers appear to maintain a full complement of key renal transporters, resulting in a more physiologically relevant, and thus predictive model of drug handling in the clinical setting.

1.5. Development of human and rat *in-vitro* models of drug transport.

As previously mentioned a major challenge in drug development is the extrapolation of drug safety information from animals to humans. Approximately 40.42 % of compound fail at Phase I (Tufts Center for the Study of Drug Development, 2014). Meaning that large numbers of animals are being sacrificed in pre-clinical trials with little to no benefit. For each drug lost at this stage $740 million is lost in developmental costs and 6.5 years in lead time to

clinic (Paul *et al.*, 2010). Overall this results in a delay in getting molecules to clinic and an increased cost of successful drug molecules.

Rat is the initial test species in drug development and safety determination (Bass *et al.*, 2009). Due to the unpredictable differences in renal drug handling between species (Rasmussen, 1983) the development of a parallel rat primary proximal tubule cell model in addition to a human is encouraged. It enables clear unambiguous transport data on the handling drug molecules in either species to be ascertained. It allows direct comparison of the renal handling of a molecule between human and rat kidney, which would flag up any differences in handling that might impact upon the progress of the candidate drug molecule into a pre-clinical study. Furthermore, the data could be crucial in validating the cell-based assay as an acceptable surrogate for renal clearance experiments in rats.

1.6. Project Aims

The aims of this project are 3-fold. Firstly; to optimise the human and rat primary proximal tubule cell isolation technique. Secondly; to characterise expression of key renal transporters in human and rat primary proximal tubular cells. Thirdly; to validate their use as a screening tool to identify drug transporter interactions and transporter mediated DDIs. In the hope that further characterisation and validation of human and rat primary proximal tubular cell model will encourage their use of as an *in-vitro* proximal tubule cell model in industry and academia.

2. Materials and Methods

2.1. Materials

2.1.1. Cell Culture

Cell culture reagents used in this project included high-glucose Dulbecco's modified eagles medium (HG-DMEM), Ham's F-12 nutrient mixture, Roswell Park Memorial Institute (RPMI)-1640 medium, foetal calf serum (FCS), penicillin, streptomycin, L-glutamine, trypsin with 0.02% ethylenediaminetetraacetic acid (EDTA), collagen, Dulbecco's phosphate-buffered saline (PBS) and mouse epidermal growth factor (EGF) purchased from Sigma-Aldrich (UK). Percoll® was bought from GE Healthcare Life Sciences (UK), type 2 collagenase from Worthington Biochemicals (USA), and 10X Hanks' balanced salt solution (HBSS) from Invitrogen (USA). Renal epithelial cell growth medium (REGM) SingleQuot kit supplements and growth factors (containing insulin, hydrocortisone, gentamycin amphotericin-B (GA) - 1000, adrenaline, tri-iodothyronine (T3), transferrin, FCS and human EGF) were procured from Lonza (Switzerland).

The renal proximal tubular epithelial cell line, RPTEC, was licensed from Evercyte (Austria), along with ProxUp-2 ready-to-use medium (consisting of HG-DMEM/Hams-F12 (1:1), 4-(2-hydroxyethyl)-1-piperazineethanesulfonic acid (HEPES) buffer, glutamax, human epidermal growth factor, tri-iodothyronine, ascorbic acid, holo-transferrin, prostaglandin E2, hydrocortisone, sodium selenite, insulin and geneticin (G418)).

Cells were grown on various cell culture vessels bought from Corning (UK). These included 24-well Transwell® permeable insert cell culture plates (with a surface area of 0.33 cm^2 per insert and polycarbonate filter pore size of 0.4 µm), plastic 96-well plates (0.33 cm^2 surface area), plastic 12-well plates (3.8 cm^2 surface area), T25 flasks (surface area 25 cm^2) and T75 flasks (surface area 75 cm^2).

2.1.2. Quantitative polymerase chain reaction

SV Total RNA isolation System, purchased from Promega (UK), was used to isolate total cell RNA. Moloney murine leukaemia virus (M-MLV) reverse transcriptase, M-MLV 5x reaction buffer, RNasin, Magnesium Chloride, deoxyribonucleotide triphosphate (dNTP) mix, 5x Green GoTaq® reaction buffer, GoTaq polymerase, and pGem-T-easy cloning vector kit (consisting of T4 DNA ligase, pGem®-T vector, 2x ligation buffers) were also procured from Promega (UK). Random hexamers were obtained from GE Healthcare Life Sciences, and MiniElute PCR purification kit from Qiagen. Agarose, EDTA, sodium hydroxide pellets, boric acid, ethidium bromide, bacto-tryptone, bacto-yeast extract, isopropyl β-D-1-thiogalactopyranoside, 5-bromo-3-indolyl β-D-galactopyranoside, dimethylformamide, ampicillin, GenElute Plasmid Miniprep were gifts from Dr Judith Hall, and sourced from Sigma-Aldrich. Competent *E.coli* strain, DH5α, was bought from New England Biolabs (UK). The 125U ThermoStart Taq DNA polymerase and 1x ThermoStart buffer were acquired from ABgene. Bespoke primers were ordered from IDT DNA (Belgium). Human and Rat Drug Transporter RT^2 Profiler PCR array plates from SABiosciences (UK).

2.1.3. Uptake and Flux Assays

Radiolabelled [1-^{14}C]-mannitol D, [^{32}P]-monosodium phosphate ([^{32}P]-P$_i$), and Optiphase Hisafe 2 scintillation solvent were purchased from PerkinElmer (USA). Bisbenzimide Hoechst 33342 (H33342), 5-(3-(2-(7-Chloroquinolin-2-yl)ethenyl)phenyl)-8-dimethylcarbamyl-4,6-dithiaoctanoic acid (MK-571), mannitol, sodium chloride, potassium chloride, monosodium dihydrogen orthophosphate, magnesium sulphate, monopotassium phosphate, calcium chloride, HEPES, glucose, tris base, ethanol, chenodeoxycholic acid (CDC), T3, rosuvastatin (RSV), cimetidine (CIM), PAH, DX, E3S, GF120918, Ko143 hydrate, heparin sodium, molecular-grade water, bovine serum albumin (BSA) and chloroform were purchased from Sigma-Aldrich. 5-chloromethylfluorescein-diacetate (CMFDA) was purchased from Invitrogen (USA), and coomassie blue dye reagent from ThermoFisher Scientific (UK). Scintillation vials were purchased from Meridian Biotechnologies Ltd (UK). TFV and radiolabelled [adenine-2,8-^{3}H]-TFV ([^{3}H]-TFV) were gifts from Gilead (USA), and sourced

from Bio-techne and Hartmann Analytic GmbH respectively. Recombinant human Klotho-α (amino acid residues 32-981) was purchased from Bio-techne (USA), recombinant fibroblast growth factor 23 (FGF-23) from BioVision (USA), and recombinant human parathyroid hormone (amino acid residues 1-84, PTH) from Cambridge Biosciences (UK). Trisodium phosphonoformate (PFA) was bought from Santa Cruz Biotechnology (USA).

2.1.4. Nephrotoxicity

CellTiter 96® AQueous one solution cell proliferation assay was purchased from Promega.

2.2. Methods and Protocols

2.2.1. Primary human proximal tubular epithelial cell isolation

Primary human proximal and distal tubular and collecting duct epithelial cells (human PTCs) were isolated from healthy human kidneys unsuitable for transplant supplied by the human tissue bank Scievita Ltd. The donations came from a variety of anonymous UK hospitals. The demographics of the donors such as age, gender and ethnicity were unknown to protect patient anonymity. Ethical approval and consent for medical research were granted to Scievita prior to tissue procurement. The work carried out at Newcastle University was approved by the Scientific Review Board at Scievita in line with the ethical approval for medical and commercial usage granted to Scievita acting as a human tissue bank.

Once excised from the donor, the kidney was stored with saline solution in sealed surgical bags placed in a polystyrene box filled with ice and transported to Newcastle University Medical School within 18 hours (hrs). All cell culture conducted at Newcastle University was performed in a class II vertical laminar flow hood to ensure sterility. The isolation procedure, summarised in Figure 2.1 has been previously published (Van der Biest *et al.*, 1994; Helbert *et al.*, 1997; Helbert *et al.*, 1999; Helbert *et al.*, 2001; Brown *et al.*, 2008).

Under sterile conditions, the kidneys were decapsulated and macroscopically normal cortex slices were dissected, cut into pieces of about 1 mm^3 and

enzymatically digested using type 2 collagenase in isolation medium. In order to optimise the enzymatic digestion phase of the isolation procedure renal cortex was incubated with different concentrations of collagenase over two different incubation periods. The cell suspension was shaken vigorously either (i) overnight at 4 °C followed by 37 °C for 1 hr (an overnight incubation) or (ii) for 2 hrs at 37 °C (an acute incubation).

Following enzymatic digestion of the renal cortex, the resulting cell suspension was passed through a 40 μm nylon mesh cell strainer to remove undigested cortex and glomerular endothelial cells. The collagenase was then removed by centrifuging the cell suspension at 1200 revolutions per minute (rpm) for 7 minutes (min) in a 4 x 200 mL swing-out rotor at 4 °C. To remove any residual collagenase the cell pellet was resuspended in fresh isolation medium and recentrifuged at 1200 rpm for 7 min, this wash process was repeated twice. After the second wash, the heterogeneous cell population was separated by gradient density centrifugation. The cell suspension was loaded on top of a discontinuous Percoll® gradient then centrifuged at 3000 rpm for 25 min (minutes) at 4 ˚C. The densities of the gradient were 1.04 g / mL and 1.07 g / mL. Proximal and distal tubular epithelial cells from the intersection of the 1.04 g / mL and 1.07 g / mL densities were carefully aspirated, washed and cultured as a mixed population of approximately 80 % proximal and 20 % distal tubule cells in 37 °C human REGM. The yield of cells collected from the isolation was quantified using a haemocytometer (Hawksley, UK). The compositions of the isolation medium and human REGM are shown in Table 2.1 and Table 2.2, respectively.

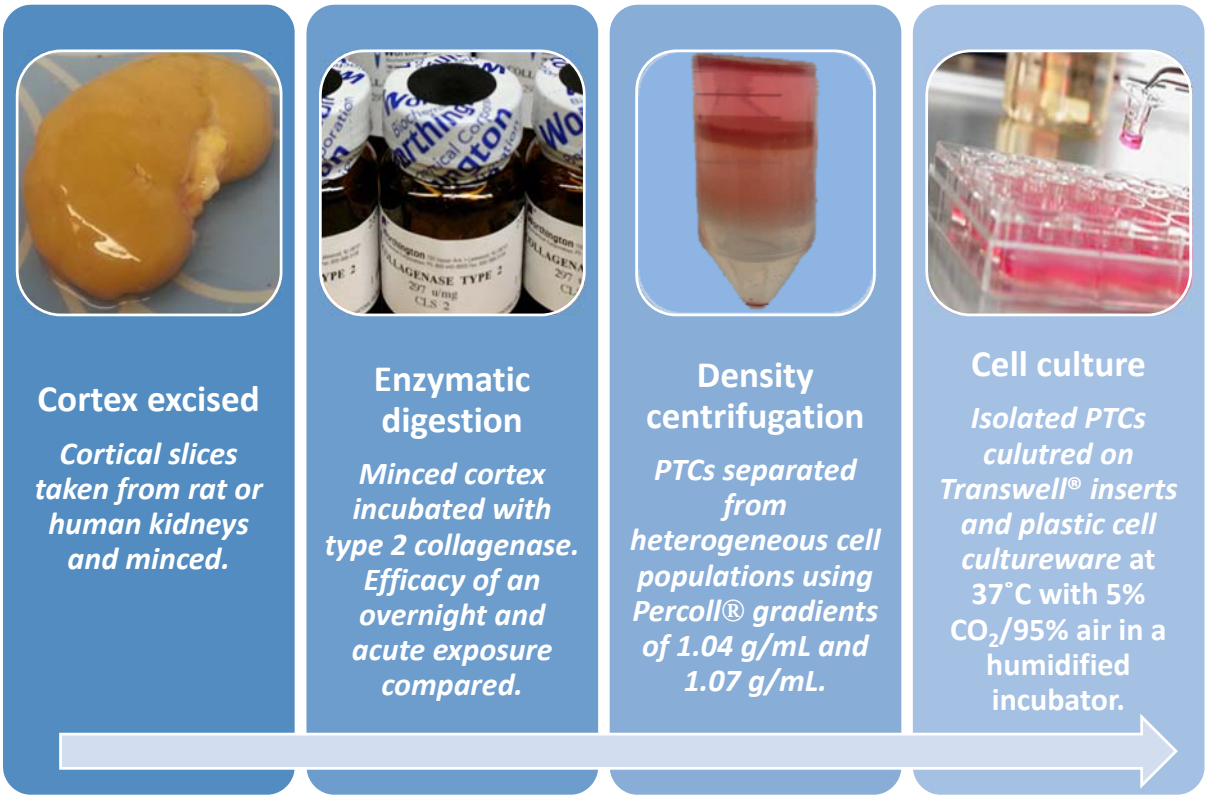

Figure 2.1: A schematic flow diagram of the proximal tubule cell isolation procedure.

The enzymatic digestion of renal cortex was optimised in both species to generate the highest yield of viable cells.

Supplements	Amount	Final concentration
Basal Medium		
RPMI-1640 Medium	500 mL	-
Supplements		
FCS	25 mL	5 %
Penicillin/Streptomycin	2.5 mL	200 units/mL, 200 µg/mL respectively.

Table 2.1:The composition of isolation medium used in both human and rat PTC isolation.

Ingredient	Amount
Basal Medium	
DMEM/Ham's F-12 (1:1)	500 mL
Supplements	
L-Glutamine	2.5 mL
Human EGF	0.5 mL
Insulin	0.5mL
Hydrocortisone	0.5 mL
GA	0.5 mL
FCS	2.5 mL
Adrenaline	0.5 mL
T_3	0.5 mL
Transferrin	0.5 mL
Penicillin/Streptomycin	2.5 mL

Table 2.2:The composition of human REGM.

The REGM SingleQuot Kit (CC-4127) was purchased from Lonza (Switzerland). The concentrations of the supplements and growth factors are withheld from consumers.

2.2.2. Primary rat proximal tubular epithelial cell isolation

Primary rat proximal and distal tubular epithelial cells (rat PTCs) were isolated from healthy 8 to 12 week old male Sprague-Dawley rats (weighing 250 - 300 g) purchased from Charles River (UK). The rats were euthanised by trained university staff in accordance with Schedule 1 of the Animals (Scientific Procedures) Act 1986. The kidneys were excised using sterile tweezers and scissors, and stored in ice-cold sterile isolation medium. The isolation procedure, which commenced within 30 min of the kidneys retrieval, was identical to the human isolation protocol described in subchapter 2.2.1. Isolated rat PTCs were cultured in rat REGM. The composition of rat REGM can be found in Table 2.3.

Ingredient	Amount
Basal Medium	
DMEM/Ham's F-12 (1:1)	500 mL
Supplements	
L-Glutamine	2.5 mL
Mouse EGF	0.5 mL
Insulin	0.5 mL
Hydrocortisone	0.5 mL
GA	0.5 mL
FCS	2.5 mL
Adrenaline	0.5 mL
T_3	0.5 mL
Transferrin	0.5 mL
Penicillin/Streptomycin	2.5 mL

Table 2.3: The composition of rat REGM.

The REGM SingleQuot Kit (CC-4127) was purchased from Lonza (Switzerland). The concentrations of the supplements and growth factors are withheld from consumers.

2.2.3. RPTEC cell line cell culture

The RPTEC cell line was also used in this project. It was developed by overexpressing the catalytic subunit of human telomerase (hTERT) in primary renal proximal tubular epithelial cells isolated from human kidney. The cells were cultured in ProxUp-2 ready-to-use medium, whose composition can be found in Table 2.4. Upon confluency, the cells were detached from the plastic flasks by incubating the cells with 5 mL trypsin/0.02 % EDTA for 5 min. After detachment of the cells, 5 mL of fresh culture medium was added to neutralised the trypsin before the cells were pelleted by centrifuging the suspension at 1500 rpm for 5 min. The cell pellet was resuspended in fresh culture medium and cell yield determined using a haemocytometer. The cells were then seeded out onto cultureware as described below. The cells were cultured up to passage 20.

Ingredient	Final concentration
DMEM/Ham's F-12 (1:1)	_
HEPES Buffer	10 mM
Glutamax	2 mM
Human EGF	10 ng / mL
T3	5 pmol
Ascorbic Acid	3.5 μg / mL
Holo Transferrin	5 μg / mL
Prostaglandin E2	25 ng / mL
Hydrocortisone	25 ng / mL
Sodium Selenite	8.65 ng / mL
Insulin	5 μg / mL
G418	100 μg / mL

Table 2.4: The composition of ProxUp-2 Medium purchased from Evercyte.

2.2.4. Cell Culture

The human PTC, rat PTC and RPTEC cells were grown on a variety of cell culture flasks and plates. They included plastic 12-well plates at a density of 200 000 cells per well with 1 mL of culture medium, plastic 96-well plates at a density of 20 000 cells per well with 200 μL of culture medium, and 24-well Transwell® inserts at a density of 75 000 cells per insert with 200 μL of culture medium in the apical chamber and a further 1000 μL in the basolateral well. All cells were also seeded on plastic T75 culture flasks at a density of 3 million cells with 25 mL of culture medium. The type of cultureware used for each experiment is defined in the relevant methods subchapter. Once seeded, cells were incubated at 37 ˚C with 5 % carbon dioxide and 95 % air in a humidified incubator.

The cells were grown until confluent to allow tight junction formation and cell polarisation. Cell confluency within 12-well, 96-well plates and T75 flasks was monitored regularly using a phase contrast microscope. Due to the opacity of

the Transwell® polycarbonate filter the confluency of cells on 24-well Transwell® inserts could not be observed using the microscope. Alternatively, the trans-epithelial electrical resistance (TEER) was measured at regular intervals to determine tight junction integrity using an epithelial voltohmmeter (EVOM, World Precision Instruments, UK). The silver metal and silver chloride chopstick electrodes were stored in 70 % ethanol to maintain sterility. The following calculation was used to determine TEER values ($\Omega.cm^2$).

$$TEER = (R_M - R_F) \times A$$

R_M = *Cell TEER measurement* (Ω)

R_F = *Resistance of the filter (80* Ω*)*

A = Area of the filter membrane (24-well filter surface area is 0.33 cm^2*)*

Experiments were performed when monolayers had a TEER value of 80 $\Omega.cm^2$ or greater.

2.2.5. Cell Growth Assays

In order to optimise the enzymatic digestion phase of the isolation procedure, samples of renal cortex were incubated with different concentrations of collagenase for an overnight and acute incubation period and the resulting yield of cells and their growth over 8 days was compared. The collagenase concentrations used to enzymatically digest human and rat renal cortex were 10, 20, 25, or 30 mg collagenase / gram of renal cortex (activity of around 300 units / mg). The yields of isolated proximal tubular cells per gram of renal cortex for each concentration of collagenase were estimated 3 times using a haemocytometer (Hawksley, UK) and the average yield was recorded (n = 3).

Following isolation the cells were seeded onto six plastic 12-well plates. In total 8 wells were seeded from cells isolated from each of the above mentioned conditions. The growth of these cells was then determined by quantifying the number of cells in the well at 24 hrs (Day 1), 48 hrs (Day 2), 72 hrs (Day 3), 96 hrs (Day 4), 120 hrs (Day 5), 144 hrs (Day 6) 168 hrs (Day 7) and 192 hrs (Day 8) after seeding. At the designated time point, the wells were washed with PBS

solution twice, trypsinised with 500 μL of trypsin / 0.02 % EDTA for 5 min at 37 °C, neutralised with 500 μL of human or rat REGM, and the number of cells in each well quantified using a haemocytometer. The number of cells in each well were counted 3 times and the average recorded (n = 3). The cell yield and growth measurements were performed in triplicate using samples derived from 3 individual kidneys (N = 3).

2.2.6. Total cell RNA isolation and quality assessment

In order to understand how cell culture conditions may affect cellular expression of transport proteins, total cell RNA was isolated from:

- Freshly isolated human PTCs and rat PTCs,
- Human PTCs, rat PTCs and RPTEC cells cultured on 24-well Transwell® inserts, and
- Human PTCs, rat PTCs and RPTEC cells cultured in plastic T25 flasks.

This was achieved using the SV Total RNA Isolation System according to the manufacturer's protocol. The yield and purity of the isolated RNA samples were determined using a NanoDrop ND-1000 UV-Vis Spectrophotometer (ThermoFisher Scientific, USA). The yield was calculated from the absorbance at 280 nm on the basis that an optical density reading of 1 is equivalent to 40 μg / mL single stranded RNA. The purity of each sample was estimated from the relative absorbance at 260 nm and 280 nm ($A_{260\ /\ 280}$) to assess protein contamination, then at 260 nm and 230 nm ($A_{260\ /\ 230}$) to determine guanidine contamination. Values of 1.8 to 2.2 for both ratios indicated the samples were of sufficient purity for downstream applications. Isolation was performed in triplicate using samples derived from 3 individual kidneys or 3 different passage numbers (N = 3).

2.2.7. Reverse transcription of total cell RNA and endpoint PCR

Total cell RNA was reverse transcribed into cDNA using MMLV-RT. Initally, 1 μg of total cell RNA was mixed with 1 μL of 0.5 mg / mL random hexamers for 5 min at 65 ˚C then immediately cooled on ice. Once cooled 0.5 μL MMLT-RT

(activity: 200 units / µL), 4 µL of 5x MMLT-RT buffer, 5 µL of 2 mM dNTPs and 0.25 µL of RNasin (a ribonuclease A inhibitor, activity: 40 units / µL) was added to create a final reaction volume of 20 µL. The reaction was performed in a Px2 Thermo Cycler (ThermoScientific, UK), where the reaction mixture was incubated at 42 ˚C for 2 hrs, then 70 ˚C for 10 min. Once the reaction was completed, the resulting cDNA was diluted using molecular grade water (1 cDNA: 3 water).

Primers for transport protein genes of interest were designed using Primer-BLAST from the National Center for Biotechnology Information website (NCBI, http://www.ncbi.nlm.nih.gov/tools/primer-blast/), unless otherwise stated. When designing the forward and reverse primer pairs, the following criteria were set:

- A product size of around 100 base pairs should be amplified by the primer pair,
- Each individual primer should be 18-22 base pairs in length,
- The total guanine and cytosine (GC) content of each primer should be 40-60 %,
- The melting temperature of each primer should be between 58 and 64 ˚C,
- Within each pair the difference in the melting temperature between the forward and reverse primer should be no more than than 2 ˚C, and
- One of the primers in the pair must cross an exon-exon boundary.

The retrieved primers by Primer-BLAST were analysed for hetero-dimer, homo-dimer, as well as hairpin formation, using the NetPrimer software (http://www.premierbiosoft.com/netprimer/). The specificity of a primer pair to the intended gene was analysed by running the basic local alignment search tool on their sequences. High performance liquid chromatography purified primers with customised sequences were then ordered from IDT DNA (Belgium). The genes of interest and their relative primer pair sequences are listed in Table 2.5 and Table 2.6.

In order to confirm the specificity of the primers, endpoint PCR followed by gel electrophoresis was carried out for each gene of interest. The endpoint PCR reaction mixture included 0.25 µL GoTaq DNA polymerase (activity: 5 units / µL), 2 µL of 2 mM dNTPs, 0.5 µM of each primer for the gene of interest (forward and reverse), 4 µL of 5x Green GoTaq buffer, 1.5 µL of cDNA template and enough molecular grade water to make the total reaction volume to 20 µL. Using a Px2 Thermo Cycler, the reaction mixture was incubated at 95 ˚C for 2 min to activate GoTaq DNA polymerase (initialising step), then amplified for 35 cycles by incubating the reaction mixture at 95 ˚C for 30 seconds (denaturation step), T_a ˚C for 30 seconds (primer annealing step) and 72 ˚C degree for 30 seconds (elongation step). This was followed by 72 ˚C for 10 min (final elongation step). T_a denotes the annealing temperature of the primer pair. The T_a was calculated by subtracting 5 ˚C from the melting temperature of the least stable primer. In order to check if the PCR had generated the anticipated DNA fragment, the PCR products were separated by agarose gel electrophoresis and visualised with ethidium-bromide staining (0.01 % volume for volume). PCR products were separated on 1.5 % agarose gels. The sizes of PCR products were determined by comparing them with DNA ladders containing fragments of known size that were run on the gels alongside the PCR products.

Gene (NCBI Reference)		Primer Sequence	T_a (°C)	Product Size (base pairs)
MATE1 (NM_018242.2)	F	^{1353}ATC GGG ATC GCG CTG ATG TT^{1372}	58	149
	R	^{1501}TGT ACC TGA GCC TGC TGA CA^{1482}		
MATE2-K (NM_152908.3)	F	^{614} TCC AGG TTG ACC CAG GAC TA^{633}	58	106
	R	^{719}CCT TCA GCC ATC CCT GAT TTT^{699}		
MDR1a/b (NM_000927.4)	F	^{1683}TTC ACT TCA GTT ACC CAT CTC^{1703}	56	76
	R	^{1758}GTC TGC CCA CTC TGC ACC TTC^{1738}		
MRP1 (NM_004996.3)	F	^{2161}TGG CAT CAC CTT CTC CAT CC^{2180}	58	81
	R	^{2241}GAG AGC AGG GAC GAC TTT CCG^{2221}		
MRP2 (NM_000392.4)	F	^{4735}CAC CAT CAT GGA CAG TGA CAA GG^{4757}	60	60
	R	^{4794}CCG CAC TCT ATA ATC TTC CCG^{4774}		
MRP3 (NM_003786.3)	F	^{3140}TCT GCA AGG GTT CTT GGT GAT G^{3161}	60	120
	R	^{3259}AAG AAG GAC TGT GGC GAG CG^{3240}		
MRP4 (NM_001105515.2)	F	^{195}CGT GTT CTT CTG GTG GCT CAA T^{216}	60	70
	R	^{264}CAT ATC ATC TTC CTC TAA TCT CCG^{241}		
BCRP (NM_001257386.1)	F	^{593}CAG GTG GAG GCA AAT CTT CG^{612}	58	54
	R	^{646}TTG GAT CTT TCC TTG CAG CTA^{626}		
URAT1 (NM_001276326.1)	F	^{241}AAA CTT AGG CCT CCC CAA GA^{260}	58	158
	R	^{398}TGA CCG GTG ACA CTT ATG GA^{379}		
OAT1 (NM_004790.4)	F	^{1586}ACCAGTCCATTGTCCGAACC^{1605}	56	116
	R	^{1701}TGTCTGCCGGATCATTGTGG^{1682}		
OAT3 (NM_001184732.1)	F	^{15}AGAGCTGAGCTGCCCTACTA^{34}	58	117
	R	^{131}AGAAGGTCATGGCACTGGTGG^{111}		
OAT4 (NM_018484.2)	F	^{879}AGG AAG CCG ATG CTG AGC TG^{898}	59	162
	R	^{1040}GGT CCA CTC CAC CAT CAG TG^{1021}		
OATP4C1		Purchased from Qiagen	60	
OCT2 (NM_003058.3)	F	^{1446}ACC TGG TGA TCT ACA ATG GCT^{1466}	58	145
	R	^{1590}TGA GGA ACA GAT GTG GAC GC^{1571}		
NPT1 (NM_005074.3)	F	^{737}TTG TGG CTG TGC CGT ATG TC^{756}	57	126
	R	^{862}CTT GAA CTG ACC TGC TGG AC^{843}		
NPT4 (NM_001098486.1)	F	^{530}GCG AGT GGT TGG CAT TTC T^{548}	51	127
	R	^{656}TAT TGA GGA CTG GCT TAG G^{638}		
NPT5 (NM_001286121.1)	F	^{1382}TCA GAT CCA GCC ACA GCA TG^{1402}	57	118
	R	^{1499}AAG CCA GTG TAC CGA GGA GC^{1479}		
NaPi-2A (NM_003052.4)	F	^{351}GAG CAG AAG CCA GAG TCC AG^{370}	50	170
	R	^{520}TCC TTG AAG ATG TCA CCA GC^{501}		
NaPi-2C (NM_001177316.1)	F	^{811}TCT TCA ACT GGC TCA CAG TGC^{831}	57	174
	R	^{984}AGT CAG CAG CTT AGC AGC CA^{965}		
PiT2 (NM_006749.4)	F	^{2173}GAC GTG AGT AAT GCC ATC GG^{2182}	57	80
	R	^{2252}GTA GCT GCT TCT TGC GTT ACC^{2231}		
GAPDH		Purchased from Primer Design	60	

Table 2.5: Sequence of human primers used in endpoint and qPCR for the amplification of drug transporters.

The number in brackets underneath the gene name is the NCBI reference number, from which the mRNA sequence of the gene was

obtained. F and R denoted forward and reverse primer sequence, respectively. The superscript numbers are the position of the bases in the mRNA sequence. T_a denotes the annealing temperature of the primer pair.

Gene (NCBI Reference)		Primer Sequence	T_a (°C)	Product Size (base pairs)
Mate1 (NM_001014118)	F	^{442}CCA GAT GTA TCC AGG CTC ACC^{462}	59	123
	R	^{564}AAC CTG AGG CAG AAC GAT GC^{545}		
Mdr1a (NM_133401.1)	F	^{5}CAG AGC CGC TGC TTC TTC C^{23}	57	195
	R	^{199}CAT TGT GAG CAC ACT GAC CGC^{179}		
Mdr1b (NM_012623.2)	F	^{129}GTT GGC ATA TTC GGG ATG TTT CGC^{152}	57	184
	R	^{312}CAC TTT GA TAG TAA CGC TCG GC^{290}		
Mdr1a/b (M81855.1)	F	^{1609}GTC AAG GAA GCC AAT GCC^{1626}	59	147
	R	^{1755}AAG GAT CTT GGG GTT GCG GAC^{1735}		
Mrp1 (NM_022281.2)	F	^{1870}AGC GTG TCC CTC AAG CGT CTC^{1890}	60	170
	R	^{2039}AAG GTG ATG CCA TTC AGT GTG^{2019}		
Mrp2 (NM_012833.2)	F	^{1063}GTT CTC GTC CTG GAA GAA GC^{1082}	57	170
	R	^{1232}TTC AGC AGC TGA GGA TTC AG^{1213}		
Mrp3 (NM_080581.1)	F	^{2439}TGT GCT GGC AGG CAA GAC TC^{2458}	59	158
	R	^{2596}TTC GGA GGA AGT TGG CAA AGG^{2576}		
Mrp4 (NM_133411.1)	F	^{2800}CAT TCA GAG GCT TGG TTC TTG^{2820}	57	185
	R	^{2984}CAC TGG AAC ATC CCC ATG AG^{2965}		
Bcrp (NM_181381.2)	F	^{836}TTG ACA GCC TCA CCT TAC TGG^{856}	59	95
	R	^{930}ACA GTG GTA ACC TGC TGA TGC^{910}		
Urat1 (NM_001034943.1)	F	^{906}ACA GCC AGC CTC TTG ATG G^{924}	55	109
	R	^{1051}ACA GCC AAC TGC AGC ATC C^{1033}		
Oat1 (NM_017224.2)	F	^{1075}ATG CTG TGG TTT GCC ACT AGC^{1095}	59	119
	R	^{1193}AAC TTG GCA GGC AGG TCC AC^{1174}		
Oat3 (NM_031332.1)	F	^{82}TCCAGCTCCAACCACCAGT^{100}	54	65
	R	^{146}TCCAGAATCTCGGAGAAGG^{128}		
Oct2 (NM_031584.2)	F	^{1358}ATC CCT GAT GAT CTA CAG TGG^{1378}	57	127
	R	^{1484}CAA GAT TCC TGA TGT ATG TGG^{1464}		
Oatp4c1 (NM_001002024)	F	^{330}AGC CCT AAC GCA AGG TAT TGT^{350}	57	101
	R	^{430}ATA TCA GGC CGG TCA GGG AA^{411}		
Gapdh		Purchased from Primer Design	60	

Table 2.6: Sequence of rodent primers used in endpoint and qPCR for the amplification of drug transporters.

The number in brackets underneath the gene name is the NCBI reference number, from which the mRNA sequence of the gene was obtained. F and R denoted forward and reverse primer sequence, respectively. The superscript numbers are the position of the bases in the mRNA sequence. T_a denotes the annealing temperature of the primer pair.

2.2.8. Quantitative real-time polymerase chain reaction

Following on from the validation of the specificity of the in-house designed primers, quantitative real-time polymercase chainr eaction (qPCR) was performed on the cDNA of:

- Freshly isolated human PTCs and rat PTCs,
- Human PTCs, rat PTCs and RPTEC cells cultured on 24-well Transwell® inserts,
- Human PTCs, rat PTCs and RPTEC cells cultured in plastic T25 flasks.

A typical qPCR reaction mixture consisted of 2.5 μL cDNA, 5 μL 2x SYBR®-green Master Mix, 0.5 μL of 10 μM mix of forward and reverse primers (1:1) and 2 μL water, contained in wells of a white 96-well format qPCR plate. In a Roche LightCycler 480 (Roche, UK), the reaction mixture was heated to 95 ˚C for 10 min to denature the initial template and activate the enzyme. The amplification of the target gene was carried out for 40 cycles by heating the sample to 95 ˚C for 10 seconds (denaturation step), T_a ˚C for 20 seconds (primer annealing step) and 72 ˚C for 10 seconds (elongation step). A melt curve was also performed (cooling to 65 ˚C followed by heating to 97 ˚C) before a final cooling step to 4 ˚C complete the reaction. The cycle number during gene amplication and its corresponding fluorescence from each sample were logged by the software LightCycler 480 (version 1.5, Roche, UK). The software calculated the fluorescence baseline during the first 15 cycles of the amplication stage to create a common starting fluorescence intensity for all the samples. A threshold level of fluorescence intensity was also defined by an algorithm showing it was significantly above the background fluorescence but still within the linear phase of amplification. The cycle at which a sample produces fluorescence intensity that crosses the threshold is termed the threshold cycle (Ct), and is correlated to the starting amount of the cDNA template; the greater the amount of starting cDNA, the earlier the Ct. As such, for the purpose of analysis, samples that produced Ct of 35 and above were disregarded. PCR analysis of gene expression was repeated 3 time using cDNA derived from 3 separate kidney preaparations.

Serially diluted endpoint PCR product of the gene of interest was also used as the DNA template and loaded on the same plate as the samples to produce a standard curve for quantification. Efficiency of the PCR was determined from this standard curve. Data generated from the qPCR were normalised to their respective species reference gene, which were human GAPDH and rat Gapdh.

2.2.9. Drug transporter RT^2 profiler array plates

Human and rat drug transporter RT^2 profiler array plates were used to charaterise drug transporter gene expression. Each PCR array plate contains 84 transporter genes and 5 house keeping genes. cDNA from freshly isolated human and rat PTCs and human and rat PTCs cultured for 7 days on plastic was combined with SYBR green quantitative PCR Master Mix according to the manufacturer's protocol. The mixture was then aliquopted onto the array plates, 25 µL per well. Real-time PCR detection was then performed using the Roche Lightcycler 480 two-step cycling programme of; 1 cycle of 10 min at 95 °C to activate the HotStart DNA polymerase, then 45 cycles of 15 seconds at 95 °C (denaturation step) and 1 min at 60 °C (annealing and elongation step) at a ramp rate of 1 °C per second. The data was analysed with Lightcycler 480 software. Second derivative maximum analysis was used to indentify the crossing point (Cp value). The manufacturer's web-based software application was used to calculate Ct values from this information. $2^{-\Delta Ct}$ values were then calculated using the following equation. The human data were normalised to GAPDH expression and the rat data to ß-actin expression.

$$2^{-\{Ct\ Gene\ of\ interest - Ct\ reference\ gene\}}$$

2.2.10. Cellular H33342 accumulation assays

H33342 is a cyan/blue fluorescent dye that binds to the minor groove of double stranded DNA without intercalation - preferably at adenine thymine-rich regions. H33342 is both cell membrane permeable and a substrate of MDR1 and BCRP. The functional activities of MDR1 and BCRP within human PTCs and rat PTCs can therefore be determined by measuring the level of intracellular retention of H33342 in the presence and absence of transporter specific inhibitors.

Cells were seeded into plastic 96-well plates at a density of 20 000 cells per well in 200 μL of medium. The cells were cultured for 6 to 8 days, with medium being replaced every 2 days, until they had formed a confluent monolayer. Cell confluency was assessed visually using a phase contrast microscope. The medium was aspirated from the wells and the cells washed twice with 200 μL of 37 °C modified Krebs buffer. The composition of the modified Krebs buffer is shown in Table 2.7. The cells were then incubated with a transporter specific inhibitor dissolved in 200 μL modified Krebs buffer for 40 min at 37 °C. GF120918 was used to inhibit the efflux of H33342 by MDR1. Ko143 hydrate (Ko143) was used to inhibit the efflux of H33342 by BCRP. Inhibitor-only buffer was then removed and replaced with 200 μL of modified Krebs buffer containing the inhibitor and H33342. The cells were incubated for a further 30 min at 37 °C. Following this, the cells were washed twice with 200 μL of ice-cold modified Krebs buffer. Cellular fluorescence levels were then determined using a FLUOstar Omega Microplate Reader (BMG Labtech, Germany). DNA complexed H33342 fluorescence was measured at 355 nm excitation and 465 nm emission, as per the manufacturer's recommendation. The number of technical replicates for each experimental condition was 6 (n = 6). Each experiment was performed 3 separate times in cells derived from 3 separate kidney preparations or passage numbers (N = 3). The concentrations of H33342, GF120918 and Ko143 used are detailed in the results chapter.

Bradford assay was performed at the end of the fluorescence readings to ascertain relative amount of protein in each well. Modified Krebs buffer was replaced with 100 μL of coomassie blue reagent and incubated at room temperature for 5 min. Thereafter, absorbance readings were taken at 595 nm using the microplate reader. A protein standard curve was also created using known amounts of BSA in the same 96-well plate as the unknown samples. The relative amount of protein in each well was thus determined by referring to the protein standard curve.

Ingredient	Concentration (mM)
Sodium Chloride (NaCl)	140
Potassium Chloride (KCl)	5.4
Magnesium Sulphate ($MgSO_4$)	1.2
Monosodium dihydrogen orthophosphate (NaH_2PO_4)	0.3
Monopotassium phosphate (KH_2PO_4)	0.3
D-Glucose ($C_6H_{12}O_6$)	5
HEPES ($C_8H_{18}N_2O_4S$)	10
Calcium Chloride ($CaCl_2$)	2
TRIS Base ($NH_2C(CH_2OH)_3$	Ad hoc to pH 7.4

Table 2.7: Composition of modified Krebs buffer.

2.2.11. Cellular glutathione methylfluorescein accumulation assays

CMFDA is a cell membrane permeable molecule that is transformed into an impermeant fluorescent product glutathione methylfluorescein (GSMF), within living cells (as shown in Figure 2.2). Cell-impermeant GSMF can be effluxed from cells through MRP (ABCC) transport proteins. Therefore, using the same protocol as stated in 2.7.1., the functional activity of the MRP family within human PTCs and rat PTCs cells was determined by measuring the level of intracellular retention of GSMF. MK-571 was used to inhibit the efflux of GSMF by the MRP family. Cellular GSMF fluorescence was measured at 492 nm excitation and 517 nm emission using a FLUOstar Omega Microplate Reader, as suggested in the manufacturers' product information sheet.

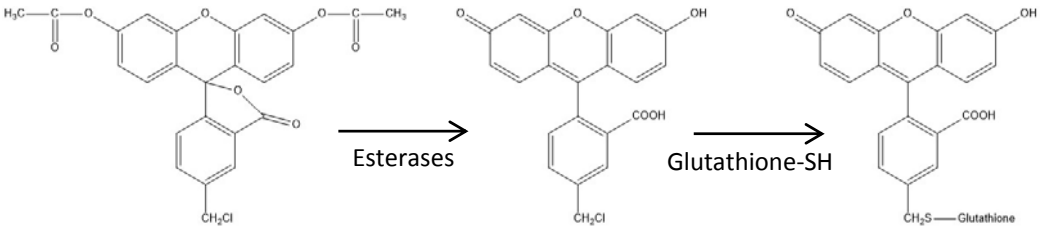

Figure 2.2: Intracellular reactions of CMFDA.

Within cells CMFDA is esterified by intracellular esterase enzymes, the chloromethyl group of this product then reacts with thiols in a glutathione mediated reaction to create a green fluorescent dye-thioether adduct, glutathione methylfluorescein (GSMF). The amount of GSMF dye can be quantified by measuring the fluorescence at 492 nm excitation and 517 nm emission. Figure created using ChemDraw.

2.2.12. Cellular radiolabelled-substrate accumulation assays in freshly isolated PTCs

In order to identify the proximal tubule cell transporters that mediate the uptake of radiolabelled substrates cells and their relative contributions, freshly isolated PTCs were incubated with the substrate of interest in the presence and absence of a combination of transporter inhibitors.

Freshly isolated human PTCs and rat PTCs were suspended at 4 million cells per mL in modified Krebs buffer. 400 000 PTCs (100 μL of the PTC mixture) were incubated with 100 μL of modified Krebs buffer in the presence and absence of a transporter inhibitor for 30 min. Uptake was initiated by adding the radiolabelled substrate (1 μCi / mL); the cells were incubated at 37 °C for 30 min with the radiolabelled substrate and inhibitor in modified Krebs buffer. The entire reaction mixtures were then overlaid onto previously prepared microcentrifuge tubes containing 100 μL of 2N sodium hydroxide (bottom layer) and 100 μL of filtration oil (middle layer, 74.5:25.5 silicon oil : mineral oil mix). Samples were centrifuged immediately at 13 000 rpm for 1 min to transfer the cells containing radiolabelled substrate through the filtration oil layer, into the sodium hydroxide layer, which lysed the cells. The samples were then frozen for at least 1 hr at -80 °C. Using a sterile razor blade the microcentrifuge tubes were cut through in the middle layer and 50 μL of the bottom aqueous layer was

collected and placed in a scintillation vial. 2 mL of Optiphase Hisafe 2 scintillation solvent was added to each vial and mixed by vortexing. The radioactivity of each vial in disintegrations per min (DPM, nuclear decays per min) was determined by liquid scintillation counting using a Beckman LS5000 liquid scintillation counter, (Beckman-Coulter Ltd, UK). The scintillation counter was normalised using a vial containing only 2 mL of scintillation fluid prior to each experiment.

The number of technical replicates for each experimental condition was 3 (n = 3). Each experiment was performed 3 separate times in cells derived from 3 separate kidney preparations (N = 3). A negative control where cells were exposed to no inhibitor and no radiolabelled substrate was included to measure machine background DPM. In addition to a positive control where cells were exposed only to the radiolabelled substrate. The following formula was used to determine the relative contributions of transporters (%).

$$Inhibtion\ of\ radiolabelled\ substrate\ uptake\ (\%) = \left({}^{DPM_{SPL}}/_{DPM_{+CTL}}\right) \times 100$$

DPM_{SPL} = The DPM reading from the sample (DPM)

DPM_{+CTL} = The average DPM reading from the positive control (DPM).

2.2.13. Cellular radiolabelled-substrate accumulation assays in PTCs cultured on 24-well Transwell® inserts

In addition to freshly isolated human PTCs and rat PTCs. Human PTCs and rat PTCs grown on 24-well Transwell® inserts were also used in the investigations of transporter functionality. Experiments were performed when monolayers had a TEER value 80 $\Omega.cm^2$ or greater. Culture medium was first aspirated from the inserts and wells. The cell monolayers were washed 3 times in 37 °C modified Krebs buffer and placed in sterile 24-well plates. Monolayers were matched according to their TEER values. 500 μL of modified Krebs buffer was added to the basolateral well and 100 μL to the apical chamber, and the monolayers left to equilibrate for at least an hr. Thereafter, the buffer in either one or both compartments of the monolayer was replaced with Krebs buffer containing the appropriate inhibitor and incubated for a further hr.

Uptake of radiolabelled substrates was initiated by introducing the radiolabelled substrate (1 μCi / mL) and [^{14}C]-mannitol-D (0.1 μCi / mL) at an equal concentration, to the appropriate compartment of the monolayer for a defined period of time. These solutions are referred to as the standard solutions. To measure uptake across the basolateral membrane the substrate of interest was added to the basolateral well, and vice versa. The activity of the radiolabelled substrates used were 1 μCi / mL. Following the incubation with the radiolabelled substrate of interest the monolayer was then washed in ice-cold modified Krebs buffer 3 times to halt all reactions and to remove extracellular isotope.

In order to measure the cellular uptake of radiolabelled substrate and the level of extracellular label left behind after washing, (i.e. the amount of [^{14}C]-mannitol-D bound to the filter), the filters and hence the adhered cell monolayers, were excised from the inserts and transferred to scintillation vials. 2 mL of Optiphase Hisafe 2 scintillation solvent was added to each vial and mixed by vortexing. The substrate and [^{14}C]-mannitol-D radioactivity of each sample was determined by liquid scintillation counting using a Beckman LS5000 liquid scintillation counter. 100 μL of the standard solutions were also transferred to scintillation vials, whose counts were used in converting the radioactivity, measured in DPM, to amount of substrate. The number of technical replicates for each experimental condition was 3 minimum ($n \geq 3$). Each experiment was performed 3 separate times in cells derived from 3 separate kidney preparations ($N = 3$). A negative control where cells were exposed to no inhibitor and no radiolabelled substrate was included to measure the machine background DPM. The following calculation was used to determine cellular uptake of radiolabelled substrate (pmol / cm^2 / min or hr) and the amount of extracellular label ([^{14}C]-mannitol-D) bound to the filter.

$$Cellular\ Uptake = \frac{\left[\left(\frac{\boldsymbol{A}_{STD}}{DPM_{STD}}\right) \times\ DPM_{SPL}\right] x\ A}{T}$$

A_{STD} = The amount of the radiolabelled substrate in 100 μL of the standard solution (pmol)

DPM_{STD} = The average DPM reading from 100 μL of the standard solution (DPM)

DPM_{SPL} = The DPM reading from the sample (DPM)

A = Area of the filter membrane (24-well filter surface area is 0.33 cm^2)
T = Exposure time to the radiolabelled substrate (min or hr)

2.2.14. Unidirectional transepithelial flux of radiolabelled substrates

In order to determine the net movement of a radiolabelled substrate across the proximal tubule epithelia, unidirectional flux of the substrate in the secretory (basolateral to apical, J_{B-A}) and absorptive (apical to basolateral, J_{A-B}) direction across PTC monolayers was compared as dpecited in Figure 2.3. Human PTCs and rat PTCs cultured on 24-well Transwells® were used in these experiments.

Experiments were performed when monolayers had a TEER value 80 $\Omega.cm^2$ or greater. The monolayers were washed as before (subchapter 2.2.13) and paired according to TEER values. After the initial incubation, the buffer in either one or both compartments of the monolayer was replaced with Krebs buffer containing the appropriate transporter inhibitor and incubated for a further hr.

Flux was initiated by introducing the radiolabelled substrate (1 μCi / mL) and [^{14}C]-mannitol-D (0.1 μCi / mL) at an equal concentration, to the appropriate monolayer compartments. These solutions are referred to as the standard solutions. Sampling of the opposite compartment was done at defined times to measure the appearance of the radiolabelled substrate by aspirating 50 µL from the apical or 250 µL from the basolateral compartment, and replacing it with equal amount of appropriate buffer. The samples and 100 μL of the standard solutions were then placed in scintillation vials and the radioactivity was measured as described in subchapter 2.2.13. In order to decipher between the transcellular and paracellular movement of the radiolabelled substrate the movement of [^{14}C]-mannitol-D was also measured as a marker of paracellular flux.

The number of technical replicates for each experimental condition was 3 minimum ($n \geq 3$). Each experiment was performed 3 separate times in cells derived from 3 separate kidney preparations (N = 3). A negative control where cells were exposed to no inhibitor and no radiolabelled substrate was included

to measure machine background DPM. The following equation was used to calculate the flux of the radiolabelled substrate and [^{14}C]-mannitol-D:

$$Flux = \frac{\left[\left(\frac{\boldsymbol{A}_{STD}}{DPM_{STD}}\right) \times (DPM_{SPL} \times D_{SPL})\right] x\, A}{T}$$

ASTD = The amount of the radiolabelled substrate in 100 μL of the standard solution (pmol)

DPMSTD = The average DPM reading from 100 μL of the standard solution (DPM)

DPMSPL = The DPM reading from the flux sample (DPM)

DSPL = The dilution factor of the flux sample

A = Area of the filter membrane (24-well filter surface area is 0.33 cm^2)

T = Exposure time to the radiolabelled substrate (min or hr)

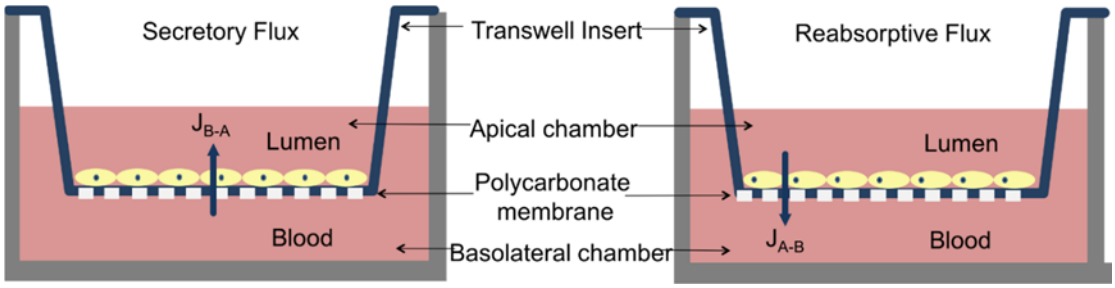

Figure 2.3: A simplified diagram of how to study unidirectional transepithelial flux.

In order to determine the net movement of a radiolabelled substrate across the proximal tubule epithelia the secretory (J_{B-A}) and absorptive (J_{A-B}) flux of radiolabelled substrate was measured in paired resistance matched monolayers. Monolayers were paired according to TEER values.

2.2.15. CellTiter 96® AQueous one solution cell proliferation assay

The CellTiter Aqueous one solution cell proliferation assay is a colorimetric method for assessing cell metabolic activity. The reagent contains [3-(4,5-dimethyl-2-yl) – 5 – (3-carboxymethoxyphenyl)-2-(4-sulfophenyl)-2H-tetrazolium

salt (MTS) and an electron coupling reagent (phenazine ethosulfate (PES). In metabolically active cells the MTS is reduced by NAD(P)H-dependent cellular oxidoreductase enzymes into an insoluble coloured formazan product, as shown in Figure 2.4. The formazan dye produced can be quantified by measuring the absorbance at 490 nm. The ability of various chemicals to affect the metabolic activity of proximal tubule epithelial cells was assessed using this reagent.

Cells seeded onto 96-well plates were used for this assay. When confluent, the cells were incubated with a range of concentrations of the compound of interest for 48 hrs. Following treatment, the medium was aspirated and the cells washed twice with 200 μL modified Krebs buffer. The cells were then incubated in 100 μL of modified Krebs buffer with 20 μL of CellTiter AQueous one solution regent added and for 120 min and maintained at 37 °C. The amount of formazan product was then quantified by measuring the absorbance at 490 nm using a FLUOstar Omega Microplate Reader. In each experiment a positive control (cells incubated with only growth medium and modified Krebs buffer, 100 % metabolic functionality), and negative control (cells incubated with 10 % Triton-X, 0 % metabolic activity) was included. The relative viabilities of the treated cells were thus calculated with reference to the positive and negative controls. The number of technical replicates for each experimental condition was 6 (n = 6). Each experiment was performed 3 separate times in cells derived from 3 separate kidney preparations or passage numbers (N = 3).

Bradford assay was performed after the absorbance readings to ascertain relative amount of protein in each well. Modified Krebs buffer containing CellTiter AQueous one solution was replaced with 100 μL of coomassie blue reagent and incubated at room temperature for 5 min. Thereafter, absorbance readings were taken at 595 nm using the microplate reader. A protein standard curve was also created using known amounts of BSA in the same 96-well plate as the unknown samples. The relative amount of protein in each well was thus determined by referring to the protein standard curve.

Figure 2.4: Intracellular reactions of MTS.

In metabolically active cells, the MTS is reduced by NAD(P)H-dependent cellular oxidoreductase enzymes into an insoluble coloured formazan product. The formazan dye produced can be quantified by measuring the absorbance at 490 nm with a plate reader. Figure created using ChemDraw.

2.3. Statistics

Data are expressed as mean ± standard error of mean (SEM) of the specified number of replicates, where "n" denotes technical replicates, and "N" denotes biological replicates. To test hypotheses normal distribution of the data and equal variance was assumed. Statistical comparison of mean values was made using a Student's *t* test. A one-way analysis of variance test (one-way ANOVA, otherwise known as the Kruskal-Wallis test) was used for multiple comparisons of 3 or more experimental conditions and significance was assigned using a Dunnett post-test. Differences in mean values were considered to be significant when $p \leq 0.05$. Non-linear regression analysis of the data and other statistical analyses were carried out using GraphPad Prism 4.0 software (GraphPad software Inc. USA).

3. Isolation and characterisation of PTCs

3.1. Background

Understanding renal drug handling in man has been hampered by the lack of a good model of the human proximal tubule. The current *in-vitro* screening tools rely on immortalised renal epithelial cell lines that are poorly predictive of *in-vivo* drug handling. Immortalised animal and human renal epithelial cell lines commonly used in pre-clinical screening include, LLC-PK1 (porcine), MDCK (canine), OK (opossum), HK-2 (human), HEK293 (human), and ciPTEC (human) cells. Several characterisation studies have reported these cells lack expression of key drug transporter and metabolic enzymes, fail to maintain brush-border microvilli, or are unable to form confluent monolayers with good tight junction integrity. The cells can be stably transfected to express missing transporters. However, transporter expression in these cell lines does not reflect the transporters' physiological expression levels as they are driven by the vector promoters and the cells' translation transcription machinery. Primary cells derived from intact tissue are a better model as they retain the characteristic biochemical and physiological properties. (See subchapters 1.4.3 and 1.4.6 for further details.)

Research has identified that time *ex-vivo*, isolation protocol and growth medium are key in maintaining primary cell differentiation (Taub *et al.*, 1989; Courjault-Gautier *et al.*, 1995). It is recommended that renal primary cell isolation begins less than 18 hrs *ex-vivo*. The human renal cortex contains at least 18 different resident cell types, 10 of which line the tubular basement membrane (Helbert *et al.*, 1999). Many renal primary cell culture techniques have been developed. Published techniques include a mixture of the following: density centrifugation, flow cytometry, free flow electrophoresis, enzymatic digestion, and differential sieving (Van der Biest *et al.*, 1994; Helbert *et al.*, 1997; Helbert *et al.*, 1999; Helbert *et al.*, 2001; Verhulst *et al.*, 2003; Verhulst *et al.*, 2004; Verhulst *et al.*, 2008). The most widely used protocol for isolating pure proximal tubular cell cultures involves enzymatic dispersion of tubular cells, followed by differential

sieving, (Percoll®) gradient centrifugation, cell labelling with a fluorescent surface marker antibody, and then fluorescence activated cell sorting (FACS) (Van der Biest *et al.*, 1994; Helbert *et al.*, 1997; Helbert *et al.*, 1999; Helbert *et al.*, 2001; Brown *et al.*, 2008). Following isolation, cells are further selected using cultured growth medium that promotes the growth of cells of interest over other cell types.

Proximal tubular cells can be distinguished from distal tubule, interstitium glomeruli and collecting duct cells through incubation with anti-human leucine aminopeptidase (LAP) monoclonal antibody (Helbert *et al.*, 1997). When compared with other fluorescent surface markers, LAP labeling of cell samples gave the clearest distinction between positive (proximal) and negative (non-proximal) cell subpopulations (93 $\pm$ 4% purity) (Helbert *et al.*, 1997). Other surface markers for proximal tubular cells include neutral endopeptidase, dipeptidyl peptidase IV, γ-glutamyl transferase, alanine aminopeptidase, TN20 antigen and intestinal type alkaline phosphatase (Helbert *et al.*, 1997). When selecting for the most appropriate surface marker antibody, it is important to consider that some characteristics may disappear from a cell type during cell culture due to dedifferentiation (Eguchi and Kodama, 1993; Hay, 1993), as has been shown for γ-glutamyl transferase and alkaline phosphatase expression on human proximal tubular cells (Trifillis *et al.*, 1985). Alternatively, certain characteristics may appear, as has been shown for dipeptidyl peptidase IV expression on distal tubular cells (Baer *et al.*, 1999).

In previous years, our research group has identified that seeding proximal tubule cultures with a proportion of distal cortical cells gave a more robust model than a pure primary proximal tubular cell culture segregated by free flow electrophoresis. mRNA expression of key transporters in native human kidney cortex and 10-day old purified proximal and distal tubule/collecting duct cell monolayers were compared using qPCR. mRNA expression of NaPi-IIa, SGLT2, OCT2, OCTN2, NBC, OAT1, OAT3, BCRP and MDR1 were restricted to native kidney and proximal tubule cells (Brown *et al.*, 2008). SGLT1, OAT4 and MRP2 on the other hand were detected in native tissue, proximal and distal tubular/collecting duct cell monolayers (Brown *et al.*, 2008). Protein expression of key transporters OAT1, OAT3 and NaPi-IIa were investigated using

immunohistochemistry and confocal microscopy. In accordance with the qPCR data, the results demonstrated the expression of OAT1, OAT3 and NaPi-IIa were restricted to human proximal tubular cells (Brown *et al.*, 2008). Correspondingly, functional characteristic studies in distal tubule / collecting duct cell monolayers showed no transcellular transport of PAH, sodium-dependent glucose uptake or endocytotic uptake of albumin (Brown *et al.*, 2008). A limitation of pure proximal tubule monolayers was the low tight junction integrity. The mean TEER value of a pure proximal tubular cell monolayer cultured on a Transwell® insert was 26 ± 0.8 Ω cm^2, compared with 205 ± 3.8 Ω cm^2 for purified distal tubular / collecting duct cell monolayers and 78.3 ± 1.7 Ω cm^2 for a co-culture of proximal and distal tubular cells (Brown *et al.*, 2008). When the monolayer tight junction integrity is low studies of secretion and absorption is not feasible because of the large paracellular movement of the substrate of interest. As a result of the low tight junction integrity of pure proximal tubule monolayers and low expression of key transport proteins in distal tubular / collecting duct cells, it was concluded that co-cultures of proximal and distal tubular cells (PTCs) were a better *in-vitro* model. Two practical advantages of human PTC and rat PTC monolayers are the cell yield generated from a single kidney is much greater and with a high TEER value transporter-mediated absorption and secretion of compounds can be studied. Analysis of the human PTC co-cultures produced with the isolation procedure detailed in subchapter 2.2.1 deduced that the co-cultures are 80% proximal tubule cells and 20% distal tubular / collecting duct cells (Brown *et al.*, 2008).

A challenge in the use of primary cells is the acquisition of tissues from which the cells are derived. The supply of fresh human kidneys is undoubtedly limited, not least because of the short fall in organ donation and the long transplant waiting list. However, in the occasions of the availability of kidneys that are unsuitable for transplants but still viable, it is paramount that an efficient isolation protocol is performed maximise the yield of cells. Rat kidneys, on the other hand, are more accessible. Nonetheless, the principles of the 3Rs of animal use should be practice. Optimisation of the isolation procedure is thus essential, and forms the basis of this chapter.

3.2. Aims

The aim of this chapter was to develop and optimise the methodology required to isolate human and rat PTCs.

In order to achieve this the enzymatic digestion phase of the isolation procedure was optimised. The yield and growth of cells isolated with a range of collagenase concentrations were studied up to day 8 of cell culture. Human PTC, rat PTC and RPTEC cell monolayer formation was assessed using TEER. The correlation between TEER and paracellular permeability of cell monolayers was studied using radiolabelled [1-^{14}C]-mannitol D. Then finally the mRNA expression of key renal drug transport proteins was evaluated in human PTCs, rat PTCs and RPTEC cells grown on different cultureware.

3.3. Results

3.3.1. Collagenase concentration and cell yield

In order to optimise the enzymatic digestion of renal cortex in terms of the yield of isolated PTCs, human or rat renal cortex was incubated with a range of concentrations of collagenase using 2 different incubation conditions. The concentrations of collagenase investigated were 10, 20, 25, and 30 mg collagenase per g of renal cortex. The activity of collagenase was approximately 300 units per mg. The tissues were exposed to the collagenase overnight (4 °C for more than 12 hrs followed by 1 hr at 37 °C) or acutely (2 hrs at 37 °C). The number of isolated PTCs per g of renal cortex were estimated using a haemocytometer.

Focusing on the human data, Figure 3.1 shows a positive correlation between collagenase concentration and human PTC yield; the higher the concentration of collagenase used, the higher the yield, which suggests enzyme concentration is the rate-limiting factor (n = 9, N = 3). In order to determine the effect of the incubation period on the yield of isolated human PTCs, the number of isolated human PTCs per g of renal cortex following an overnight incubation was compared to an acute incubation for each collagenase concentration. Except at 10 mg collagenase per g of tissue, which gave 1.58 ± 0.09 million cells with an overnight incubation and 2.13 ± 0.04 million cells with an acute incubation (** $P < 0.01$), the incubation period did not affect cell yield. For instance, overnight and acute incubation of human renal cortex with 30 mg collagenase per g of tissue yielded 3.07 ± 0.09 million and 3.07 ± 0.03 million cells, respectively. Similarly, 25 mg collagenase per g of tissue gave 2.80 ± 0.01 million and 2.62 ± 0.16 million cells with overnight and acute incubation, respectively. 20 mg collagenase per g of tissue gave 2.56 ± 0.04 million and 2.40 ± 0.13 million cells with overnight and acute incubation, respectively.

Enzymatic digestion of rat renal cortex produced similar findings, shown in Figure 3.2 (n = 9, N = 3). The number of isolated rat PTCs following an overnight or acute incubation at each collagenase concentration was compared and no significant difference in the cell yield was found. For instance, an

overnight and acute incubation of rat renal cortex with 30 mg collagenase per g of tissue yielded 13.75 ± 0.05 million and 13.76 ± 0.73 million cells, respectively. 25 mg collagenase per g of tissue yielded 11.19 ± 0.36 million and 11.11 ± 0.42 million cells from an overnight and acute digest, respectively. 20 mg collagenase per g of tissue yielded 4.60 ± 0.10 million and 4.51 ± 0.37 million cells from an overnight and acute digest, respectively. The lowest concentration of collagenase (10 mg collagenase per g of renal cortex) yielded 3.36 ± 0.04 million and 3.31 ± 0.17 million cells from overnight and acute digests, respectively. The significance of the difference in cell yield using an overnight and acute incubation was determined using a Student's t-test.

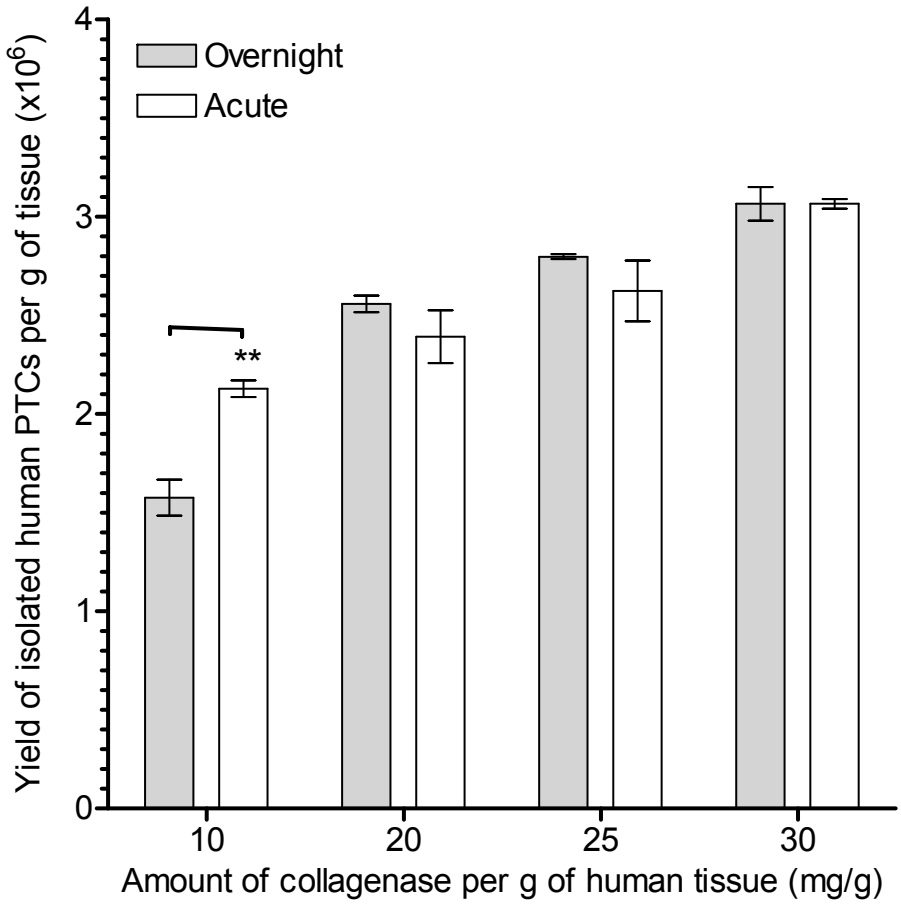

Figure 3.1: The yield of isolated human PTCs following an overnight and acute incubation with different concentrations of collagenase.

*Samples of human renal cortex were incubated with 10, 20, 25 or 30 mg collagenase per g of renal cortex. Cell numbers were estimated using a haemocytometer. There were no differences in the number of isolated human PTCs per g of tissue in an overnight incubation compared to an acute incubation when using 20, 25 and 30 mg collagenase per g of tissue. Cell isolation with 30 mg collagenase per g of renal cortex gave the highest cell yield, at 3.07 ± 0.09 million cells per g of tissue from an overnight digest, and 3.07 ± 0.03 million cells per g of tissue from an acute digest. 25 mg collagenase per g of tissue yielded 2.80 ± 0.01 million cells from an overnight digest and 2.62 ± 0.16 million cells from an acute digest. 20 mg collagenase per g of renal cortex yielded 2.56 ± 0.04 million cells from an overnight digest and 2.40 ± 0.13 million cells from an acute digest. However, 10 mg collagenase per g of tissue yielded a significantly lower number of cells in an overnight digest with 1.58 ± 0.09 million cells per g of tissue compared to an acute digest with 2.13 ± 0.04 million cells per g of tissue (** P < 0.01). The results are expressed as the mean ± SEM from 3 samples of renal cortex derived from 3 individual kidneys. The significance of the difference in cell yield using an overnight and acute incubation was determined using a Student's t-test.*

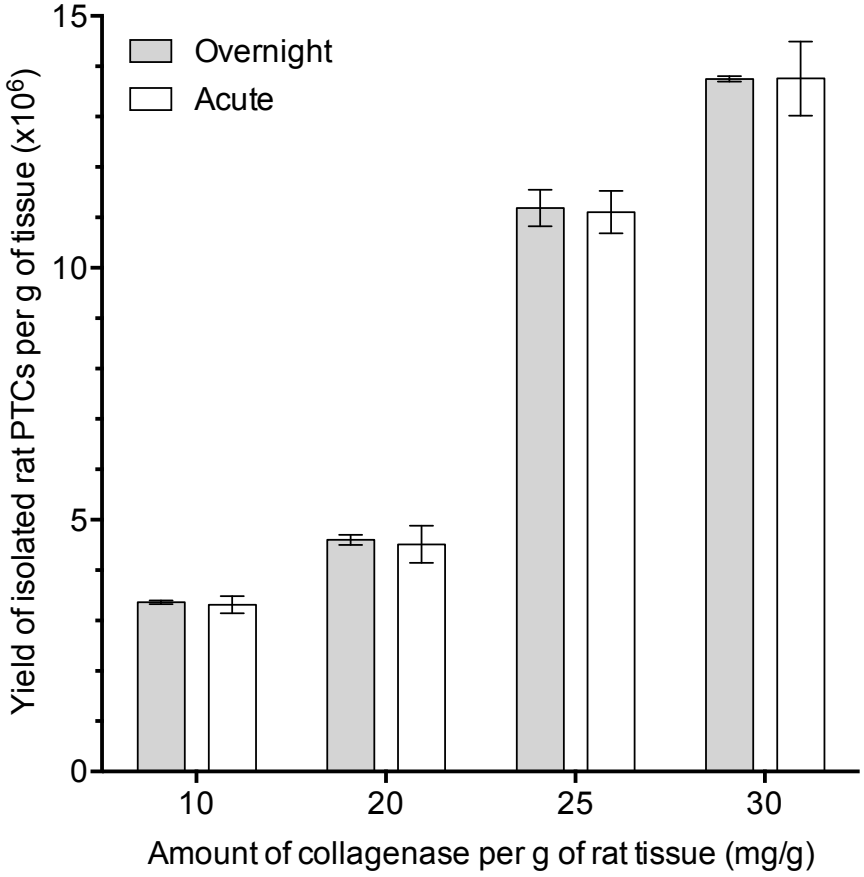

Figure 3.2: The yield of isolated rat PTCs following an overnight and acute incubation with different concentrations of collagenase.

Samples of rat renal cortex were incubated with 10, 20, 25, or 30 mg collagenase per g of tissue. The number of cells was estimated using a haemocytometer. The mean number of isolated rat PTCs following an overnight and acute incubation at each concentration of collagenase was compared and no significant difference was found. Using 30 mg of collagenase per g of tissue gave the highest yield of rat PTCs; 13.75 ± 0.05 million cells per g of tissue was isolated from an overnight digest, and 13.76 ± 0.73 million cells per g of tissue from an acute digest. 25 mg collagenase per g of tissue yielded 11.19 ± 0.36 million cells in an overnight digest and 11.11 ± 0.42 million cells from an acute digest. 20 mg collagenase per g of renal cortex yielded 4.60 ± 0.10 million cells in an overnight digest and 4.51 ± 0.37 million cells from an acute digest. 10 mg collagenase per g of tissue yielded 3.36 ± 0.04 million cells in an overnight digest and 3.31 ± 0.17 million cells in an acute digest. The results are expressed as the mean ± SEM from 3 samples of renal cortex derived from 3 individual kidneys. The significance of the difference in cell yield using an overnight and acute digest was determined using a Student's t-test.

3.3.2. Collagenase concentration and cell viability.

The collagenase used in the isolation process contained a mixture of protease enzymes. It has been reported that prolonged exposure to high concentrations of protease enzymes can affect cell viability (Boogaard *et al.*, 1990; Cummings *et al.*, 2000). In order to determine the effect of collagenase concentration and incubation condition upon cell health, growth assays were performed. Isolated cells were seeded into plastic 12-well plates at a density of 200 000 cells per well. The number of cells in a well per cm^2 at 1, 2, 3, 4, 5, 6, 7, and 8 days of cell culture were quantified using a haemocytometer.

Figure 3.3 shows the number of human PTCs per cm^2 over 8 days following an (a) overnight and (b) acute incubation with different concentrations of collagenase (n = 9, N = 3). For both incubation periods, the cells isolated using 25 mg collagenase per g of tissue displayed the highest rate of cell propagation. At day 8 of cell culture, following an overnight incubation, the number of human PTCs per cm^2 was significantly greater for cells isolated using 25 mg collagenase per g of tissue (220 000 $\pm$ 3 824) compared to 10 (127 000 $\pm$ 3 163, **** P < 0.0001), 20 (195 000 $\pm$ 3 039, ** P < 0.01) and 30 (197 000 $\pm$ 4 558, * P < 0.05) mg collagenase per g of tissue. Similarly, at day 8 of cell culture following an acute incubation, the number of human PTCs per cm^2 was significantly greater for cells isolated using 25 mg collagenase per g of tissue (221 000 $\pm$ 3 039) compared to 10 (87 000 $\pm$ 1 519, **** P < 0.0001), 20 (188 000 $\pm$ 4 642, ** P < 0.01) and 30 (182 000 $\pm$ 2 321, *** P < 0.001) mg collagenase per g of tissue. In order to determine if one incubation period led to better cell health the number of cells per cm^2 at day 8 following isolation with 25 mg collagenase per g of tissue was compared. No significant difference in the cell number per cm^2 was found between an overnight and acute incubation period (P > 0.05). Significance was determined using a Student's t-test.

Figure 3.4 shows the number of rat PTCs per cm^2 over 8 days following an (a) overnight and (b) acute incubation with different concentrations of collagenase (n = 9, N = 3). Once again, cells isolated using 25 mg of collagenase per g of tissue displayed the highest rate of cell proliferation. At day 8 of culture the number of rat PTCs per cm^2 was significantly greater for cells isolated overnight with 25 mg collagenase per g of tissue (242 000 $\pm$ 2 589) compared to 10 (122

000 ± 2 321, **** P < 0.0001), and 30 (174 000 ± 7 982, ** P < 0.01) mg collagenase per g of tissue. Similarly, at day 8 following an acute incubation, the number of rat PTCs per cm^2 was significantly greater for cells isolated using 25 mg collagenase per g of tissue (192 000 ± 3 044) compared to 10 (21 000 ± 382, **** P < 0.0001), 20 (166 000 ± 4 487, ** P < 0.01) and 30 (29 000 ± 1 379, **** P < 0.0001) mg collagenase per g of renal cortex. When the number of cells per cm^2 at day 8 following an overnight and acute incubation with 25 mg collagenase per g of renal cortex was compared, the number of cells at day 8 following an overnight incubation was significantly greater (P < 0.001, ***). This suggests that an overnight enzymatic digestion of rat renal cortex is better for cell health. Significance was determined using a Student's t-test.

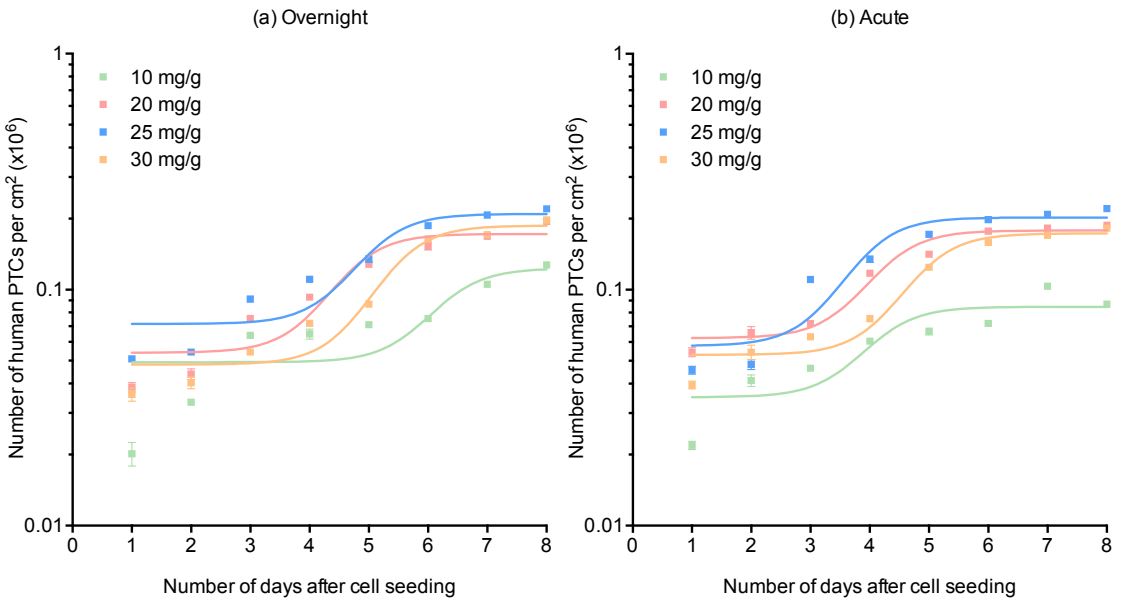

Figure 3.3: The growth of isolated human PTCs over 8 days following an (a) overnight and (b) acute incubation with different concentrations of collagenase.

The number of cells per cm² was estimated at day 1, 2, 3, 4, 5, 6, 7, and 8 of culture using a haemocytometer. The results are expressed as the mean ± SEM from 9 human PTC monolayers derived from 3 individual kidneys. (a) Following an overnight incubation the highest number of cells per cm² at each time point was cells isolated using 25 mg of collagenase per g of human renal cortex. The number of human PTCs was 187 000 ± 3 039 per cm² at day 6, 207 000 ± 2 321 per cm² at day 7 and 220 000 ± 3 824 per cm² at day 8. The number of human PTCs for 20 and 30 mg collagenase per g of renal cortex were very similar, 164 000 ± 2 321 versus 153 000 ± 5 478 per cm² at day 6, 171 000 ± 4 020 versus 168 000 ± 1 519 per cm² at day 7 and 197 000 ± 4 558 versus 195 000± 3 039 per cm² at day 8, respectively. The lowest number of cells per cm² at each time point was wells containing cells isolated using 10 mg of collagenase per g of human renal cortex. (b) After an acute incubation the highest number of cells per cm² was cortex digested with 20 mg collagenase per g of human renal cortex at day 1 and 2 of cell culture, then cells isolated using 25 mg collagenase per g of human renal cortex from day 3 of cell culture onwards. For cells isolated using 25 mg collagenase per g of renal cortex the number of human PTCs was 198 000 ± 2 321 per cm² at day 6, 209 000 ± 2 321 per cm² at day 7 and 221 000 ± 3 039 per cm² at day 8. The number of human PTCs for 20 and 30 mg collagenase per g of renal cortex were very similar, 177 000 ± 3 163 versus 159 000 ± 3 163 per cm² at day 6, 182 000 ± 2 321 versus 170 000 ± 3 163 per cm² at day 7 and 188 000 ± 4 642 versus 182 000± 2 321 per cm² at day 8, respectively. The lowest number of cells per cm² at each time point was wells containing cells isolated using 10 mg of collagenase per g of human renal cortex.

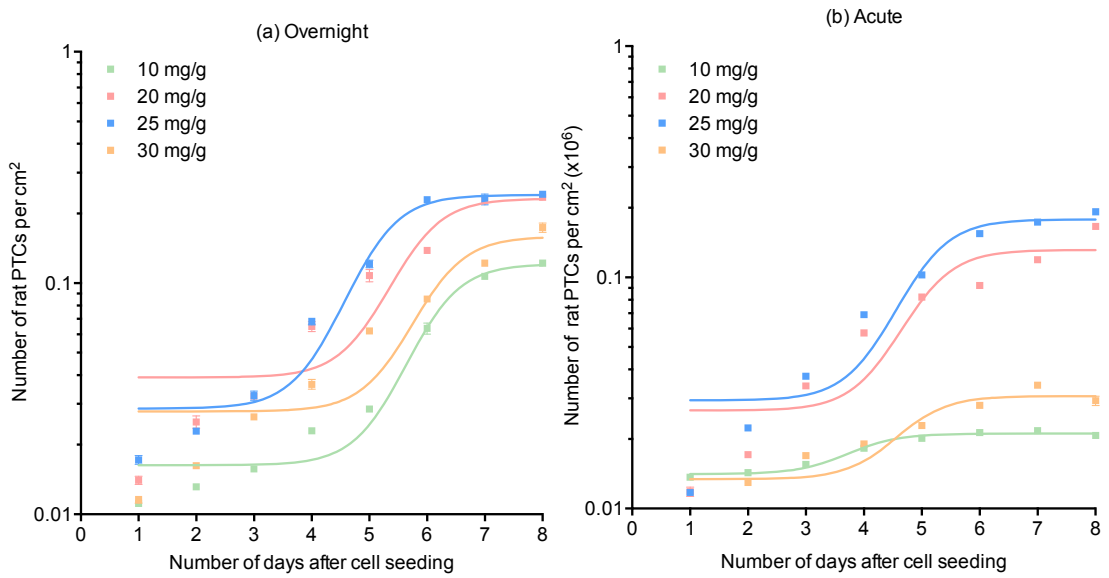

Figure 3.4: The growth of isolated rat PTCs over 8 days following an (a) overnight and (b) acute incubation with different concentrations of collagenase.

The number of cells per cm² was estimated at day 1, 2, 3, 4, 5, 6, 7, and 8 of culture using a haemocytometer. The results are expressed as the mean ± SEM from 9 rat PTC monolayers derived from 3 individual kidneys.(a) In an overnight isolation the highest number of cell per cm² at each time point, with the exception of day 3, was cell isolates using 25 mg of collagenase per g of tissue. The number of rat PTCs was 229 000 ± 1 529 per cm² at day 6, 230 000 ± 12 281 per cm² at day 7 and 242 000 ± 2 589 per cm² at day 8. The number of rat PTCs for 20 mg collagenase per g of renal cortex was 138 000 ± 2 191 per cm² at day 6, 228 000 ± 6 265 per cm² at day 7 and 235 000 ± 3 267 per cm² at day 8. The number of rat PTCs for 30 mg collagenase per g of renal cortex was 85 000 ± 2 339 per cm² at day 6, 122 000 ± 3 824 per cm² at day 7 and 174 000 ± 7 982 per cm² at day 8. The lowest number of cells per cm² at each time point was wells containing cells isolated using 10 mg of collagenase per g of human renal cortex. (b) In an acute isolation the highest numbers of cells per cm2 from day 2 to day 8 were cells isolated using 25 mg of collagenase per g of rat renal cortex. For cells isolated using 25 mg collagenase per g of renal cortex the number of rat PTCs was 154 000 ± 2 510 per cm² at day 6, 174 000 ± 1 959 per cm² at day 7 and 192 000 ± 3 044 per cm² at day 8. The number of rat PTCs for 20 mg collagenase per g of renal cortex was 92 000 ± 1 444 per cm² at day 6, 119 000 ± 3 441 per cm² at day 7 and 166 000 ± 4 487 per cm² at day 8. The number of rat PTCs for 30 mg collagenase per g of renal cortex was 28 000 ± 749 per cm² at day 6, 34 000 ± 608 per cm² at day 7 and 29 000 ± 1 379 per cm² at day 8. The lowest number of cells per cm² at each time point was wells containing cells isolated using 10 mg of collagenase per g of human renal cortex.

3.3.3. Cell yield per g of cortex.

As a result of the growth study findings, human PTCs were isolated from human renal cortex by incubating tissue samples with 25 mg collagenase per g of renal cortex. Figure 3.5 is a summary of the number of isolated human PTCs per g of renal cortex (N = 100). The relationship between number of isolated human PTCs and weight of human renal cortex shows strong positive correlation. Correlation analysis of the sample data gave a Pearson correlation coefficient of 0.90 and a coefficient of determination of 0.82. Due to the small p value ($p < 0.0001$) we can conclude that the correlation is not due to random sampling. The numbers of isolated human PTCs from samples weighting less than 2 g were negligible.

Due to the growth assay findings, rat PTCs were isolated from rat renal cortex by incubating tissue samples overnight with 25 mg collagenase per g of tissue. Figure 3.6 is a summary of the number of isolated rat PTCs per g of renal cortex (N = 100). The relationship between number of isolated rat PTCs and weight of rat renal cortex appears to have positive correlation. Correlation analysis of the sample data gave a Pearson correlation coefficient of 0.715 and a coefficient of determination of 0.511. Due to the small p value ($p < 0.0001$) we can conclude that the correlation is not due to random sampling.

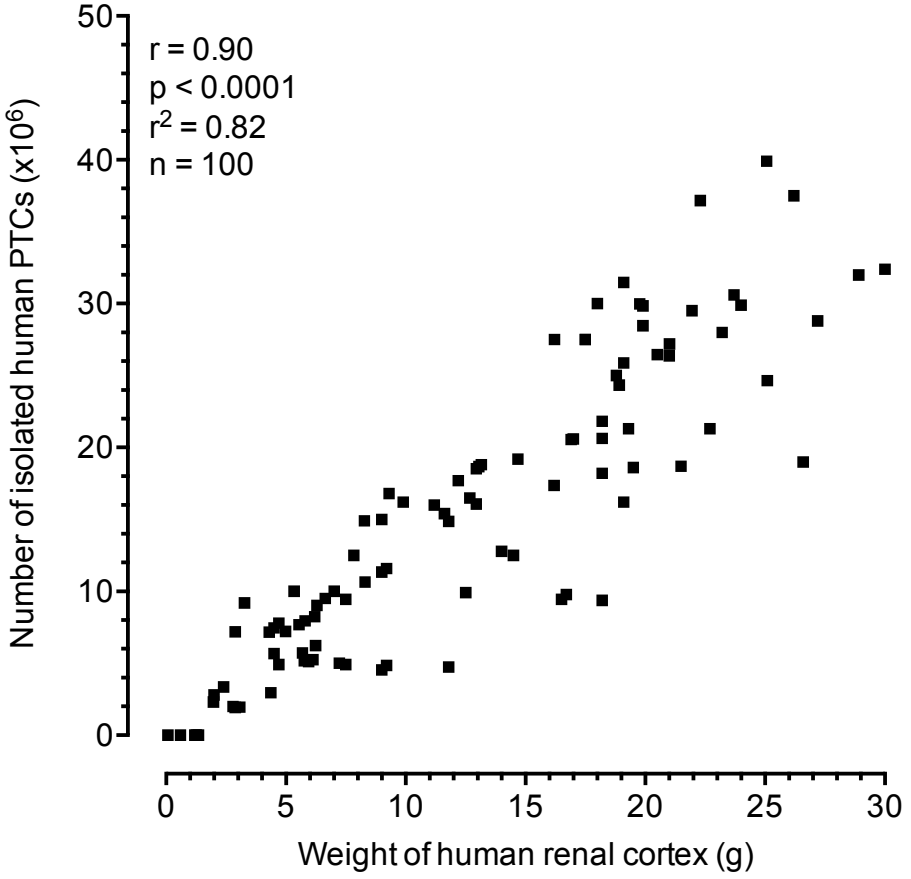

Figure 3.5: A summary of the number of isolated human PTCs per g of human renal cortex.

Correlation analysis of the sample data gave a Pearson correlation coefficient (r) of 0.90, coefficient of determination (r^2) of 0.82 and p value < 0.0001. This suggests that the number of isolated human PTCs is strongly correlated to the weight of human renal cortex used and not the result of random sampling. The numbers of isolated human PTCs obtained from samples weighting less than 2 g were negligible. The sample size (n) was 100.

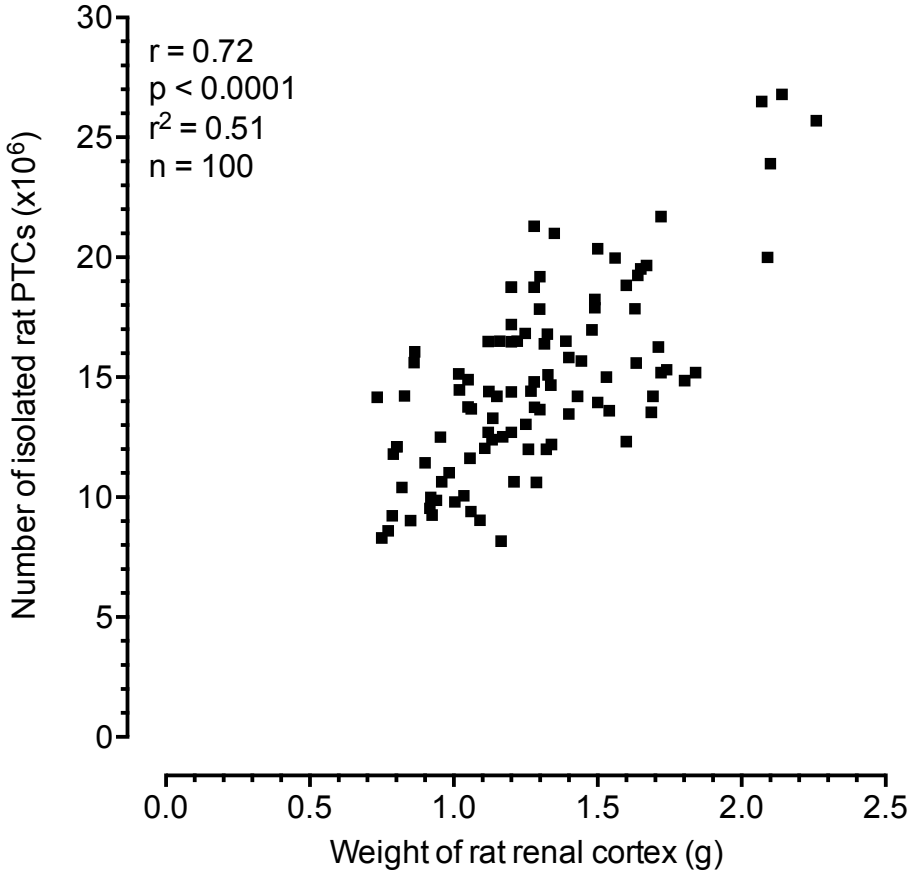

Figure 3.6: A summary of the number of isolated rat PTCs per g of rat renal cortex.

Correlation analysis of the sample data gave a Pearson correlation coefficient (r) of 0.72, coefficient of determination (r^2) of 0.51 and p value < 0.0001. This suggests that the number of isolated rat PTCs is correlated to the weight of rat renal cortex used and not the result of random sampling. The sample size (n) was 100.

3.3.4. TEER of human PTC, rat PTC and RPTEC monolayers.

A characteristic feature of epithelial cells is the formation of intercellular junctions. Formation of these tight junctions results in a cellular barrier separating the apical membrane from the basolateral membrane and apical-basal polarity. Epithelial cells connect to one another as they grow via these tight junctions to form polarised epithelial monolayers. TEER measurements are a convenient, reliable and non-destructive method of quantitatively evaluating the growth of epithelial tissue cultures on Transwell® inserts and cell monolayer permeability *in-vitro*.

Human PTCs, rat PTCs and RPTEC cells were seeded on to 24-well Transwell® inserts at a density of 75 000 cells per insert with 200 μL of culture medium in the apical chamber and a further 1000 μL in the basolateral well. The TEER of each monolayer was measured daily using an epithelial voltohmmeter to determine growth and permeability.

TEER values of human PTC monolayers grown on Transwell® inserts are shown in Figure 3.7 (n = 72, N = 3). The human PTC monolayers developed TEER. TEER increased steadily from day 1 to 6. Resistance reached a plateau of around 120 $\Omega.cm^2$ between day 6 and 8, with readings of 110.30 ± 1.00 $\Omega.cm^2$ at day 6, 129.60 ± 0.87 $\Omega.cm^2$ at day 7, and 135.50 ± 1.04 $\Omega.cm^2$ at day 8. Resistance then decreased at day 9 and 10 but was still significantly above a threshold value of 80 $\Omega.cm^2$. Mean rat PTC monolayer TEER values, shown in Figure 3.8, were very similar to that of the human monolayers (n = 72, N = 3). rat PTC TEER values plateaued around 110 $\Omega.cm^2$. The mean TEER at day 6 was 107.50 ± 0.84 $\Omega.cm^2$, day 7 was 114.30 ± 1.09 $\Omega.cm^2$, and 98.90 ± 0.12 $\Omega.cm^2$ at day 8. RPTEC monolayers, on the other hand, had very low TEER readings in comparison to the primary cells, as shown in Figure 3.9 (n = 24, N = 3). The highest individual reading was 27.92 ± 0.33 $\Omega.cm^2$ at day 9. The results are expressed as the mean ± SEM.

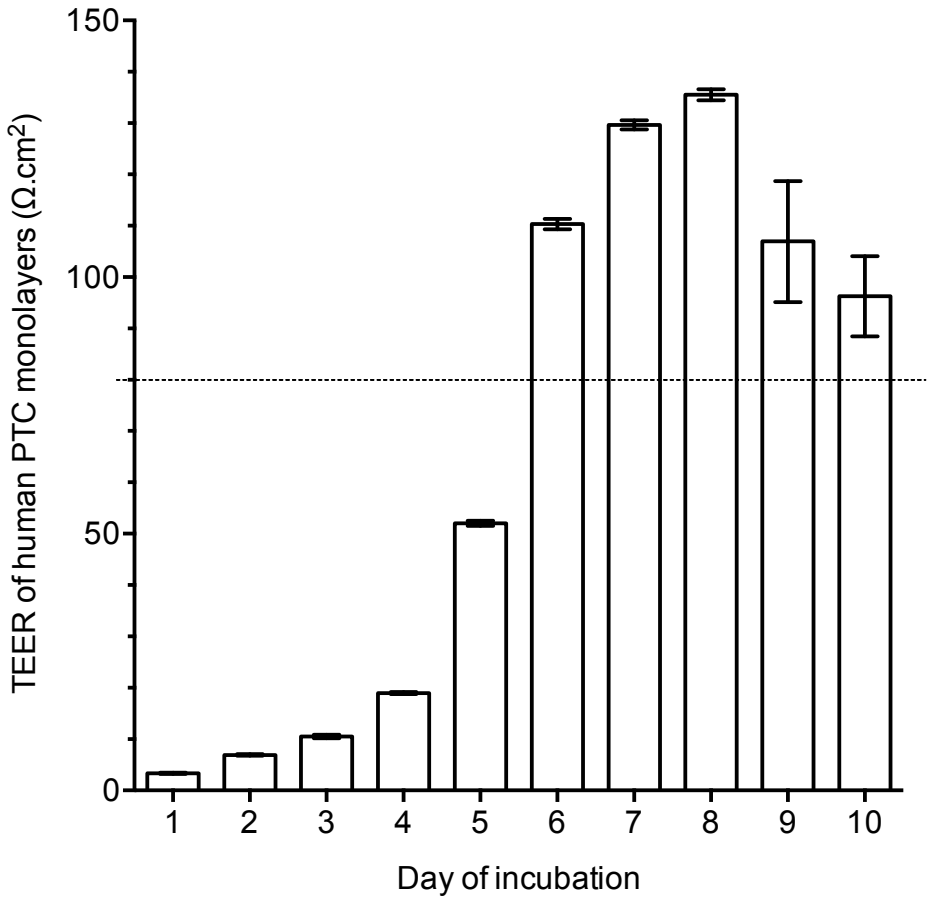

Figure 3.7: TEER of human PTC monolayers grown on Transwell® inserts.

Human PTCs were seeded on to 24-well Transwell® inserts at a density of 75 000 cells per insert with 200 μL of culture medium in the apical chamber and a further 1000 μL in the basolateral well. TEER of each monolayer was measured daily using an epithelial voltohmmeter to determine growth and permeability. TEER developed and increased steadily in culture from day 1 to 6 (Day 1: 3.35 ± 0.14 Ω.cm², Day 2: 6.93 ± 0.15 Ω.cm², Day 3: 10.47 ± 0.35 Ω.cm², Day 4: 18.96 ± 0.18 Ω.cm², Day 5: 51.97 ± 0.52 Ω.cm², Day 6: 110.30 ± 1.00 Ω.cm²). Resistance reached a plateau of around 120 Ω.cm² between 6 and 8 days in culture (Day 7: 129.60 ± 0.87 Ω.cm², Day 8: 135.50 ± 1.04 Ω.cm²). Then decreased to 106.9 ± 1.39 Ω.cm² and 96.45 ± 0.92 Ω.cm² at day 9 and 10, respectively. The results are expressed as the mean ± SEM from 72 monolayers derived from 3 individual kidneys.

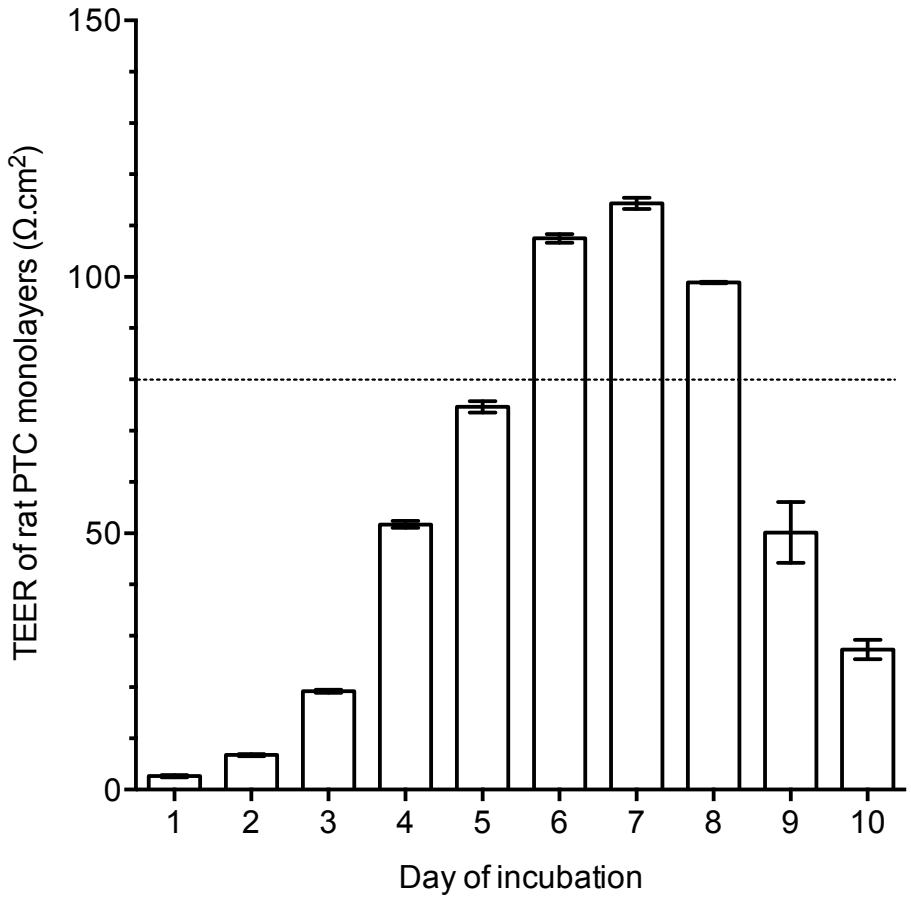

Figure 3.8: TEER of rat PTC monolayers grown on Transwell® inserts.

Rat PTCs were seeded on to 24-well Transwell® inserts at a density of 75 000 cells per insert with 200 μL of culture medium in the apical chamber and a further 1000 μL in the basolateral well. TEER of each monolayer was measured daily using an epithelial voltohmmeter to determine growth and permeability. TEER increased steadily from day 1 to 7 (Day 1: 2.64 ± 0.22 Ω.cm², Day 2: 6.76 ± 0.20 Ω.cm², Day 3: 19.19 ± 0.30 Ω.cm², Day 4: 51.74 ± 0.65 Ω.cm², Day 5: 74.65 ± 1.14 Ω.cm², Day 6: 107.50 ± 0.84 Ω.cm², Day 7: 114.30± 1.09 Ω.cm²). Resistance then decreased from between 8 and 10 days in culture (Day 8: 98.90 ± 0.12 Ω.cm², Day 9: 50.17 ± 0.70 Ω.cm² and Day 10: 27.35 ± 0.22 Ω.cm²). The results are expressed as the mean ± SEM from 72 monolayers derived from 3 individual kidneys.

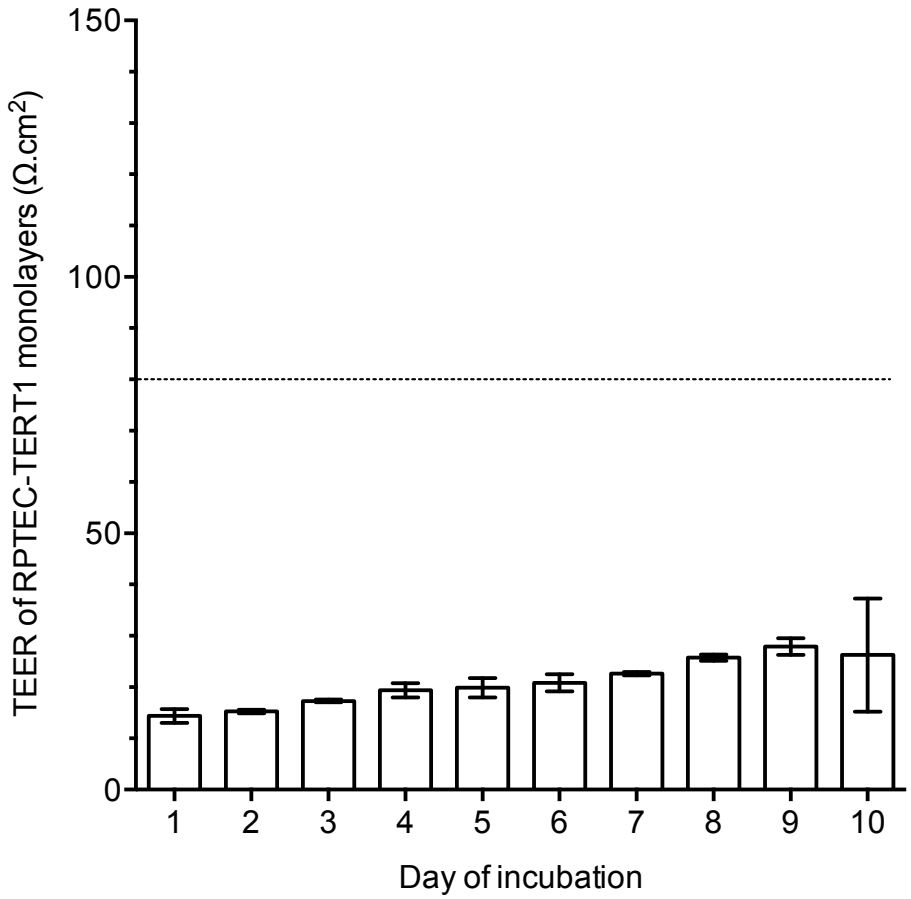

Figure 3.9: TEER of RPTEC monolayers grown on Transwell® inserts.

RPTEC cells were seeded on to 24-well Transwell® inserts at a density of 75 000 cells per insert with 200 μL of culture medium in the apical chamber and a further 1000 μL in the basolateral well. TEER of each monolayer was measured daily using an epithelial voltohmmeter to determine growth and permeability. Resistance was low throughout culture. The highest reading was 27.92 ± 0.33 Ω.cm² at day 9. The results are expressed as the mean ± SEM from 24 monolayers derived from 3 individual passages.

3.3.5. The correlation between TEER and paracellular permeability.

In order to determine the efficiency of TEER as a measurement of epithelial cell monolayer permeability, the correlation between TEER and paracellular permeability was investigated. Radiolabelled [1-^{14}C]-mannitol D is a non-metabolised small molecular weight probe (112 kiloDaltons) that can be used to determine paracellular permeability. Human and rat PTCs, as well as RPTEC cells, were seeded on to 24-well Transwell® inserts. The TEER of monolayers was measured prior to mannitol flux experiments in the absorptive direction (J_{A-B}). Radiolabelled [1-^{14}C]-mannitol D (10 μM, radioactivity 0.1 μCi / mL) was introduced into the apical chamber of the Transwell® inserts and its appearance in the basolateral well after 1 hr was measured to quantify the paracellular permeability of the monolayers.

Figure 3.10 and Figure 3.11 show the inverse relationship between monolayer TEER and paracellular permeability (n = 200, N = 25). As human PTC and rat PTC monolayer TEER increased, the paracellular movement of mannitol decreased until it reached a plateau of 12.89 ± 8.29 pmol / hr / cm^2 and 7.24 ± 11.05 pmol / hr / cm^2, respectively. In both species there was a mannitol flux of 30 pmol / hr / cm^2 or less when monolayer TEER was greater than 80 Ω.cm^2. This equated to a mannitol paracellular flux of less than 0.01 % of the total amount of mannitol used. As shown in Figure 3.12 , RPTEC monolayers that failed to develop a high TEER showed a high mannitol flux and permeability.

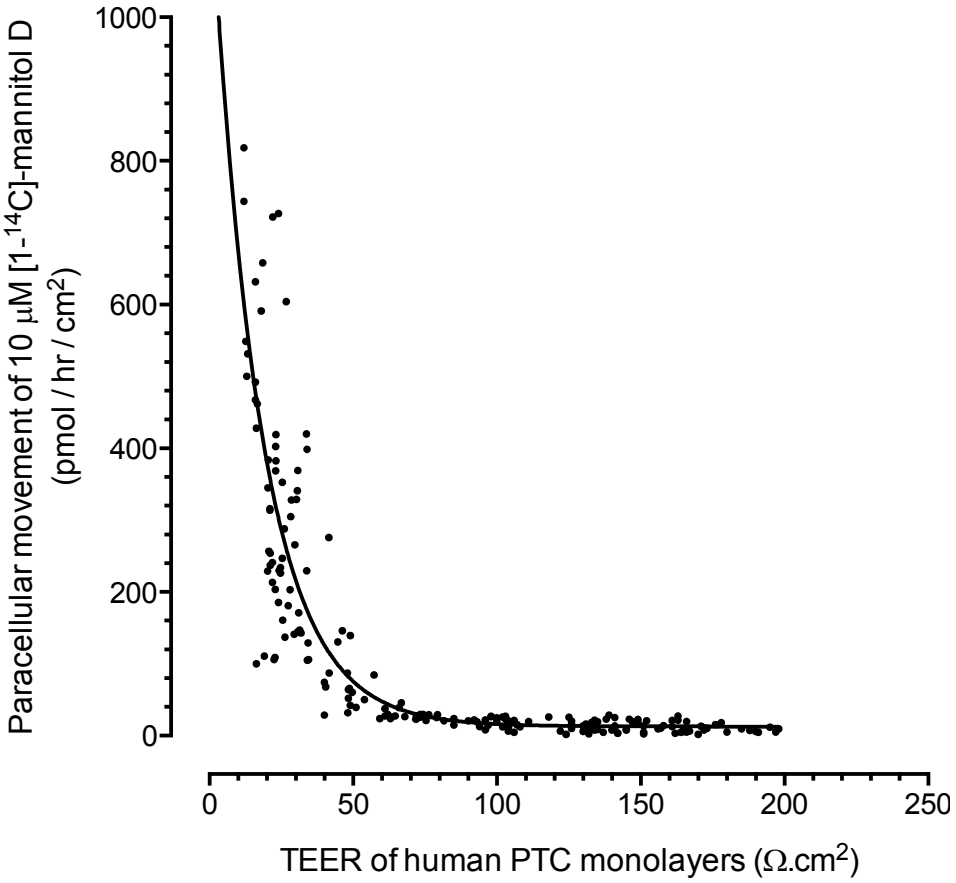

Figure 3.10: The correlation between TEER of human PTC monolayers and paracellular movement of radiolabelled 10 μM [1-^{14}C]-mannitol D.

An inverse relationship between the TEER value and mannitol paracellular flux was observed. As monolayer TEER increased, the paracellular movement of mannitol decreased until it reached a plateau of 12.89 ± 8.29 pmol / hr / cm^2. Monolayers with TEER of 50 Ω.cm^2 or lower showed a high amount of mannitol flux and thus had a high permeability. This is in contrast to monolayers with TEER of 80 Ω.cm^2 or greater that showed low mannitol flux (30 pmol / hr / cm^2 or less) and thus had a low permeability. Each dot represents the TEER of the monolayer and the paracellular movement of mannitol across the monolayer in the absorptive direction (J_{A-B}). The sample size (n) was 200.

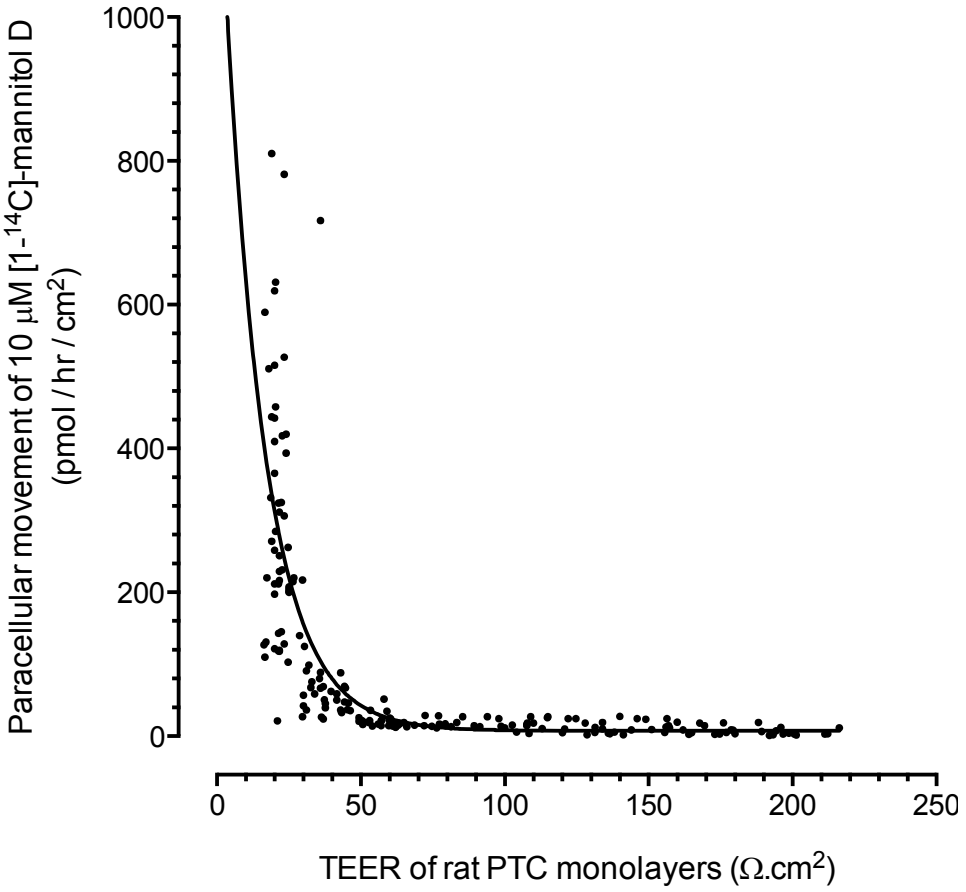

Figure 3.11: The correlation between TEER of rat PTC monolayers and paracellular movement of radiolabelled 10 μM [1-^{14}C]-mannitol D.

An inverse relationship between TEER values and mannitol paracellular flux was observed. As monolayer TEER increased, the paracellular movement of mannitol decreased until it reached a plateau of 7.24 ± 11.05 pmol / hr / cm^2. Monolayers with TEER of 40 Ω.cm^2 and lower had a high permeability, whereas monolayers with TEER of 80 Ω.cm^2 and greater had a low permeability. Each dot represents the TEER of the monolayer and the paracellular movement of mannitol across the monolayer in the absorptive direction (J_{A-B}). The sample size (n) was 200.

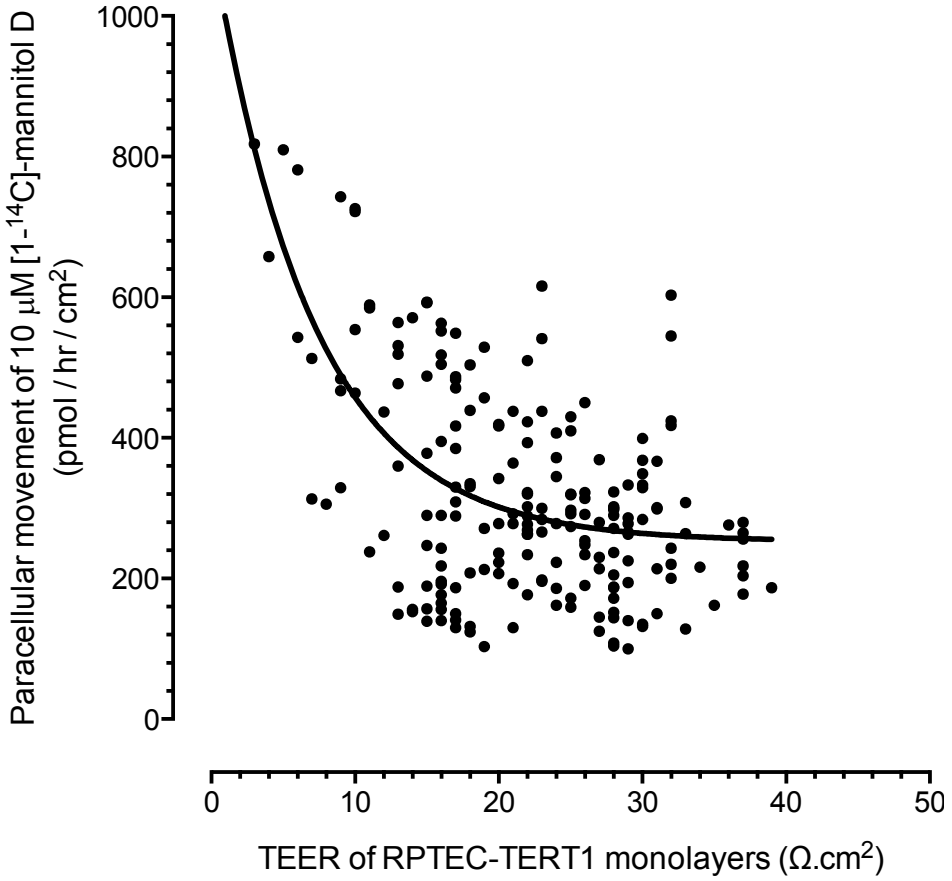

Figure 3.12: The correlation between TEER of RPTEC monolayers and paracellular movement of radiolabelled 10 μM [1-^{14}C]-mannitol D.

The monolayers failed to develop high TEER values. The maximum TEER value was 39 Ω.cm^2. Correspondingly, the monolayers showed a high paracellular flux of mannitol and thus permeability. Each dot represents the TEER of the monolayer and the paracellular movement of mannitol across the monolayer in the absorptive direction (J_{A-B}). The sample size (n) was 200.

3.3.6. mRNA expression of key renal drug transporters.

In order to understand how primary cell cultureware and immortalisation of primary proximal tubular cells may affect cellular mRNA expression of transport proteins, total cell RNA was isolated from

- freshly isolated human and rat PTCs,
- human and rat PTCs cultured on 24-well Transwell® inserts®,
- human and rat PTCs cultured in plastic T25 flasks, and
- RPTEC cells (immortalised human PTCs) cultured in plastic T25 flasks.

The total cell RNA was reverse transcribed into cDNA using MMLV-RT before qPCR. The mRNA expression levels of human drug transporters, OAT1, OAT3, URAT1, OATP4C1, OCT2, BCRP, MATE1, MATE2-K, MDR1, MRP1, MRP2, MRP3, and MRP4 following culture on Transwell® inserts and plastic cultureware, and human PTC immortalisation with TERT (RPTEC cell line) relative to freshly isolated cells are shown in Figure 3.13, Figure 3.14, Figure 3.15, Figure 3.16, Figure 3.17, Figure 3.18, Figure 3.19, Figure 3.20, Figure 3.21, Figure 3.22, Figure 3.23, Figure 3.24, and Figure 3.25, respectively. The data are summarised in Table 3.1. The mRNA expression levels of rat drug transporters, Oat1, Urat1, Oatp4c1, Oct2, Bcrp, Mate1, Mdr1, and Mrp2, following culture on Transwell® inserts and plastic cultureware relative to freshly isolated cells are summarised in Table 3.2. This data was produced in collaboration with Git Chung. The expression levels had been normalised to reference gene GAPDH/Gapdh expression level prior to comparison. The data are presented as the mean ± SEM percentage change in expression levels from 3 separate batches of RNA (N = 3).

Human PTCs cultured on Transwell® inserts maintained expression of all the key renal transport proteins investigated. At day 8 in culture, there was however a significant fall in the mRNA expression of OAT1, URAT1, OATP4C1, OCT2, BCRP, MATE1, MDR1, MRP3 and MRP4 compared with mRNA expression levels in freshly isolated human PTCs. On average the human PTCs at day 7 had expression levels around 40-50% of fresh tissue, with some exceptions.

Similarly, human PTCs cultured on plastic cultureware maintained a similar expression of all transporters proteins tested, again with a significant decrease in the expression of OAT1, OAT3, URAT1, OATP4C1, OCT2, BCRP, MATE1, MDR1, MRP1, MRP3 and MRP4 when compared with freshly isolated human PTCs. In stark contrast, immortalised primary proximal tubule cells (RPTEC) showed a profound loss of transporter expression compared with fresh tissue there was a significant fall in the expression of all transporters following immortalisation.

Expression in human PTCs cultured on Transwell® inserts was compared against cells cultured on plastic. The data show expression of OAT3, OATP4C1, BCRP, MRP1, MRP3 and MRP4 was significantly higher following culture on Transwell® inserts suggesting that cells grown on Transwell® inserts may retain more differentiation than cells grown on plastic.

Rat PTCs cultured on both Transwell® inserts and plastic showed an almost identical pattern with maintained expression of all the key renal transport proteins investigated, but with expression levels of all transporters significantly lower than freshly isolated rat PTCs, (approximately 80 to 70% lower). In contrast to the human PTC data, no significance in expression levels was observed between the two culture conditions with rat PTCs. Significance was determined using a Student's t-test.

Relative drug transporter gene expression was compared using human and rat drug transporter RT^2 profiler PCR array plates. The plates screen expression of 84 drug transporter genes and 5 reference genes. Drug transporter expression in freshly isolated human and rat PTCs, and human and rat PTCs cultured for 7 days on plastic were charactersied. In correlation with the other data the results in Figure 3.26 and Figure 3.27 show drug transporter mRNA levels were lower in cells cultured on plastic.

The data in Figure 3.26 show high expression of OAT1 and OCT2 in fresh human PTCs and expression of OAT2, OAT3, OATP1A2, OCT3, BCRP, MDR1, MRP1, MRP2, MRP3, MRP4, MRP5, and MRP6 at lower levels. Human PTCs cultured for 7 days on plastic showed expression of OCT2, MDR1, MRP1, MRP3, MRP4, and MRP5. Drug transporters of interest absent from the PCR

array panel include OAT4, URAT1, OATP4C1, MATE1 and MATE2-K. Expression had been normalised to the reference gene, GAPDH. The results are representative of a single batch of RNA derived from a single individual (N = 1).

Figure 3.27 shows high expression of Oat3 and Oct1 in fresh rat PTCs and expression of Oat1, Oat2, Oct2, Bcrp, Mdr1b, Mrp1, Mrp2, Mrp3, Mrp4, Mrp5, and Mrp6 at lower levels. Rat PTCs cultured for 7 days on plastic showed expression of Bcrp, Mdr1b, Mrp1, Mrp4, and Mrp5. Drug transporters of interest absent from the PCR array panel include Urat1, Oatp4c1, Oatp1a isoforms, and Mate1. Expression had been normalised to the reference gene, ß-actin. The results are representative of a single batch of RNA derived from a single individual (N = 1).

The expression of non-proximal tubule drug transporters was also assessed to determine cell contamination. Expression of V-ATPase a marker of collecting duct cells and MCT8 a marker of loop of Henle and colecting duct cells was very low in all samples. This suggests that proximal tubule cells predominate the human and rat PTC cell populations.

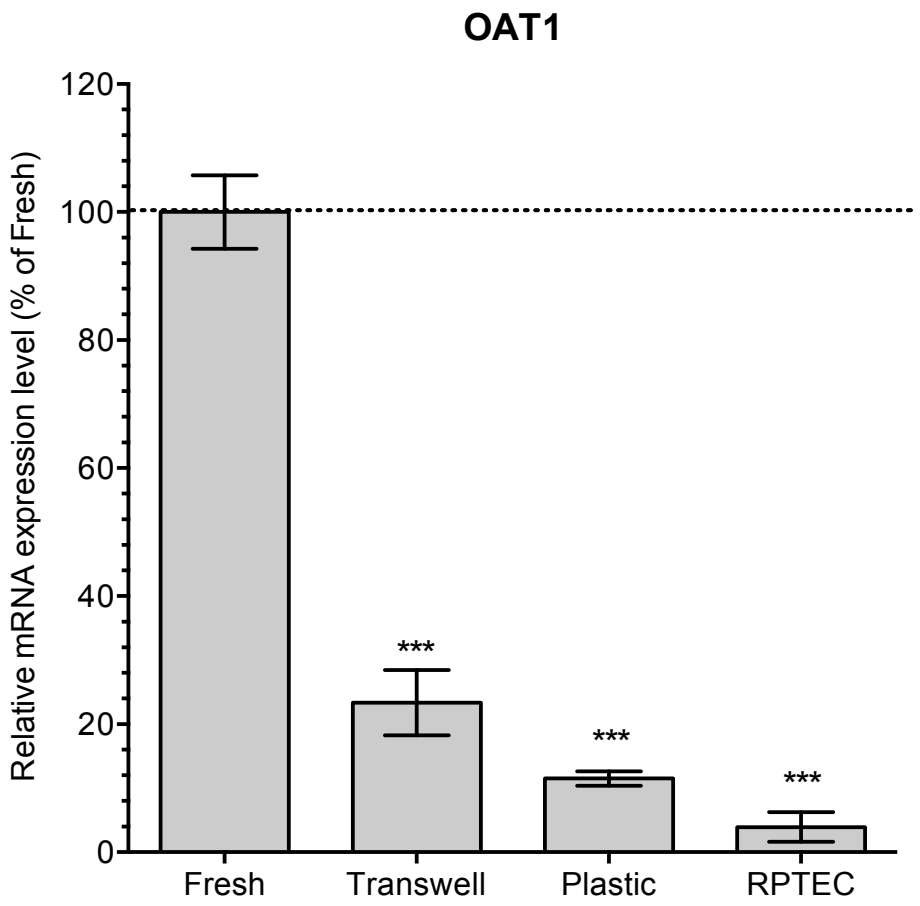

Figure 3.13: The mRNA expression of OAT1 in human PTCs under different culture conditions.

*OAT1 mRNA expression levels are expressed as percentage expression relative to freshly isolated human PTCs. Human PTCs cultured for 7 days on Transwell inserts and plastic showed a 76.61 ± 5.10 % and 88.49 ± 1.11 % decrease in expression in comparison to freshly isolated cells (100.00 ± 5.72 %), respectively. The immortalised RPTEC cell line showed a 96.05 ± 2.32 % decrease in expression in comparison to freshly isolated cells. The expression levels had been normalised to reference gene GAPDH expression level prior to comparison. The results are expressed as the mean ± SEM from 3 separate batches of RNA derived from 3 individual kidneys. One-way ANOVA statistical test was performed on the data set to determine significance, *** P < 0.001.*

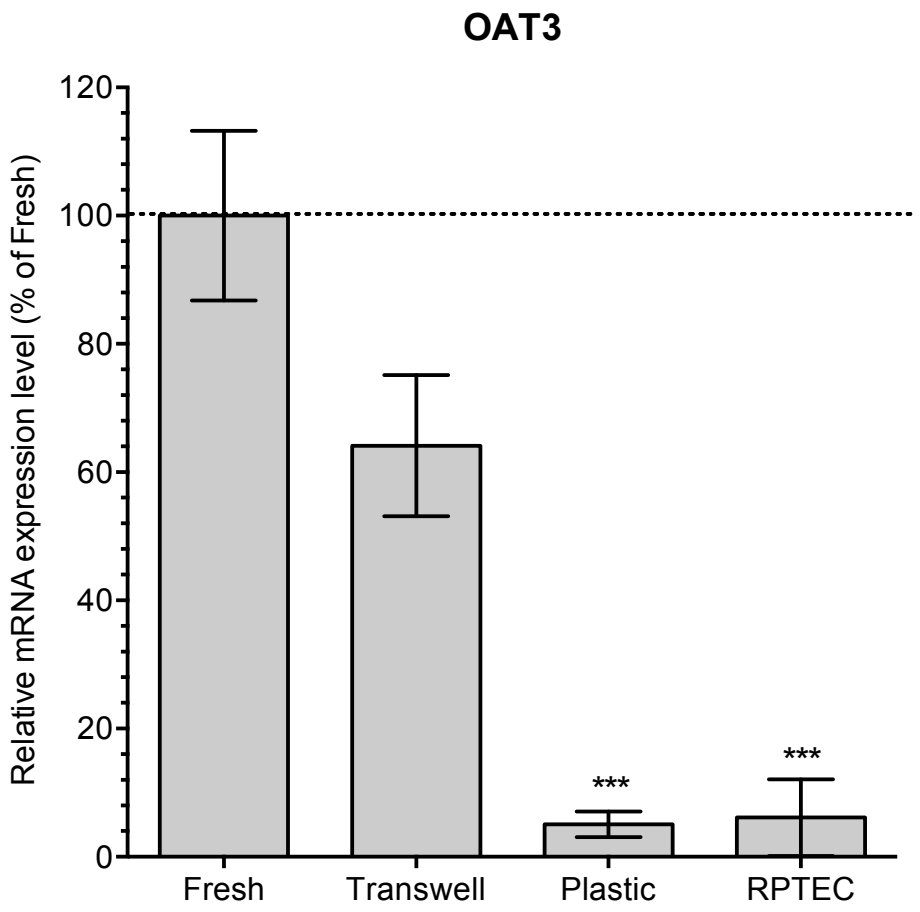

Figure 3.14: The mRNA expression of OAT3 in human PTCs under different culture conditions.

*OAT3 mRNA expression levels are expressed as percentage expression relative to freshly isolated human PTCs. Human PTCs cultured for 7 days on Transwell inserts and plastic showed a 35.88 ± 11.01 % and 94.93 ± 1.99 % decrease in expression in comparison to freshly isolated cells (100.00 ± 13.25 %), respectively. The immortalised RPTEC cell line showed a 93.90 ± 5.98 % decrease in expression in comparison to freshly isolated cells. The expression levels had been normalised to reference gene GAPDH expression level prior to comparison. The results are expressed as the mean ± SEM from 3 separate batches of RNA derived from 3 individual kidneys. One-way ANOVA statistical test was performed on the data set to determine significance, *** P < 0.001.*

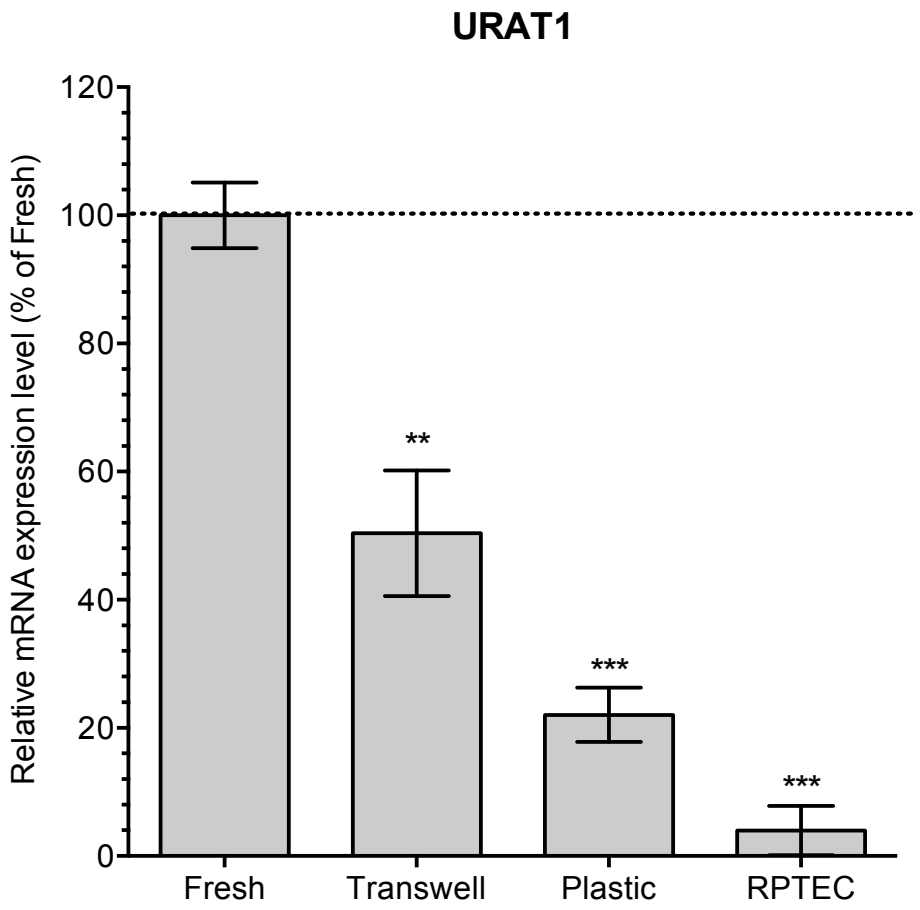

Figure 3.15: The mRNA expression of URAT1 in human PTCs under different culture conditions.

*URAT1 mRNA expression levels are expressed as percentage expression relative to freshly isolated human PTCs. Human PTCs cultured for 7 days on Transwell inserts and plastic showed a 49.61 ± 9.79 % and 77.96 ± 4.23 % decrease in expression in comparison to freshly isolated cells (100.00 ± 5.12 %), respectively. The immortalised RPTEC cell line showed a 96.03 ± 3.84 % decrease in expression in comparison to freshly isolated cells. The expression levels had been normalised to reference gene GAPDH expression level prior to comparison. The results are expressed as the mean ± SEM from 3 separate batches of RNA derived from 3 individual kidneys. One-way ANOVA statistical test was performed on the data set to determine significance, ** P < 0.01, *** P < 0.001.*

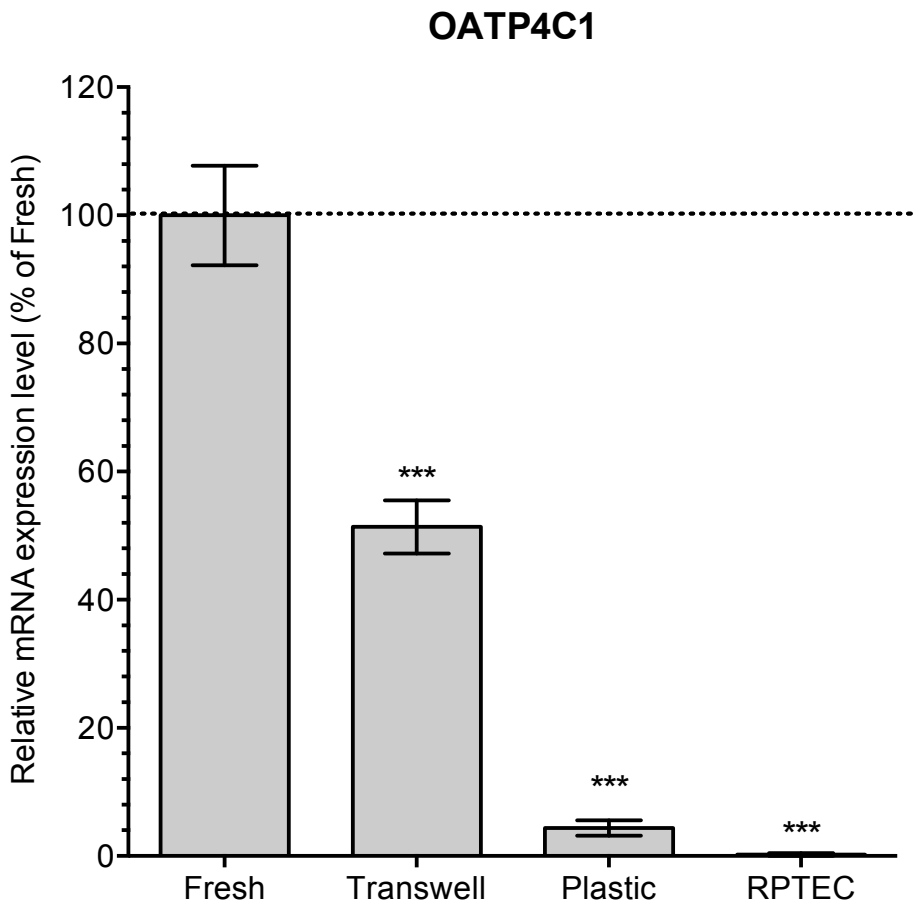

Figure 3.16: The mRNA expression of OATP4C1 in human PTCs under different culture conditions.

OATP4C1 mRNA expression levels are expressed as percentage expression relative to freshly isolated human PTCs. Human PTCs cultured for 7 days on Transwell inserts and plastic showed a 48.63 ± 4.13 % and 95.62 ± 1.21 % decrease in expression in comparison to freshly isolated cells, (100.00 ± 7.77 %), respectively. The immortalised RPTEC cell line showed a 99.79 ± 0.20 % decrease in expression in comparison to freshly isolated cells. The expression levels had been normalised to reference gene GAPDH expression level prior to comparison. The results are expressed as the mean ± SEM from 3 separate batches of RNA derived from 3 individual kidneys. One-way ANOVA statistical test was performed on the data set to determine significance, *** $P < 0.001$.

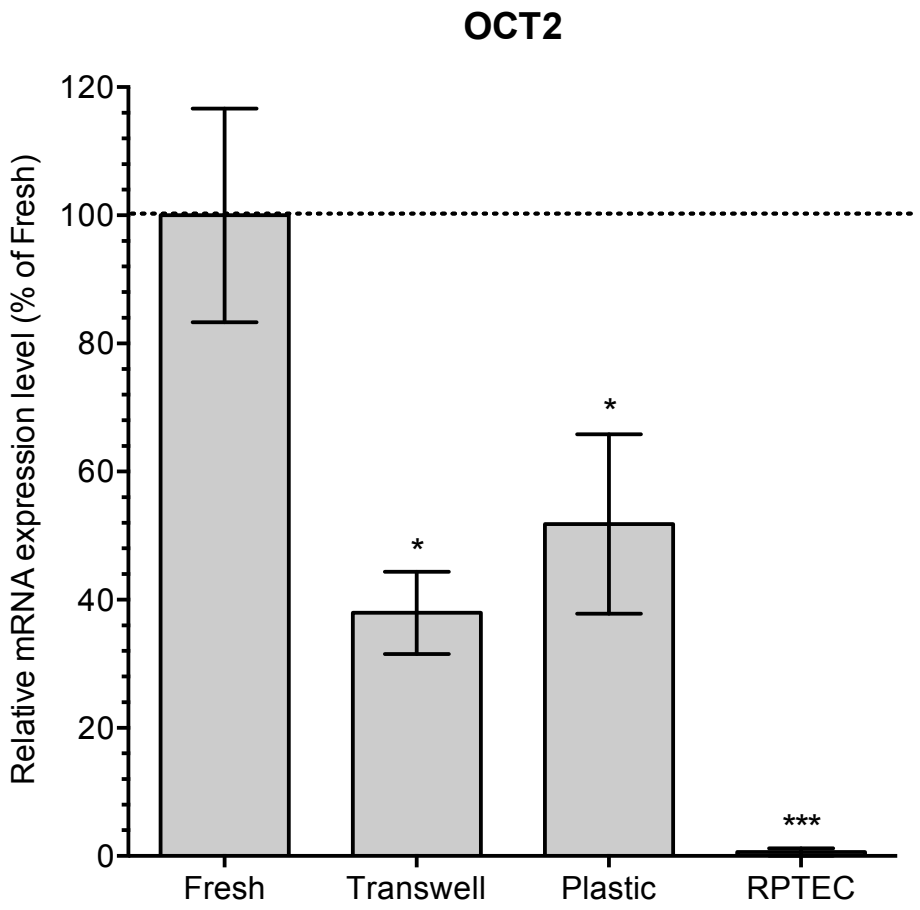

Figure 3.17: The mRNA expression of OCT2 in human PTCs under different culture conditions.

*OCT2 mRNA expression levels are expressed as percentage expression relative to freshly isolated human PTCs. Human PTCs cultured for 7 days on Transwell inserts and plastic showed a 62.04 ± 6.43 % and 48.16 ± 13.99 % decrease in expression in comparison to freshly isolated cells, (100.00 ± 16.67 %), respectively. The immortalised RPTEC cell line showed a 99.38 ± 0.56 % decrease in expression in comparison to freshly isolated cells. The expression levels had been normalised to reference gene GAPDH expression level prior to comparison. The results are expressed as the mean ± SEM from 3 separate batches of RNA derived from 3 individual kidneys. One-way ANOVA statistical test was performed on the data set to determine significance, * P < 0.05, *** P < 0.001.*

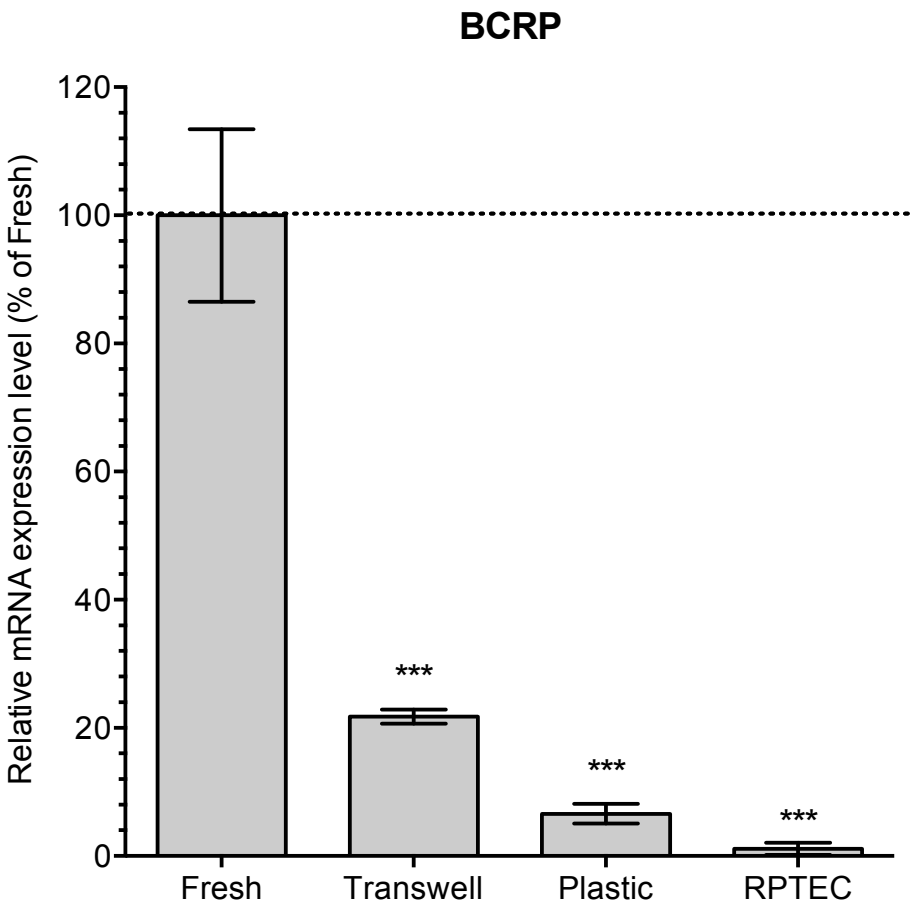

Figure 3.18: The mRNA expression of BCRP in human PTCs under different culture conditions.

BCRP mRNA expression levels are expressed as percentage expression relative to freshly isolated human PTCs. Human PTCs cultured for 7 days on Transwell inserts and plastic showed a 78.21 ± 1.09 % and 93.41 ± 1.52 % decrease in expression in comparison to freshly isolated cells, (100.00 ± 13.46 %), respectively. The immortalised RPTEC cell line showed a 98.89 ± 0.94 % decrease in expression in comparison to freshly isolated cells. The expression levels had been normalised to reference gene GAPDH expression level prior to comparison. The results are expressed as the mean ± SEM from 3 separate batches of RNA derived from 3 individual kidneys. One-way ANOVA statistical test was performed on the data set to determine significance, *** $P < 0.001$.

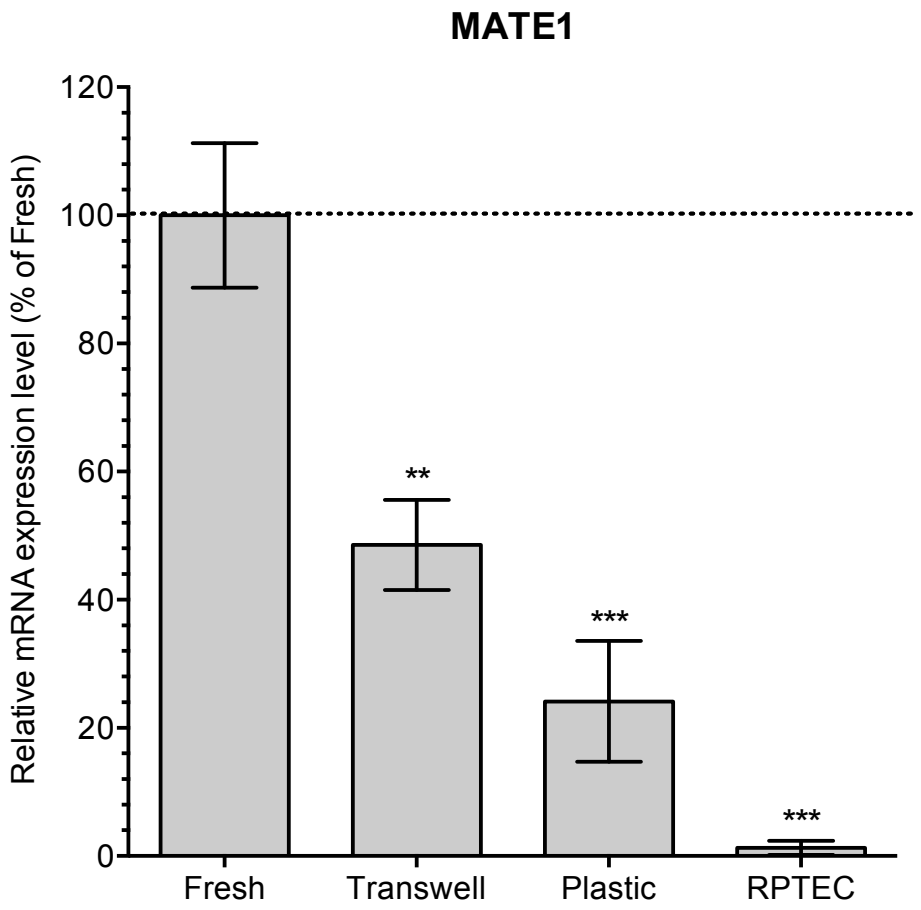

Figure 3.19: The mRNA expression of MATE1 in human PTCs under different culture conditions.

*MATE1 mRNA expression levels are expressed as percentage expression relative to freshly isolated human PTCs. Human PTCs cultured for 7 days on Transwell inserts and plastic showed a 51.44 ± 7.01 % and 75.86 ± 9.42 % decrease in expression in comparison to freshly isolated cells, (100.00 ± 11.28 %), respectively. The immortalised RPTEC cell line showed a 98.71 ± 1.11 % decrease in expression in comparison to freshly isolated cells. The expression levels had been normalised to reference gene GAPDH expression level prior to comparison. The results are expressed as the mean ± SEM from 3 separate batches of RNA derived from 3 individual kidneys. One-way ANOVA statistical test was performed on the data set to determine significance, ** P < 0.01, *** P < 0.001.*

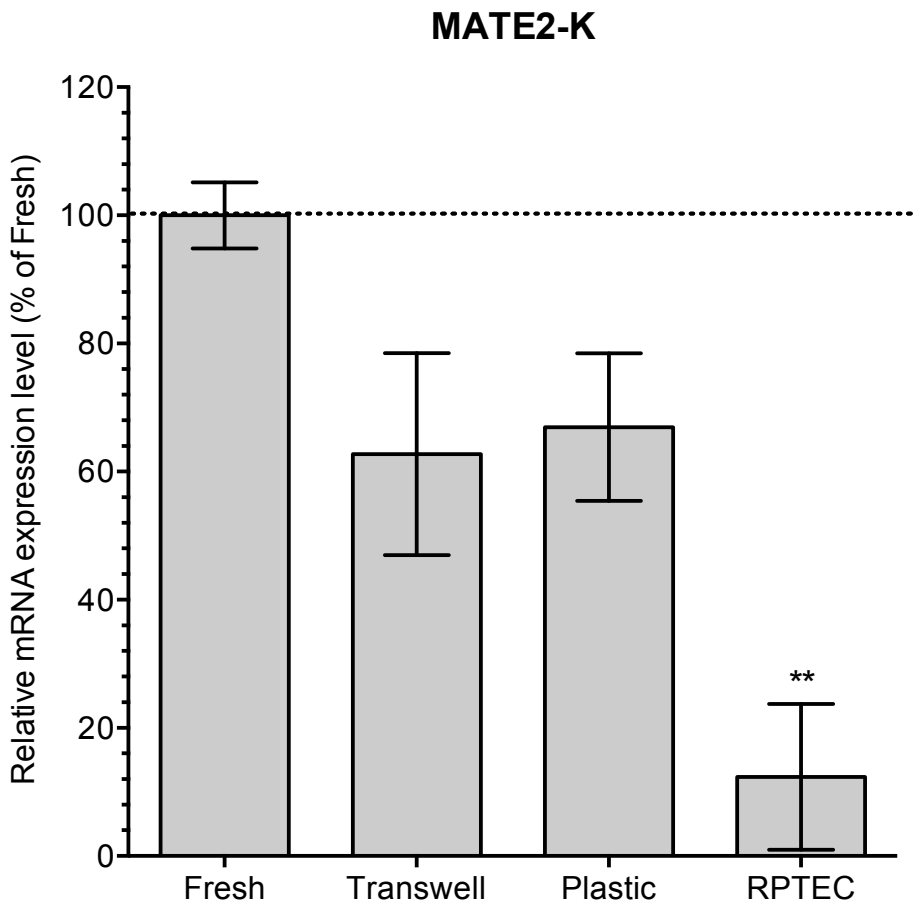

Figure 3.20: The mRNA expression of MATE2-K in human PTCs under different culture conditions.

*MATE2-K mRNA expression levels are expressed as percentage expression relative to freshly isolated human PTCs. Human PTCs cultured for 7 days on Transwell inserts and plastic showed a 37.25 ± 15.80 % and 33.05 ± 11.55 % decrease in expression in comparison to freshly isolated cells, (100.00 ± 5.16 %), respectively. The immortalised RPTEC cell line showed an 87.66 ± 11.37 % decrease in expression in comparison to freshly isolated cells. The expression levels had been normalised to reference gene GAPDH expression level prior to comparison. The results are expressed as the mean ± SEM from 3 separate batches of RNA derived from 3 individual kidneys. One-way ANOVA statistical test was performed on the data set to determine significance, ** P < 0.01.*

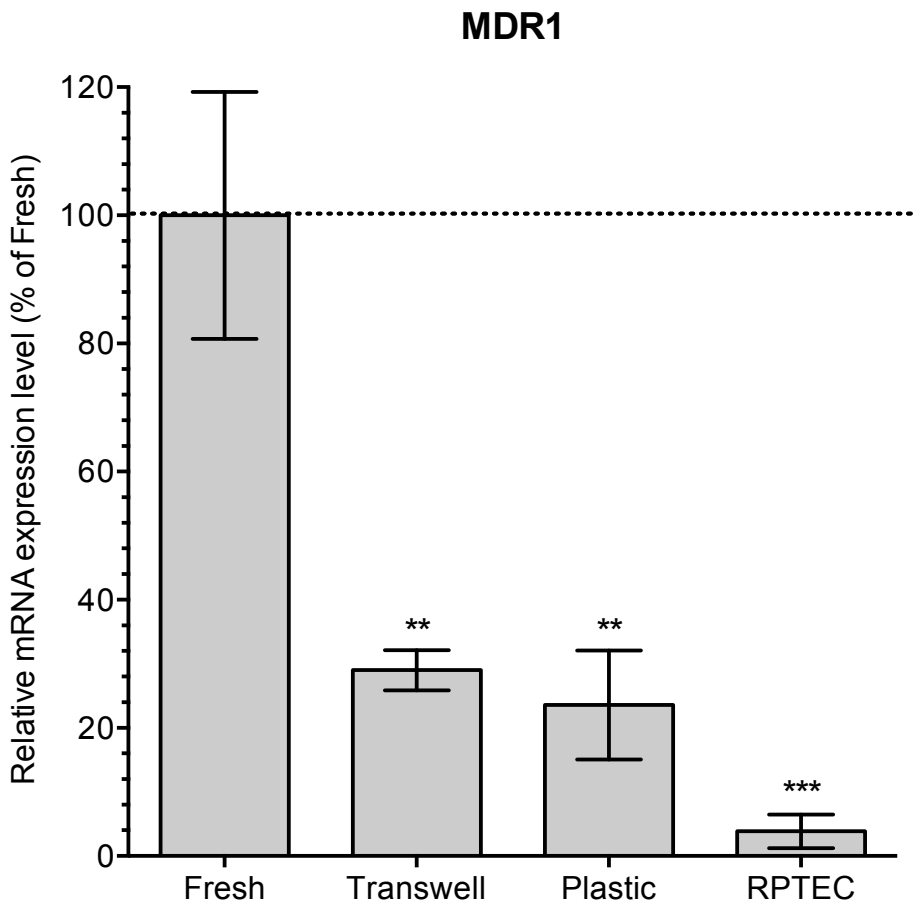

Figure 3.21: The mRNA expression of MDR1 in human PTCs under different culture conditions.

*MDR1 mRNA expression levels are expressed as percentage expression relative to freshly isolated human PTCs. Human PTCs cultured for 7 days on Transwell inserts and plastic showed a 70.99 ± 3.12 % and 76.42 ± 8.51 % decrease in expression in comparison to freshly isolated cells, (100.00 ± 19.26 %), respectively. The immortalised RPTEC cell line showed a 96.13 ± 2.62 % decrease in expression in comparison to freshly isolated cells. The expression levels had been normalised to reference gene GAPDH expression level prior to comparison. The results are expressed as the mean ± SEM from 3 separate batches of RNA derived from 3 individual kidneys. One-way ANOVA statistical test was performed on the data set to determine significance, ** P < 0.01, *** P < 0.001.*

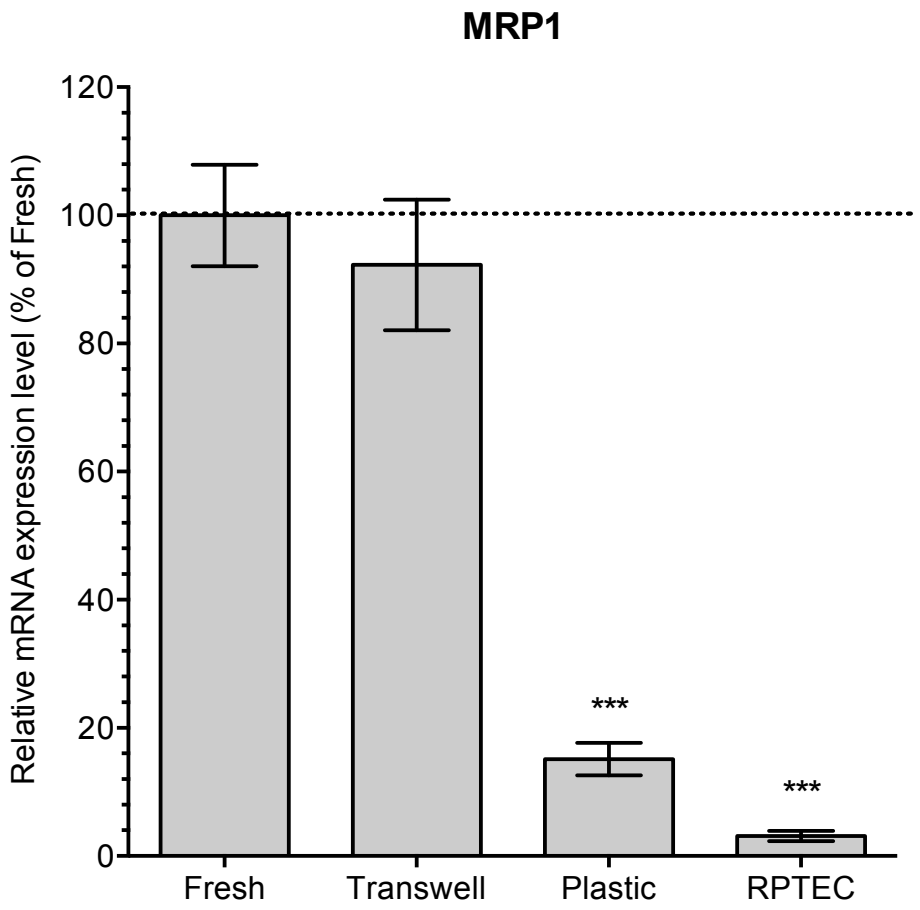

Figure 3.22: The mRNA expression of MRP1 in human PTCs under different culture conditions.

*MRP1 mRNA expression levels are expressed as percentage expression relative to freshly isolated human PTCs. Human PTCs cultured for 7 days on Transwell inserts and plastic showed a 7.71 ± 10.20 % and 84.87 ± 2.56 % decrease in expression in comparison to freshly isolated cells, (100.00 ± 7.91 %), respectively. The immortalised RPTEC cell line showed a 96.87 ± 0.81 % decrease in expression in comparison to freshly isolated cells. The expression levels had been normalised to reference gene GAPDH expression level prior to comparison. The results are expressed as the mean ± SEM from 3 separate batches of RNA derived from 3 individual kidneys. One-way ANOVA statistical test was performed on the data set to determine significance, *** P < 0.001.*

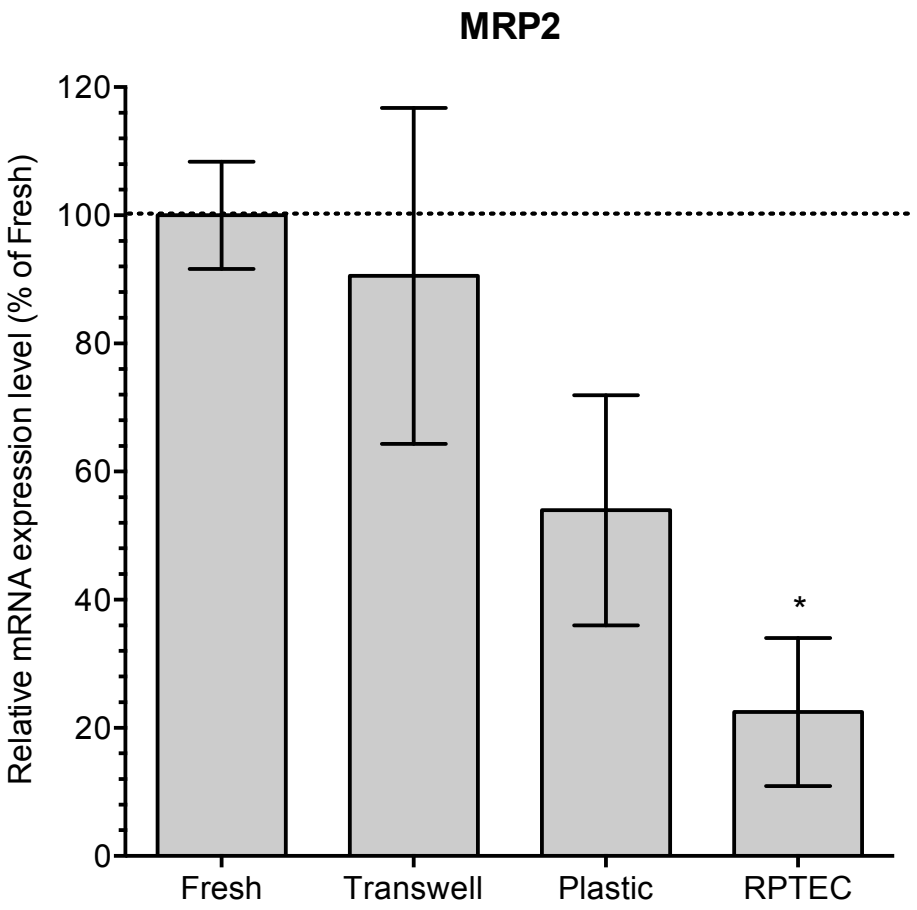

Figure 3.23: The mRNA expression of MRP2 in human PTCs under different culture conditions.

*MRP2 mRNA expression levels are expressed as percentage expression relative to freshly isolated human PTCs. Human PTCs cultured for 7 days on Transwell inserts and plastic showed a 9.44 ± 26.22 % and 46.03 ± 17.97 % decrease in expression in comparison to freshly isolated cells, (100.00 ± 8.38 %), respectively. The immortalised RPTEC cell line showed a 77.53 ± 11.54 % decrease in expression in comparison to freshly isolated cells. The expression levels had been normalised to reference gene GAPDH expression level prior to comparison. The results are expressed as the mean ± SEM from 3 separate batches of RNA derived from 3 individual kidneys. One-way ANOVA statistical test was performed on the data set to determine significance, * P < 0.05.*

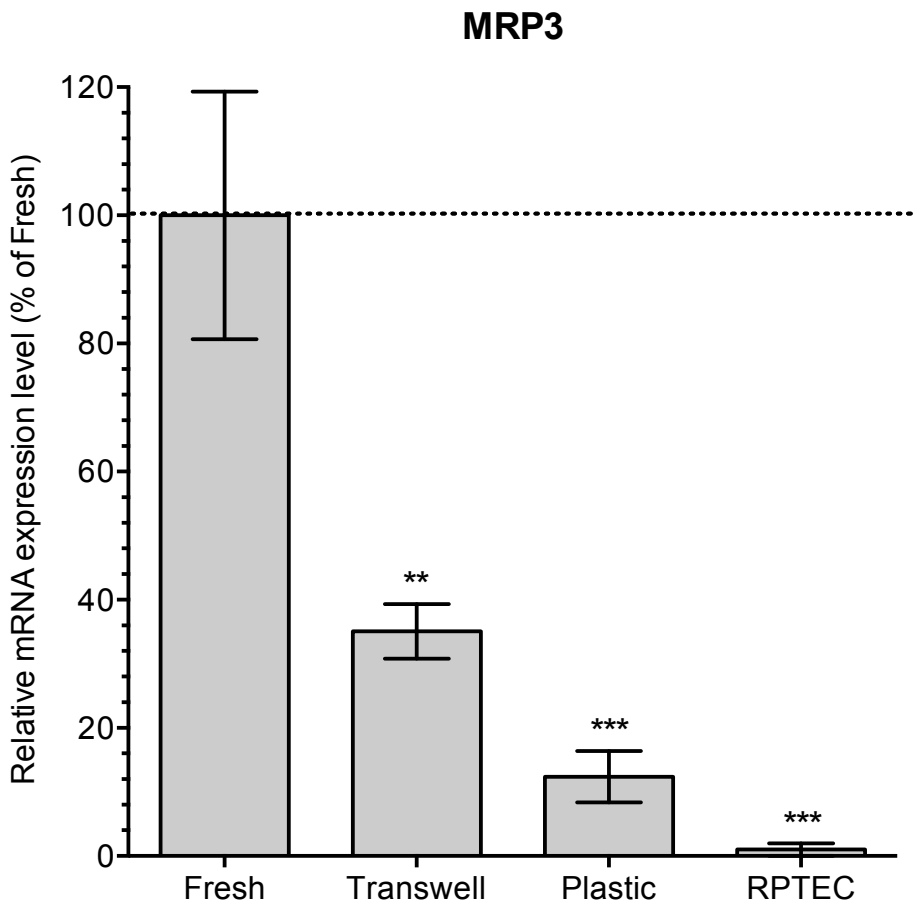

Figure 3.24: The mRNA expression of MRP3 in human PTCs under different culture conditions.

*MRP3 mRNA expression levels are expressed as percentage expression relative to freshly isolated human PTCs. Human PTCs cultured for 7 days on Transwell inserts and plastic showed a 64.91 ± 4.26 % and 87.62 ± 4.00 % decrease in expression in comparison to freshly isolated cells, (100.00 ± 19.33 %), respectively. The immortalised RPTEC cell line showed a 99.00 ± 0.96 % decrease in expression in comparison to freshly isolated cells. The expression levels had been normalised to reference gene GAPDH expression level prior to comparison. The results are expressed as the mean ± SEM from 3 separate batches of RNA derived from 3 individual kidneys. One-way ANOVA statistical test was performed on the data set to determine significance, ** P < 0.01, *** P < 0.001.*

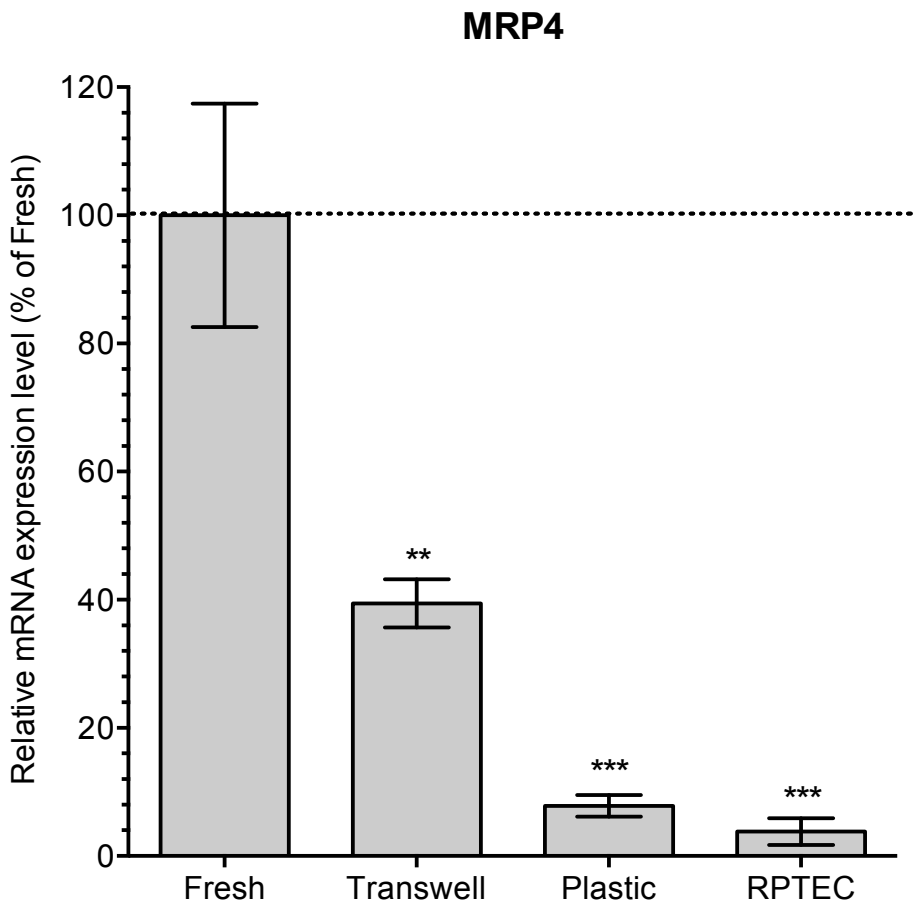

Figure 3.25: The mRNA expression of MRP4 in human PTCs under different culture conditions.

*MRP4 mRNA expression levels are expressed as percentage expression relative to freshly isolated human PTCs. Human PTCs cultured for 7 days on Transwell inserts and plastic showed a 60.57± 3.76 % and 92.18 ± 1.71 % decrease in expression in comparison to freshly isolated cells, (100.00 ± 17.42 %), respectively. The immortalised RPTEC cell line showed a 96.20 ± 2.05 % decrease in expression in comparison to freshly isolated cells. The expression levels had been normalised to reference gene GAPDH expression level prior to comparison. The results are expressed as the mean ± SEM from 3 separate batches of RNA derived from 3 individual kidneys. One-way ANOVA statistical test was performed on the data set to determine significance, ** P < 0.01, *** P < 0.001.*

Transporter	% expression compared to fresh human PTCs (Mean ± SEM)		
	Transwell®	Plastic	RPTEC
OAT1	23.39 ± 5.10 ***	11.51 ± 1.11 ***	3.95 ± 2.32 ***
OAT3	64.12 ± 11.01	5.07 ± 1.99 ***	6.11 ± 5.98 ***
URAT1	50.39 ± 9.79 **	22.04 ± 4.23 ***	3.97 ± 3.84 ***
OATP4C1	51.37 ± 4.13 ***	4.38 ± 1.21 ***	0.21 ± 0.20 ***
OCT2	37.96 ± 6.43 *	51.84 ± 13.99 *	0.62 ± 0.56 ***
BCRP	21.79 ± 1.09 ***	6.59 ± 1.52 ***	1.12 ± 0.94 ***
MATE1	48.56 ± 7.01 **	24.14 ± 9.42 ***	1.29 ± 1.11 ***
MATE-2K	62.75 ± 15.80	66.95 ± 11.55	12.34 ± 11.37 **
MDR1	29.01 ± 3.12 **	23.58 ± 8.51 **	3.87 ± 2.62 ***
MRP1	92.29 ± 10.20	15.13 ± 2.56 ***	3.13 ± 0.81 ***
MRP2	90.56 ± 26.22	53.97 ± 17.97	22.47 ± 11.54 *
MRP3	35.09 ± 4.26 **	12.38 ± 4.00 ***	1.00 ± 0.96 ***
MRP4	39.43 ± 3.76 **	7.82 ± 1.71 ***	3.80 ± 2.05 ***

Table 3.1: Summary of the change in relative mRNA expression levels of key drug transporters when human PTCs are cultured on Transwell® inserts, plastic cultureware and immortalised in comparison to freshly isolated human PTCs.

*mRNA expression levels are expressed as percentage expression relative to freshly isolated human PTCs. The data show that expression of many of the key renal transporters was significantly lower in cultured cells. Expression of OAT3, OATP4C1, BCRP, MRP1, MRP3 and MRP4 was significantly higher following culture on Transwell® inserts when compared with plastic. The expression levels had been normalised to reference gene GAPDH expression level prior to comparison. The results are expressed as the mean ± SEM from 3 separate batches of RNA derived from 3 individual kidneys. One-way ANOVA statistical test was performed on the data set to determine significance, * $P < 0.05$, ** $P < 0.01$, *** $P < 0.001$.*

Transporter	% expression compared to fresh rat PTCs (Mean ± SEM)	
	Transwell®	Plastic
Oat1	24.97 ± 7.51 ***	16.50 ± 4.93 ***
Urat1	19.05 ± 6.20 **	25.17 ± 4.53 **
Oatp4c1	22.81 ± 10.68 **	12.46 ± 7.57 **
Oct2	36.98 ± 17.71 **	27.68 ± 16.88 **
Bcrp	24.98 ± 8.50 **	20.23 ± 6.32 **
Mate1	28.09 ± 6.00 **	18.93 ± 9.44 **
Mdr1	72.81 ± 5.39 *	60.25 ± 7.07 *
Mrp2	37.71 ± 4.30 **	21.19 ± 10.33 **

Table 3.2: Summary of the change in relative mRNA expression levels of key drug transporters in rat PTCs cultured on Transwell® inserts and plastic cultureware compared to freshly isolated rat PTCs.

*mRNA expression levels are expressed as percentage expression relative to freshly isolated rat PTCs. The data show that expression of all key renal transporters was significantly lower in cultured cells. The expression levels had been normalised to reference gene Gapdh expression level prior to comparison. The results are expressed as the mean ± SEM from 3 separate batches of RNA derived from 3 individual kidneys. One-way ANOVA statistical test was performed on the data set to determine significance, * $P < 0.05$, ** $P < 0.01$, *** $P < 0.001$.*

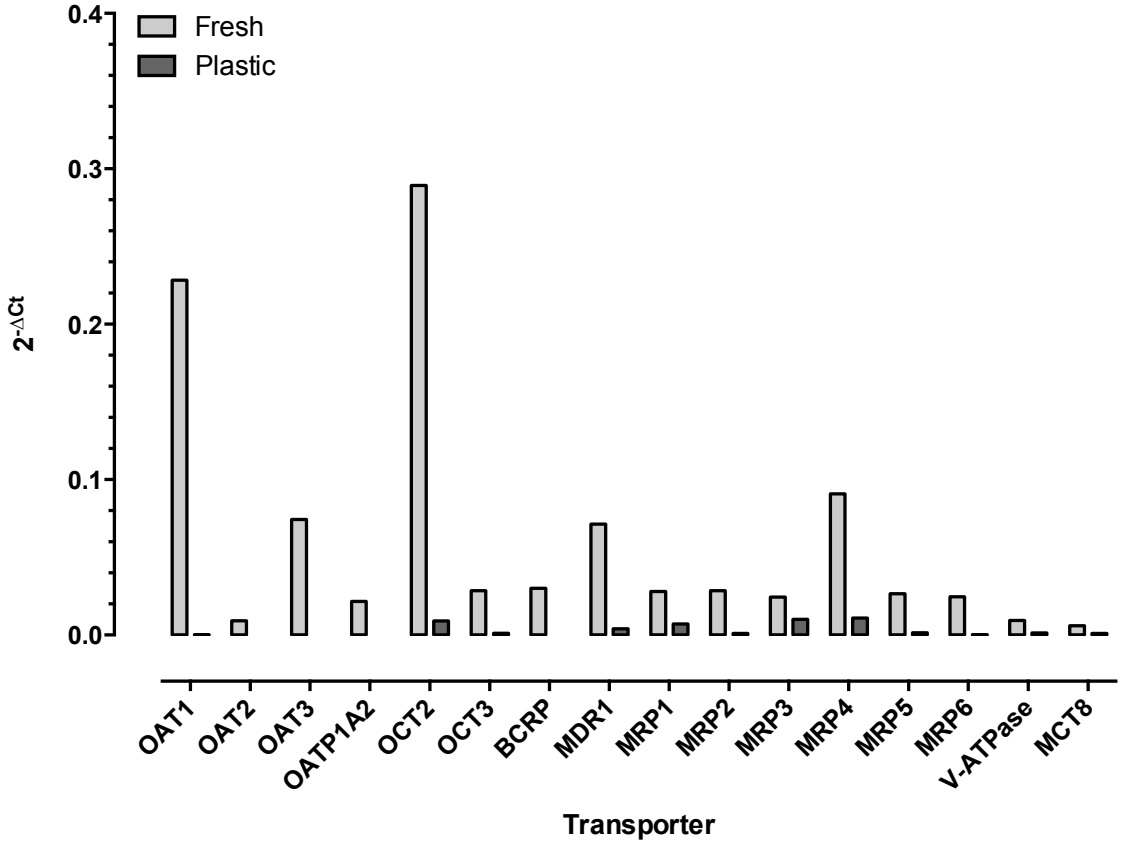

Figure 3.26: Characterisation of proximal and non-proximal tubular drug transporter expression using the human drug transporter RT² Profiler PCR array.

The human drug transporter RT² profiler PCR array was used to characterise drug transporter gene expression in freshly isolated human PTCs and human PTCs cultured for 7 days on plastic. The data shows a fall in drug transporter expression in cell culture on plastic. Fresh human PTCs showed high expression of OAT1 (0.228) and OCT2 (0.289). OAT2 (0.009), OAT3 (0.074), OATP1A2 (0.022), OCT3 (0.029), BCRP (0.030), MDR1 (0.071), MRP1 (0.028), MRP2, (0.029), MRP3 (0.025), MRP4 (0.091), MRP5 (0.027), MRP6 (0.025) were expressed at lower levels. The expression of non-proximal markers was also assessed to determine cell contamination. Expression of V-ATPase (0.009), a marker of collecting duct cells, and MCT8 (0.006), a marker of loop of Henle and distal tubular cells was very low. Human PTCs cultured for 7 days on plastic showed low expression of OCT2 (0.009), MDR1 (0.004), MRP1 (0.007), MRP3 (0.010), MRP4 (0.011) and MRP5 (0.002). Expression of the non-proximal tubule cell markers V-ATPase (0.001) and MCT8 (0.001) was minimal. Drug transporters of interest absent from the PCR array panel include OAT4, URAT1, OATP4C1, MATE1 and MATE2-K. The expression levels had been normalised to the reference gene, GAPDH, prior to comparison. The results are representative of a single batch of RNA derived from a single individual.

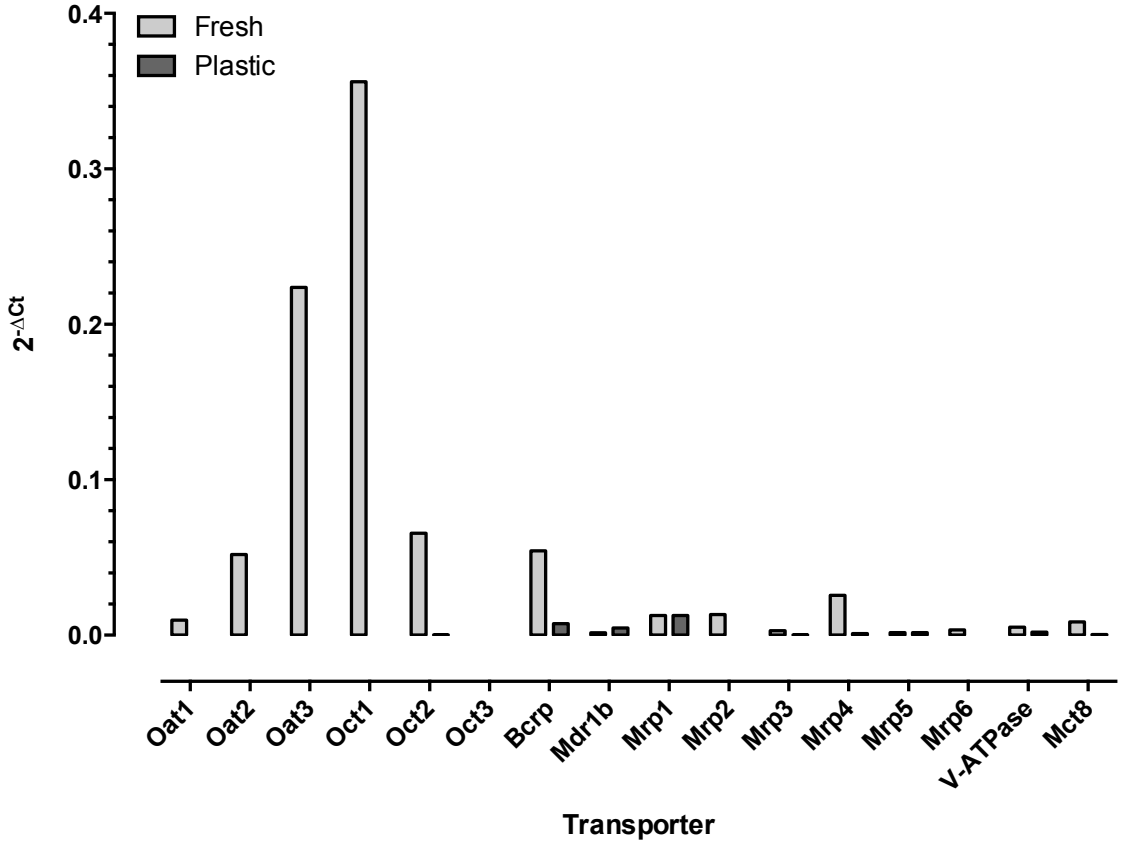

Figure 3.27: Characterisation of proximal and non-proximal tubular drug transporter expression using the rat drug transporter RT² Profiler PCR array.

The rat drug transporter RT² profiler PCR array was used to characterise drug transporter gene expression in freshly isolated rat PTCs and rat PTCs cultured for 7 days on plastic. The data shows a fall in drug transporter expression in cell culture on plastic. Fresh rat PTCs showed high expression of Oat3 (0.224) and Oct1 (0.356). Oat1 (0.010), Oat2 (0.052), Oct2 (0.066), Bcrp (0.054), Mdr1b (0.002), Mrp1 (0.013), Mrp2, (0.013), Mrp3 (0.003), Mrp4 (0.026), Mrp5 (0.002), Mrp6 (0.003) were expressed at lower levels. The expression of non-proximal markers was also assessed to determine cell contamination. Expression of V-ATPase (0.005) and Mct8 (0.009) was very low. Rat PTCs cultured for 7 days on plastic showed low expression of Bcrp (0.007), Mdr1b (0.005), Mrp1 (0.013), Mrp4 (0.001) and Mrp5 (0.002). Expression of the non-proximal tubule cell markers V-ATPase (0.002) and Mct8 (0.001) was minimal. Drug transporters of interest absent from the PCR array panel include Oat4, Urat1, Oatp4c1, Oatp1a isoforms, and Mate1. The expression level had been normalised to the reference gene, ß-actin, prior to comparison, as Gapdh was not included on the PCR array panel. The results are representative of a single batch of RNA derived from a single individual.

3.4. Discussion

The proximal tubule plays a pivotal role in the renal clearance of xenobiotic and endogenous metabolites. The uptake and efflux of molecules across the cell membrane of proximal tubule epithelial cells are achieved by the polar distribution of transport proteins to either the basolateral or apical membrane. From a molecular approach, a good understanding of the substrate profiles of the transporters expressed in the proximal tubule has been obtained, but we have little knowledge of the contribution of individual transporters or how transporters integrate to produce an efficient secretory or absorptive mechanism. A holistic model of the proximal tubule epithelial is needed to address this problem.

Many pre-clinical models of transport in the kidney are based on transfected or animal cells, which express a limited number of human renal transporters and consequently are not accurate models. In contrast, primary renal proximal tubule cells retain the full complement of key renal transporters. This makes them a more physiologically relevant and therefore predictive model of renal handling. Species differences in the properties and expression patterns of renal transporters are making data derived from animal studies difficult to extrapolate to humans. This highlights the importance of conducting parallel studies using primary human and rat models of the proximal tubule. In this chapter, a previously published method of isolating primary human proximal tubule cells was optimised, and was also adapted to isolate rat proximal tubule cells.

Samples of renal cortex tissue were enzymatically digested with collagenase into a single cell suspension. The cell suspension was then divided in to the constituent cell types by sieving and Percoll® density gradient centrifugation. In order to optimise the enzymatic digestion of the renal cortex, chopped samples (approximately 1 mm^3) were incubated overnight or acutely with different concentrations of collagenase and the yield of isolated PTCs was compared. In both species, higher concentrations of collagenase resulted in greater enzymatic digestion of renal cortex, and naturally larger yields of PTCs. As shown in Figure 3.1 and Figure 3.2, the incubation period had no significant

effect on the cell yield when using 20, 25, or 30 mg collagenase per g of renal cortex.

An issue of enzymatic digestion of renal cortex is that the enzyme mixtures contain protease enzymes that can be detrimental to cell viability at high concentrations (Boogaard *et al.*, 1990; Cummings *et al.*, 2000). In order to evaluate the effect of collagenase concentration upon cell health, growth assays were conducted on the isolated cells. The numbers of cells per cm^2 over an 8-day period of cell culture were quantified. As shown in Figure 3.3, human PTC growth was significantly greater when cells were incubated with 25 mg of collagenase per g of tissue. No significant difference was found in cell viability human PTC at day 8 of culture following an overnight or acute incubation with the same concentration of collagenase ($P > 0.05$). As a result of these findings, samples of human renal cortex were incubated with 25 mg of collagenase per g of renal cortex in the enzymatic digestion phase of human PTC isolation, despite 30 mg of collagenase per g of renal cortex producing a greater yield of cells. This concentration provides a good compromise on cell yield and viability, with the latter being crucial for downstream experiments. As the incubation period of the tissue with collagenase appeared to have no effect upon cell growth, convenience dictated the period of exposure of the human tissue to collagenase. Rat renal cortex tissues, on the other hand, were incubated with 25 mg of collagenase per g of tissue and incubated overnight in this project. This is because when rat PTC numbers in Figure 3.4 at day 8 of culture following an overnight or acute incubation were compared, the former produced significantly greater number of viable cells rat PTC ($P < 0.001$).

A limitation of this proximal tubule isolation technique is that the isolated cells are a mixture of proximal and distal tubular cells. Our research group has previously cultured and characterised transporter expression of pure human proximal and distal tubular / collecting duct cell monolayers (Brown *et al.*, 2008). qPCR and immunohistochemistry studies of drug transporter expression found that pure cultures of distal tubule / collecting duct cells lack expression of key drug transport proteins and thus are effectively ‘silent’ in these co-cultures of proximal and distal tubular cells. In addition, pure proximal tubular cell monolayers have very low TEER values. Therefore, to improve cell yield and

monolayer permeability a mixture of proximal and distal tubule cells was used rather than a pure culture of proximal tubule cells. A further constraint is that this isolation technique is not efficient enough to isolate human PTCs from human renal tissue samples weighing less than 2 g. A number of renal cortex resection samples from the nephrology unit of the Freeman hospital were donated to our research cause, but we were unable to obtain cells from the majority of these samples. As shown in Figure 3.5 and Figure 3.6, the weight of renal cortex was positively correlated to the number of isolated PTCs.

Isolated primary cells were then grown on plastic cell cultureware and Transwell® polycarbonate inserts. Growth of cells on polycarbonate inserts with microporous membranes has numerous advantages over solid plastic cell growth platforms. Permeable Transwell® inserts permit cells to take up and secrete molecules on both their basal and apical membranes. This environment is a closer representation of the *in-vivo* environment and thus improves cell polarisation, transporter expression and viability (Fulcher *et al.*, 2005). Cellular functions such as transport, absorption and secretion can also be studied since cells grown on permeable supports provide access to their apical and basolateral plasma membranes.

Cell confluency on plastic cell culture ware was assessed visually using a phase contrast microscope throughout the culture. Due to the opacity of the Transwell® inserts, the confluency of cells grown on 24-well Transwell® inserts was determined by measuring the TEER of the monolayer daily with an epithelial voltohmmeter. TEER is a reliable, quantitative measure of barrier strength. In this instance, TEER was used to indicate the confluency and permeability of the cell monolayers. TEER values of human PTC monolayers up to day 10 of cell culture are shown in Figure 3.7. The findings strongly correlate with the human PTC cell growth curves in Figure 3.3. The lag phase of cell growth characterised by low growth and TEER was from day 1 to 3 of cell culture. After this period of acclimatisation to the new environment, cell numbers and TEER increased exponentially until day 6. Cell growth and resistance plateaued at around 210 000 human PTCs per cm^2 and 120 $\Omega.cm^2$ between day 6 and 8. Then cell number and TEER decreased from day 9 onwards as cell death began. Cell growth and TEER of rat PTCs shown in Figure 3.4 and

Figure 3.8 showed very similar trends. Cell growth and TEER plateaued at 230 000 rat PTCs per cm^2 and 110 $\Omega.cm^2$ from day 6 to 7 of cell culture.

In order to determine the efficiency of TEER as a measure of epithelial cell monolayer permeability, the correlation between TEER and paracellular flux of radiolabelled [1-^{14}C]-mannitol D was studied. Figure 3.10 and Figure 3.11 show an inverse relationship between the two. As human PTC and rat PTC monolayer TEER increased, the paracellular movement of mannitol decreased until it reached a plateau of 12.89 $\pm$ 8.29 pmol / hr / cm^2 and 7.24 $\pm$ 11.05 pmol / hr / cm^2 respectively. In both primary cell culture models there was a mannitol flux of 30 pmol / hr / cm^2 or less when monolayer TEER was greater than 80 $\Omega.cm^2$, which equates to a mannitol paracellular flux of less than 0.01% of the total amount of mannitol used. These results indicate confluent monolayer formation, high tight junction integrity and low paracellular permeability. As a consequence of these findings, only monolayers with a TEER greater than 80 $\Omega.cm^2$ were used in transporter absorption and secretion studies.

The mRNA expression levels of several transporters following incubation on two different cell cultureware materials were analysed by qPCR. Human and rat PTCs cultured on Transwell® inserts and plastic were compared to freshly isolated PTCs. The freshly isolated cells were considered to be representative of the native proximal tubule *in-vivo*. The findings shown in Table 3.1 and Table 3.2 show that human and rat PTCs cultured on both Transwell® inserts and plastic maintained expression of all the key renal transport proteins investigated. Including the basolateral uptake transporters OAT1/Oat1, OAT3, and OCT2/Oct2 commonly absent from immortalised renal epithelial cell lines (Gstraunthaler *et al.*, 1985; Pfaller and Gstraunthaler, 1998; Jenkinson *et al.*, 2012; Jansen *et al.*, 2014). Although there was a significant fall in the expression of most transporters in comparison to freshly isolated cells the expression levels are substantially higher than those seen in any previous *in-vitro* kidney model. Comparison of mRNA drug transporter expression in human and rat PTCs using drug transporter RT^2 profiler array plates in Figure 3.26 and Figure 3.27 showed little expression of non-proximal tubular cell markers. This suggests that proximal tubular cells perdominate the human and rat PTC cell populations.

A limitation of using primary cell cultures is the finite lifespan of the isolated cells. As our results have shown, renal primary cells have a short life span, cell death occurred from day 9 onwards regardless of nutrient availability. A number of preservation techniques were attempted unsuccessfully. For instance, cells were subcultured once confluency was reached. However, many subcultured cells were unable to adhere to the culture vessel, and attached cells failed to proliferate. Isolated proximal-distal cells were also cryopreserved. Cryopreservation involved suspending cells in serum rich medium containing DMSO as a cryoprotectant, then cooling cells to -135 °C. However, upon thawing, the primary cells also failed to attach to the cell culture vessel.

Due to the difficulties of primary cell preservation, primary proximal tubule cells have been immortalised. There are several publications in the literature that highlights the advantages of using the immortalised cells. A good example is that of the renal proximal tubule epithelial cells transfected with TERT1 (RPTEC). However, contradictory to some of the publications, RPTEC monolayers exhibited very low TEER values (Figure 3.9), when compared to human or rat PTCs (Wieser *et al.*, 2008) and high paracellular permeability (Figure 3.12) making if difficult to perform transepithelial studies with this cell line. Furthermore, the cells appear to lose differentiation. mRNA expression of key renal transport proteins were analysed in RPTEC cells. Expression relative to freshly isolated human PTCs is shown in Table 3.1. Transporter mRNA expression in RPTEC was very low in comparison to freshly isolated cells. In all these findings suggest that this cell line may not be a suitable *in-vitro* model of the proximal tubule in this instance.

3.5. Summary

Primary cultures of human and rat PTCs were successfully isolated. The enzymatic digestion phase of the isolation procedure was optimised to improve cell viability. When grown on Transwell® inserts the primary cultures formed confluent monolayers of good tight junction integrity and low paracellular permeability. When mRNA expression of transporters following culture on Transwell® inserts and plastic were compared, human PTCs cultured on Transwell® inserts showed greater expression of many transporters. However,

there was a significant fall in the mRNA expression of most transporters in cultured cells comparison to freshly isolated cells. In comparison, the immortalised human proximal tubule epithelial cell line, RPTEC, failed to form a monolayer with low paracellular permeability and transporter mRNA expression was very low in comparison to freshly isolated cells. Suggesting that primary PTCs are a better *in-vitro* cell model of the proximal tubule for safety pharmacology studies.

4. TFV handling by PTCs

4.1. Background

The previous chapter characterised transporter mRNA expression in human and rat primary PTC monolayers, this chapter expands on this to demonstrate the utility of human and rat PTC monolayers as predictive *in-vitro* models of proximal tubule drug handling with a focus on the proximal tubule handling of TFV. Pharmacokinetic *in-vivo* studies in animals and man had previously shown that the elimination of TFV is a combination of glomerular filtration and tubular secretion (Shaw et al., 1997; Kearney et al., 2004). As such, this molecule was an ideal candidate for use in demonstrating the models as suitable screening platforms for drug transporter and DDI studies by investigating the renal handling of TFV.

TFV is widely prescribed as part of a combination therapy for the treatment of human immunodeficiency 1 (HIV-1) infection in patients 10 years of age and older, and chronic hepatitis B virus (HBV) infection in patients 12 years of age and older (Gilead Sciences, 2015). TFV alone has poor oral bioavailability, due to a negatively charged phosphonate moiety. In order to improve bioavailability it is administered as a pro-drug formulation named tenofovir disoproxil fumarate (TDF, Viread®). In the pro-drug form the two negative charges of the TFV phosphonic group are masked by isopropyloxycarbonyloxymethyl moieties, which increase the lipophilicity of the compound and thus its permeation across membranes (van Gelder *et al.*, 2002). The chemical structure of these molecules can be seen in Figure 4.1.

The enzymatic activation of TDF into its active component is shown in Figure 4.1. TDF is rapidly converted to TFV in the intestine and systemic circulation through esterase hydrolysis (van Gelder *et al.*, 2002). TFV is then di-phosphorylated by adenylate kinase and nucleoside diphosphate kinase to form the active metabolite TFV diphosphate (TFVpp) (Merta *et al.*, 1992; De Clercq and Holy, 2005). TFVpp inhibits the activity of HIV reverse transcriptase by

competing with the natural substrate deoxyadenosine 5'-triphosphate. The incorporation of a molecule of TFVpp at the 3' end causes replication of the viral DNA to cease. TFV can be activated in both living and resting cells to TFVpp (Robbins *et al.*, 1998). TFVpp inhibits HIV replication in macrophages and other non-dividing cells (Kearney *et al.*, 2004). TFVpp is also a weak inhibitor of mammalian DNA polymerases α, β, and mitochondrial DNA polymerase γ (Birkus *et al.*, 2002).

The pharmacokinetics of TDF are dose-proportional, and similar in healthy individuals and HIV-1 infected patients. The oral bioavailability of TFV from TDF is approximately 25 %. Following oral administration of a single 300 mg dose to fasted HIV-1 patients, maximum serum concentrations (C_{max}) are achieved in 1.0 $\pm$ 0.4 hrs. C_{max} and area under the curve (AUC) values are 0.3 $\pm$ 0.1 μg/mL and 2.29 $\pm$ 0.69 μg.h.mL, respectively. Following the achievement of C_{max}, TFV concentration decline in a biphasic manner, with an apparent elimination half-life of 17 hrs. TFV C_{max} and AUC are dose-proportional over a dose range of 75 to 600 mg and unaffected by repeated dosing. *In-vitro* binding studies found that binding of TFV to human plasma or serum proteins is less than 0.7 and 7.2%, respectively, over the TFV concentration range of 0.01 to 0.25 μg/mL. The volume of distribution at steady state is 1.3 $\pm$ 0.6 L/kg. *In-vitro* and *in-vivo* studies indicate that neither TFV nor TDF are substrates, inducers or inhibitors of cytochrome P450 enzymes. Following steady-state dosing, 32 $\pm$ 10 % of the administered dose is recovered in urine over 24 hrs. Studies have shown that the pharmacokinetics of TDF are unaltered by most other antiretroviral agents or by concomitant medications that are frequently prescribed to the HIV-1 infected population. Although clinically important pharmacokinetic interactions do occur with didanosine and atazanavir, adjustment of the dosages of these agents can readily be accomplished using commercially available dosage forms. In HIV-1 infected patients with renal impairment, adjustment of the TDF is warranted and accomplished by extension of the dosage interval. This clinical pharmacology data has been published by the department of pharmacology and pharmacokinetics at Gilead Sciences, Inc (Kearney *et al.*, 2004; Gilead Sciences, 2015).

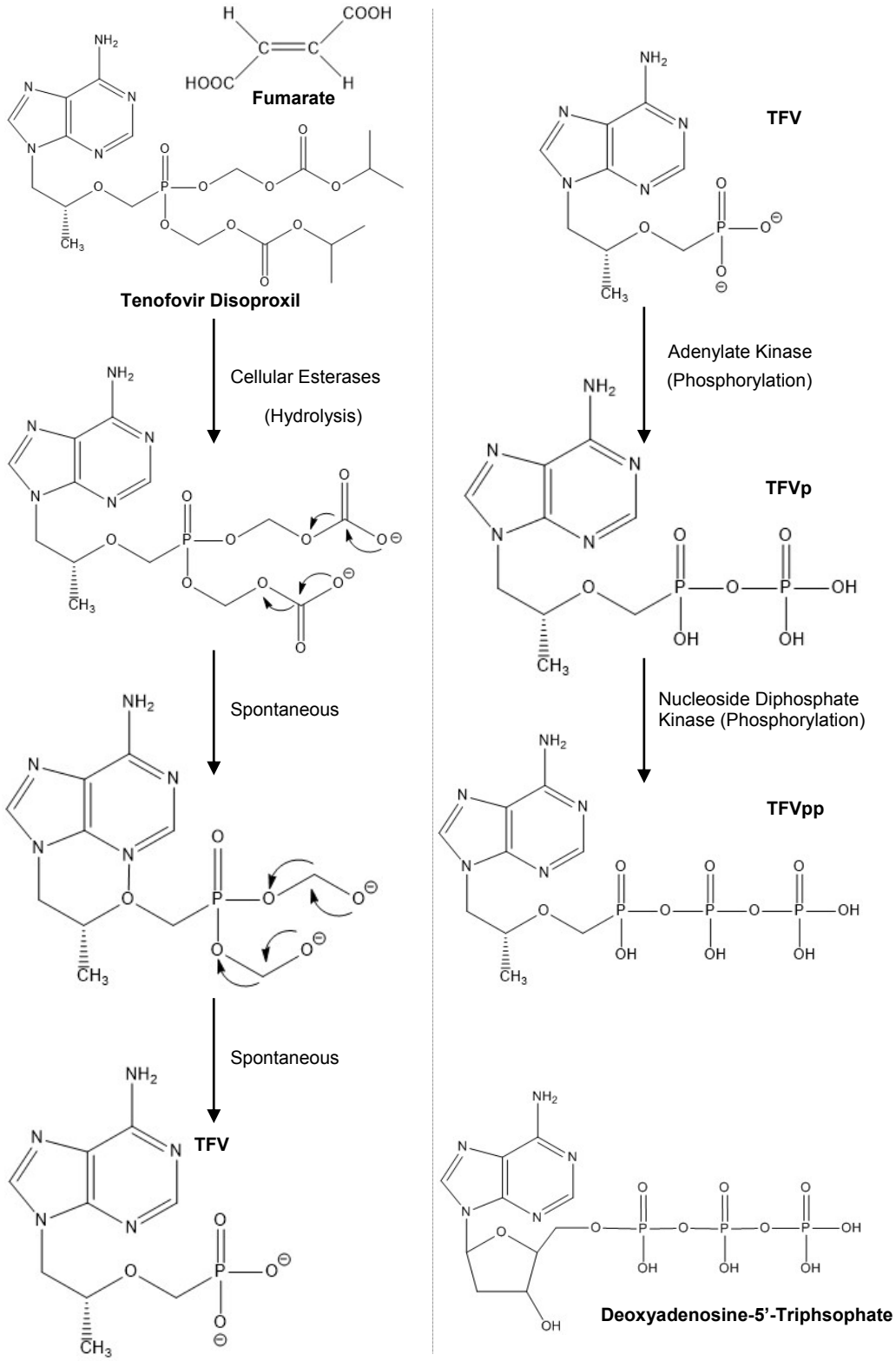

Figure 4.1: The enzymatic activation of TDF into its active component, TFVpp.

Figure created using ChemDraw.

Post-marketing safety data covering 455 392 patient years of TDF exposure showed renal serious adverse events (acute/chronic renal failure, Fanconi syndrome) in only 0.5 % of patients and graded elevations in serum creatinine in 2.2 % of patients (Nelson *et al.*, 2007; Herlitz *et al.*, 2010; Fernandez-Fernandez *et al.*, 2011). Reports of proximal tubule dysfunction, Fanconi syndrome and acute kidney injury associated with TDF have been published in multiple individual case reports and case series. Retrospective histological and ultrastructural studies conducted in renal biopsies have demonstrated a distinctive pattern of proximal tubule injury characterised by severe mitochondrial damage, supporting a mechanism of drug induced-mitochondrial toxicity (Cote *et al.*, 2006; Kohler *et al.*, 2009; Herlitz *et al.*, 2010; Perazella, 2010). Pathology studies indicate that the accumulation of TFV within proximal tubule cells results in host cell toxicity (Kohler *et al.*, 2009; Fernandez-Fernandez *et al.*, 2011; Kohler *et al.*, 2011). At high intracellular concentrations TFV inhibits mitochondrial DNA polymerase γ (Martin *et al.*, 1994; Birkus *et al.*, 2002; Fernandez-Fernandez *et al.*, 2011). As a result, a number of the encoded enzymes involved in the electron transport chain and oxidative phosphorylation become depleted, resulting in disturbed mitochondrial cell function, a deficit in ATP production, impaired cell function, cell injury and apoptosis. This in turn leads to proximal tubular cell death, and endogenous metabolites such as glucose, amino acids, uric acid, phosphate and bicarbonate are passed into the urine instead of being reabsorbed. These manifest as polyuria, glycosuria, proteinuria, hyperuricosuria, hypophosphatemia, osteomalacia, hypokalemia and acidosis in patients. TFV discontinuation has been associated with significant renal recovery, however, many patients may suffer from chronic kidney disease (Herlitz *et al.*, 2010).

The literature proposes the uptake of TFV from the basolateral circulation into epithelial proximal tubule cells is predominantly mediated by OAT1 with minor contribution from OAT3 (Cihlar *et al.*, 1999; Cihlar and Ho, 2000; Ho *et al.*, 2000; Cihlar *et al.*, 2001; Cihlar *et al.*, 2007; Uwai *et al.*, 2007; Mandikova *et al.*, 2013). TFV is then effluxed into the urine through apical transporters MRP2 and MRP4 (Schuetz *et al.*, 1999; Izzedine *et al.*, 2006; Cihlar *et al.*, 2007; Imaoka *et al.*, 2007; Uwai *et al.*, 2007; Mandikova *et al.*, 2013). However, a critique of the current proposition is that these studies were performed in poor renal

experimental models. Heterologous expression of individual renal transporters in expression systems and transfected cells have given crucial information about substrate specificities and the potential for DDIs at the level of an individual transport system. However, there are no studies in physiologically relevant intact cell models to investigate how a plethora of individual transporters combine and integrate to form an efficient secretory pathway. In addition to investigating the renal handling of TFV by primary models, the results from this study may also elucidate the mechanism behind TFV accumlation within the proximal tubules, and validate the use of the models in drug development studies.

4.2. Aims

The aim of this chapter was to demonstrate the utility of human and rat PTC monolayers as predictive *in-vitro* models of proximal tubule drug handling, using TFV as a model substrate.

Firstly, the uptake and flux of [^{3}H]-TFV in human PTC and rat PTC monolayers over time were studied to select a suitable time point to conduct transport experiments under initial rate conditions. Once a time point had been selected, the unidirectional transepithelial fluxes of [^{3}H]-TFV were measured in the secretory and absorptive direction across paired human and rat PTC monolayers. Uptake of [^{3}H]-TFV across the basolateral and apical membrane of human and rat PTC monolayers were also measured. Kinetics parameters such as the maximum rate of [^{3}H]-TFV uptake (V_{max}) and the affinity of [^{3}H]-TFV for PTC uptake transporters (K_m) were determined in both models. Then to identify the transporters responsible for the uptake of TFV across the basolateral membrane, the secretory flux and uptake of [^{3}H]-TFV were measured in the presence of various competitive substrates of basolateral uptake transport. Similarly, the transporters responsible for the efflux of TFV across the apical membrane were characterised by measuring the secretory flux and intracellular accumulation of [^{3}H]-TFV in the presence of various competitive substrates of apical efflux transport proteins.

4.3. Results

4.3.1. Flux and uptake of TFV by human PTC monolayers over time.

In order to ensure the renal handling of TFV was measured under initial rate conditions, the rate of TFV unidirectional fluxes and uptake over time were studied. The secretory and absorptive fluxes of 10 μM [^{3}H]-TFV across human PTC monolayers following 20, 40, and 60 min of exposure were measured. Additionally, the uptake of [^{3}H]-TFV across the basolateral membrane of human PTC monolayers was measured at 15, 30, 45, 60, and 90 min of exposure. Figure 4.2 shows the secretory, absorptive and net fluxes of [^{3}H]-TFV increased linearly between the defined time-points (n = 9, N = 3). Correspondingly, the uptake of [^{3}H]-TFV increased linearly between 0 and 90 min, with a gradient of 0.50 ± 0.01 pmol / cm^2 / min (n = 9, N = 3), as shown in Figure 4.3. We can thus deduce that 0 to 90 min lies within the linear rate of TFV transport, and subsequent experiments of TFV renal handling were performed within the 60-min time point. The non-specific binding of [^{3}H]-TFV to the Transwell® insert was also found to be 0.96 ± 0.11 pmol / cm^2, which was considered to be negligible.

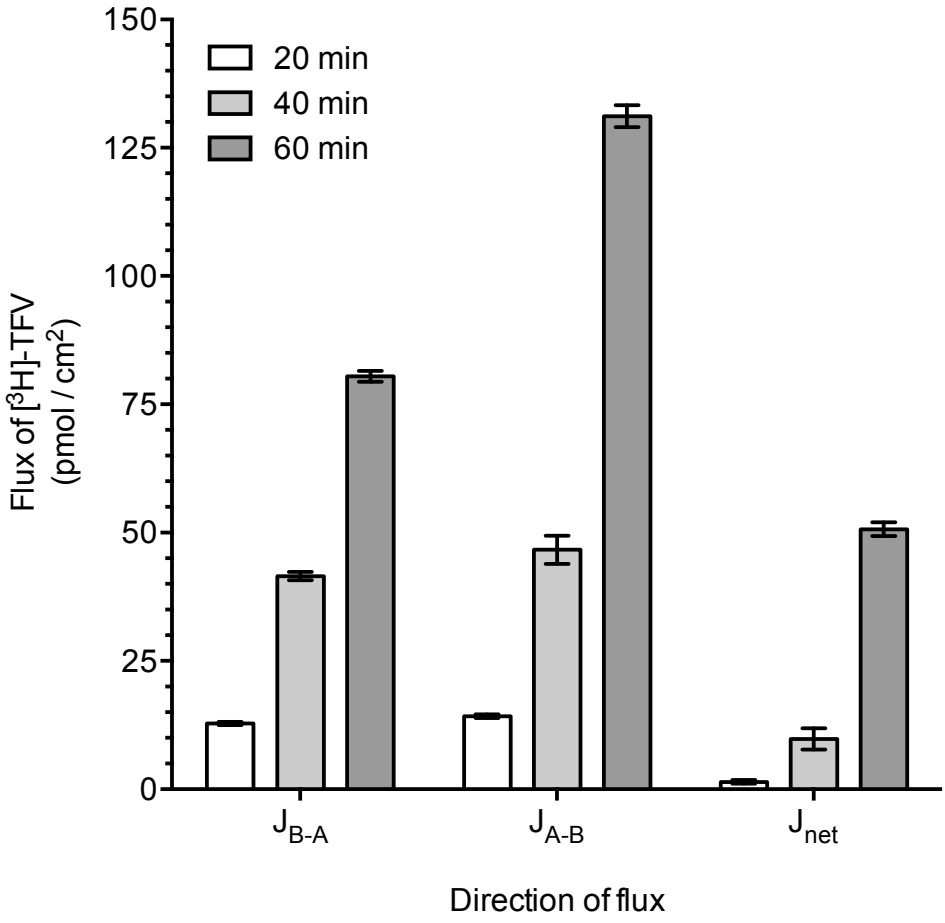

Figure 4.2: Time course of unidirectional fluxes of 10 μM [³H]-TFV across human PTC monolayers.

The fluxes of 10 μM [³H]-TFV across human PTC monolayers over the defined periods of time are shown. The fluxes of [³H]-TFV were within the initial rate period between 0 and 60 min as secretory, absorptive and net fluxes were linear over this time period. The results are expressed as the mean ± SEM from 9 human PTC monolayers derived from 3 individual kidneys.

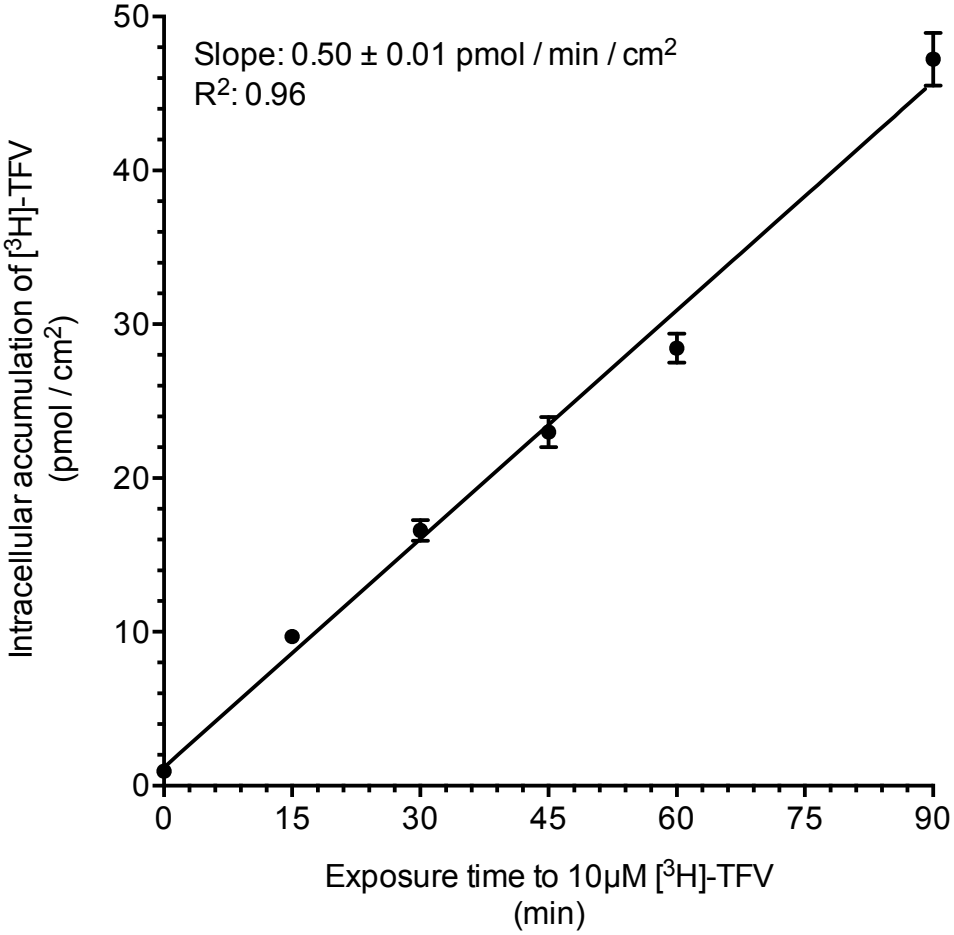

Figure 4.3: Time course of 10 µM [^{3}H]-TFV uptake across the basolateral membrane of human PTC monolayers.

The basolateral membranes of the monolayers were incubated with 10 µM [^{3}H]-TFV for 0, 15, 30, 45, 60 or 90 min. The rate of uptake of [^{3}H]-TFV was linear within the time period investigated. Linear regression analysis of the data gave a slope of 0.50 ± 0.01 pmol / cm^2 / min (R^2: 0.96). The non-specific binding of [^{3}H]-TFV to the Transwell® insert was 0.96 ± 0.11 pmol / cm^2. The results are expressed as the mean ± SEM from 9 human PTC monolayers derived from 3 individual kidneys.

4.3.2. Flux and uptake of TFV by human PTC monolayers.

Unidirectional transepithelial fluxes of 10 μM [^{3}H]-TFV over 60 min in both the secretory (J_{B-A}) and absorptive (J_{A-B}) direction were studied in the human PTC monolayer model. The net flux (J_{net}) was calculated from the difference between the two fluxes. Uptake of TFV across the basolateral or apical membranes were also determined by assaying the amount of intracellular [^{3}H]-TFV accumulated within the human PTC monolayers at the end of the experiment.

Figure 4.4 shows a net absorption of TFV (50.69 ± 1.35 pmol / hr / cm^2) across human PTC monolayers. The absorptive movement of [^{3}H]-TFV (131.16 ± 2.15 pmol / hr / cm^2) was 1.63-fold greater than the secretory movement of [^{3}H]-TFV (80.47 ± 1.00 pmol / hr / cm^2) (**** $P < 0.0001$, $n = 9$, $N = 3$). Figure 4.5 shows the intracellular concentration of [^{3}H]-TFV, which was representative of [^{3}H]-TFV uptake across the basolateral or apical membranes of the human PTC monolayers. [^{3}H]-TFV uptake across the basolateral and apical membrane were 39.09 ± 1.31 pmol / hr / cm^2 and 6.67 ± 0.46 pmol / hr / cm^2, respectively; uptake across the basolateral membrane was 5.86-fold greater than across the apical membrane (**** $P < 0.0001$, $n = 9$, $N = 3$). When cellular uptake was expressed as cell-to-medium ratio, see calculation below, the findings indicated a cell to media ratio greater than 1. Implying TFV is accumulated into the proximal tubule cells across the basolateral membrane.

The cell-to-medium ratio was calculated by dividing the intracellular concentration of TFV (μM) by the concentration of test compound in the transport medium (μM). Assumptions made in this calculation are the height of a proximal tubule epithelial cell is 10 microns i.e. 0.001 cm as measured by transmission electron microscopy (Dorup and Maunsbach, 1997), cell monolayers form a cylinder, and intracellular space does not contain subcellular compartments. These assumptions give ratios which probably substantially underestimate the true accumulation

Volume occupied by a monolayer per 24-well Transwell® insert (surface area 0.33 cm^2) = π.radius^2.height
If radius = 0.32 cm, and height = 0.001 cm,
Volume (per 0.33cm^3)= 0.00032 cm^3 = 0.332 μL

Volume (per cm^3) = 0.332 µL x 3 = 0.996 µL

TFV concentration per cm^3 = 39.09 pmol / cm^3

Intracellular concentration of TFV = 39.09 pmol / 0.996 µL i.e. 39.25 µM

Extracellular concentration of TFV = 10 µM

Cell-to-medium ratio = 39.25 µM ÷ 10 µM = 3.93

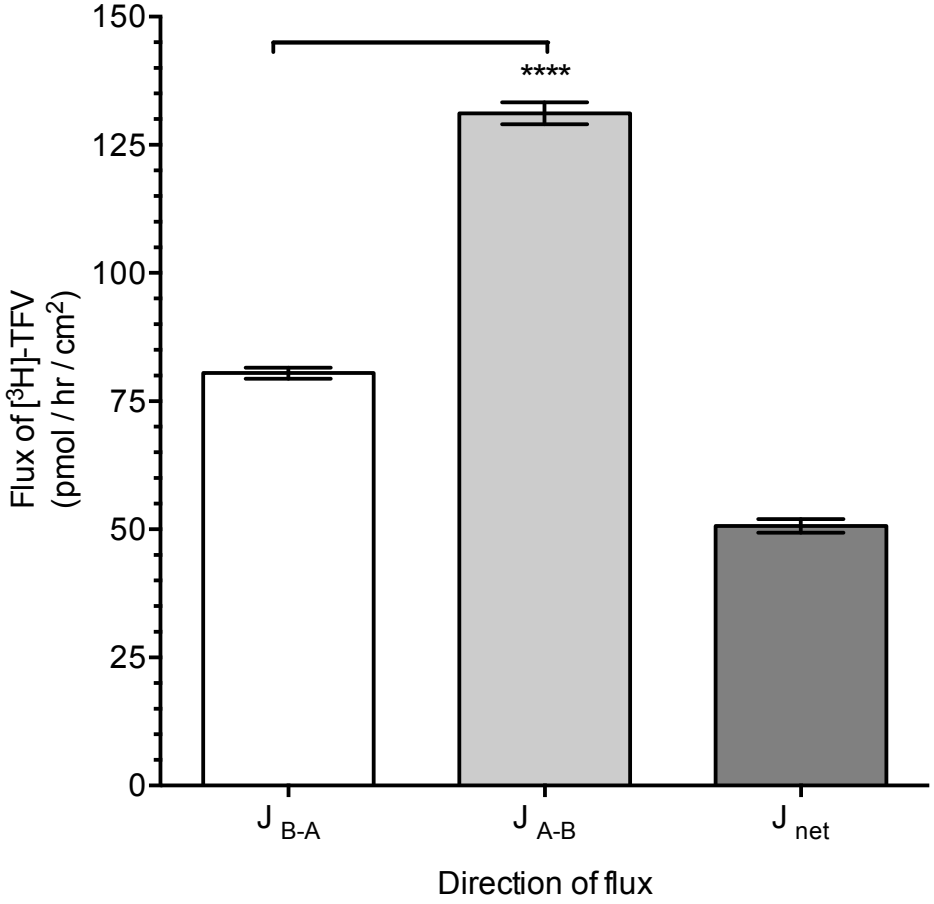

Figure 4.4: Unidirectional fluxes of 10 µM [^{3}H]-TFV by human PTC monolayers.

*In order to determine the secretory and absorptive fluxes of TFV through human PTC monolayers, paired monolayers were incubated with 10 µM [^{3}H]-TFV at either the basolateral or apical chamber. Buffer samples were collected from the opposing chambers after a 60 min incubation period. The amount of [^{3}H]-TFV in each sample was measured using scintillation counting. The results show a net absorptive flux (50.69 ± 1.35 pmol / hr / cm^2). The absorptive movement of [^{3}H]-TFV (131.16 ± 2.15 pmol / hr / cm^2) was 1.63-times greater than the secretory movement (80.47 ± 1.00 pmol / hr / cm^2) (**** P < 0.0001). The results are expressed as the mean ± SEM from 9 human PTC monolayers derived from 3 individual kidneys. Significance was determined by a Student's t-test.*

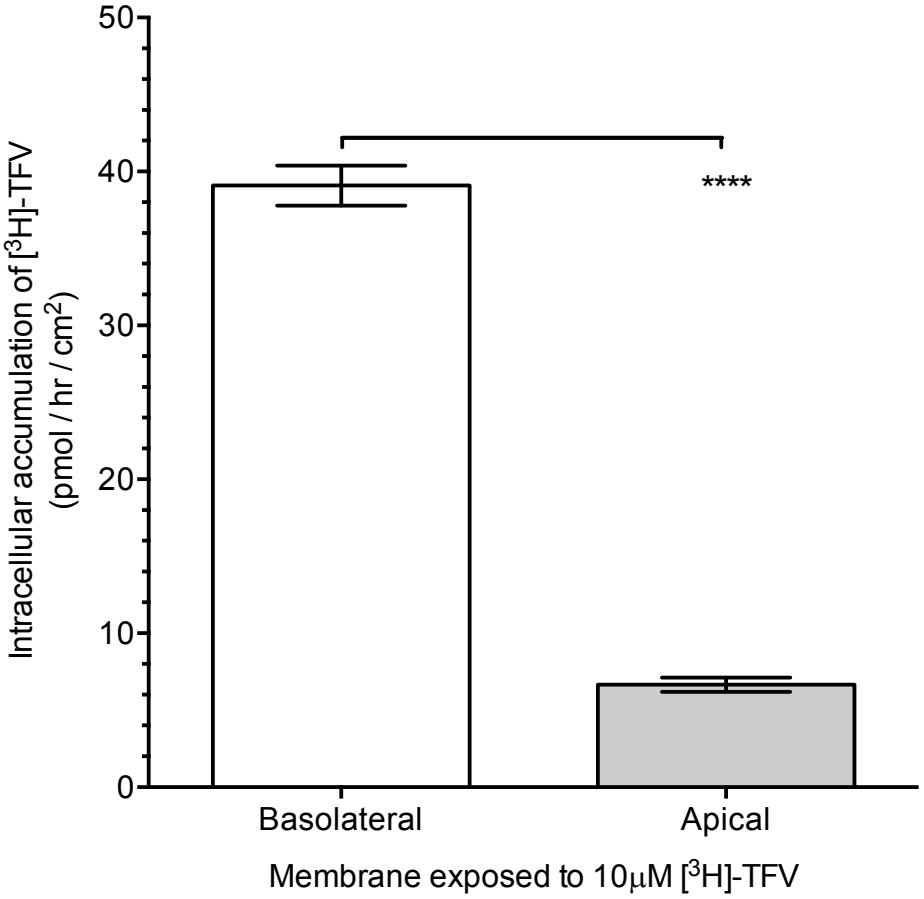

Figure 4.5: Uptake of 10 μM [^{3}H]-TFV across the basolateral and apical membrane of human PTC monolayers.

*Paired monolayers were incubated with 10 μM [^{3}H]-TFV at either the basolateral or apical chamber for 60 min. The data show that the uptake of [^{3}H]-TFV across the basolateral membrane (39.09 ± 1.31 pmol / hr / cm^2) was 5.86-times greater than across the apical membrane (6.67 ± 0.46 pmol / hr / cm^2) (**** P < 0.0001). The results are expressed as the mean ± SEM from 9 human PTC monolayers derived from 3 individual kidneys. Significance was determined by a Student's t-test.*

4.3.3. The effect of pH upon TFV renal handling.

In order to ascertain if pH had an effect upon TFV renal handling, the unidirectional fluxes and uptake of [^{3}H]-TFV by human PTC monolayers at pH 6.80 and 7.40 were compared. The results in Figure 4.6 show pH had no effect upon the secretory, absorptive and thus net movement of [^{3}H]-TFV across human PTC monolayers ($P > 0.05$, $n = 9$, $N = 3$). In accordance with these findings, the data in Figure 4.7 show pH had no effect upon the uptake of [^{3}H]-TFV across the basolateral and apical membrane of human PTC monolayers ($P > 0.05$, $n = 9$, $N = 3$).

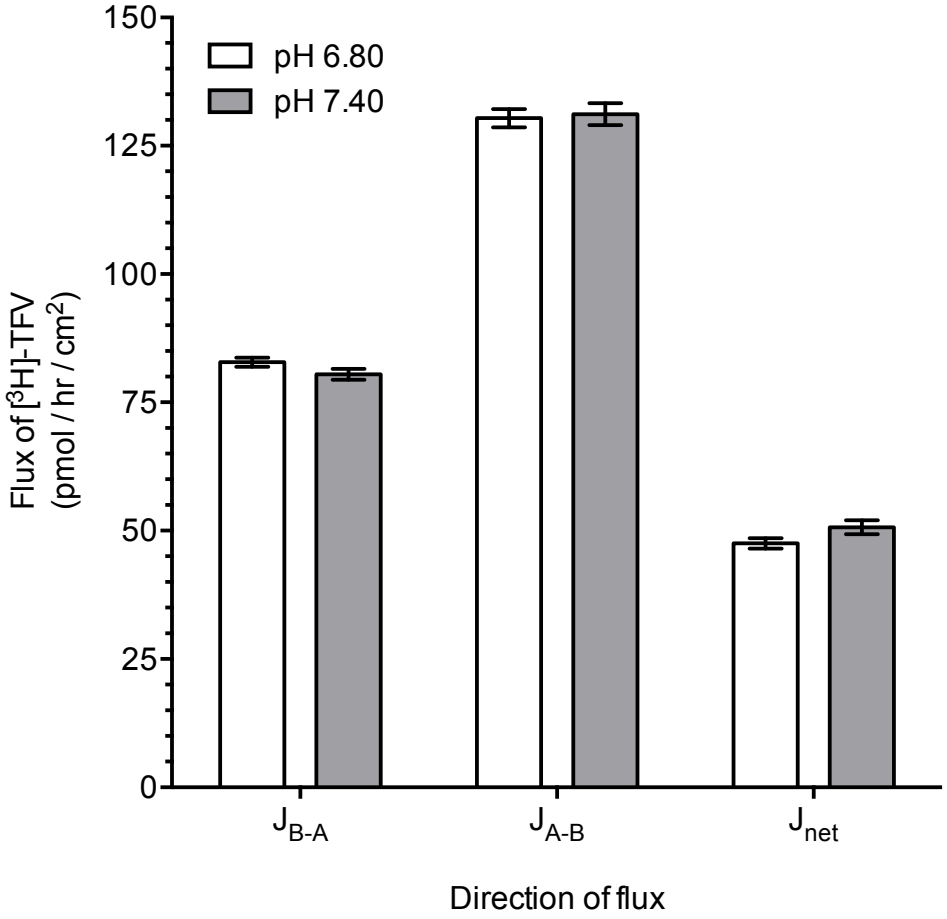

Figure 4.6: Unidirectional fluxes of 10 μM [^{3}H]-TFV at pH 6.80 and 7.40 by human PTC monolayers.

The effects of extracellular pH upon the secretory and absorptive fluxes of TFV by human primary tubular cells were investigated. The results show no significant difference in the secretory flux; 82.83 ± 0.88 pmol / hr / cm^2 at pH 6.80 versus 80.47 ± 1.09 pmol / hr / cm^2 at pH 7.40. Absorptive fluxes of [^{3}H]-TFV at pH 6.8 (130.38 ± 1.79 pmol / hr / cm^2) and at pH 7.4 (131.16 ± 2.15 pmol / hr / cm^2) were also not significantly different. The results are expressed as the mean ± SEM from 9 human PTC monolayers derived from 3 individual kidneys. Significance was determined by a Student's t-test.

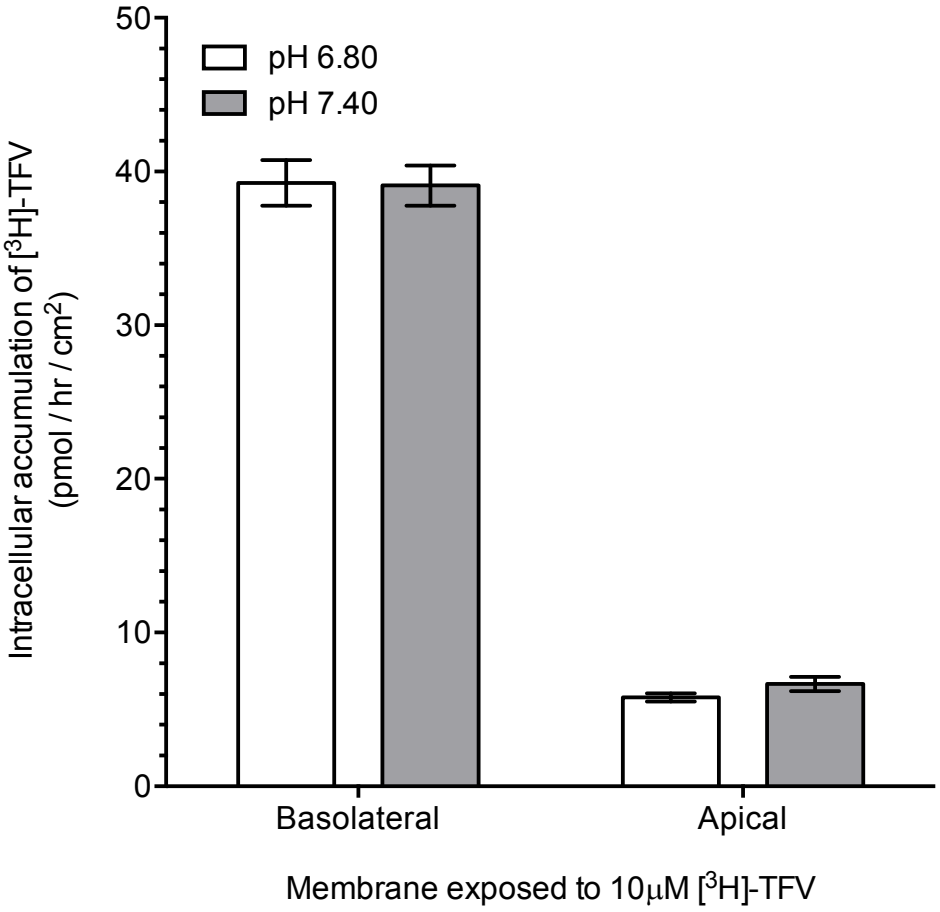

Figure 4.7: Uptake of 10 μM [^{3}H]-TFV across the basolateral and apical membrane of human PTC monolayers at pH 6.80 and 7.40.

The effect of extracellular pH upon the uptake of TFV across the basolateral and apical membrane of human PTC monolayers were investigated. The results show uptake of [^{3}H]-TFV across the basolateral and apical membrane were not affected by extracellular pH. Uptake of [^{3}H]-TFV across the basolateral membrane at pH 6.80 was 39.27 ± 1.48 pmol / hr / cm^2 compared with 39.09 ± 1.31 pmol / hr / cm^2 at pH 7.40, and uptake of [^{3}H]-TFV across the apical membrane at pH 6.80 was 5.78 ± 0.27 pmol / hr / cm^2 compared with 6.67 ± 0.46 pmol / hr / cm^2. The results are expressed as the mean ± SEM from 9 human PTC monolayers derived from 3 individual kidneys. Significance was determined by a Student's t-test.

4.3.4. Kinetics of TFV transport by human PTC monolayers.

The kinetic parameters of TFV transport by human PTC monolayers were calculated. Human PTC monolayers were incubated at the basolateral membrane with various concentrations of [^{3}H]-TFV (1 to 5000 μM) for 60 min and the intracellular accumulation of [^{3}H]-TFV was measured. Figure 4.8 shows the relationship between [^{3}H]-TFV concentration and uptake of [^{3}H]-TFV across the basolateral membrane of human PTC monolayers (n = 9, N = 3). Non-linear regression analysis of the data gave a V_{max} of 1214.11 ± 134.57 pmol / hr / cm^2 and an apparent K_m value of 756.86 ± 166.48 μM.

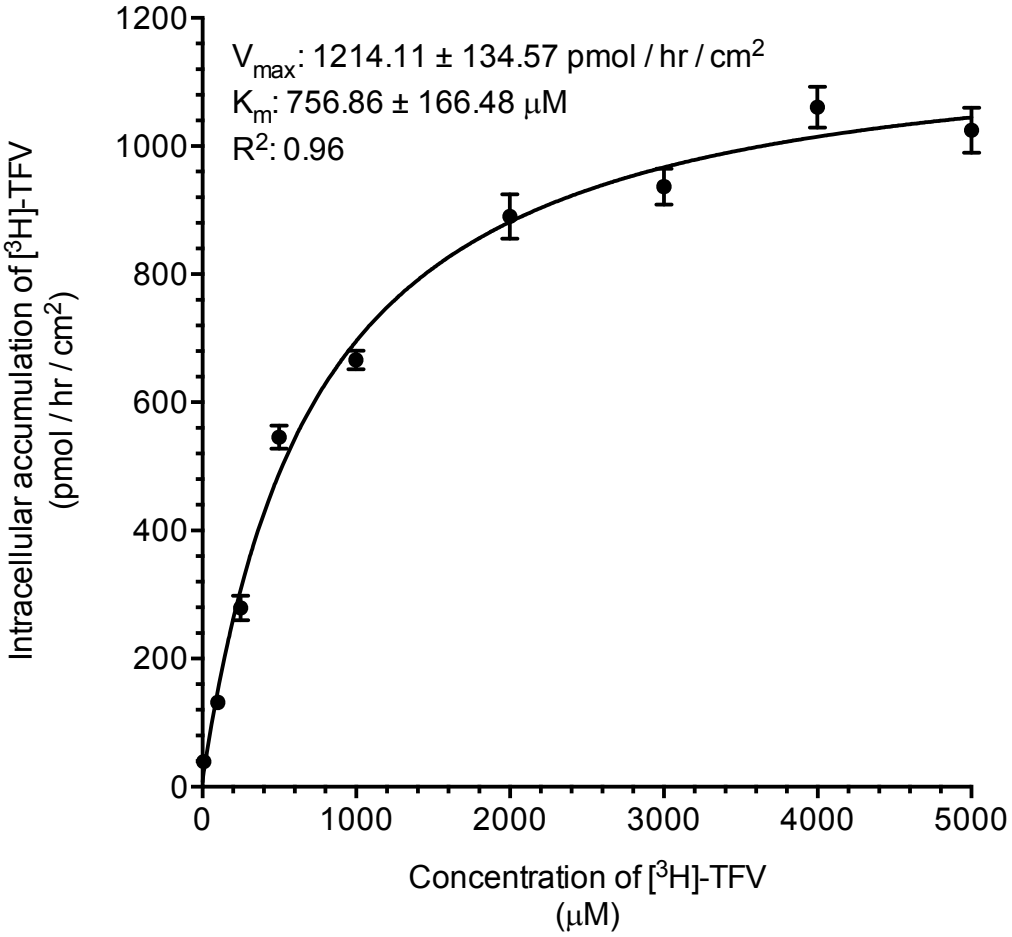

Figure 4.8: Kinetic data on [^{3}H]-TFV uptake across the basolateral membrane of human PTC monolayers under initial rate conditions.

In order to obtain kinetic data on TFV uptake under initial rate conditions, the monolayers were incubated with a range of [^{3}H]-TFV concentrations (1 to 5000 μM) for 60 min. Non-linear regression analysis of the data gave a V_{max} of 1214.11 ± 134.57 pmol / hr / cm^2 and an apparent K_m value of 756.86 ± 166.48 μM. The results are expressed as the mean ± SEM from 9 human PTC monolayers derived from 3 individual kidneys.

4.3.5. Identifying the transporters mediating the uptake of TFV across the basolateral membrane of human PTC monolayers.

The contributions of various uptake transport proteins in the tubular handling of TFV were quantified by measuring unidirectional fluxes and uptake of 10 μM [^{3}H]-TFV in the presence and absence of various competitive substrates of uptake transport proteins. A schematic of this technique is shown in Figure 4.9. The inhibitors were added at concentrations that would as selectively as possible inhibit the activity of transporters that were expected to be involved in the uptake of TFV. Table 4.1 shows the competitive substrates and their affinity values (K_m) for the corresponding transporter(s).

The effect of competitive substrates on the secretory and absorptive fluxes of [^{3}H]-TFV by human PTC monolayers is shown in Figure 4.10 (n = 9, N = 3). The presence of 50 μM PAH, an OAT1 and OAT3 substrate, reduced [^{3}H]-TFV secretory flux by 27.64 ± 1.69 % of control (**** P < 0.0001), whilst the presence of the OAT3 substrate rosuvastatin (RSV, 20 μM) had no significant effect (P > 0.05). The presence of the OATP4C1 substrates triiodothyronine (T3, 10μM) and chenodeoxycholic acid (CDC, 10μM) also resulted in a marked decrease in [^{3}H]-TFV secretory flux (69.26 ± 1.33 % **** P < 0.0001 and 74.34 ± 0.99 % **** P < 0.0001, respectively). The presence of the competitive substrates had no effect on absorptive flux (P > 0.05).

Figure 4.11 shows the effect of competitive substrates on the uptake of [^{3}H]-TFV across the basolateral and apical membrane of human PTC monolayers (n = 9, N = 3). The presence of 50 μM PAH reduced [^{3}H]-TFV uptake across the basolateral membrane by 23.11 ± 1.10 % of control (**** P < 0.0001), whilst 20 μM RSV had no effect (P > 0.05). The presence 10 μM T3 and 10 μM CDC decreased basolateral [^{3}H]-TFV uptake by 74.47 ± 1.90 % of control (**** P < 0.0001) and 81.92 ± 2.07 % (**** P < 0.0001), respectively. The presence of the competitive substrates had no effect on apical uptake of TFV. In agreement with the flux experimental data, these results suggest both OATP4C1 and OAT1 mediate the initial uptake of TFV across the basolateral membrane in TFV renal secretion.

A substantial role for OATP4C1 in the basolateral uptake of TFV had not previously been reported. In order to determine if the apparent important role for OATP4C1 resulted from a loss of OAT1 and OAT3 expression and function as the cells were maintained in culture, the inhibition study was repeated in freshly isolated human PTCs. The results are shown in Figure 4.12 (n = 9, N = 3). In corroboration with the previous findings, 50 µM PAH, 10 µM T3 and 10 µM CDC reduced TFV uptake by 18.16 ± 0.84 % (**** P < 0.0001), 57.25 ± 2.19 % (**** P < 0.0001) and 44.64 ± 2.02 % of control (**** P < 0.0001), respectively. Additionally , a role of OCTs in the basolateral uptake of TFV was ruled out as the presence of 1.5 mM cimetidine (CIM, OCT2 substrate) had no effect on the uptake of [^{3}H]-TFV across the basolateral membrane of human PTC cells.

In Figure 4.13 the uptake of [^{3}H]-TFV in (a) fresh and (b) cultured human PTC monolayers is compared. The results are normalised to uptake per 300 000 cells. The data show that uptake of 10 µM [^{3}H]-TFV in the cells cultured for 7-days on Transwell® inserts was around 20% of that in freshly isolated cells (19.81 ± 0.79 pmol / hr / 300 000 cells v 89.35 ± 2.30 pmol / hr / 300 000 cells). The presence of 50 µM PAH reduced [^{3}H]-TFV accumulation by 18.16 ± 0.84 % in freshly isolated cells and 23.11 ± 1.10 % in cultured cells, which suggests a similar contribution of OATs. In contrast, the presence of 10 µM T3 and CDC reduced [^{3}H]-TFV uptake by 57.25 ± 2.19 % and 44.64 ± 2.02 % in freshly isolated cells, respectively, and by 74.47 ± 1.90 % and 81.92 ± 2.07 % in cultured cells, respectively.

The identification of OATP4C1 as a transporter of TFV is novel. This important discovery can be used to identify potentially toxic DDIs.

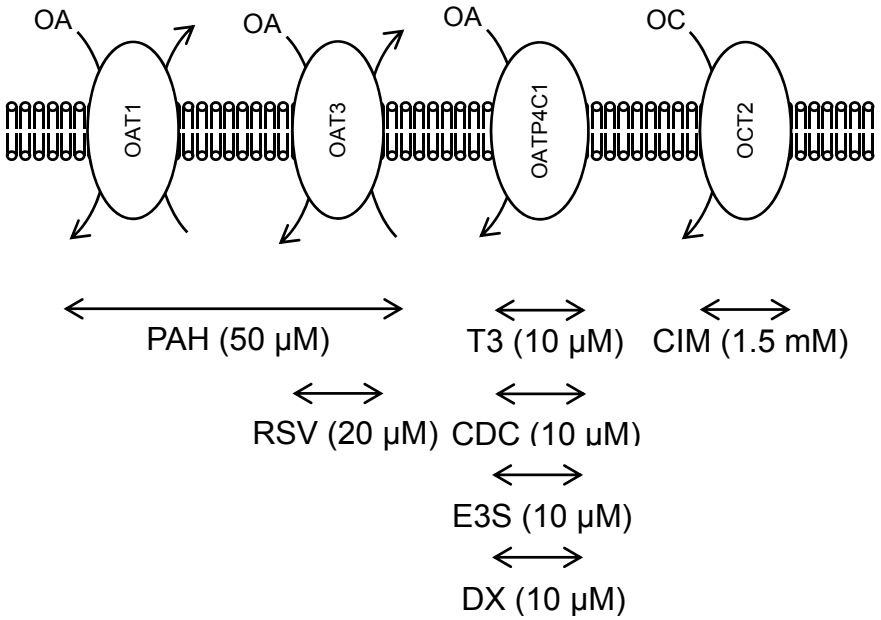

Figure 4.9: Substrate inhibition scheme to determine the contributions of OAT1, OAT3, OATP4C1 and OCT2 to TFV uptake and flux in human and rat PTC monolayers.

Substrate	Transporter	System	K_m (µM)	Reference
PAH	hOAT1	*X.Laevis* oocytes	9.3 ± 1.0	(Hosoyamada *et al.*, 1999)
PAH	hOAT3	*X.Laevis* oocytes	87.2 ± 11.1	(Cha *et al.*, 2001)
RSV	hOAT3	*X.Laevis* oocytes	7.4 ± 2.5	(Windass *et al.*, 2007)
T3	hOATP4C1	MDCK	5.9 ± 2.1	(Mikkaichi *et al.*, 2004)
CDC	hOATP4C1	–	–	(Yamaguchi *et al.*, 2010)
CIM	hOCT2	HEK293	72.6 ± 13.9	(Tahara *et al.*, 2005)

Table 4.1: Competitive substrates used to identify transporters mediating the uptake of TFV.

Listed are competitive substrate of hOAT1, hOAT3 and hOATP4C1. The apparent affinity (K_m) values of the substrates for transporters are shown.

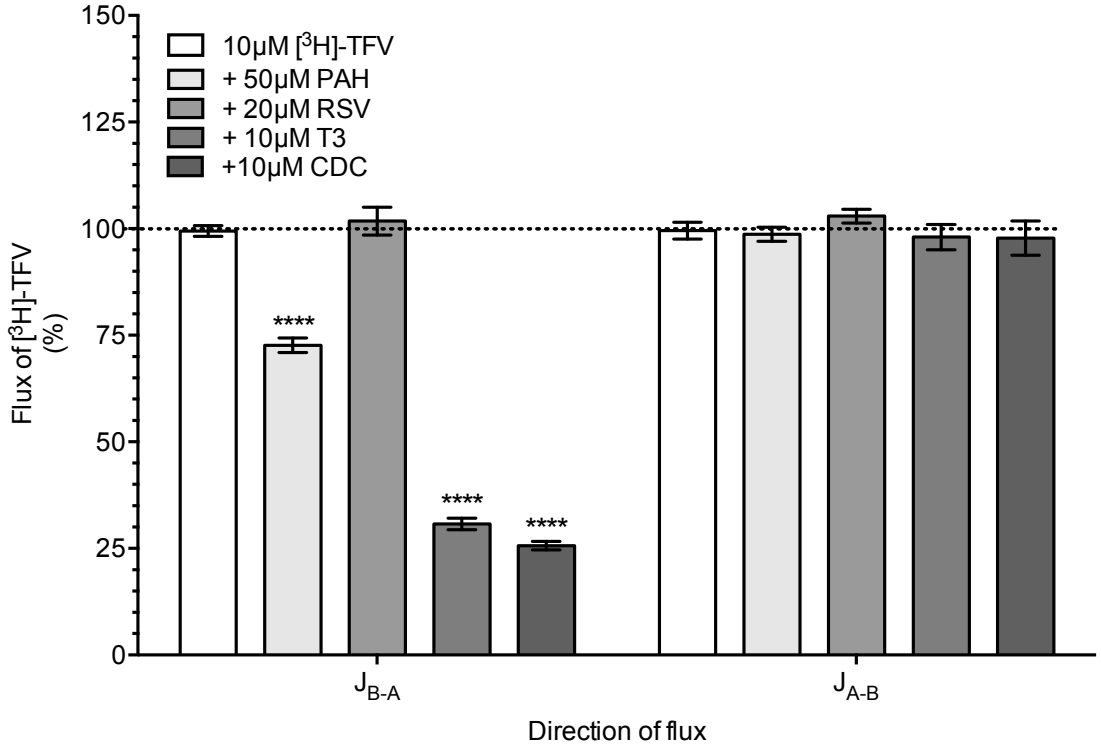

Figure 4.10: Identifying the transporters mediating the uptake of TFV in the unidirectional fluxes of [^{3}H]-TFV across the human PTC monolayer.

*The secretory and absorptive fluxes of 10 μM [^{3}H]-TFV were measured in the presence of various competitive substrates of uptake transport proteins. The presence of 50 μM PAH reduced [^{3}H]-TFV secretory flux (27.64 ± 1.69 %, **** P < 0.0001), whilst 20 μM RSV had no effect. The presence of T3 (10 μM, substrate of OATP4C1) and CDC (10 μM, substrate of OAT1) also resulted in a marked decrease in [^{3}H]-TFV tubular secretion (69.26 ± 1.33 % **** P < 0.0001 and 74.34 ± 0.99 % **** P < 0.0001, respectively). The presence of the competitive substrates had no effect on absorptive flux. These findings suggest both OATP4C1 and OAT1 mediate the uptake of TFV across the basolateral membrane. The results are expressed as the mean ± SEM from 9 human PTC monolayers derived from 3 individual kidneys. Significance was determined using ANOVA and a Dunnett's post-test.*

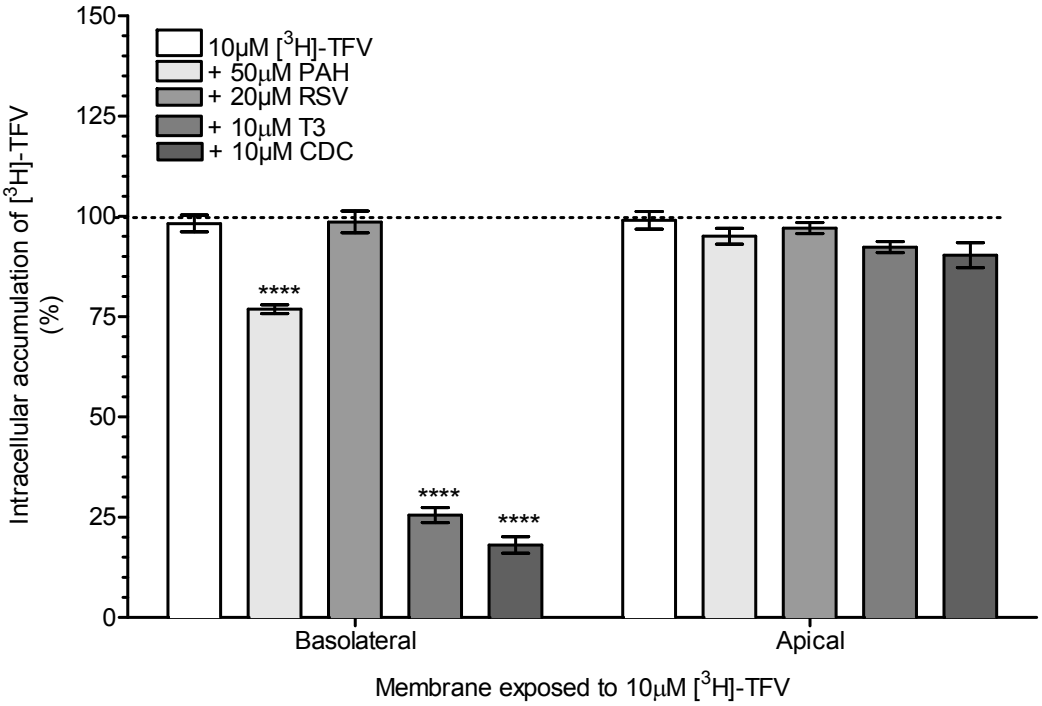

Figure 4.11: Identifying the transporters mediating the uptake of [³H]-TFV in to human PTC monolayers.

*Uptake of 10 μM [³H]-TFV was measured across either the apical or basolateral membrane in the presence of various competitive substrates of uptake transport proteins. The presence of 50 μM PAH reduced [³H]-TFV uptake across the basolateral membrane (23.11 ± 1.10 % decrease, **** P < 0.0001), whilst 20 μM RSV had no effect. The presence of 10 μM T3 and CDC also resulted in a marked decrease in [³H]-TFV basolateral uptake (74.47 ± 1.90 % **** P < 0.0001 and 81.92 ± 2.07 % **** P < 0.0001, respectively). The presence of the competitive substrates had no effect on apical uptake of TFV. These findings suggest both OATP4C1 and OAT1 mediate the basolateral uptake of TFV in the tubular secretion. The results are expressed as the mean ± SEM from 9 human PTC monolayers derived from 3 individual kidneys. Significance was determined using ANOVA and a Dunnett's post-test.*

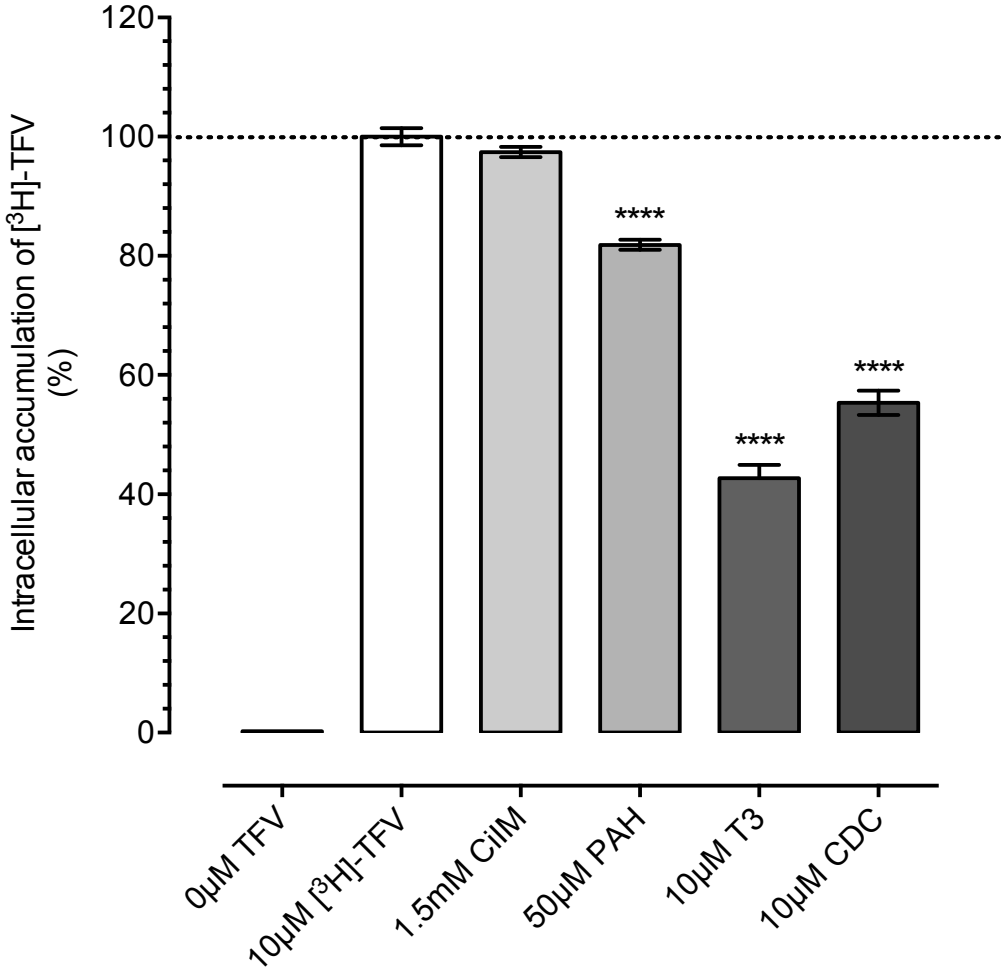

Figure 4.12: Identifying the transporters mediating the uptake of [^{3}H]-TFV in freshly isolated human PTCs.

*The presence of 1.5 mM CIM (OCT2 substrate) had no effect on intracellular accumulation of [^{3}H]-TFV. 50 μM PAH reduced [^{3}H]-TFV accumulation by 18.16 ± 0.84 % of control (**** P < 0.0001). The presence of 10 μM T3 and 10 μM CDC reduced [^{3}H]-TFV uptake to 57.25 ± 2.19 % (**** P < 0.0001) and 44.64 ± 2.02 % of control (**** P < 0.0001), respectively. These findings suggest both OATP4C1 and OAT1 mediate the uptake of TFV across the basolateral membrane in the tubular secretion of TFV in freshly isolate human PTCs. The results are expressed as the mean ± SEM from 9 human PTCs samples derived from 3 individual kidneys. Significance was determined using ANOVA and a Dunnett's post-test.*

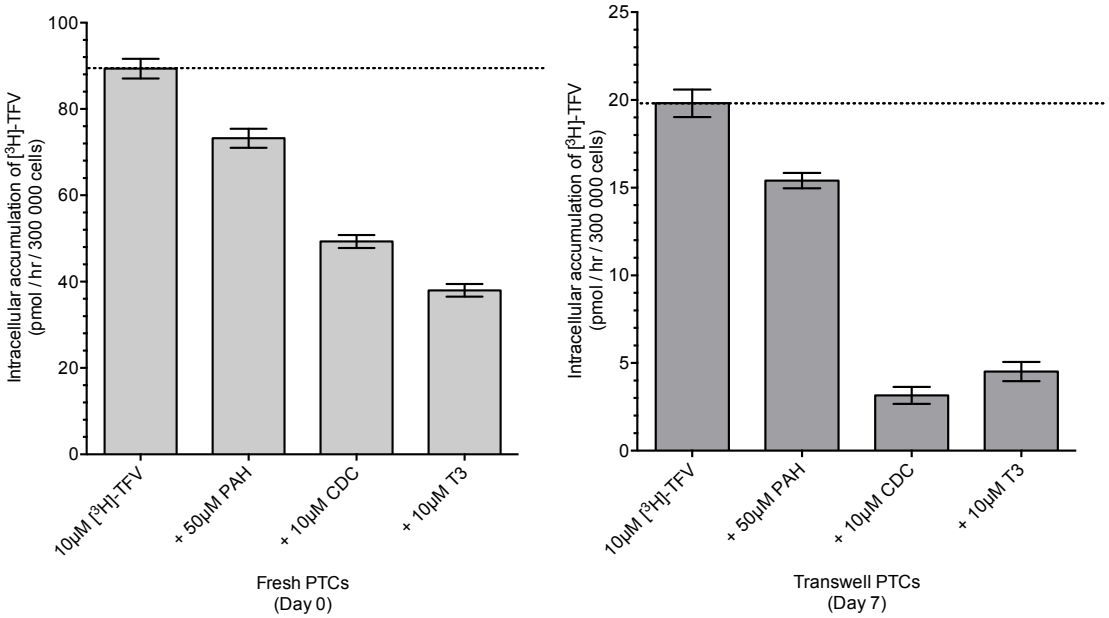

Figure 4.13: A comparison of the uptake of [^{3}H]-TFV in 300 000 (a) fresh and (b) cultured human PTC monolayers.

The uptake of 10 μM [^{3}H]-TFV was 4.51-fold lower in the cells cultured for 7-days on Transwell® inserts (19.81 ± 0.79 pmol / hr / 300 000 cells) when compared to freshly isolated cells (89.35 ± 2.30 pmol / hr / 300 000 cells). 50 µM PAH reduced [^{3}H]-TFV accumulation by 18.16 ± 0.84 % in freshly isolated cells and 23.11 ± 1.10 % in cultured cells. 10 µM T3 reduced [^{3}H]-TFV accumulation by 57.25 ± 2.19 % in freshly isolated cells and 74.47 ± 1.90 % in cultured cells. 10 µM CDC reduced [^{3}H]-TFV accumulation by 44.64 ± 2.02 % in freshly isolated cells and 81.92 ± 2.07 % in cultured cells. The results are expressed as the mean ± SEM from 9 human PTCs samples derived from 3 individual kidneys.

4.3.6. Transport of TFV mediated by OATP4C1

OATP4C1 is known to possess multiple substrate recognition sites. So far, two distinct recognition sites for DX and E3S have been characterised. The affinity values (K_m) of these substrates for OATP4C1 are listed in

Substrate	Transporter	System	Km (μM)	Reference
E3S	hOATP4C1	MDCK	26.6 ± 4.9	(Yamaguchi *et al.*, 2010)
DX	hOATP4C1	MDCK	7.8 ± 2.0	(Mikkaichi *et al.*, 2004)

Table 4.2. In order to determine if TFV binds to the same recognition site as DX or E3S, the basolateral uptake of 10 μM [^{3}H]-TFV across human PTC monolayers in the presence of various concentrations of DX and E3S (0.1 to 50 μM) were measured.

The uptake of 10 μM [^{3}H]-TFV across the basolateral membrane of human PTC monolayers in the presence of various concentrations of E3S and DX are shown in Figure 4.14 (n = 9, N = 3). At concentrations of 1 μM DX and greater, basolateral uptake of TFV was significantly inhibited, whilst concentrations of 10 μM E3S and greater significantly inhibited uptake. Non-linear regression analysis of the data suggested that DX and E3S are only able to bind one binding site. With apparent IC_{50} values of 0.38 ± 0.10 μM for DX and 1198 μM for E3S. These findings indicate that TFV has a higher affinity for the DX recognition site compared with the E3S recognition site.

Substrate	Transporter	System	K_m (μM)	Reference
E3S	hOATP4C1	MDCK	26.6 ± 4.9	(Yamaguchi *et al.*, 2010)
DX	hOATP4C1	MDCK	7.8 ± 2.0	(Mikkaichi *et al.*, 2004)

Table 4.2: Competitive substrates used to identify which hOATP4C1 recognition site mediates the uptake of TFV.

Two distinct recognition sites of hOATP4C1 have been identified using E3S and DX. The affinity values (K_m) of these substrates for OATP4C1 are listed.

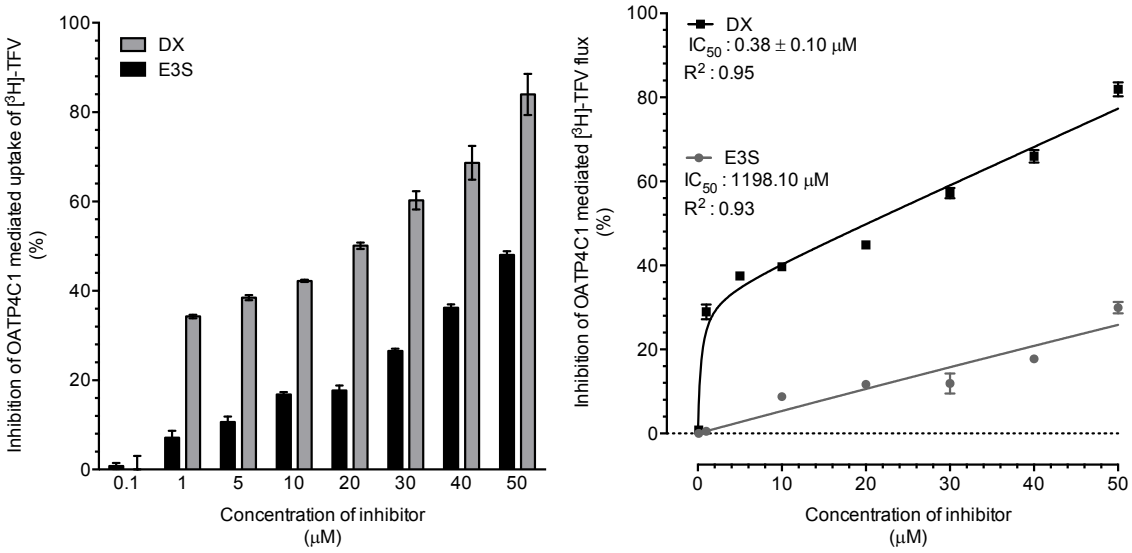

Figure 4.14: Identifying the recognition site of OATP4C1 mediating the uptake of [^{3}H]-TFV across the basolateral membrane of human PTC monolayers.

To identify which substrate recognition site of OATP4C1 TFV binds, basolateral uptake of 10 μM [^{3}H]-TFV in the presence various concentrations (0.1 to 50 μM) of E3S and DX was measured. DX inhibition of [^{3}H]-TFV uptake was greater than E3S inhibition at each concentration. Non-linear regression analysis of the data suggested that DX and E3S are only able to bind one binding site, with apparent IC_{50} values of 0.38 ± 0.10 μM for DX and 1198 μM for E3S. These findings indicate that TFV has a higher affinity for the DX recognition site compared with the E3S binding site. The results are expressed as the mean ± SEM from 9 human PTC monolayers derived from 3 individual kidneys.

4.3.7. Identifying the transporters mediating the efflux of TFV across the apical membrane of human PTC monolayers.

The contributions of various efflux transport proteins in the tubular handling of TFV were characterised by measuring unidirectional fluxes and intracellular concentrations of [^{3}H]-TFV in the presence and absence of various inhibitors of apical efflux transport proteins. A schematic of this technique is shown in Figure 4.15. The inhibitors were added at concentrations that would selectively inhibit the activity of transporters. Reported IC_{50} values for the inhibitors are shown in Table 4.3.

The effect of efflux transport protein inhibitors on the secretory and absorptive fluxes of [^{3}H]-TFV across human PTC monolayers are shown in Figure 4.16 (n = 9, N = 3). The presence of the MRP2/MRP4 inhibitor MK-571 (5 μM), BCRP inhibitor Ko 143 (2 μM), and MDR1 inhibitor GF120918 (5 μM) had no effect on the secretory and absorptive fluxes of 10 μM [^{3}H]-TFV. Similarly, these compounds had no effect on the intracellular accumulation of 10 μM [^{3}H]-TFV, as shown in Figure 4.17 (n = 9, N = 3). These findings imply that TFV has a low affinity for MRP2, MRP4, BCRP, and MDR1 under physiological conditions.

In order to determine if the poor affinity of TFV for efflux transport proteins resulted from a loss of MRP2, MRP4, MDR1 or BCRP expression in culture, the functionality of MRPs, MDR1, and BCRP, in cultured human PTCs were investigated. H33342 is a fluorescent substrate of MDR1 and BCRP. Figure 4.18 shows the presence of the BCRP inhibitor Ko 143 (2 μM) and MDR1 inhibitor GF120918 (2 μM) increased human PTC intracellular retention of H33342 2.11-fold (**** $P < 0.0001$) and 1.43-fold (**** $P < 0.0001$), respectively. The CMFDA metabolite GSMF is a fluorescent substrate of MRPs. Figure 4.19 shows the presence of the MRP inhibitor MK-571 (5 μM) increased the intracellular retention of GSMF 2.39-fold (**** $P < 0.0001$). This information confirms functional expression of BCRP, MDR1 and the MRP transport family in human PTCs.

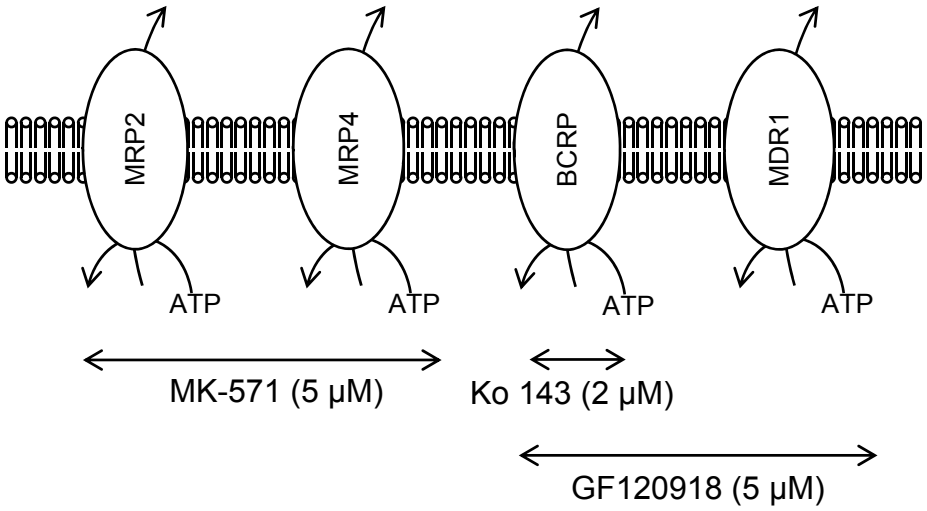

Figure 4.15: Substrate inhibition scheme to determine the contributions of MRP2, MRP4, BCRP and MDR1 to TFV efflux and flux in human and rat PTC monolayers.

Inhibitor	Transporter	System	Substrate	IC_{50} (µM)	Reference
MK-571	hMRP2	Caco-2	IRT	50.0	(Luo *et al.*, 2002)
MK-571	hMRP4	HEK293 vesicles	PMEA	10	(Reid *et al.*, 2003)
Ko 143	hBCRP	MDCK-II	PH-A	0.01	(Weiss *et al.*, 2007)
GF120918	hBCRP	HEK293	MT	0.31	(Ahmed-Belkacem *et al.*, 2005)
GF120918	hMDR1	MDCK-II	DX	0.18	(Keogh and Kunta, 2006)

Table 4.3: Inhibitors used to characterise the efflux pathway of TFV in human PTC monolayers.

Listed are inhibitors of MRP2, MRP4, BCRP and MDR1 used to characterise efflux transport of TFV. Reported IC_{50} values for the inhibitors are shown. Acronyms – IRT: Irinotecan, PMEA: para-methoxyethylamphetamine, PH-A: Phenophorbide, MT: mitoxantrone

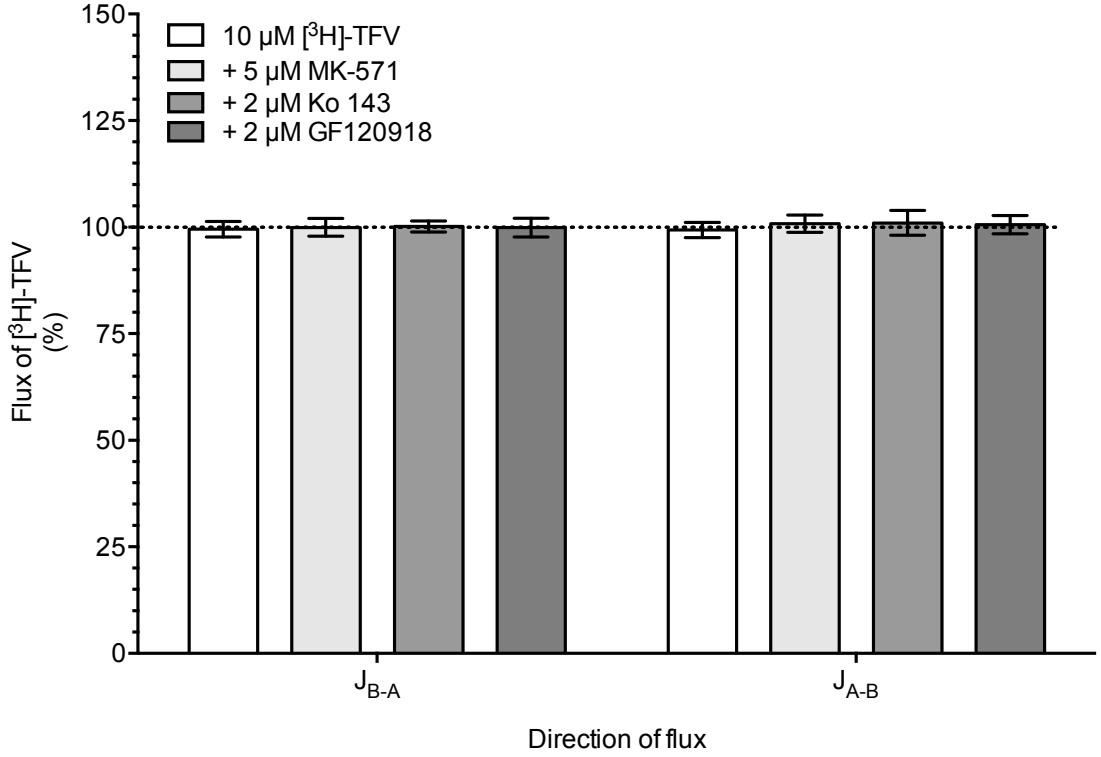

Figure 4.16: Identifying the transporters mediating the efflux of TFV in [^{3}H]-TFV flux across the human PTC monolayer.

Secretory and absorptive fluxes of 10 μM [^{3}H]-TFV were measured in the presence of various competitive substrates of apical efflux transport proteins. The presence of 5 µM MK-571, 2 µM Ko 143, and 2 µM GF120918 had no effect on the secretory flux of [^{3}H]-TFV. This indicates that TFV has a low affinity for MRP2, MRP4, BCRP, and MDR1 under physiological conditions. The presence of the competitive substrates also had no effect on absorptive flux. The results are expressed as the mean ± SEM from 9 human PTC monolayers derived from 3 individual kidneys Significance was determined using ANOVA and a Dunnett's post-test.

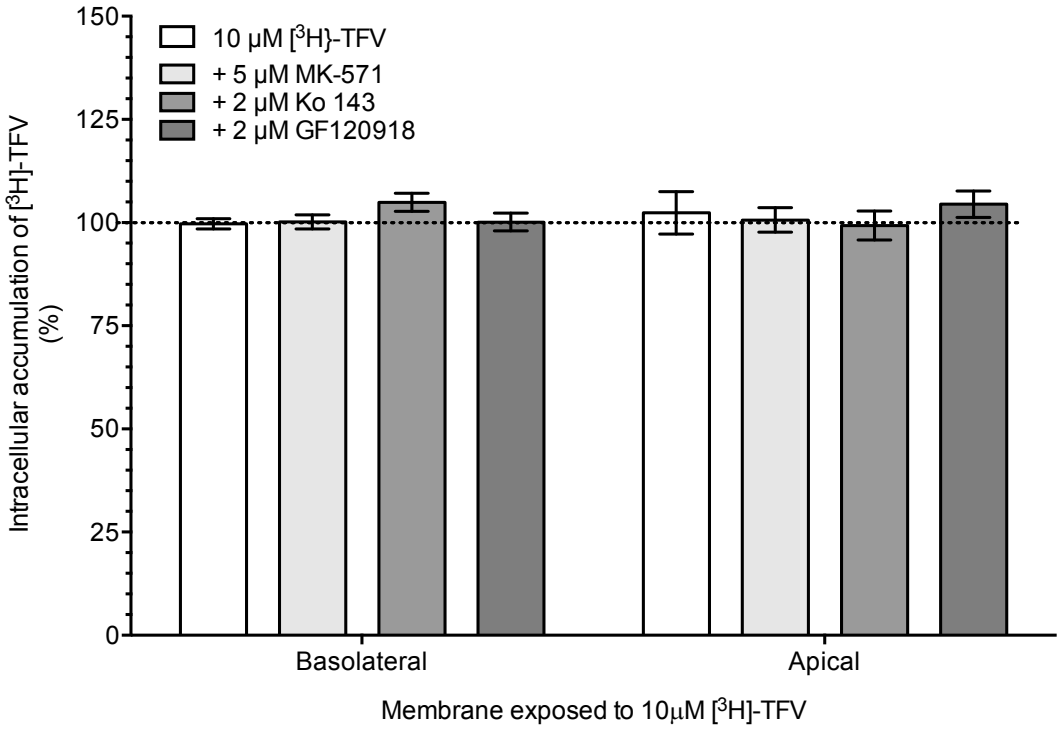

Figure 4.17: Identifying the transporters mediating the efflux of [^{3}H]-TFV from the human PTC monolayer.

Intracellular accumulation of [^{3}H]-TFV by the monolayers was measured in the presence of various competitive substrates of apical efflux transport proteins. The presence of 5 µM MK-571, 2 µM Ko 143, and 2 µM GF120918 at both the apical and basolateral membrane had no effect on the intracellular concentration of [^{3}H]-TFV. This suggests TFV has a low affinity for MRP2, MRP4, BCRP, and MDR1 under physiological conditions. The results are expressed as the mean ± SEM from 9 human PTC monolayers derived from 3 individual kidneys. Significance was determined using ANOVA and a Dunnett's post-test.

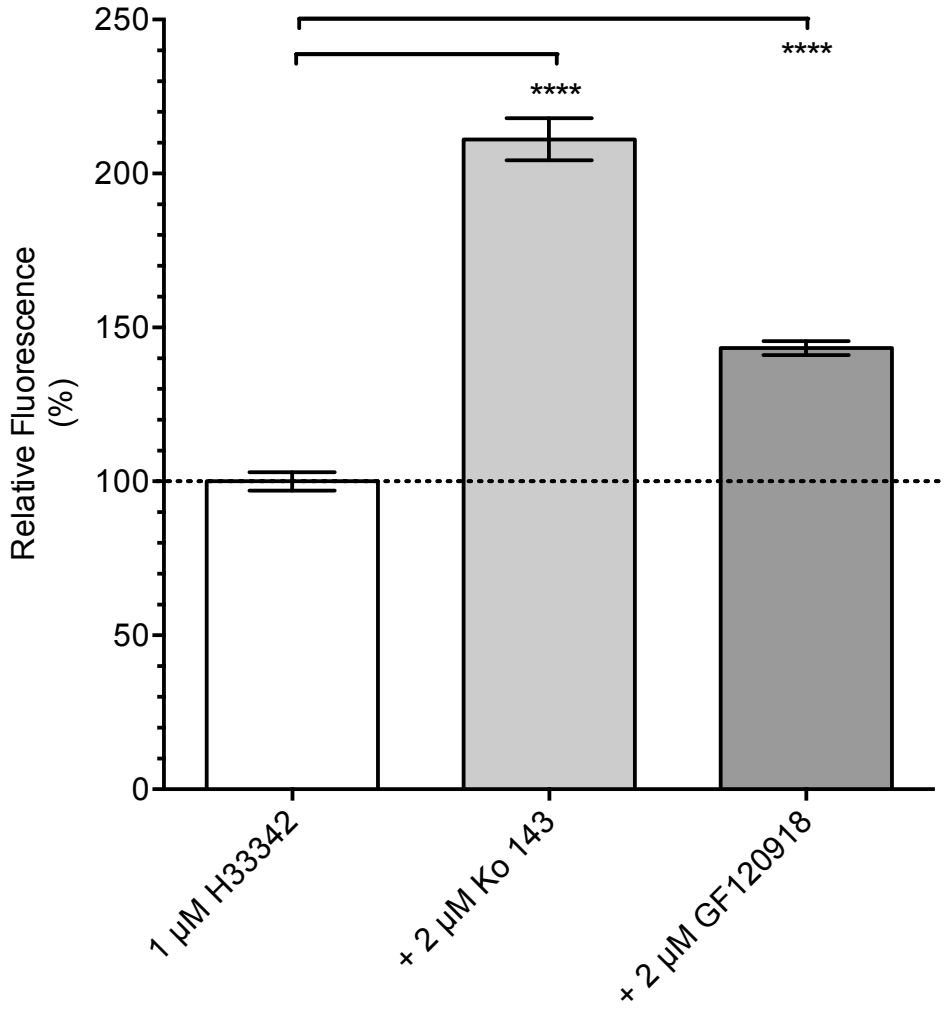

Figure 4.18: Measurement of H33342 retention in human PTCs to demonstrate functional activity of BCRP and MDR1.

*Intracellular retention of H33342 was measured in the presence of various competitive substrates of apical efflux transport proteins. The presence of 2 μM Ko143 increased the intracellular retention of H33342 2.11-fold (**** P < 0.0001). The presence of 2 μM GF120918 increased the intracellular retention of H33342 1.43-fold (**** P < 0.0001). The results are expressed as the mean ± SEM from 18 human PTC monolayers derived from 3 individual kidneys. Significance was determined using ANOVA and a Dunnett's post-test.*

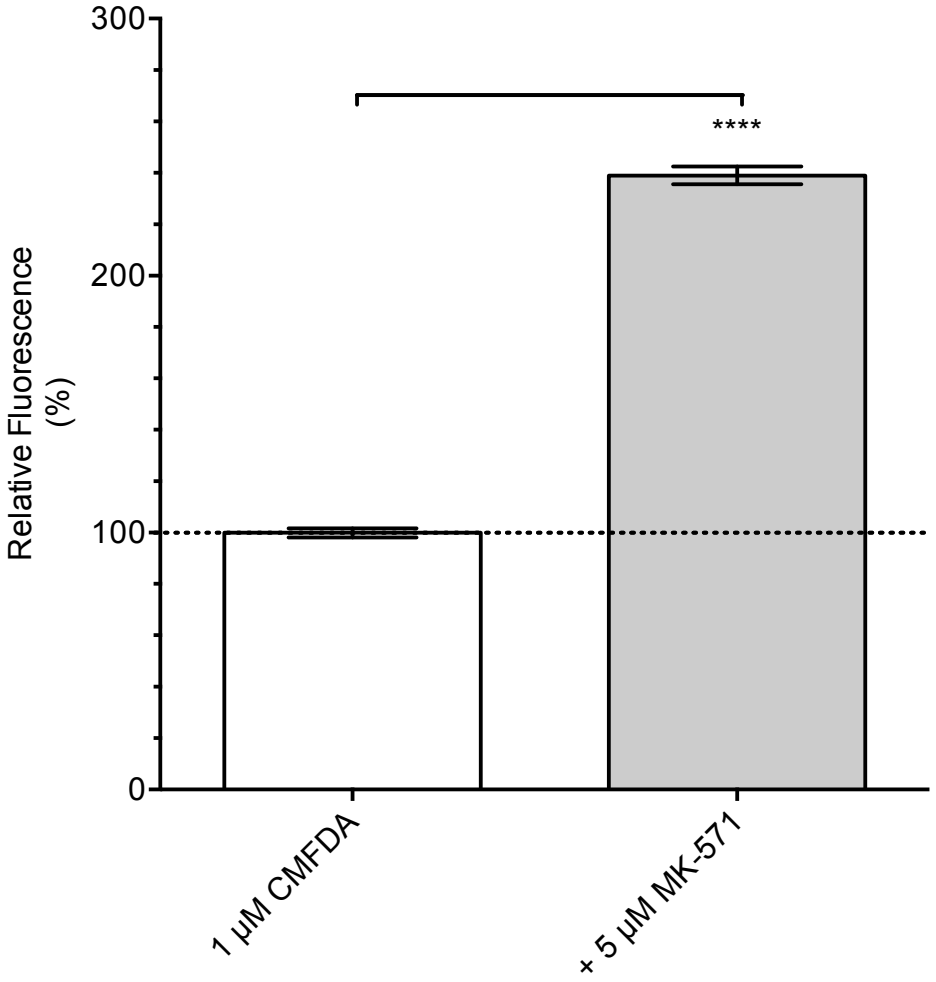

Figure 4.19: Measurement of GSMF retention in human PTCs to demonstrate functional activity of MRP transporters.

*Intracellular retention of GSMF was measured in the presence of presence of 5 μM MK-571. The presence of 5 μM MK-571 increased the intracellular retention of GSMF 2.39-fold (**** P < 0.0001). The results are expressed as the mean ± SEM from 18 human PTC monolayers derived from 3 individual kidneys. Significance was determined by a Student's t-test.*

4.3.8. The effect of TFV on metabolic activity of human PTCs.

The effect of TFV on the metabolic activity of human PTC monolayers was measured using the CellTiter 96® AQ_{ueous} assay (MTS). Monolayers were incubated for 2 or 7 days with a range of concentrations (0 to 500 μM) of TFV in the culture medium. The metabolic activity of monolayers was quantified by measuring the cellular production of a coloured formazan product via an absorbance reading. Formazan is produced through the reduction of MTS by NAD(P)H-dependent cellular oxidoreductase enzymes.

Figure 4.20 shows the effect of prolonged incubation with the concentrations of TFV on the metabolic activity of human PTC monolayers (n = 18, N = 3). At physiologically relevant concentrations of TFV there was no inhibition of human PTC metabolic activity. An extracellular TFV concentration of 50 μM or greater significantly reduced metabolic activity following a two day incubation period (**** $P < 0.0001$). In comparison, an extracellular TFV concentration of 10 μM or greater significantly reduced metabolic activity after a 7 day incubation period (**** $P < 0.0001$). Non-linear regression analysis of the data gave an apparent IC_{50} value of 354.20 ± 60.74 μM following a 2 day and 113.20 ± 1.30 μM following a 7 day incubation with TFV.

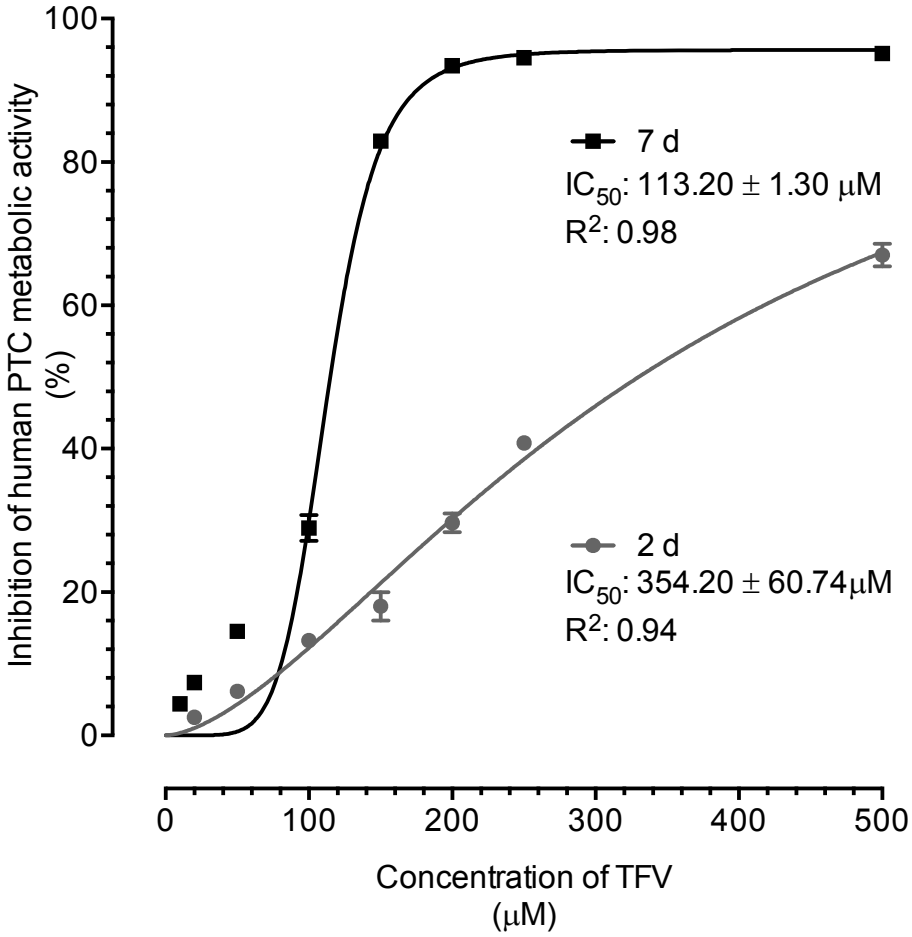

Figure 4.20: The effect of TFV on metabolic activity of human PTC monolayers.

In order to determine the effect of TFV on cellular metabolic activity, human PTC monolayers were incubated with a range of concentrations of TFV (0 to 500 μM) for 2 or 7 days. The metabolic activity of cells was measured using MTS. Exposure to high concentrations of TFV significantly reduced human PTC metabolic activity. However, there was no inhibition of human PTC metabolic activity at physiologically relevant concentrations. Non-linear regression analysis of the data gave an apparent IC_{50} value of 354.20 ± 60.74 μM following two days and 113.20 ± 1.30 μM following 7 days incubation with TFV. The results are expressed as the mean ± SEM from 18 human PTC monolayers derived from 3 individual kidneys.

4.3.9. Flux and uptake of TFV by rat PTC monolayers over time.

The rate of TFV unidirectional fluxes and uptake over time were studied by measuring the secretory and absorptive fluxes of 10 μM [^{3}H]-TFV across rat PTC monolayers following 20, 40, and 60 min of exposure. Additionally, the uptake of [^{3}H]-TFV across the basolateral membrane of rat PTC monolayers was measured at 15, 30, 45, 60, and 90 min of exposure.

Figure 4.21 shows the secretory, absorptive and net fluxes of [^{3}H]-TFV increased linearly between 0 and 60 min (n = 12, N = 3). Furthermore, as shown in Figure 4.22, uptake of [^{3}H]-TFV increased linearly between 0 and 90 min, with a gradient of 0.43 $\pm$ 0.01 pmol / cm^2 / min (n = 9, N = 3). From these findings we can deduce the initial rate period of TFV transport lies within 0 to 90 min. A time point of 60 min was therefore selected to conduct future studies to ensure linearity in rate of flux and uptake.

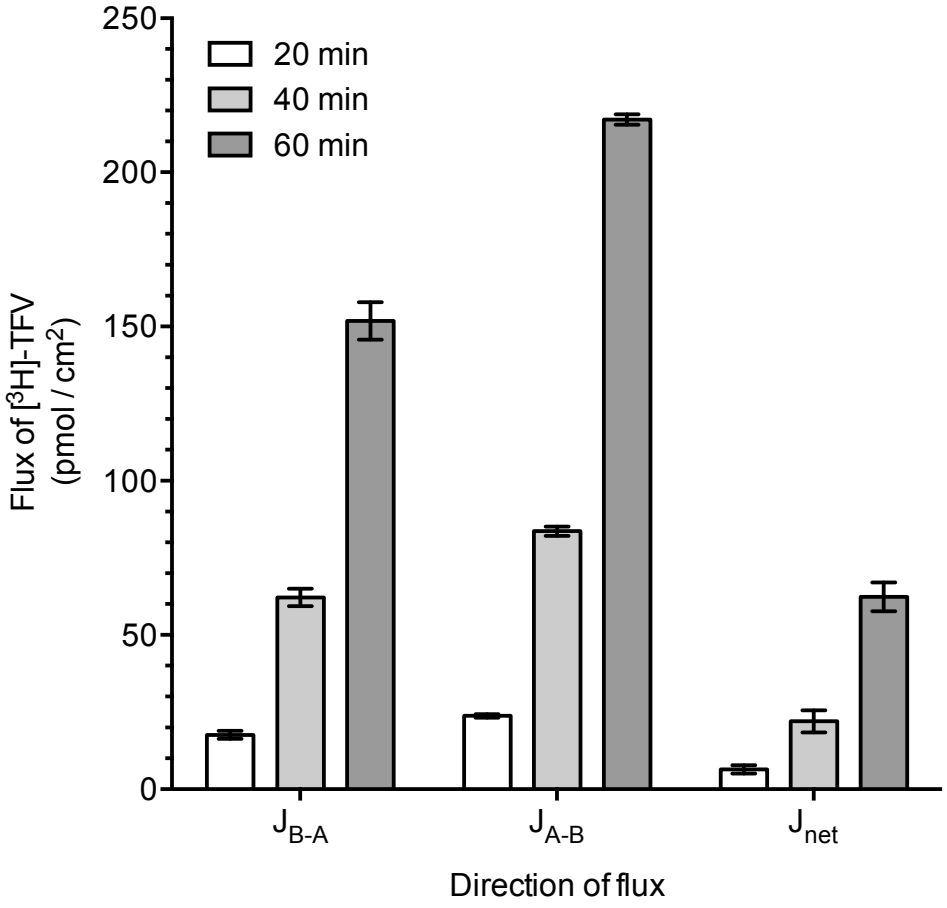

Figure 4.21: Time course of 10 μM [^{3}H]-TFV flux by rat PTC monolayers.

The flux of 10 μM [^{3}H]-TFV across rat PTC monolayers over time is shown. The flux of [^{3}H]-TFV was within the initial rate period between 0 and 60 min as flux was linear over this time period. The results are expressed as the mean ± SEM from 12 rat PTC monolayers derived from 3 individual kidneys.

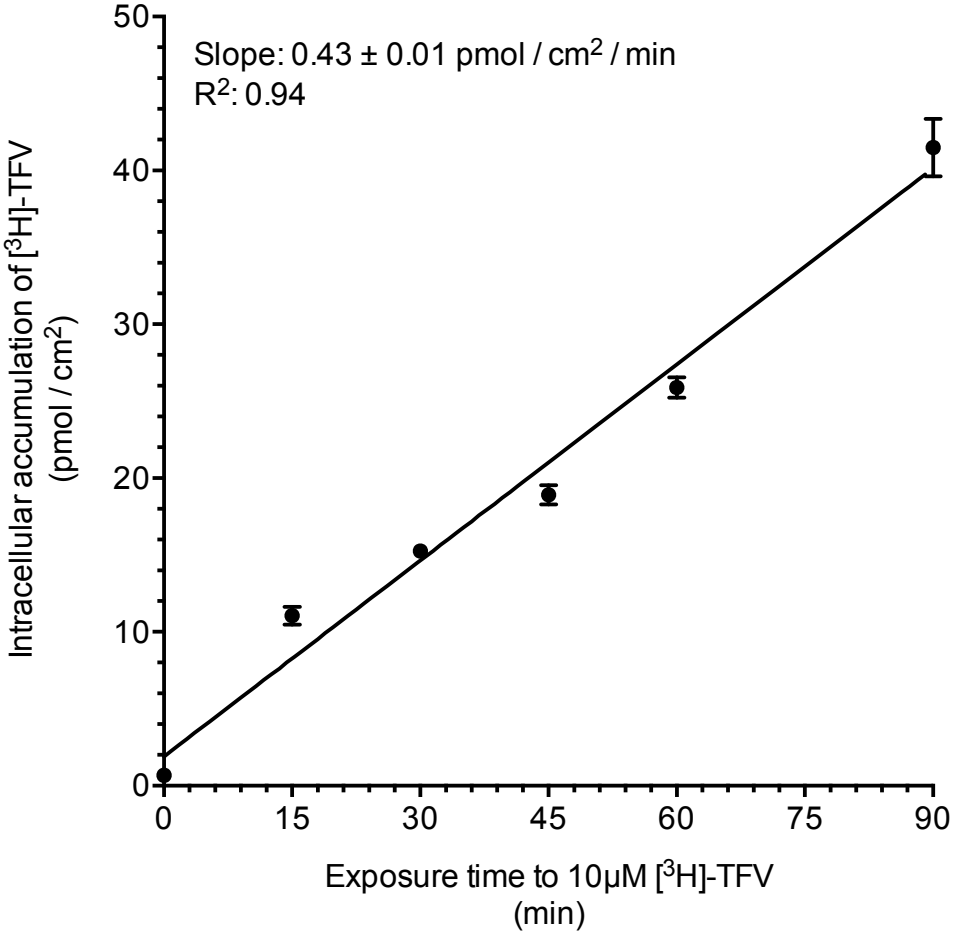

Figure 4.22: Time course of 10 µM [³H]-TFV uptake across the basolateral membrane of rat PTC monolayers.

A progress curve was created by measuring the uptake of 10 µM [³H]-TFV across the basolateral membrane of rat PTC monolayers over time. The uptake of [³H]-TFV between 0 and 90 min was linear. Linear regression analysis of the data gave a slope of 0.43 ± 0.01 pmol / cm² / min (R^2: 0.96). The non-specific binding of [³H]-TFV to the Transwell® insert was 0.68 ± 0.04 pmol / cm². The results are expressed as the mean ± SEM from 9 rat PTC monolayers derived from 3 individual kidneys.

4.3.10. Flux and uptake of TFV by rat PTC monolayers.

Unidirectional transepithelial fluxes of 10 μM [^{3}H]-TFV the secretory and absorptive direction were studied in the rat PTC monolayer model. Furthermore, uptake of [^{3}H]-TFV across the basolateral and apical membranes was determined from intracellular accumulation of [^{3}H]-TFV in rat PTC monolayers.

The results in Figure 4.23 exhibit a net absorption of TFV (62.34 ± 4.70 pmol / hr / cm^2) by rat PTC monolayers. Absorption of [^{3}H]-TFV (217.20 ± 1.66 pmol / hr / cm^2) was 1.40-fold greater than secretion (154.80 ± 5.09 pmol / hr / cm^2, **** $P < 0.0001$, n = 12, N = 3). Figure 4.24 shows the amount of [^{3}H]-TFV taken up across the basolateral and apical membranes of the rat PTC monolayers were 25.89 ± 0.68 pmol / hr / cm^2 and 18.15 ± 0.28 pmol / hr / cm^2, respectively; uptake of TFV was 1.43-fold greater across the basolateral membrane (**** $P < 0.0001$, n = 9, N = 3). These findings, coupled with the human data, indicate a cell to media ratio greater than 1 (See calculation below). This implies TFV is accumulated within the proximal tubule cells via the basolateral membrane.

The cell-to-medium ratio was calculated by dividing the intracellular concentration of TFV (μM) by the concentration of test compound in the transport medium (μM). Assumptions made in this calculation are the height of a proximal tubule epithelial cell is 10 microns i.e. 0.001 cm as measured by transmission electron microscopy (Dorup and Maunsbach, 1997), cell monolayers form a cylinder, and intracellular space does not contain subcellular compartments. These assumptions give ratios which probably substantially underestimate the true accumulation.

Volume occupied by a monolayer per 24-well Transwell® insert (surface area 0.33 cm^2) = π.radius^2.height
If radius = 0.32 cm, and height = 0.001 cm,
Volume (per 0.33cm^3)= 0.00032 cm^3 = 0.332 μL
Volume (per cm^3) = 0.332 μL x 3 = 0.996 μL
TFV concentration per cm^3 = 25.89 pmol / cm^3
Intracellular concentration of TFV = 25.89 pmol / 0.996 μL i.e. 25.99 μM
Extracellular concentration of TFV = 10 μM
Cell-to-medium ratio = 26:10 μM = 2.60

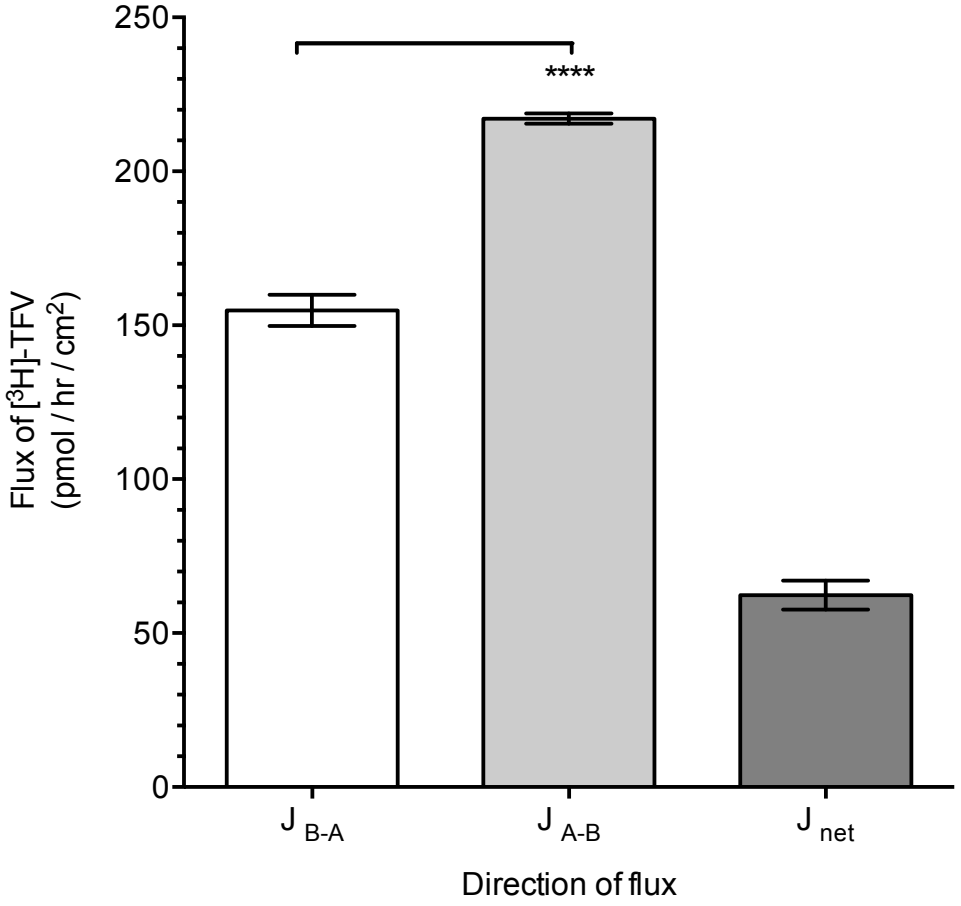

Figure 4.23: Unidirectional flux of 10 μM [^{3}H]-TFV by rat PTC monolayers.

*In order to determine the secretory and absorptive flux of TFV through rat PTC monolayers, paired monolayers were incubated with 10 μM [^{3}H]-TFV at either the basolateral or apical chamber. The results show a net absorptive flux (62.34 ± 4.70 pmol / hr / cm^2). The absorptive movement of [^{3}H]-TFV (217.20 ± 1.66 pmol / hr / cm^2) was significantly greater than the secretory movement (154.80 ± 5.09 pmol / hr / cm^2) (**** P < 0.0001). The results are expressed as the mean ± SEM from 12 rat PTC monolayers derived from 3 individual kidneys. Significance was determined by a Student's t-test.*

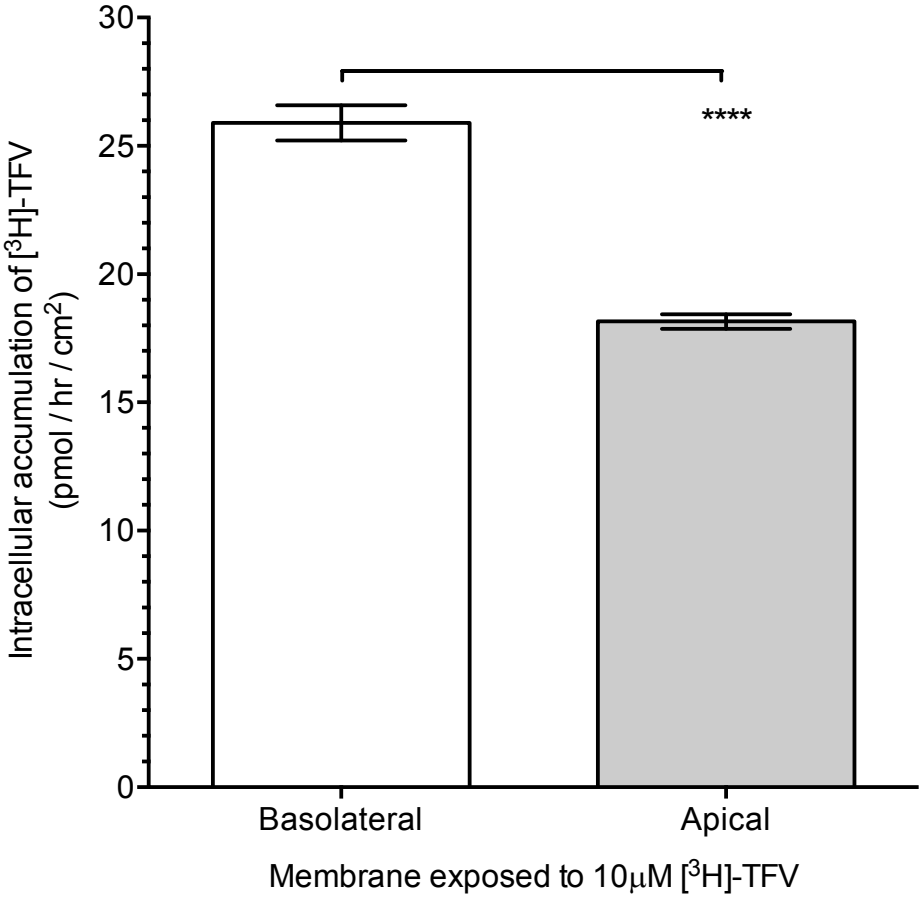

Figure 4.24: Uptake of 10 μM [^{3}H]-TFV across the basolateral and apical membrane of rat PTC monolayers.

*In order to measure the uptake of TFV across the basolateral and apical membrane of rat PTC monolayers, paired monolayers were incubated with 10 μM [^{3}H]-TFV at either the basolateral or apical chamber for 60 min. The data show that the uptake of [^{3}H]-TFV across the basolateral membrane (25.89 ± 0.68 pmol / hr / cm^2) was significantly greater than the apical membrane (18.15 ± 0.28 pmol / hr / cm^2) (**** P < 0.0001). The results are expressed as the mean ± SEM from 9 rat PTC monolayers derived from 3 individual kidneys. Significance was determined by a Student's t-test.*

4.3.11. Kinetics of TFV flux and uptake by rat PTC monolayers.

Rat PTC monolayers were incubated at the basolateral membrane with a range of [^{3}H]-TFV concentrations (1 to 5000 μM) for 60 min and the intracellular accumulation of [^{3}H]-TFV was measured, so as to calculate the kinetic parameters of TFV transport. Figure 4.25 shows the sigmoidal relationship between [^{3}H]-TFV concentration and uptake of [^{3}H]-TFV across the basolateral membrane of rat PTC monolayers (n = 9, N = 3). Non-linear regression analysis of the data gave a V_{max} of 1597.62 ± 131.70 pmol / hr / cm^2 and an apparent K_m value of 2482.40 ± 404.87 μM.

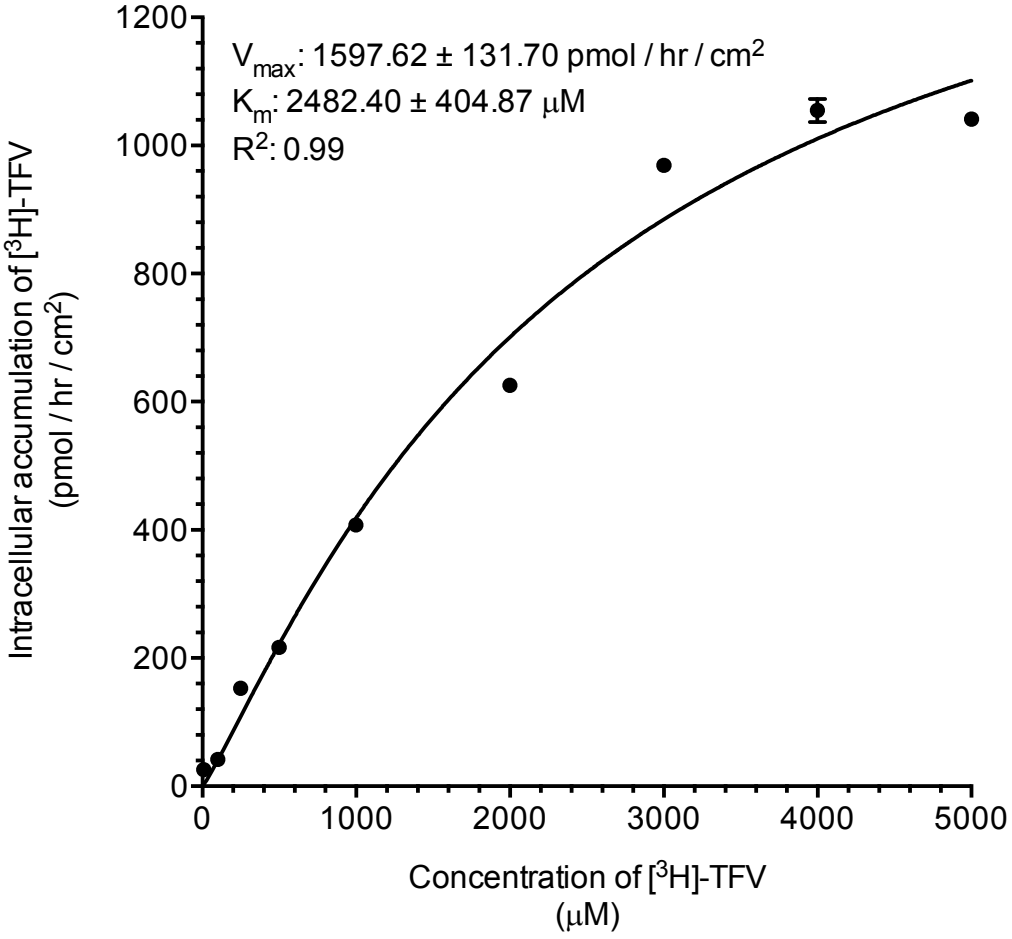

Figure 4.25: Kinetic data on the uptake of [^{3}H]-TFV across the basolateral membrane of rat PTC monolayers under initial rate conditions.

Rat PTC monolayers were incubated with a range of [^{3}H]-TFV concentrations (1 to 5000 μM) for 60 min. Non-linear regression analysis of the data gave a V_{max} of 1597.62 ± 131.70 pmol / hr / cm^2 and an apparent K_m value of 2482.40 ± 404.87 μM. The results are expressed as the mean ± SEM from 9 rat PTC monolayers derived from 3 individual kidneys.

4.3.12. Identifying the transporters mediating the uptake of TFV across the basolateral membrane of rat PTC monolayers.

The contributions of various uptake transport proteins in the rat tubular handling of TFV were quantified by measuring unidirectional fluxes and uptake of 10 μM [^{3}H]-TFV in the presence and absence of various competitive substrates of uptake transport proteins. The inhibitors were added at concentrations that would selectively inhibit the activity of transporters that were expected to be involved in the uptake of TFV. Table 4.4 shows the competitive substrate and its affinity value (K_m) for its corresponding transporter(s).

The effect of competitive substrates on the secretory and absorptive fluxes of [^{3}H]-TFV across rat PTC monolayers is shown in Figure 4.26 (n = 9, N = 3). The presence of PAH (50 μM) reduced [^{3}H]-TFV secretory flux to 19.07 ± 1.36 % (**** P < 0.0001), whilst RSV (20 μM) had no effect. Additionally, the presence of T3 (10 μM), CDC (10 μM) and DX (10 μM) reduced [^{3}H]-TFV secretory fluxes to 52.68 ± 2.03 % (**** P < 0.0001), 58.42 ± 2.29 % (**** P < 0.0001), and 53.15 ± 1.03 % (**** P < 0.0001), respectively, when compared to the control. The presence of the competitive substrates had no effect on absorptive flux.

Figure 4.27 shows the effect of competitive substrates on the uptake of [^{3}H]-TFV across the basolateral and apical membrane of rat PTC monolayers (n = 9, N = 3). The presence of 50 μM PAH reduced [^{3}H]-TFV uptake across the basolateral membrane to 18.78 ± 0.67 % of control (**** P < 0.0001), whilst 20 μM RSV had no effect. The presence of 10 μM T3, 10 μM CDC, and 10 μM DX decreased basolateral [^{3}H]-TFV uptake to 70.51 ± 1.22 % (**** P < 0.0001), 68.75 ± 0.88 % and 63.36 ± 1.44 % (**** P < 0.0001) of the control, respectively. The presence of the competitive substrates had no effect on apical uptake of TFV. In agreement with the flux experimental data, these findings suggest both Oatp4c1 and Oat1 mediate the uptake of TFV across the basolateral membrane.

As with the human transporter characterisation studies, in order to determine if the low contribution of rOat1 and rOat3 were the result of a loss of functionality or expression during cell culture, the inhibition study was repeated in freshly isolated rat PTCs (Figure 4.28). The presence of the Oct2 substrate CIM (1.5mM) had no effect on the uptake of [^{3}H]-TFV. Like the previous findings, 50

µM PAH, 10 µM T3 and 10 µM CDC reduced TFV uptake to 19.36 ± 2.31 % (**** P < 0.0001), 54.13 ± 1.93 % (**** P < 0.0001) and 44.41 ± 2.90 % (**** P < 0.0001) of control, respectively.

Substrate	Transporter	System	K_m (µM)	Reference
PAH	rOat1	*X.Laevis* oocytes	14.3 ± 2.9	(Sekine *et al.*, 1997)
PAH	rOat3	*X.Laevis* oocytes	64.7 ± 10.0	(Kusuhara *et al.*, 1999)
RSV	rOat3	*X.Laevis* oocytes	4.7 ± 0.7	(Windass *et al.*, 2007)
T3	rOatp4c1	MDCK	1.9 ± 0.6	(Mikkaichi *et al.*, 2004)
CDC	rOatp4c1	_	_	_
DX	rOatp4c1	MDCK	8.0 ± 2.2	(Mikkaichi *et al.*, 2004)
CIM	rOct2	HEK293	68.8 ± 8.0	(Tahara *et al.*, 2005)

Table 4.4: Competitive substrates used to identify transporters mediating the uptake of TFV.

Listed are competitive substrate of rOat1, rOat3 and Oatp4c1. The apparent affinity (K_m) values of the substrates for transporters are shown.

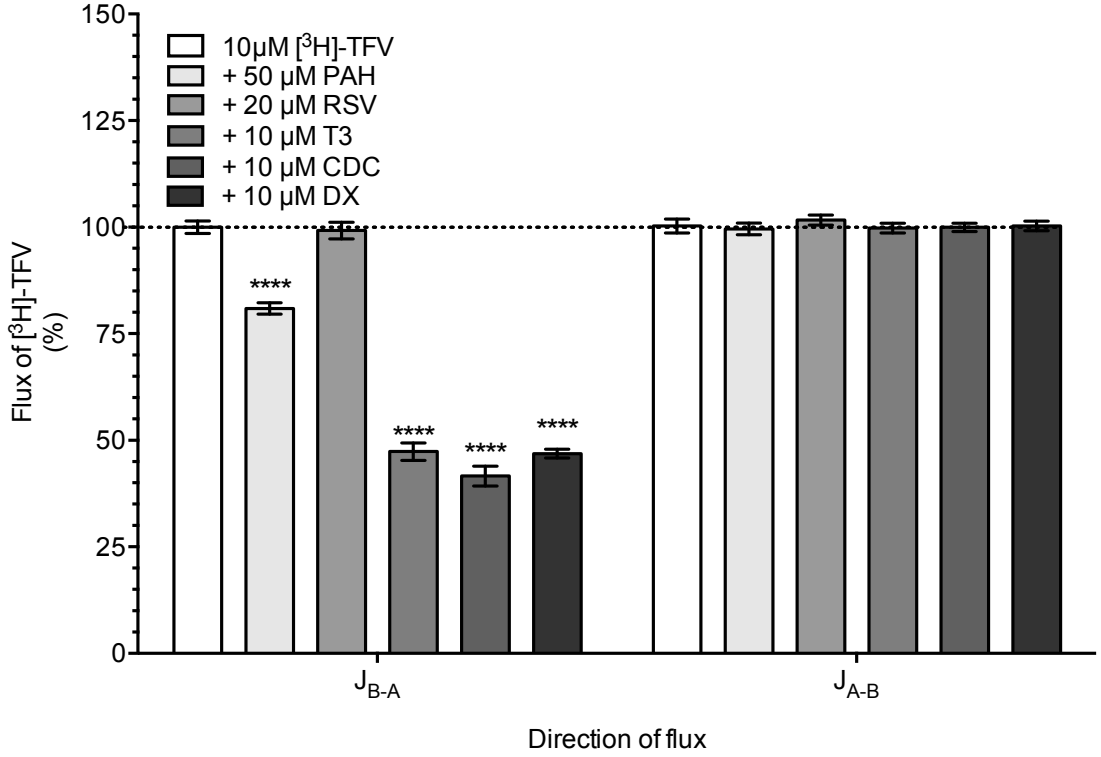

Figure 4.26: Identifying the transporters mediating the uptake of [^{3}H]-TFV in [^{3}H]-TFV flux across the rat PTC monolayer.

*Secretory and absorptive fluxes of 10 μM [^{3}H]-TFV were measured in the presence of various competitive substrates of uptake transport proteins. The presence of 50 μM PAH significantly reduced TFV secretory flux when compared to the control (19.07 ± 1.37 %, **** P < 0.0001), while 20 μM RSV had no effect. The presence of 10 μM T3, 10 μM CDC, and 10 μM DX also resulted in a marked decrease in TFV secretory flux (52.68 ± 2.03 % **** P < 0.0001, 58.42 ± 2.29 % **** P < 0.0001, and 53.15 ± 1.03 % **** P < 0.0001, respectively). The data suggest both Oatp4c1 and Oat1 are transporters that mediate the uptake of TFV across the basolateral membrane. The presence of the competitive substrates had no effect on the absorptive flux. The results are expressed as the mean ± SEM from 9 rat PTC monolayers derived from 3 individual kidneys. Significance was determined by a Student's t-test.*

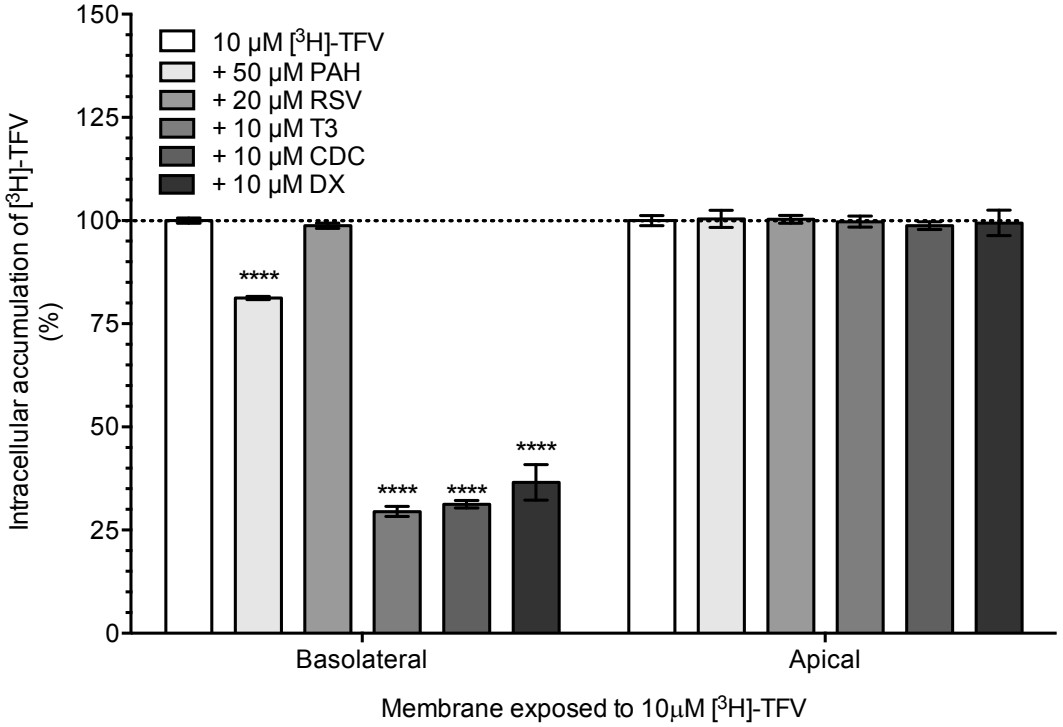

Figure 4.27: Identifying the transporters mediating the uptake of [^{3}H]-TFV in to rat PTC monolayers.

*Uptake of 10 µM [^{3}H]-TFV across the apical and basolateral membrane in the presence of various competitive substrates of uptake transport proteins was measured. At the basolateral membrane of rat PTC monolayers 50 µM PAH reduced [^{3}H]-TFV uptake to 18.78 ± 0.35 % of control (**** P < 0.0001). 20 µM RSV had no effect while 10 µM T3 reduced uptake to 70.51 ± 1.22 % of control (**** P < 0.0001), 10 µM CDC reduced uptake to 68.75 ± 0.88 % of control (**** P < 0.0001) and 10 µM DX reduced uptake to 63.46 ± 1.44 % (**** P < 0.0001). In agreement with the flux data these findings suggest Oatp4c1 and Oat1 are the transporters that mediate the uptake of TFV across the basolateral membrane. The presence of the competitive substrates had no effect on apical uptake of TFV. The results are expressed as the mean ± SEM from 9 rat PTC monolayers derived from 3 individual kidneys. Significance was determined by a Student's t-test.*

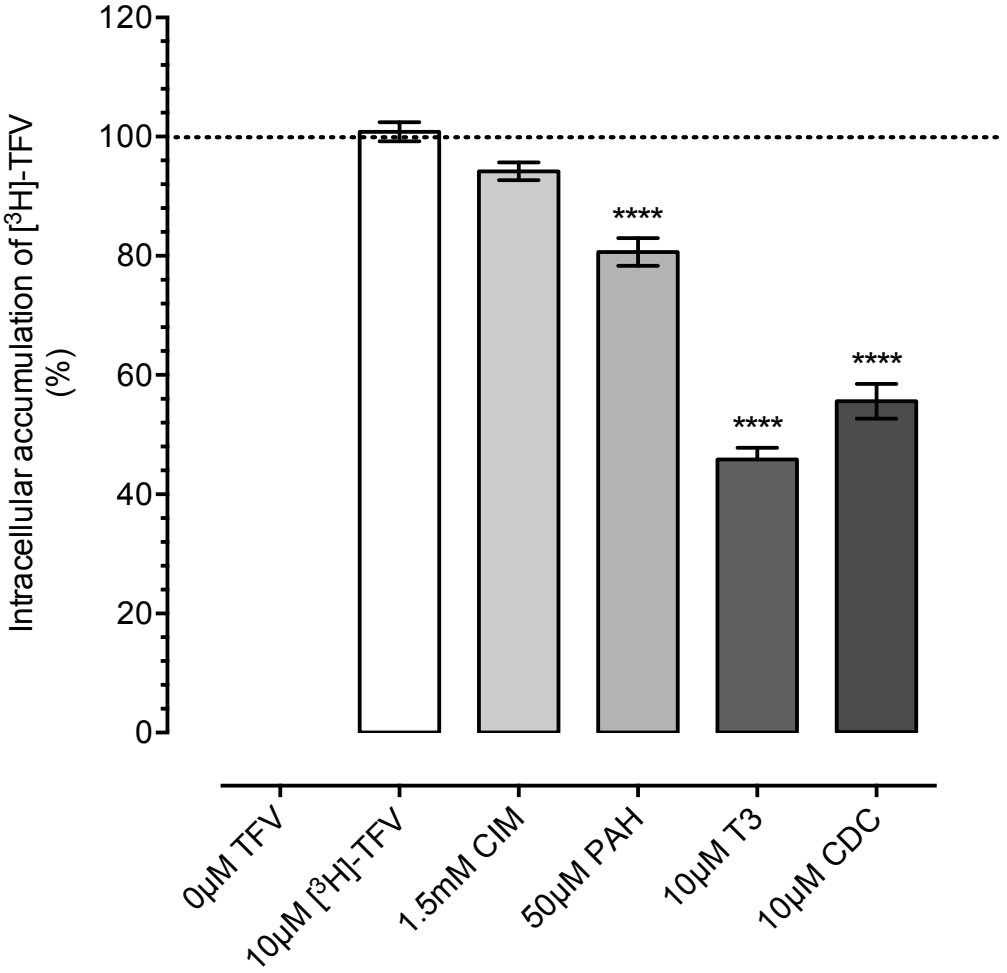

Figure 4.28: Identifying the transporters mediating the uptake of [^{3}H]-TFV in freshly isolated rat PTCs.

*Uptake of 10 μM [^{3}H]-TFV was measured in suspended rat PTCs in the presence of various competitive substrates of uptake transport proteins The presence of 1.5 mM CIM had no effect on intracellular accumulation of [^{3}H]-TFV. 50 μM PAH reduced TFV accumulation to 19.36 ± 2.31 % when compared to the control (**** P < 0.0001). 10 μM T3 and 10 μM CDC resulted in a marked decrease in TFV accumulation when compared to the control (54.13 ± 1.93 % **** P < 0.0001 and 44.41 ± 2.90 % **** P < 0.0001, respectively). These findings suggest both Oatp4c1 and Oat1 are the transporters that mediate the uptake of TFV across the basolateral membrane. The results are expressed as the mean ± SEM from 12 rat PTCs samples derived from 3 individual kidneys. Significance was determined by a Student's t-test.*

4.3.13. Identifying the transporters mediating the efflux of TFV across the apical membrane of rat PTC monolayers.

The contributions of various efflux transport proteins in the tubular handling of TFV by rat PTC monolayers were characterised by measuring unidirectional fluxes and intracellular concentrations of [^{3}H]-TFV in the presence and absence of various inhibitors of apical efflux transport proteins. The inhibitors were added at concentrations that would selectively inhibit the activity of transporters..

The effect of efflux transport protein inhibitors on the secretory and absorptive fluxes of [^{3}H]-TFV across rat PTC monolayers are shown in Figure 4.29 (n = 9, N = 3). The presence of MK-571 (5 μM), and Ko 143 (2 μM) had no effect on the secretory and absorptive fluxes of 10 μM [^{3}H]-TFV. The same compounds also had no effect on the intracellular accumulation of 10 μM [^{3}H]-TFV when compared to the control (Figure 4.30). The functionality of these transporters within rat PTC monolayers have previously been confirmed. Therefore, these findings imply that TFV has a poor affinity for Mrp2, Mrp4 and Bcrp under physiological conditions.

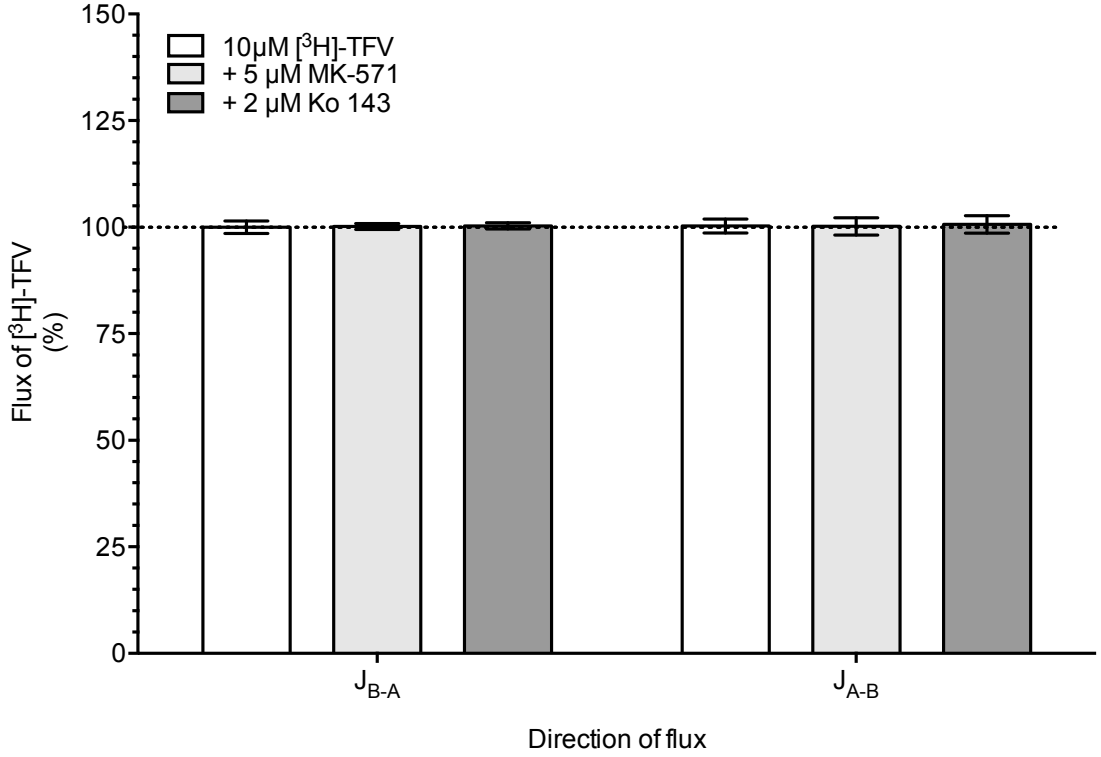

Figure 4.29: Identifying the transporters mediating the efflux of [^{3}H]-TFV by rat PTC monolayers.

Secretory and absorptive fluxes of 10 μM [^{3}H]-TFV were measured in the presence of various competitive substrates of apical efflux transport proteins. The presence of 5 µM MK-571 and 2 µM Ko 143 had no effect on the secretory nor the absorptive flux of [^{3}H]-TFV. This indicates that TFV has a poor affinity for Mrp2, Mrp4 and Bcrp under physiological conditions. The results are expressed as the mean ± SEM from 9 rat PTC monolayers derived from 3 individual kidneys. Significance was determined by a Student's t-test.

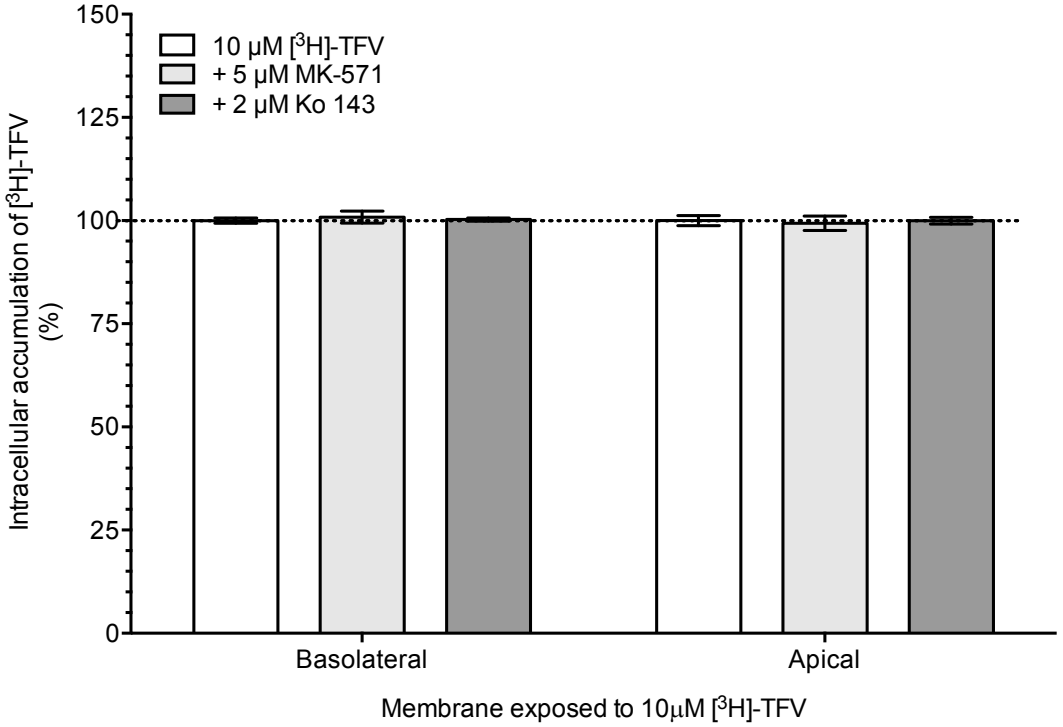

Figure 4.30: Identifying the transporters mediating the efflux of [3H]-TFV from the rat PTC monolayer.

Intracellular accumulation of [^{3}H]-TFV in the monolayers was measured in the presence of various competitive substrates of apical efflux transport proteins. The monolayers were incubated at either the basolateral or apical membrane with 10 μM [^{3}H]-TFV in the presence or absence of competitive substrates for 60 min. The presence of 5 µM MK-571 and 2 µM Ko 143 had no effect on the intracellular concentration of [^{3}H]-TFV, suggesting that TFV has a poor affinity for Mrp2, Mrp4, and Bcrp under physiological conditions. The results are expressed as the mean ± SEM from 9 rat PTC monolayers derived from 3 individual kidneys. Significance was determined by a Student's t-test.

4.4. Discussion

In this chapter the renal handling of TFV by human and rat PTC monolayers was studied to investigate their use as platforms to predict renal drug handling, DDIs and nephrotoxicity. From *in-vivo* studies it is known that TFV is cleared in the kidney by a combination of glomerular filtration and tubular secretion, and that it is a substrate of multiple transporters in the kidney. Following on from marketing approval, a low rate of nephrotoxicity has been reported with long-term TFV therapy.

Unidirectional transepithelial fluxes of radiolabelled [^{3}H]-TFV (10 µM) in both the secretory and absorptive direction were measured over 1 hr in paired monolayers of human and rat PTCs grown on 24-well Transwell® inserts. In the human PTC monolayers, we observed net absorption of TFV (50.69 $\pm$ 1.35 pmol / hr / cm^2) as shown in Figure 4.4. The absorptive movement of [^{3}H]-TFV (131.16 $\pm$ 2.15 pmol / hr / cm^2) was 1.63-fold greater than the secretory movement of [^{3}H]-TFV (80.47 ± 1.00 pmol / hr / cm^2). Figure 4.5 shows uptake of TFV across the basolateral membrane (39.09 ± 1.31 pmol / hr / cm^2) was 5.86-fold higher than apical uptake (6.67 ± 0.46 pmol / hr / cm^2). Similarly, in rat PTC monolayers, Figure 4.23 and Figure 4.24, the absorptive movement of [^{3}H]-TFV (217.20 ± 1.66 pmol / hr / cm^2) was 1.40-fold greater than the secretory movement of [^{3}H]-TFV (154.80 ± 5.09 pmol / hr / cm^2) and the uptake of TFV across the basolateral membrane (25.89 ± 0.68 pmol / hr / cm^2) was 1.43-fold higher than apical uptake (18.15 ± 0.28 pmol / hr / cm^2). Within the PTCs these findings would result in a cell to media ratio greater than 1 across the basolateral membrane suggesting that TFV is accumulated within the proximal tubule cells. These findings support the *in-vivo* pathology studies which have reported an accumulation of TFV within the same cells (Cote *et al.*, 2006; Kohler *et al.*, 2009; Herlitz *et al.*, 2010; Perazella, 2010; Fernandez-Fernandez *et al.*, 2011; Kohler *et al.*, 2011).

The rate of transporter-mediated movement of a drug molecule is approximately linear for a period of time once exposure begins; this is known as the initial rate period. As the rate of transport proceeds the substrate concentration decreases, consequently the rate decelerate. In order to measure the maximum rate of

transport, transporter assays are typically carried out in the 'linear' initial rate period. The length of the initial rate period for each molecule depends on the assay conditions and can be milliseconds to hrs. To ensure the flux and uptake of TFV was measured under initial rate conditions, the experiments were performed at defined time points. From the findings in Figure 4.2, Figure 4.3, Figure 4.21 and Figure 4.22 we can deduce the linear initial rate period of TFV transport was between 0 to 90 min for both human and rat. Therefore, a time point of 60 min was selected to conduct subsequent studies as it was within the linear initial rate. This would also ensure the reactions had progressed enough to be measured within the radiation detection instrument's sensitivity.

The kinetic parameters, V_{max} and K_m, of TFV uptake across the basolateral membrane of both human and rat PTC monolayers were quantified by incubating the monolayers with various concentrations of [^{3}H]-TFV. In order to determine the maximum rate of TFV uptake, the limiting factor must be the transporter activity and not the amount of substrate. Between 0 to 2000 µM [^{3}H]-TFV in the human monolayers and 0 to 3000 µM [^{3}H]-TFV in the rat, there was an exponential increase in the rate of uptake with increasing substrate concentration. Within these conditions the rate limiting factor was the concentration of TFV, as the substrate recognition site of the transporters mediating uptake were unsaturated. As the concentration of [^{3}H]-TFV increased beyond 2000 µM in man and 3000 µM in rat, the transporters mediating TFV uptake were saturated with substrate and the rate limiting factor was transporter activity. Adding more TFV did not significantly affect the rate of uptake. On the graph this is represented as a plateau. The maximum rate of TFV uptake when the transporter is saturated with a substrate is known as the maximum initial velocity (V_{max}). Non-linear regression analysis of the data in Figure 4.8 and Figure 4.25 gave a V_{max} of 1214.11 $\pm$ 134.57 pmol [^{3}H]-TFV / hr / cm^2 in human PTC monolayers and 1597.62 $\pm$ 131.70 pmol [^{3}H]-TFV / hr / cm^2 in rat PTC monolayers.

The relationship between the rate of uptake and concentration of TFV depends on the affinity of the transporter for the substrate. This is usually expressed as the K_m of the transporter for the substrate. In this instance, K_m is the concentration of TFV which permits the uptake of TFV to achieve half of V_{max}. A

transporter with a high K_m has a low affinity for its substrate, and requires a greater concentration of substrate to achieve V_{max}. The basolateral membrane transporters within rat and human PTC appeared to have low affinities for TFV. Non-linear regression analysis of the data in Figure 4.8 and Figure 4.25 gave an apparent K_m value of 756.86 ± 166.48 μM [^{3}H]-TFV in human PTC monolayers and 2482.40 ± 404.87 μM [^{3}H]-TFV in rat PTC monolayers. The kinetic parameters from previously published in-vitro studies modelling TFV uptake are shown in

Table 4.5. The reason why the K_m values generated in our models were higher than those published is that our system expresses a full complement of renal transporters involved in the renal handling of TFV whilst the published studies conducted in transfected cells only expressed a single transporter, for instance hOAT1 or hMRP4.

System	K_m (μM)	V_{max}	Reference
hOAT1 oocyte	25.0	129 pmol / oocyte / h	(Moss *et al.*, 2011)
hOAT1 HEK293	400.0 ± 80.0	5500 ± 400 pmol / min / mg	(Riches, 2010)
hOAT1 CHO	33.8 ± 3.4	110 ± 12 pmol / 10^6 cells. min	(Cihlar *et al.*, 2001)
hMRP4 HEK293 vesicles	>1000		(Imaoka *et al.*, 2007)

Table 4.5: A summary of published V_{max} and K_m values for TFV uptake.

TFV is reported to be a substrate for multiple transporters in the kidney. There are two methods to elucidate the contribution of individual transporters in the renal handling of TFV. The first is the relative activity factor method: selective substrates for each individual transporter are used to estimate the contribution of transporters to the flux and uptake of drugs when multiple transporters are involved (Hirano *et al.*, 2004). However, this method is commonly infeasible due to the overlapping substrate specificity of many transporters. Alternatively, a method in which the use of available transporter specific inhibitors in

combination with a cocktail of inhibitors with known but overlapping inhibitory potencies toward multiple transporters can be used. The method is depicted in Figure 4.9 and Figure 4.15.

The transporters that were initially considered to be involved in the renal handling of TFV were OAT1, OAT3, MRP2 and MRP4. Current literature proposes that TFV secretion in the kidney begins with the basolateral uptake of the compound from general circulation into the epithelial proximal tubule cells via OAT1 and OAT3. It is then effluxed into urine through apically located MRP2 and MRP4. This is also the secretory pathway proposed for similar molecules such as adefovir and cidofovir (Cihlar et al., 1999; Schuetz et al., 1999; Cihlar and Ho, 2000; Ho et al., 2000; Cihlar et al., 2001; Izzedine et al., 2006; Cihlar et al., 2007; Imaoka et al., 2007; Uwai et al., 2007; Weiss et al., 2007; Kohler et al., 2011; Moss et al., 2011; Mandikova et al., 2013).

The transporters responsible for the uptake of TFV across the basolateral membrane of human and rat PTC monolayers were identified with a combination of substrates for those transporters. The findings revealed that a significant component of carrier mediated basolateral uptake of TFV was unaccounted for. Uptake studies with RSV showed that TFV was not a substrate for OAT3. This finding is highly significant as OAT3 is highly expressed within the kidney (Hilgendorf *et al.*, 2007). OAT1 was identified as a key transporter in the uptake to TFV using a combination of PAH and RSV. However, the relative contribution of this transporter in the basolateral uptake of TFV was lower than expected. The contribution of OAT1 in human PTC monolayers was around 20 to 30 % (Figure 4.10 and Figure 4.11) and around 20 % in rat PTC monolayers (Figure 4.26 and Figure 4.27). Hence other proteins known to transport anions were considered, and OATP4C1 was chosen for further investigation.

OATP4C1 was confirmed as a transporter in the basolateral uptake of TFV with the co-administration of TFV with T3 and CDC. The contribution of OATP4C1 in TFV uptake was around 70 to 80 % in human monolayers (Figure 4.10 and Figure 4.11) and, 50 to 70 % in rat monolayers (Figure 4.26 and Figure 4.27). It was thus shown that OAT1 and OATP4C1 were responsible for the basolateral uptake of TFV. In order to determine if TFV transport via OATP4C1 was the

result of a loss in OAT1 and OAT3 expression or functionality during PTC cell culture, the inhibition study was repeated in freshly isolated human and rat PTCs. The findings in Figure 4.12 and Figure 4.28, confirmed that OATP4C1 was the predominant transporter of TFV; it mediated the 45 to 55 % of the basolateral uptake of TFV whereas OAT1 contributed only around 20 %. Uptake of 10 μM [^{3}H]-TFV was 4.51-fold lower in the human cells cultured for 7-days on Transwell® inserts when compared to freshly isolated cells. The data shown in Figure 4.13 suggested that the loss of OATP4C1 expression in cultured cells is not as great as loss of OAT expression. This result is consistent with the mRNA data in Table 3.1, which reported a 4.27-fold decrease in expression of OAT1 and a 1.95 decrease in the expression OATP4C1 in human PTCs cultured on Transwell® inserts when compared to freshly isolated cells. The identification of OATP4C1 as a key transporter in the renal elimination of TFV is novel.

OATP4C1 is reported to possess multiple substrate recognition sites. Two distinct recognition sites for DX and E3S have been characterised (Mikkaichi et al., 2004). Apparent K_m values of these substrates for OATP4C1 are listed in Table 4.2. In order to determine if TFV binds to the same recognition site as DX or E3S, the basolateral uptake of 10 μM [^{3}H]-TFV across human PTC monolayers in the presence of various concentrations of DX and E3S (0.1 to 50 μM) were plotted to generate IC_{50} values. IC_{50} represents the concentration of an inhibitor required for 50 % inhibition of a cellular response. Non-linear regression analysis of the data in Figure 4.14 suggested that DX and E3S are only able to bind one binding site. With apparent IC_{50} values of 0.38 ± 0.10 μM for DX and 1198 μM for E3S. These findings indicate that TFV has a higher affinity for the DX recognition site of OATP4C1 than the E3S recognition site.

Using the Cheng-Prusoff equation, these information, in combination with the kinetic data of TFV uptake in human PTC monolayers, the inhibition constants (K_i) were calculated. K_i is the concentration of the inhibitor that is required to decrease the maximal rate of reaction by half. Therefore, the smaller the K_i the smaller the amount of drug was needed to inhibit the basolateral uptake of TFV in human PTC monolayers. The calculated K_i values for DX and E3S were 0.38 ± 0.10 and 1182.38 μM, respectively. If the K_i value is much larger than the maximal plasma drug concentrations a patient is exposed to from typical dosing,

as is the case in this example, then the drug is not likely to inhibit the uptake of TFV *in-vivo*.

OATP4C1 is the only member of the OATP family expressed on the basolateral membrane of proximal tubules in humans and rodents. The overall homology between human OATP4C1 and rat Oatp4c1 was found to be 80.4% at the amino acid level (Mikkaichi T, 2004). OATP4C1 and Oatp4c1 also have a moderate sequence homology with other OATP family members (below 35%) (Mikkaichi T, 2004). Oatp4c1 mRNA expression is male-predominat in mouse kidneys (Cheng X and Klaassen CD, 2009). Using gonadectomized and *lit/lit* mouse models, gender divergent regulation of Oatp4c1 in mouse kidneys was shown to be controlled by sex hormones (Cheng X and Klaassen CD, 2009). Based upon these findings, males could be more prone to tenofovir induced nephrotoxicity as a result of greater renal expression of OATP4C1.

The transporters responsible for the efflux of TFV across the apical membrane were characterised by measuring the secretory flux and intracellular concentration of TFV in the absence and presence of various competitive substrates of apical efflux transport proteins. The presence of MK-571 (5μM, MRP substrate), Ko 143 (2 μM, BCRP substrate) or GF120918 (5 μM, MDR1 substrate) had no effect on the secretory flux and intracellular concentration of [^{3}H]-TFV in human (Figure 4.16 and Figure 4.17, respectively) and rat PTC monolayers (Figure 4.29 and Figure 4.30, respectively). We have confirmed in Figure 4.18 and Figure 4.19 that human PTC monolayers exhibit functional expression of apical MRP, BCRP and MDR1. Their functional expression in rat PTC monolayers has also been characterised by colleagues. Therefore, these findings, in contrast to the majority of the published literature, suggest TFV is a weak substrate of MRP, BCRP and MDR1 under physiological conditions.

In conjunction with our findings that the absorptive flux of TFV was significantly greater than the secretory flux, the information suggests that TFV accumulates within the proximal tubule cells due to the lack of an efficient secretory route. TFV enters the tubular cells at the basolateral membrane through OATP4C1 and OAT1, at a higher rate than the efflux of TFV due to the low affinity for efflux transporters; TFV thus accumulates or exits through membrane permeation. Similarly, adefovir and cidofovir have been reported to accumulate

in the proximal tubule cells and cause nephrotoxicity. The expression of hOAT1 has been observed to induce the cytotoxicity in the presence of adefovir and cidofovir in hOAT1-CHO cells (Ho *et al.*, 2000). Co-administration of cidofovir with the OAT1/OAT3 inhibitor has been shown to ameliorate nephrotoxicity. In animal toxicity studies, oral probenecid treatment decreased the concentration of cidofovir in the cortex of the kidney, whilst levels in other tissues have remained unaffected as a result of the reduced renal clearance (Cundy *et al.*, 1995; Cundy *et al.*, 1996; Lacy *et al.*, 1998; Ho *et al.*, 2000; Mandikova *et al.*, 2013). Probenecid inhibition studies have also found that tubular secretion of low doses of cidofovir are unaffected by probenecid co-administration (Cundy *et al.*, 1995). This suggests another unknown transporter maybe involved in cidofovir tubular secretion, which could be OATP4C1 based on our findings. At low cidofovir doses, the drug may be cleared from the serum by this high-affinity unknown transporter (OATP4C1), while at higher cidofovir doses this system may be saturated, requiring cidofovir to be transported by a probenecid-sensitive mechanism (OAT1 and 3).

The literature associates TFV accumulation with proximal tubulopathies such as acute kidney, injury and Fanconi syndrome by disrupting proximal tubule cell mitochondrial function (Rifkin and Perazella, 2004; Cote *et al.*, 2006; Kohler *et al.*, 2009). The mitochondrial activity of human PTC monolayers following a 2 and 7 day exposure to different concentrations of TFV was assessed using MTS. In metabolically active cells MTS is reduced by NAD(P)H-dependent cellular oxidoreductase enzymes into a soluble coloured formazan product. As shown in Figure 4.20, at physiologically relevant concentrations of TFV there was no inhibition of human PTC metabolic activity. Non-linear regression analysis of the data gave an apparent IC_{50} value of 354.20 ± 60.74 μM TFV following a 2 day and 113.20 ± 1.30 μM TFV following a 7 day incubation. A limitation of conducting this study and other measures of nephrotoxicity in our primary human PTC model is that the length of exposure to the nephrotoxic molecule is limited by the finite lifespan of the cells.

The information gathered on the renal handling of TFV in the human and rat PTC monolayers will have a large translational impact. TFV in combination with other antivirals is a first line therapy for both HIV-1 and HBV infected patients,

as recommended by the World Health Organisation (WHO, 2014; WHO, 2015a). The organisation estimates that in 2014, 36.9 million people were living with HIV and 240 million with HBV globally (WHO, 2015c; WHO, 2015b). Approximately 14.9 million people living with HIV (40.4%) were receiving HIV antiretroviral therapy (ART) in 2014 (WHO, 2015c). The number of people taking this medication is certain to increase in the future due to the substantial progress in access to HIV-1 treatment and the introduction of 'pre-exposure prophylaxis'.

The novel identification of OATP4C1 as a key transporter in the renal elimination of TFV using the primary models has led Gilead to invest in developing assays for OATP4C1 DDI. The life expectancy of HIV-1 and HBV infected patients is now comparable to the general population. Therefore, it is important to be aware of any potential DDIs that may occur with co-medication. Known substrates of OATP4C1 include cardiac glycosides (DX and ouabain), thyroid hormones (T3 and T4), cAMP and methotrexate. In addition, the work has generated commercial renal drug screening contracts with Gilead and Chimerix, which in turn has resulted in a reduction in animal use at both companies. Furthermore, this work in combination with other studies has led to the FDA flagging OATP4C1 as a key renal drug transporter. The use of the primary models as screening platforms for drug transporter and DDI studies have thus been validated in this chapter.

4.5. Summary

In both human and rat PTC monolayers the uptake of TFV was greater across the basolateral membrane in comparison to the apical. We also observed a predominant absorptive pathway of TFV. Within the PTCs this would result in a cell to media ratio greater than 1 across the basolateral membrane suggesting that TFV is accumulating with the tubular cells. The transporters mediating the transport of TFV were identified using a cocktail of transporter inhibitors. The predominant basolateral uptake transporter was OATP4C1, followed by OAT1, with a negligible contribution from OAT3. TFV had low affinities for the apical efflux transporters MRP2, MRP4, MDR1 and BCRP. The novel identification of OATP4C1 as a TFV transporter has led Gilead to develop assays for investigating OATP4C1 DDI and also the FDA to recognise OATP4C1 as a key renal transporter. The primary models has thus been validated as a good model for such studies.

5. P_i handling by PTCs

5.1. Background

Phosphorus is an essential mineral. In mammals, it is required for cell structural integrity (phospholipid membranes and skeletal tissue), protein synthesis (DNA), energy production (ADP, ATP), and cell signalling (IP_3, cAMP, cGMP). Phosphorus exists freely in plasma as either monovalent ($H_2PO_4^-$) or divalent (HPO_4^{2-}) phosphate and these are collectively referred to as inorganic phosphate (P_i). Plasma P_i is maintained within a narrow range of 0.8 to 1.5 mM (Biber *et al.*, 2013).

As summarised in Figure 5.1, this balance is achieved by four separate but intertwined physiological systems – the gastrointestinal, renal, musculoskeletal and endocrine systems. On average, 1200 mg of phosphorus is ingested in dietary products each day (Hruska *et al.*, 2008). Of this intake, around 950 mg is absorbed at the small intestine into the exchangeable P_i pool by either paracellular movement or active transport across the intestinal mucosa, whilst the remainder is excreted with faeces (Hruska *et al.*, 2008). *In-vitro* preparations of rat small intestine have demonstrated the duodenum and jejunum are responsible for the bulk of P_i absorption (Walling, 1977; Marks *et al.*, 2007). The active uptake of P_i is mediated by a series of specialised sodium dependent P_i transporters NaPi-IIb (SLC34A2), PiT1 (SLC20A1), and PiT2 (SLC20A2). Once absorbed P_i enters the exchangeable phosphorus pool which consists of intracellular P_i (70 %), the skeletal mineralisation store (29 %), and plasma P_i (1 %) *(Hruska et al., 2008)*. P_i exits the pool via changes in skeletal disposition, renal excretion and intestinal secretion. Approximately 300 mg day^{-1} of serum P_i undergoes continuous exchange with the conjugates of phosphate that make up bone (Hruska *et al.*, 2008). This constant balance between bone reabsorption and formation is a process known as bone turnover. The kidney plays a key role in regulating plasma P_i. Within the kidney, P_i is freely filtered in the glomeruli of the kidney. Approximately 800 mg day^{-1} (80%) of the filtered load is reabsorbed in the proximal tubule by the specialised sodium dependent P_i transporters

NaPi-IIa (SLC34A1), NaPi-IIc (SLC34A3) and PiT2 (SLC20A2), whilst the rest is excreted in urine. The endocrine system uses hormones to regulate the processes of gastrointestinal absorption, bone turnover and tubular reabsorption to keep serum P_i levels normal despite fluctuations in dietary intake, elimination and physiologic need.

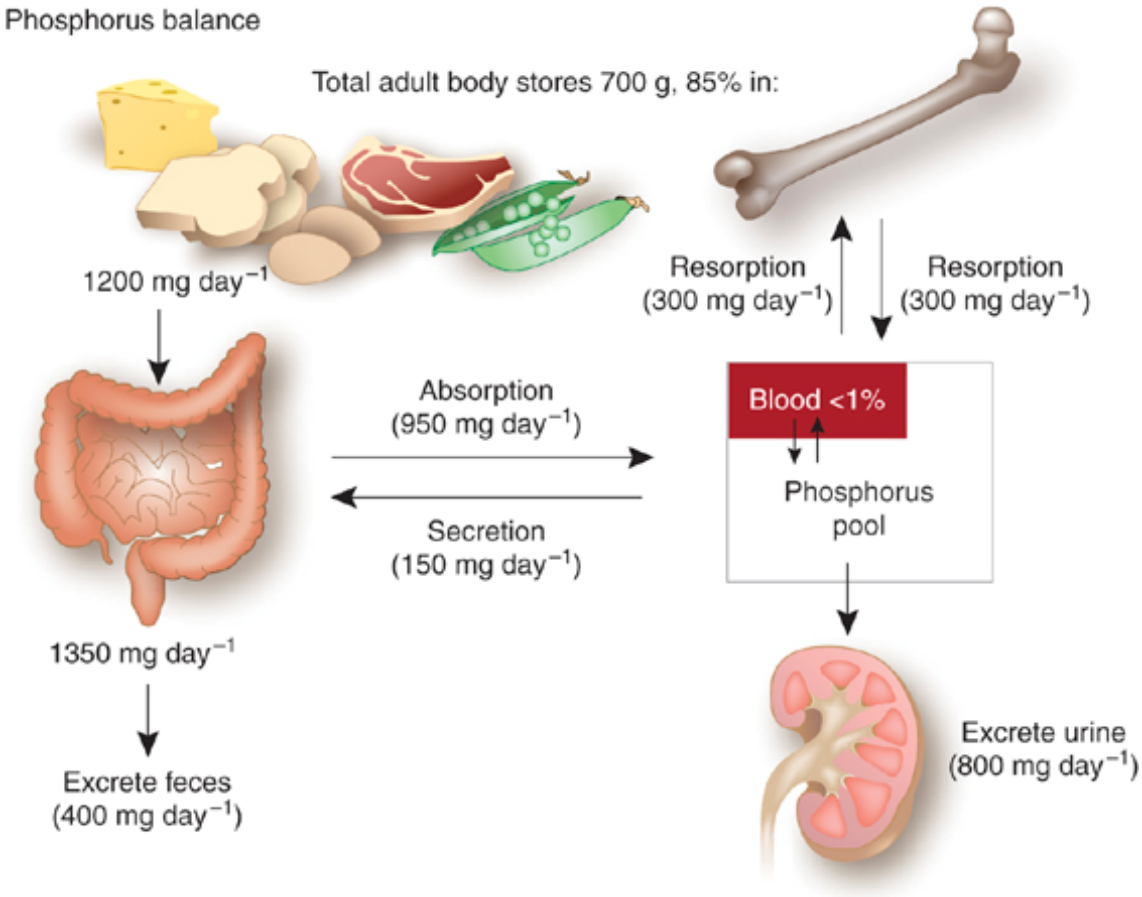

Figure 5.1: Overview of human P_i homeostasis.

The major source of phosphorus is the diet. Dietary P_i is absorbed in the small intestine. The skeleton is the major storage pool for P_i, it contains around 85% of the total body phosphorous. The main route by which P_i is lost from the body is excretion in the urine. Diagram taken from Hruska et al., 2008.

The three major hormones that regulate P_i homeostasis are parathyroid hormone (PTH), fibroblast growth factor 23 (FGF-23) and calcitriol (the active form of vitamin D: 1,25-$(OH)_2$ cholecalciferol). PTH is produced by chief cells of the parathyroid glands. It acts through the PTH receptor 1 (PTHR1) in the kidney to downregulate the key renal transporters, NaPi-IIa, NaPi-IIc and PiT2,

which are abundantly expressed in the proximal tubule, and mediates the reabsorption of P_i (Traebert *et al.*, 2000; Yang *et al.*, 2004; Bacic *et al.*, 2006; Forster *et al.*, 2006). More P_i is excreted in the urine in response to the down regulation of these transporters. Through the same receptors, PTH also stimulates the production of calcitriol through stimulation of 1α-hydroxylase (Torres and De Brauwere, 2011).

Calcitriol acts in the negative feedback loop to inhibit the secretion of PTH, in addition to stimulating NaPi-IIb and PiT2 in the GI tract, which mediate the dietary P_i absorption (Ritter *et al.*, 2006; Torres and De Brauwere, 2011). Calcitriol also stimulates the production of FGF-23 in osteocyte cells of the bone (Torres and De Brauwere, 2011). FGF-23 acts on the kidney through FGF receptors in conjunction with the co-factor, klotho-α (Kuro-o *et al.*, 1997; Hu *et al.*, 2010; Kuro, 2011). FGF-23 also down regulates NaPi-IIa, NaPi-IIc and PiT2 expression in the proximal tubules (Biber *et al.*, 2013). Removal of these transporters reduces the proximal tubule reabsorption of P_i and that enhances urinary P_i excretion. In contrast to PTH, FGF-23 is a potent inhibitor of 1α-hydroxylase and thus calcitriol production (Kuro-o *et al.*, 1997; Prie *et al.*, 2009; Torres and De Brauwere, 2011). Dentrin matrix acidic phosphoprotein 1, Ectonucleotide pyrophosphatase/phosphodiesterase 1 and phosphate-regulating neutral endopeptidase are several regulators of FGF-23 that have been identified (Martin *et al.*, 2012).

Serum P_i levels in healthy adults ranges from 2.5 to 4.5 mg/dL (0.81 to 1.45 mmol/L). A drop in this level can lead to hypophosphatemia, and can be defined as mild (2 to 2.5 mg/dL, or 0.65 to 0.81 mmol/L), moderate (1 to 2.5 mg/dL or 0.32 -0.65 mmol/L), or severe (<1 mg/dL, or <0.32 mmol/L). Moderate to severe hypophosphatemia is observed in 4 to 32 % of HIV-1 patients on ART (Badiou et al., 2006; Buchacz et al., 2006). This adverse reaction is generally related to increased urinary excretion of phosphorous (hyperphosphaturia), but the underlying aetiology is not completely understood, although HIV infection and ART are risk factors for the development of hypophosphatemia (Paccou et al., 2009). In a study of hypophosphatemia prevalence in HIV-positive patients, hypophosphatemia was more frequent in those who were on ART than ART-naïve (35% versus 10%, n = 123, P = 0.0001) (Wainwright et al., 2013). Of the

ARTs, TDF is most frequently associated with hypophosphatemia, hyperphosphaturia, and osteomalacia (defective bone mineralisation) (Buchacz et al., 2006; Labarga et al., 2009; Cooper et al., 2010; Judd et al., 2010; Calza et al., 2011; Havens et al., 2013; Ezinga et al., 2014; Giacomet et al., 2015; Lim et al., 2015).

In drug development toxicology studies conducted in rats, dogs, and monkeys, TDF administration caused bone toxicity at exposures greater than those observed in humans (based on AUCs) (Gilead Sciences, 2015). In monkeys the bone toxicity was diagnosed as osteomalacia and appeared to be reversible upon dose reduction or discontinuation of TDF. In rats and dogs, bone toxicity manifested as reduced bone mineral density. In addition, increases in phosphaturia, calciuria and decreases in serum P_i were observed to varying degrees in all species at exposures 2 to 20 times higher than those observed in humans. Disappointingly, the mechanism underlying bone toxicity was not investigated further.

In a human clinical phase study conducted in 600 HIV-1 infected adults over 144 weeks, significant decrease in bone mineral density was reported at the lumbar spine in subjects receiving a cocktail of medications containing TDF, compared to subjects taking medications with a TDF substitute (Gilead Sciences, 2015). The majority of the reduction in bone mineral density occurred in the first 24 to 48 weeks of the trial and this reduction was sustained through to week 144. In addition, there were more biochemical markers of bone metabolism, higher serum PTH levels, and higher calcitriol levels in the TDF-treatment group relative to the non-TDF-treatment group. However, except for bone-specific alkaline phosphatase, despite the increase in levels, the values remained within the normal range. Similar findings were observed in other paediatric HIV-1 clinical studies (Gilead Sciences, 2015). Indeed, since the approval of TDF use, there have been over 45 published cases that reports the association of TDF treatment with hypophosphatemia. TDF discontinuation is associated with a significant increase in serum P_i levels (Herlitz et al., 2010; Judd et al., 2010; Bech et al., 2012b; Lim et al., 2015; Magalhaes-Costa et al., 2015). But there is no conclusive evidence of a causal link.

Predominantly, the literature suggests that TDF-induced hypophosphatemia is the result of TFV induced Fanconi syndrome. TFV accumulation within the proximal tubular cells results in inhibition of mitochondrial DNA polymerase-γ. As a result, the enzymes involved in the electron transport chain and oxidative phosphorylation become depleted. Mitochondrial function is disturbed, followed by a deficit in ATP production, impaired cell function, cell injury, and eventually apoptosis. Endogenous metabolites such P_i and calcium are passed in urine instead of being reabsorbed (hyperphosphaturia) with proximal tubule cell death (Martin et al., 1994; Birkus et al., 2002; Cote et al., 2006; Kohler et al., 2009; Herlitz et al., 2010; Perazella, 2010; Fernandez-Fernandez et al., 2011; Kohler et al., 2011). A decrease in P_i reabsorption from ultrafiltrate results in low serum P_i levels (hypophosphatemia). When the body recognises there is a low P_i serum concentration, bone demineralisation can occur to increase serum P_i levels, which could lead to osteomalacia. However medically induced renal tubular damage leading to Fanconi syndrome occurs in less than 0.1% of patients on TDF and thus cannot account for the high prevalence of hypophosphatemia (Nelson *et al.*, 2007; Herlitz *et al.*, 2010; Fernandez-Fernandez *et al.*, 2011). Recent clinical studies in HIV+ patients on TDF found that renal P_i loss was not caused by hyper-secretion of PTH or FGF-23, nor by calcium or vitamin D deficiency either (Saidenberg-Kermanac'h *et al.*, 2011; Bech *et al.*, 2012a; Bech *et al.*, 2012b). This suggests that other factors, possibly a transporter-related one, may be involved in the aetiology of the clinical symptoms (Nelson et al., 2007; Hall et al., 2011; Bech et al., 2012a; Bech et al., 2012b).

In fact, a trend between the years of TDF therapy and P_i reabsorption rate of patients has suggested that TFV may inhibit P_i reabsorption (Bech et al., 2012a), which could lead to the observed TDF related adverse effects. This chapter shall therefore consider the renal handling of P_i using the human and rat PTC monolayers, and assess their suitability as *in-vitro* models for the investigation of TFV-induced toxicity.

5.2. Aims

The aims of the chapter were threefold (i) to investigate the handling of P_i, (ii) to investigate the regulation of P_i handling by PTH, FGF-23 and α-klotho, and (iii) to investigate the impact of acute exposure to TFV upon the kinetics of P_i transport in human and rat PTC monolayers.

Firstly, the uptake and flux of radiolabelled [^{32}P]-P_i in human and rat PTC monolayers over time were studied to select a suitable time point to conduct transport experiments under initial rate conditions. Once a time point had been selected, the unidirectional transepithelial fluxes of [^{32}P]-P_i were measured in the secretory and absorptive direction across paired human and rat PTC monolayers. Uptake of [^{32}P]-P_i across the basolateral and apical membrane of human and rat PTC monolayers were also measured. Kinetics parameters such as the maximum rate of [^{32}P]-P_i uptake (V_{max}) and the affinity of [^{32}P]-P_i for PTC uptake transporters (K_m) were determined in both models. Following this the effect of the following compounds on [^{32}P]-P_i uptake across the apical membrane of human and rat PTC monolayers were measured:

- Sodium
- extracellular pH
- phosphonoformic acid (PFA)
- PTH
- FGF-23
- Klotho-α
- TFV

5.3. Results

5.3.1. mRNA expression of P_i transporters in human PTC monolayer.

qPCR was performed to confirm mRNA expression of P_i transporters by human PTCs in different culture conditions (N = 3). The mRNA expression levels of NaPi-IIa, NaPi-IIc, PiT2, NPT1, NPT4 and NPT5 following culture on Transwell® inserts and plastic cultureware relative to freshly isolated cells are shown in Figure 5.2, Figure 5.3, Figure 5.4, Figure 5.5, Figure 5.6 and Figure 5.7, respectively. The data are summarised in Table 5.1 The expression levels had been normalised to the reference gene GAPDH prior to comparison. Human PTCs maintained expression of key renal P_i transporters, NaPi-IIa, NaPi-IIc and PiT2, as well as NPT1, NPT4 and NPT5 under both culture conditions. However, there was a significant fall in the expression of NaPi-IIc, PiT2 and NPT1 when compared with freshly human PTCs. No statistical difference in expression level was observed between the two culture conditions for any of the transporters.

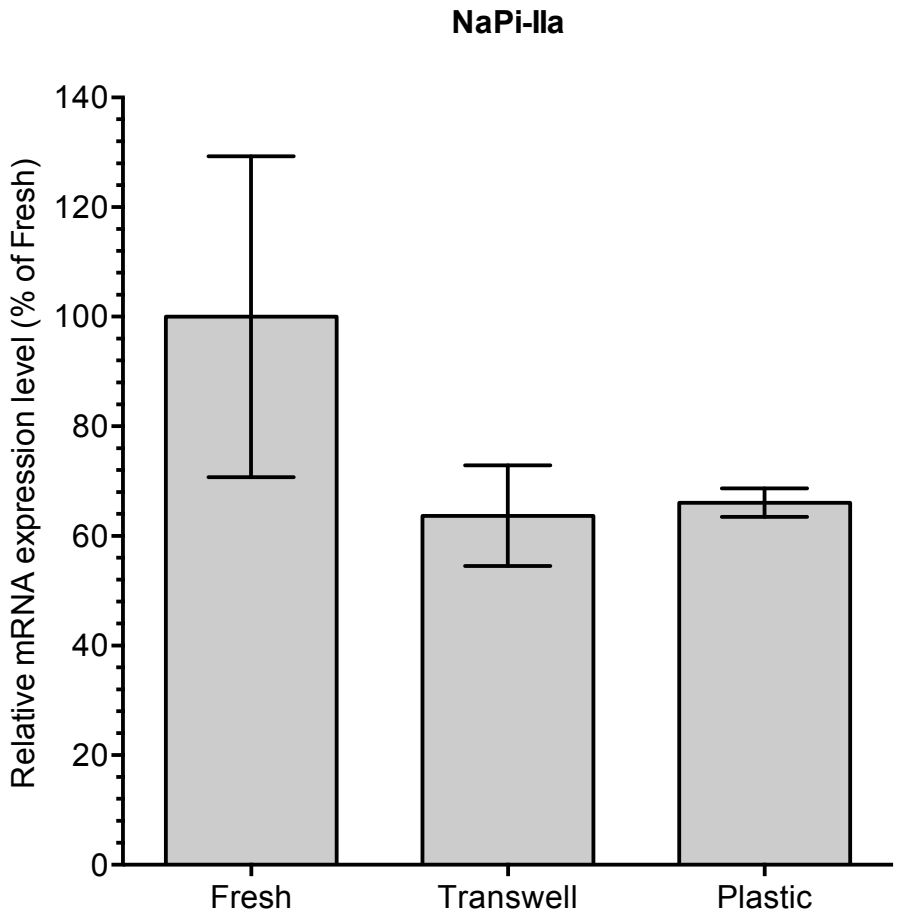

Figure 5.2: The mRNA expression of NaPi-IIa in human PTCs under different culture conditions.

NaPi-IIa mRNA expression levels are expressed as percentage expression relative to freshly isolated human PTCs. Human PTCs cultured for 7 days on Transwell inserts and plastic showed a 36.31 ± 9.18 % and 33.91 ± 2.60 % decrease in expression in comparison to freshly isolated cells (100.00 ± 29.28 %), respectively. The expression levels had been normalised to reference gene GAPDH expression level prior to comparison. The results are expressed as the mean ± SEM from 3 separate batches of RNA derived from 3 individual kidneys. One-way ANOVA statistical test was performed on the data set to determine significance.

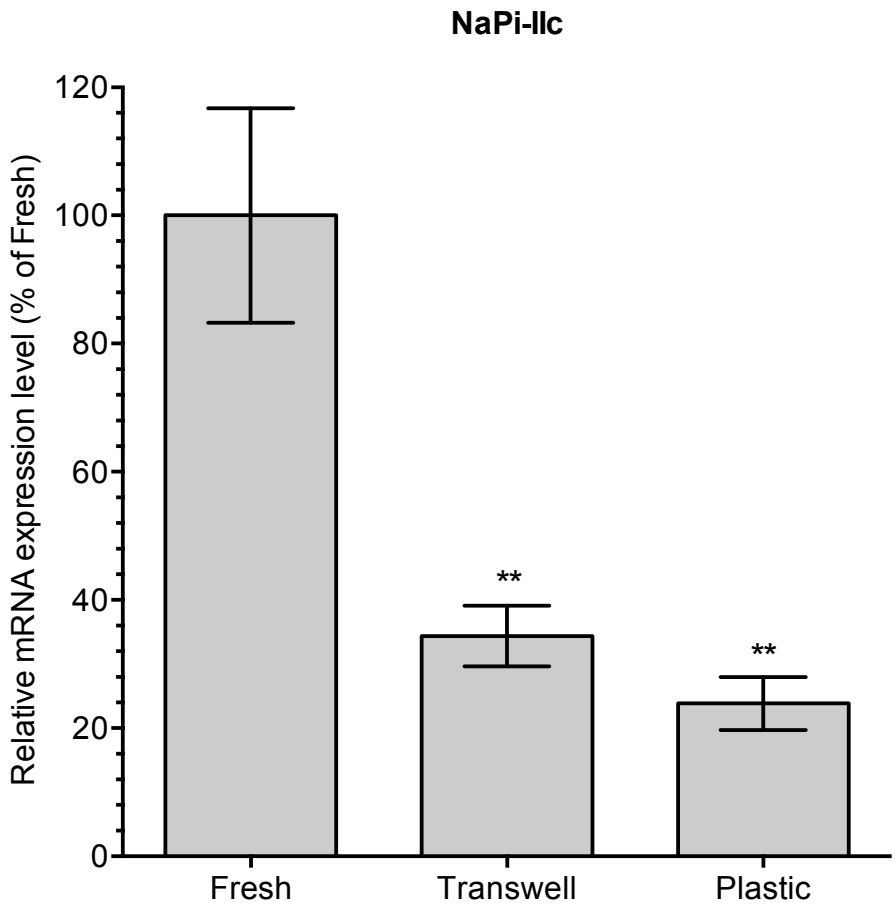

Figure 5.3: The mRNA expression of NaPi-IIc in human PTCs under different culture conditions.

*NaPi-IIc mRNA expression levels are expressed as percentage expression relative to freshly isolated human PTCs. Human PTCs cultured for 7 days on Transwell inserts and plastic showed a 65.62 ± 4.75 % and 76.13 ± 4.12 % decrease in expression in comparison to freshly isolated cells (100.00 ± 16.74 %), respectively. The expression levels had been normalised to reference gene GAPDH expression level prior to comparison. The results are expressed as the mean ± SEM from 3 separate batches of RNA derived from 3 individual kidneys. One-way ANOVA statistical test was performed on the data set to determine significance, ** P < 0.01.*

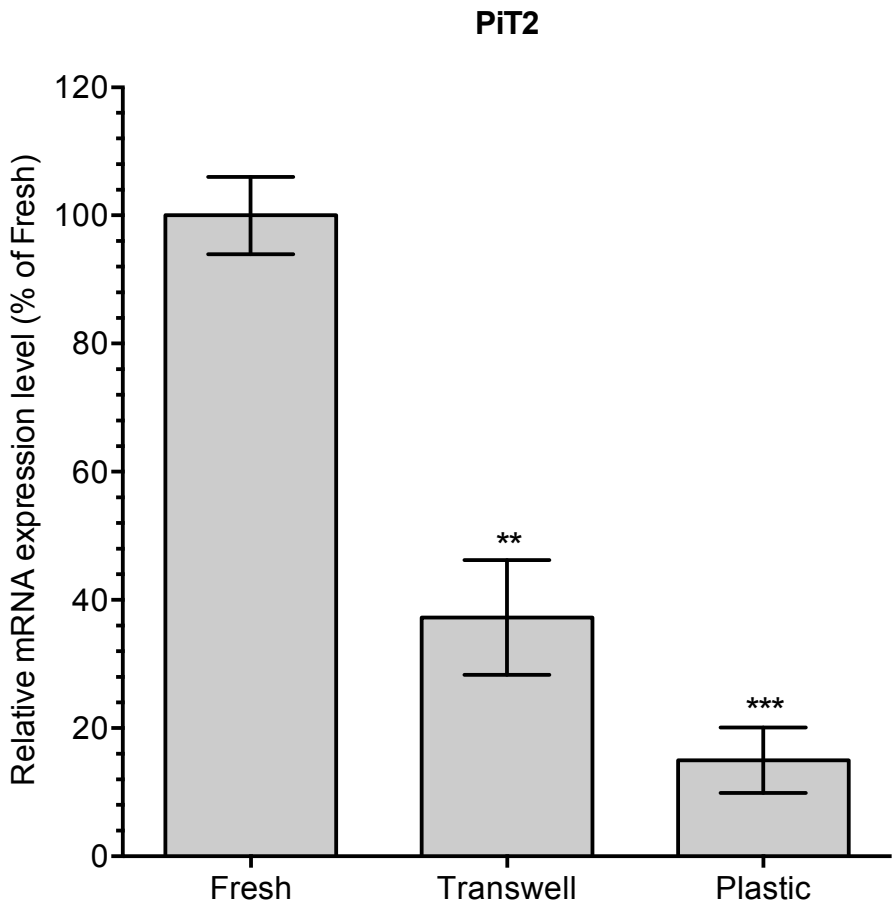

Figure 5.4: The mRNA expression of PiT2 in human PTCs under different culture conditions.

*PiT2 mRNA expression levels are expressed as percentage expression relative to freshly isolated human PTCs. Human PTCs cultured for 7 days on Transwell inserts and plastic showed a 62.71 ± 8.95 % and 85.01 ± 5.13 % decrease in expression in comparison to freshly isolated cells (100.00 ± 6.04 %), respectively. The expression levels had been normalised to reference gene GAPDH expression level prior to comparison. The results are expressed as the mean ± SEM from 3 separate batches of RNA derived from 3 individual kidneys. One-way ANOVA statistical test was performed on the data set to determine significance, ** P < 0.01, *** P < 0.001.*

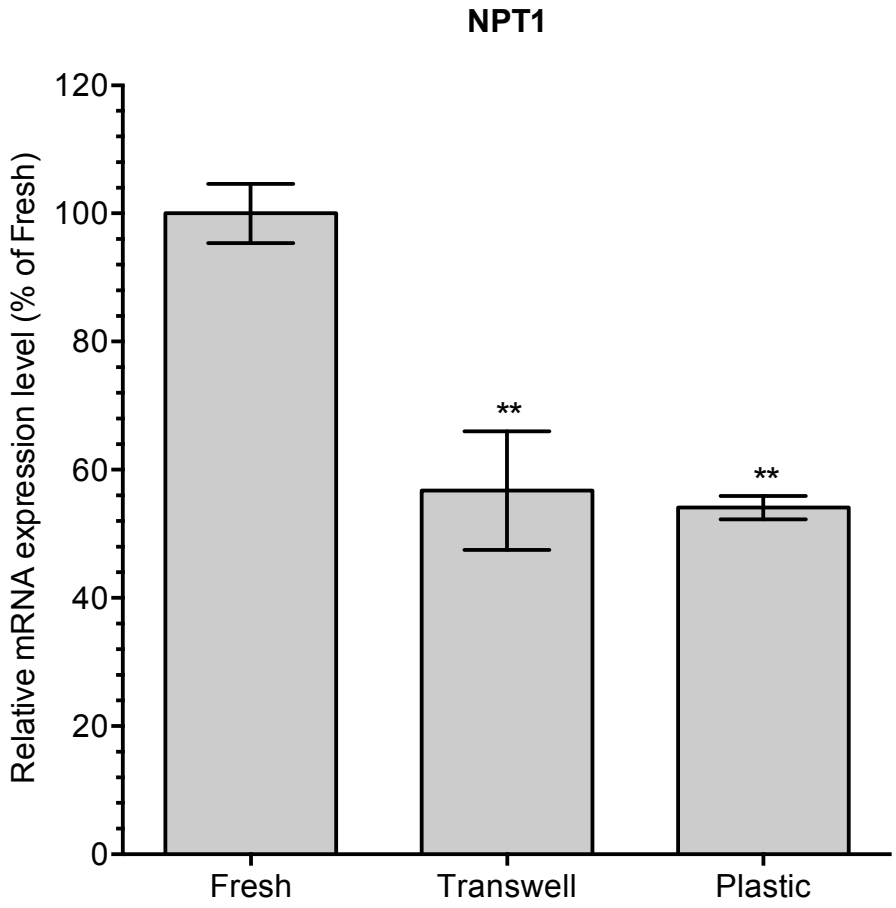

Figure 5.5: The mRNA expression of NPT1 in human PTCs under different culture conditions.

*NPT1 mRNA expression levels are expressed as percentage expression relative to freshly isolated human PTCs. Human PTCs cultured for 7 days on Transwell inserts and plastic showed a 43.26 ± 9.26 % and 45.89 ± 1.82 % decrease in expression in comparison to freshly isolated cells (100.00 ± 4.65 %), respectively. The expression levels had been normalised to reference gene GAPDH expression level prior to comparison. The results are expressed as the mean ± SEM from 3 separate batches of RNA derived from 3 individual kidneys. One-way ANOVA statistical test was performed on the data set to determine significance, ** P < 0.01.*

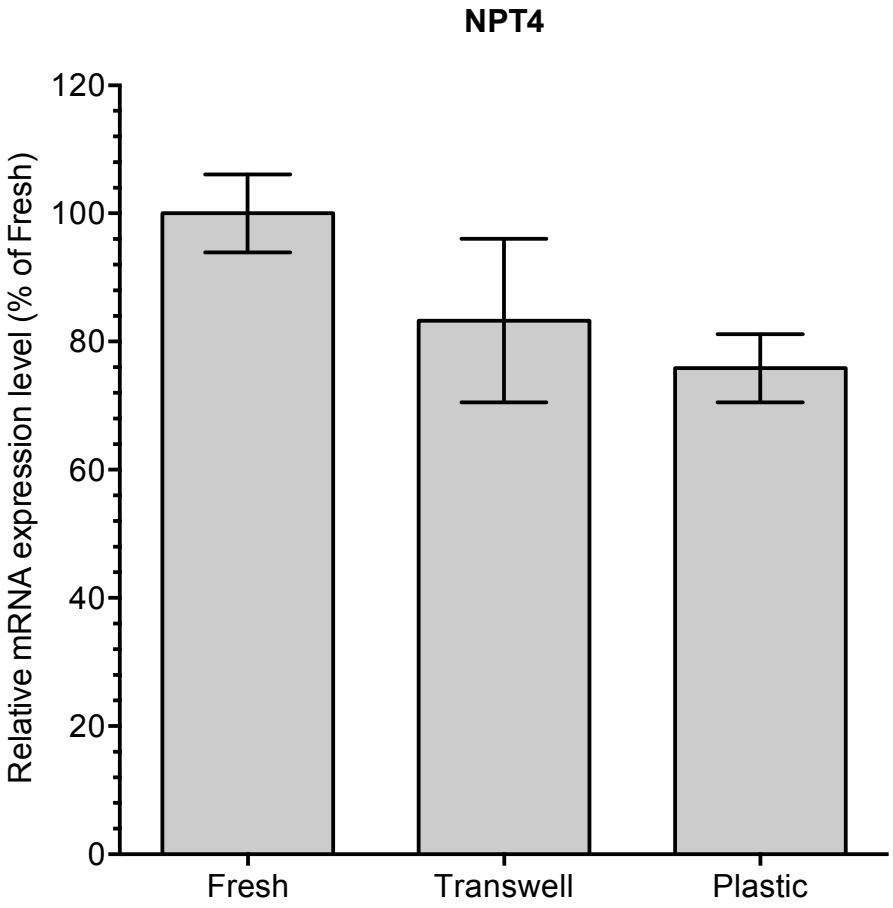

Figure 5.6: The mRNA expression of NPT4 in human PTCs under different culture conditions.

NPT4 mRNA expression levels are expressed as percentage expression relative to freshly isolated human PTCs. Human PTCs cultured for 7 days on Transwell inserts and plastic showed a 16.72 ± 12.78 % and 24.15 ± 5.32 % decrease in expression in comparison to freshly isolated cells (100.00 ± 6.06 %), respectively. The expression levels had been normalised to reference gene GAPDH expression level prior to comparison. The results are expressed as the mean ± SEM from 3 separate batches of RNA derived from 3 individual kidneys. One-way ANOVA statistical test was performed on the data set to determine significance.

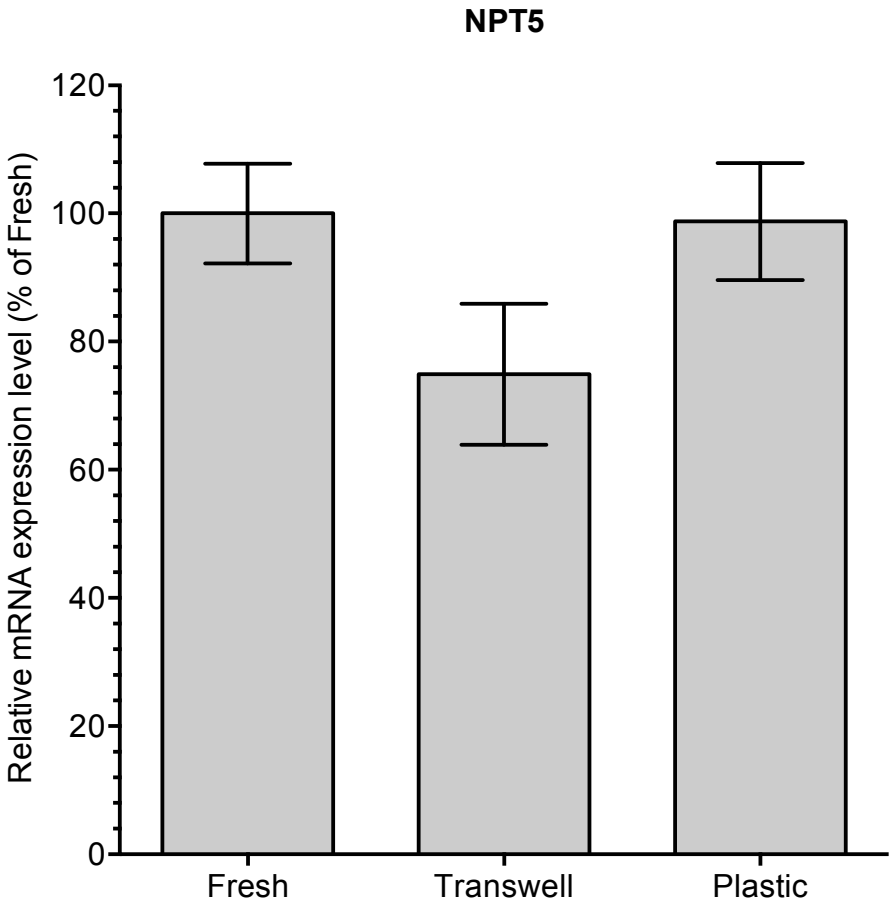

Figure 5.7: The mRNA expression of NPT5 in human PTCs under different culture conditions.

NPT5 mRNA expression levels are expressed as percentage expression relative to freshly isolated human PTCs. Human PTCs cultured for 7 days on Transwell inserts and plastic showed a 25.08 ± 10.99 % and 1.24 ± 9.12 % decrease in expression in comparison to freshly isolated cells (100.00 ± 7.77 %), respectively. The expression levels had been normalised to reference gene GAPDH expression level prior to comparison. The results are expressed as the mean ± SEM from 3 separate batches of RNA derived from 3 individual kidneys. One-way ANOVA statistical test was performed on the data set to determine significance.

Transporter	% Expression compared to fresh PTCs	
	Transwell®	Plastic
NaPi-IIa	63.69 ± 9.18	66.09 ± 2.60
NaPi-IIc	34.38 ± 4.75 **	23.87 ± 4.12 **
PiT2	37.29 ± 8.95 **	14.99 ± 5.13 ***
NPT1	56.74 ± 9.26 **	54.11 ± 1.82 **
NPT4	83.28 ± 12.77	75.85 ± 5.34
NPT5	74.90 ± 10.99	98.70 ± 9.12

Table 5.1: Percentage change in mRNA expression of P_i transporters in human PTCs cultured on plastic and Transwell® inserts when compared to freshly isolated PTCs.

*mRNA expression levels of NaPi-IIa, NaPi-IIc, PiT2, NPT1, NPT4 and NPT5 were measured using qPCR and shown as a percentage of freshly isolated cells. Expression levels had been normalised to GAPDH expression levels. Data are the mean ± SEM of expression levels determined from 3 batches of RNA derived from 3 individual kidneys. One-way ANOVA statistical test was performed on the data set to determine significance, ** P < 0.01, *** P < 0.001.*

5.3.2. Flux and uptake of P_i by human PTC monolayers over time.

In order to ensure the renal handling of P_i was measured under initial rate conditions, the rate of P_i unidirectional transepithelial flux and uptake over fixed periods of time were studied. The secretory and absorptive flux of 100 μM [^{32}P]-P_i across human PTC monolayers at 20, 40, and 60 min of exposure were measured. Additionally the apical uptake of 100 μM [^{32}P]-P_i in human PTC monolayers was measured at 0, 1, 5, 10, and 20 min of exposure.

Figure 5.8 shows the secretory, absorptive and net fluxes of 100 μM [^{32}P]-P_i increased linearly between the defined time-points (n = 9, N = 3). Correspondingly, the uptake of 100 μM [^{32}P]-P_i increased linearly between 0 and 20 min, with a gradient of 70.18 ± 1.38 pmol / cm^2 / min (n = 9, N = 3), as shown in Figure 5.9. Non-specific binding of [^{32}P]-P_i to the Transwell® insert

was also found to be 1.62 ± 0.14 pmol / cm^2, which was considered to be negligible.

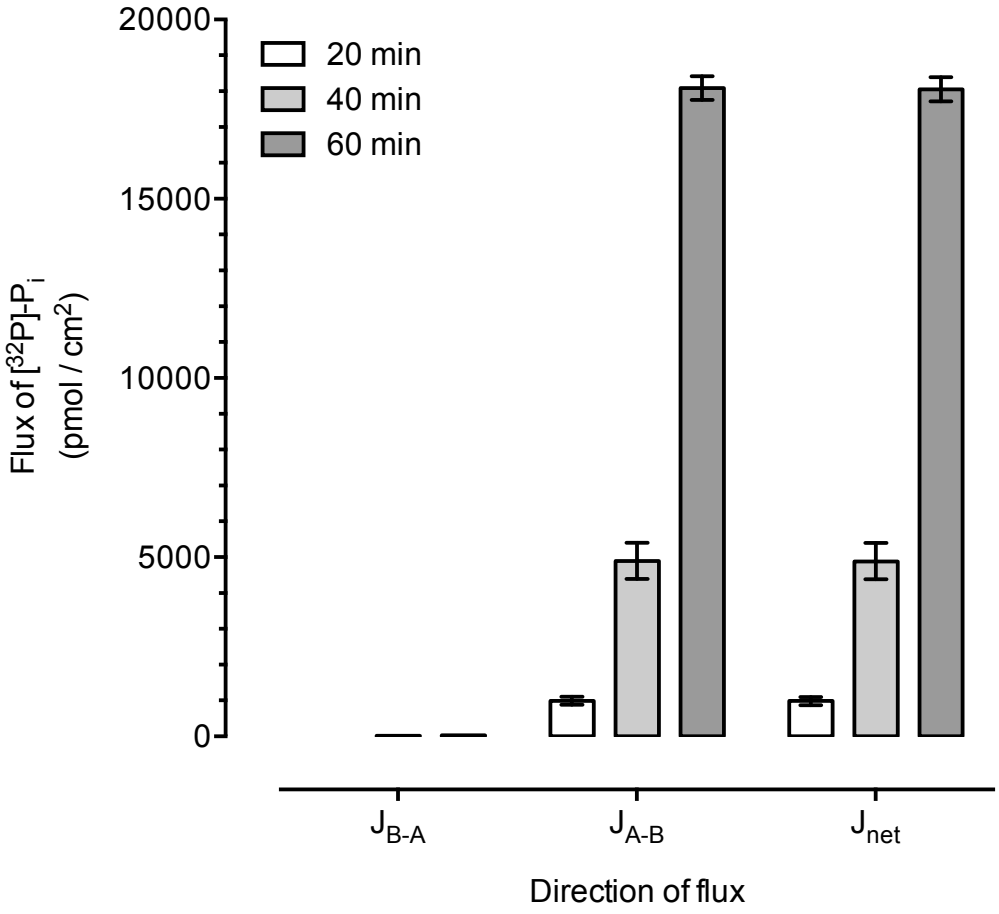

Figure 5.8: Time course of unidirectional transepithelial fluxes of 100 μM [^{32}P]-P_i across human PTC monolayers.

The fluxes of 100 μM [^{32}P]-P_i across human PTC monolayers at 20, 40 and 60 min of exposure are shown. The secretory, absorptive and net fluxes of [^{32}P]-P_i were within the linear initial rate period between 0 and 60 min. The results are expressed as the mean ± SEM from 12 human PTC monolayers derived from 3 individual kidneys.

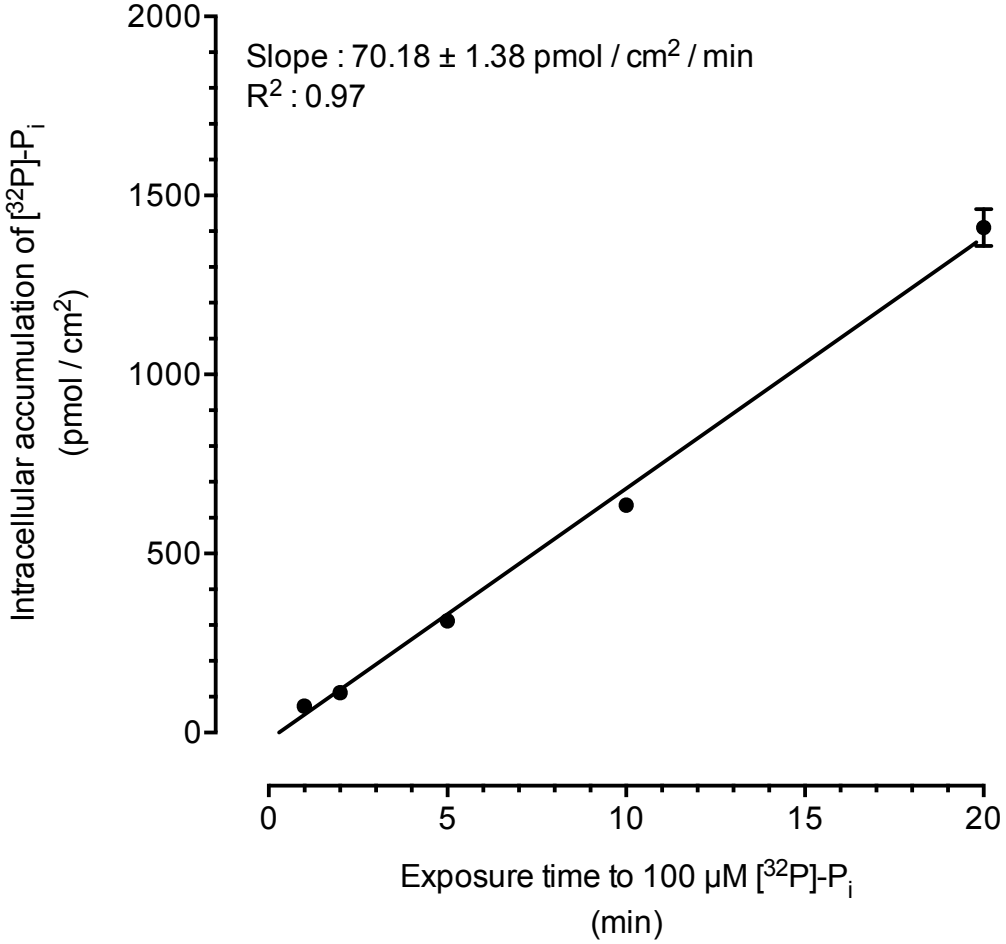

Figure 5.9: Time course of 100 µM [^{32}P]-P$_i$ uptake across the apical membrane of human PTC monolayers.

The apical membranes of the monolayers were incubated with 100 µM [^{32}P]-P$_i$ for 0, 1, 2, 5, 10 or 20 min. The intracellular accumulation of [^{32}P]-P$_i$ was linear over this time period. Linear regression analysis of the data gave a slope of 70.18 ± 1.38 pmol / cm^2 / min (R^2: 0.97). The non-specific binding of [^{32}P]-P$_i$ to the Transwell® insert was 1.62 ± 0.14 pmol / cm^2. The results are expressed as the mean ± SEM from 12 human PTC monolayers derived from 3 individual kidneys.

5.3.3. Flux and uptake of P_i by human PTC monolayers

Unidirectional transepithelial fluxes of 100 μM [^{32}P]-P_i over 60 min in both the secretory (basolateral to apical, J_{B-A}) and absorptive (apical to basolateral, J_{A-B}) direction were studied in the human PTC monolayer model. The net flux was calculated from the difference between the two fluxes. Initial rates of uptake of P_i across the basolateral or apical membrane of monolayer was also determined by measuring the intracellular accumulation of [^{32}P]-P_i in human PTC monolayers after a 5-minute incubation time.

Figure 5.10 shows a net absorption of P_i (300.94 ± 5.56 pmol / minute / cm^2) predominates across human PTC monolayers. The absorptive and secretory movement of [^{32}P]-P_i were 301.46 ± 5.56 pmol / minute / cm^2 and 0.52 ± 0.02 pmol / minute / cm^2, respectively (**** $P < 0.0001$, $n = 12$, $N = 3$). Figure 5.11 shows the intracellular accumulation of [^{32}P]-P_i, which was representative of [^{32}P]-P_i uptake across the basolateral or apical membranes of human PTC monolayers. [^{32}P]-P_i uptake across the apical membrane (312.36 ± 5.13 pmol / minute / cm^2) was 4.72-times greater than across the basolateral membrane (66.22 ± 1.50 pmol / minute / cm^2) (**** $P < 0.0001$, $n = 12$, $N = 3$). This information suggests the transporters responsible for P_i uptake are predominantly located on the apical membrane of human PTC monolayers.

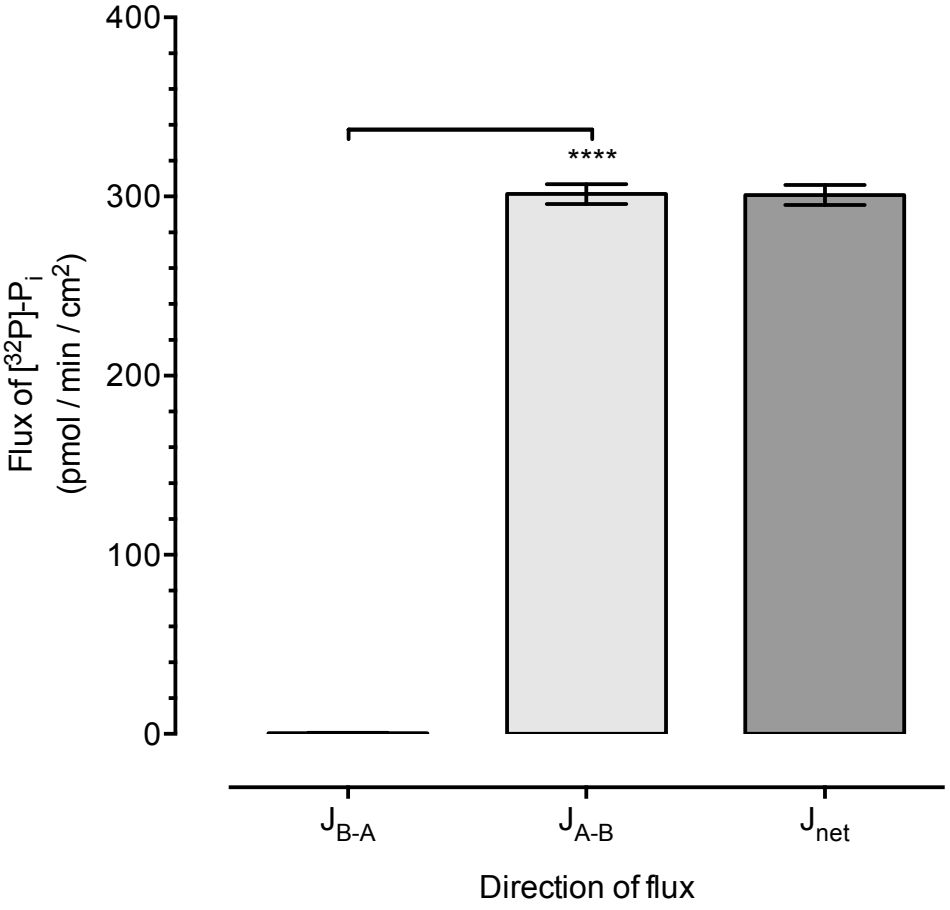

Figure 5.10: Unidirectional transepithelial fluxes of 100 μM [^{32}P]-P$_i$ across human PTC monolayers.

*In order to determine the secretory and absorptive fluxes of P$_i$ across human PTC monolayers, paired monolayers were incubated with 100 μM [^{32}P]-P$_i$ at either the basolateral or apical chamber for 60 min. The results show a net absorptive flux (300.94 ± 5.56 pmol / minute / cm^2). The absorptive movement of [^{32}P]-P$_i$ was 301.46 ± 5.56 pmol / minute / cm^2, whilst the secretory movement was negligible (0.52 ± 0.02 pmol / minute / cm^2) (**** P < 0.0001). The results are expressed as the mean ± SEM from 12 human PTC monolayers derived from 3 individual kidneys. Significance was determined by a Student's t-test.*

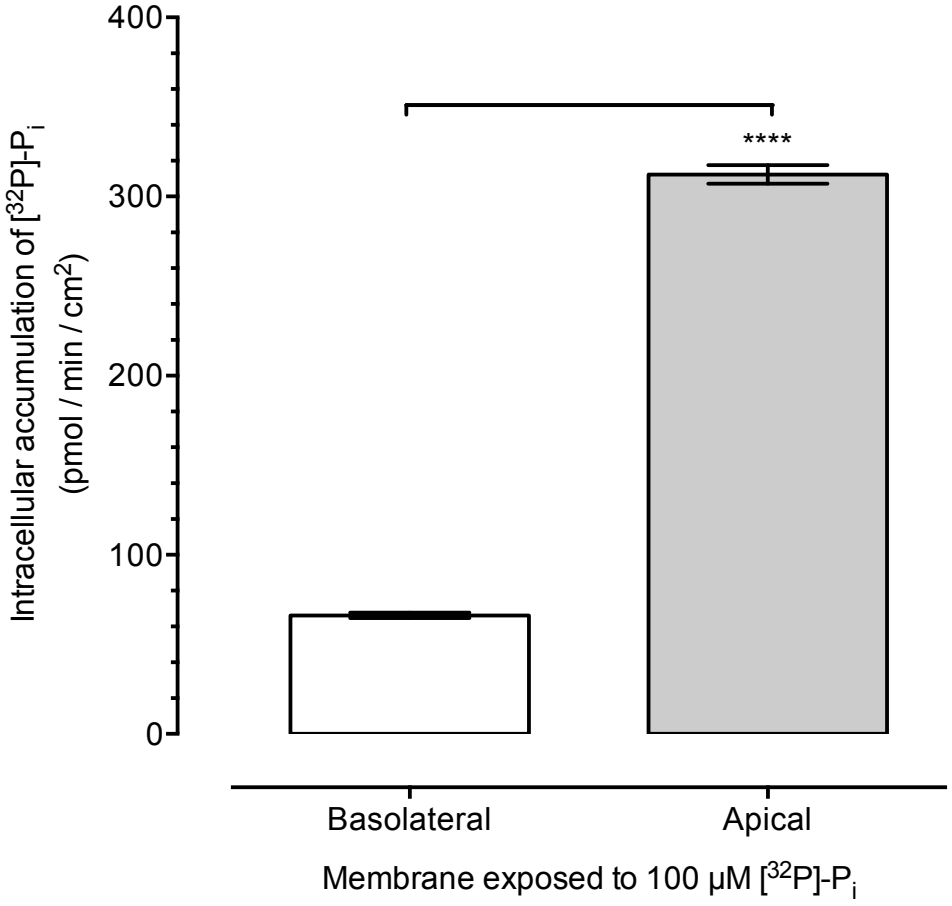

Figure 5.11: Uptake of 100 µM [^{32}P]-P$_i$ across the basolateral and apical membrane of human PTC monolayers.

*Paired monolayers were incubated with 100 µM [^{32}P]-P$_i$ at either the basolateral or apical chamber for 5 min. The data show that the initial rates of uptake of [^{32}P]-P$_i$ across the apical membrane (312.36 ± 5.13 pmol / minute / cm^2) was 4.72-times greater than across the basolateral membrane (66.22 ± 1.50 pmol / minute / cm^2) (**** P < 0.0001). The results are expressed as the mean ± SEM from 12 human PTC monolayers derived from 3 individual kidneys. Significance was determined by a Student's t-test.*

5.3.4. Kinetics of P_i transport by human PTC monolayers.

Kinetic parameters of P_i uptake across the apical membrane of human PTC monolayers were also calculated. Monolayers were incubated at the apical membrane with a range of [^{32}P]-P_i concentrations (10 to 500 μM) for 5 min and the intracellular accumulation of [^{32}P]-P_i was measured. Figure 5.12 shows the relationship between extracellular [^{32}P]-P_i concentration and intracellular accumulation of [^{3}H]-TFV (n = 9, N = 3). Non-linear regression analysis of the data gave a V_{max} of 562.90 ± 99.18 pmol / minute / cm^2 and an apparent K_m value of 106.05 ± 36.40 μM.

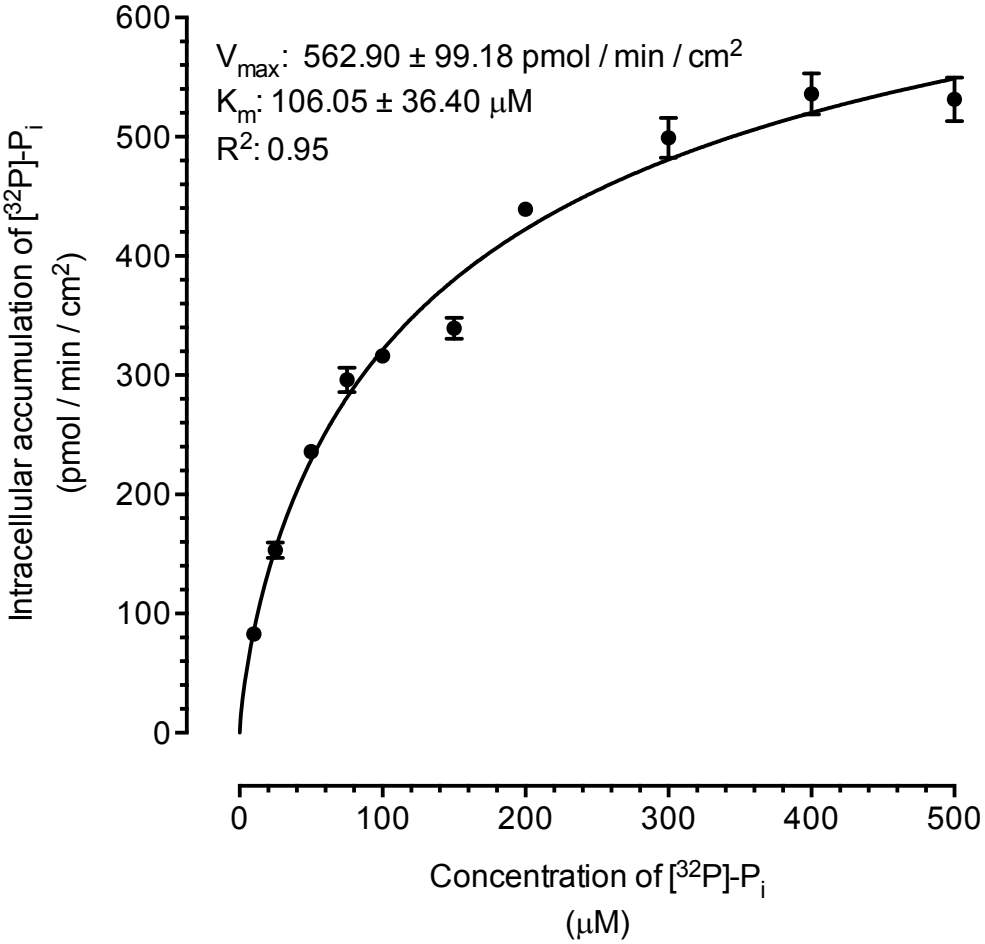

Figure 5.12: Kinetic data on [^{32}P]-P_i uptake across the apical membrane of human PTC monolayers under initial rate conditions.

In order to obtain kinetic data on P_i uptake under initial rate conditions, the monolayers were incubated with a range of [^{32}P]-P_i concentrations (10 to 500 μM) for 5 min. Non-linear regression analysis of the data gave a V_{max} of 562.90 ± 99.18 pmol / minute / cm^2 and an apparent K_m value of 106.05 ± 36.40 μM. The results are expressed as the mean ± SEM from 9 human PTC monolayers derived from 3 individual kidneys.

5.3.5. The effect of sodium concentration upon P_i renal handling by human PTC monolayers.

The key renal P_i transporters expressed in proximal tubule cells are sodium (Na^+) dependent. Therefore the Na^+ dependence of P_i uptake at the apical membrane was investigated in human PTC monolayers. The uptake of 100 μM [^{32}P]-P_i was measured in the presence and absence of Na^+ over several time points. In addition, the kinetics of apical P_i uptake in the presence of a range of Na^+ concentrations (0 to 150 mM) were also determined.

Figure 5.13 shows the apical uptake of P_i was significantly attenuated by the absence of Na^+ (n = 12, N = 3). Linear regression analysis of the data gave a slope of 70.18 ± 1.38 pmol / cm^2 / minute in the presence of 137 mM Na^+, and 0.66 ± 0.11 pmol / cm^2 / minute in the absence of Na^+. Furthermore, a strong correlation between Na^+ concentration and apical uptake of 100 μM [^{32}P]-P_i was observed in Figure 5.14 and Figure 5.15 (n = 12, N = 3). Na^+ uptake increased linearly with Na^+ concentration up to 120 mM. Uptake then plateaued between 120 and 137 mM Na^+. The buffer solution used in this experiment was hypertonic at 150 mM Na^+, which resulted in cell crenation and little uptake of P_i. The maximum rate of P_i uptake was 312.36 ± 5.13 pmol / minute / cm^2 at 137 mM Na^+. When the data was plotted as shown in Figure 5.15, non-linear regression analysis of the data gave an estimated Hill coefficient of 1.88 ± 0.16, and K_m value of 38.15 ± 1.89 mM Na^+.

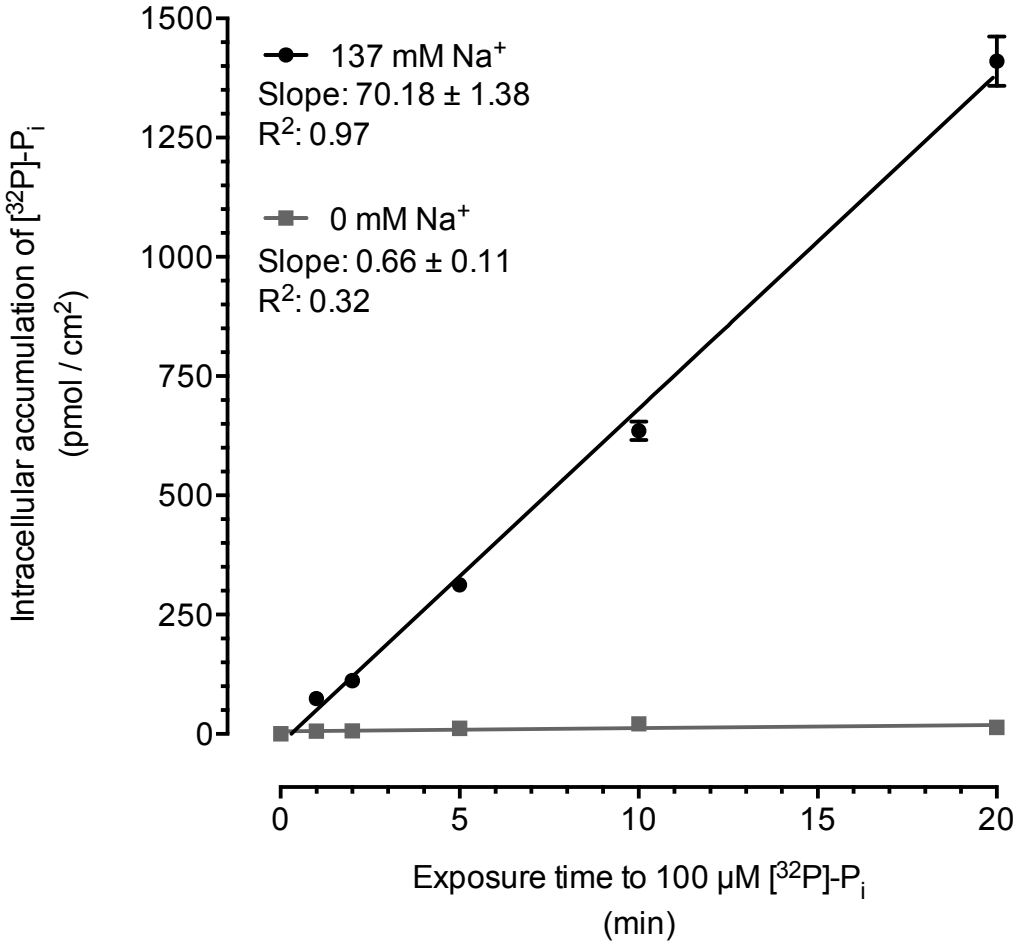

Figure 5.13: The effect of Na^+ on uptake of 100 μM [^{32}P]-P_i across the apical membrane of human PTC monolayers.

Uptake of 100 μM [^{32}P]-Pi across the apical membrane of human PTC monolayers was measured in the presence and absence of Na^+ over several time points (0 to 20 min). The results show uptake of [^{32}P]-P_i across the apical membrane was Na^+ dependent. Linear regression analysis of the data gave a slope of 70.18 $\pm$ 1.38 pmol / cm^2 / min in the presence of 137 mM Na^+, and 0.66 $\pm$ 0.11 pmol / cm^2 / min in the absence (0 mM) Na^+. The results are expressed as the mean ± SEM from 12 human PTC monolayers derived from 3 individual kidneys.

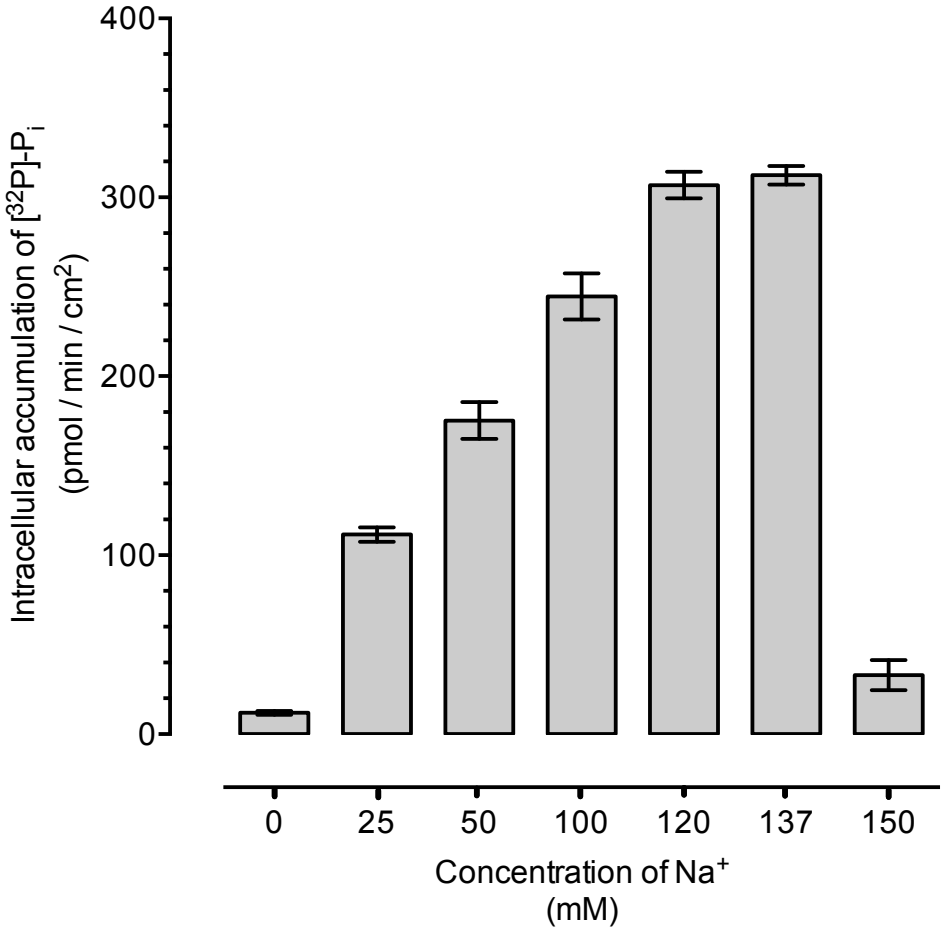

Figure 5.14: The effect of Na^+ concentration on uptake of 100 μM [^{32}P]-P_i across the apical membrane of human PTC monolayers.

Uptake of 100 μM [^{32}P]-P_i across the apical membrane of human PTC monolayers was measured over a range of Na^+ concentrations (0 to 150 mM). The results show uptake of [^{32}P]-P_i across the apical membrane was Na^+ dependent. Uptake of [^{32}P]-P_i was 11.93 $\pm$ 1.09 pmol / minute / cm^2 at 0 mM Na^+, 111.56 $\pm$ 4.10 pmol / minute / cm^2 at 25 mM Na^+, 175.29 $\pm$ 10.31 pmol / minute / cm^2 at 50 mM Na^+, 244.63 $\pm$ 12.90 pmol / minute / cm^2 at 100 mM Na^+, 306.88 $\pm$ 7.48 pmol / minute / cm^2 at 120 mM Na^+, 312.36 $\pm$ 5.13 pmol / minute / cm^2 at 137 mM Na^+, and 33.07 $\pm$ 8.46 pmol / minute / cm^2 at 150 mM Na^+. The results are expressed as the mean ± SEM from 12 human PTC monolayers derived from 3 individual kidneys.

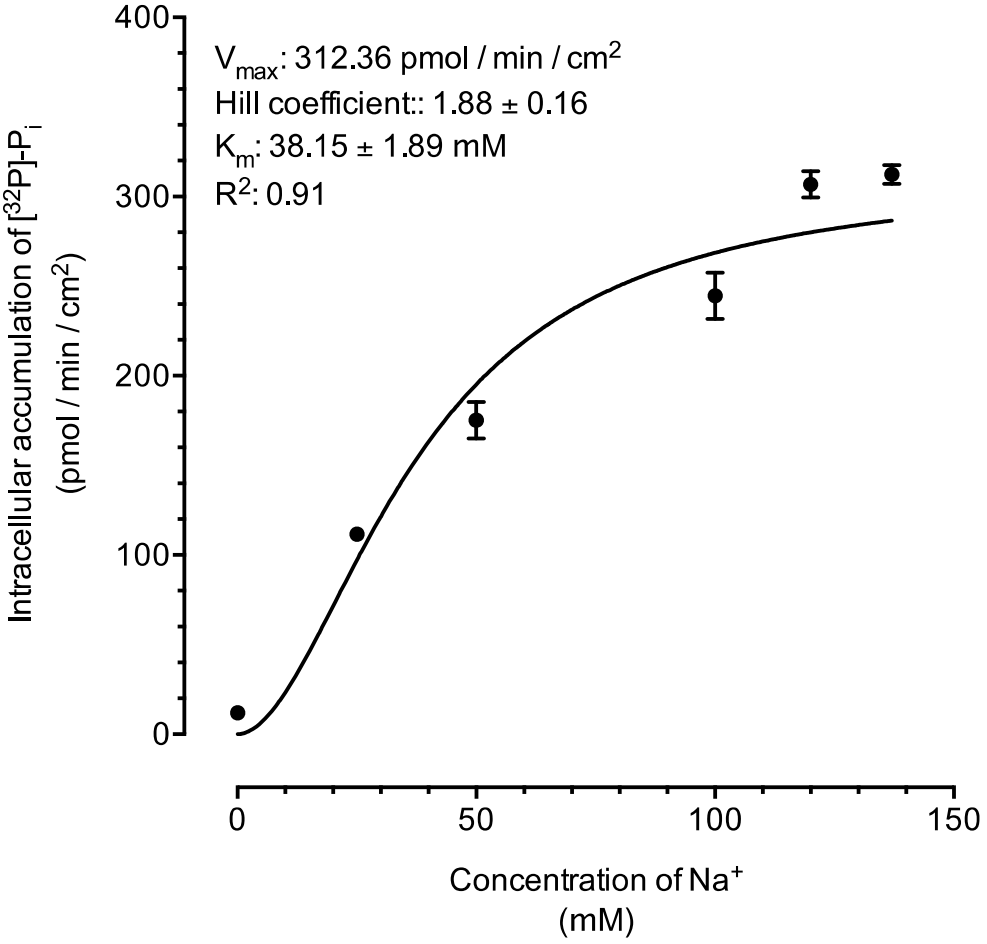

Figure 5.15: The kinetics of Na^+ and uptake of 100 μM [^{32}P]-P_i across the apical membrane of human PTC monolayers.

Uptake of 100 μM [^{32}P]-P_i across the apical membrane of human PTC monolayers was measured in a range of concentrations of Na^+ (0 to 137 mM). The results show uptake of [^{32}P]-P_i across the apical membrane was Na^+ dependent. The V_{max} was constrained to 312.36 pmol / min / cm^2 based upon previous findings. Non-linear regression analysis of the data gave an estimated Hill coefficient of 1.88 $\pm$ 0.16, and K_m value of 38.15 $\pm$ 1.89 mM Na^+. The results are expressed as the mean ± SEM from 12 human PTC monolayers derived from 3 individual kidneys.

5.3.6. The effect of pH upon P_i renal handling by human PTC monolayers.

The effect of pH on the rate of P_i uptake was studied in human PTC monolayers. The apical uptake of 100 μM [^{32}P]-P_i was measured in experimental buffer of pH 6.0, 6.5, 7.0, 7.5 and 8.0. As shown in Figure 5.16, the rate of P_i uptake was dependent on pH. For instance increasing the pH from 6.0 (154.45 ± 12.64 pmol / minute / cm^2) to 7.5 (317.09 ± 4.43 pmol / minute / cm^2) doubled the rate of P_i uptake.

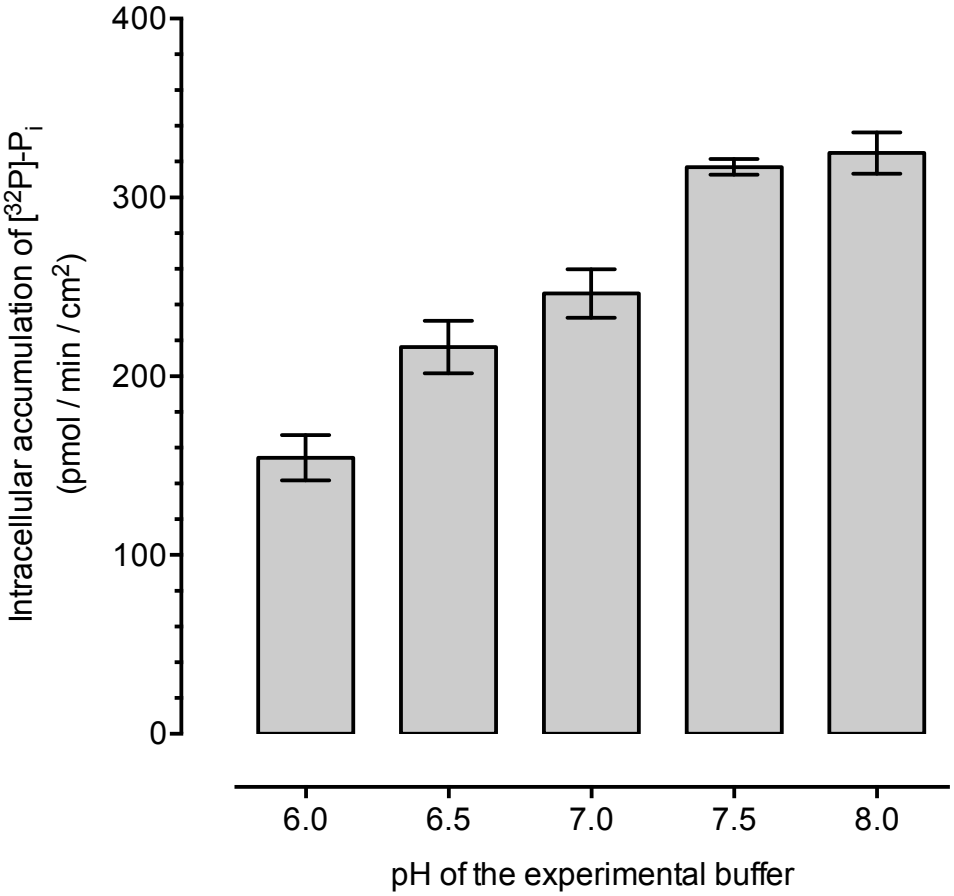

Figure 5.16: The effect of pH on uptake of 100 μM [^{32}P]-P_i across the apical membrane of human PTC monolayers.

The uptake of 100 μM [^{32}P]-P_i across the apical membrane of human PTC monolayers was measured in experimental buffer of pH 6.0, 6.5, 7.0, 7.5 and 8.0. The results show uptake of [^{32}P]-P_i across the apical membrane was pH dependent. Uptake of [^{32}P]-P_i was 154.45 ± 12.64 pmol / minute / cm^2 at pH 6.0, 216.37 ± 14.71 pmol / minute / cm^2 at pH 6.5, 246.28 ± 13.66 pmol / minute / cm^2 at pH 7.0, 317.09 ± 4.43 pmol / minute / cm^2 at pH 7.5, and 324.83 ± 11.51 pmol / minute / cm^2 at pH 8.0. The results are expressed as the mean ± SEM from 12 human PTC monolayers derived from 3 individual kidneys.

5.3.7. The effect of PFA upon P_i renal handling by human PTC monolayers.

PFA has been shown to competitively inhibit both NaPi-IIa and NaPi-IIc cotransport. In order to confirm expression of NaPi-IIa, NaPi-IIc or both, the effect of PFA on the rate of P_i uptake was studied in human PTC monolayers. Apical uptake of 100 μM [^{32}P]-P_i was measured in the presence of a range of PFA concentrations (100 to 1500 μM). The results in Figure 5.17 show the presence of PFA significantly inhibited P_i uptake (n = 9, N = 3). Non-linear regression analysis of the data gave an apparent IC_{50} value of 570.35 ± 62.50 μM. This observation confirms human PTC monolayers express NaPi-IIa and/or NaPi-IIc at a functional level.

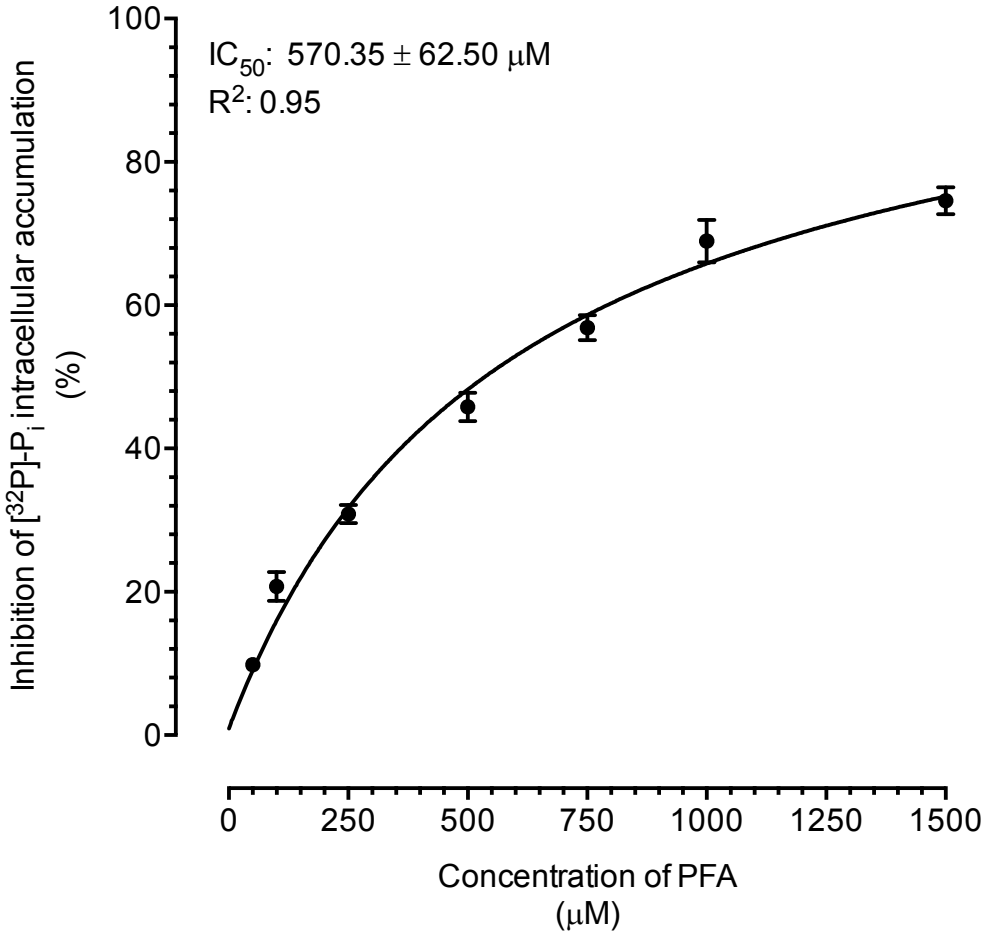

Figure 5.17: The effect of PFA on the renal handling of 100 μM [^{32}P]-P$_i$ by human PTC monolayers.

The uptake of 100 μM [^{32}P]-P$_i$ across the apical membrane of human PTC monolayers was measured in the presence of a range of concentrations of PFA (10 to 1500 μM). The presence of PFA significantly inhibited P$_i$ uptake. Non-linear regression analysis of the data gave an apparent IC$_{50}$ value of 570.35 ± 62.50 μM. The results are expressed as the mean ± SEM from 9 human PTC monolayers derived from 3 individual kidneys.

5.3.8. The effect of PTH upon P_i renal handling by human PTC monolayers.

As previously mentioned, PTH binding to PTHR1 on the basolateral membrane of proximal tubular cells down regulates expression of NaPi-IIa, NaPi-IIc, and PiT2. In order to confirm human PTC cells retain PTH intracellular signalling pathways, the effect of PTH on the rate of P_i uptake was studied in human PTC monolayers. The uptake of 100 μM [^{32}P]-P_i across the apical membrane of human PTC monolayers was measured in the presence of a range of PTH concentrations (0 to 10 nM). The presence of PTH significantly inhibited P_i uptake in a concentration dependent manner, as illustrated by the results in Figure 5.18 (n = 12, N = 3). These findings confirm the PTH intracellular signalling pathways were retained during culture of human PTCs.

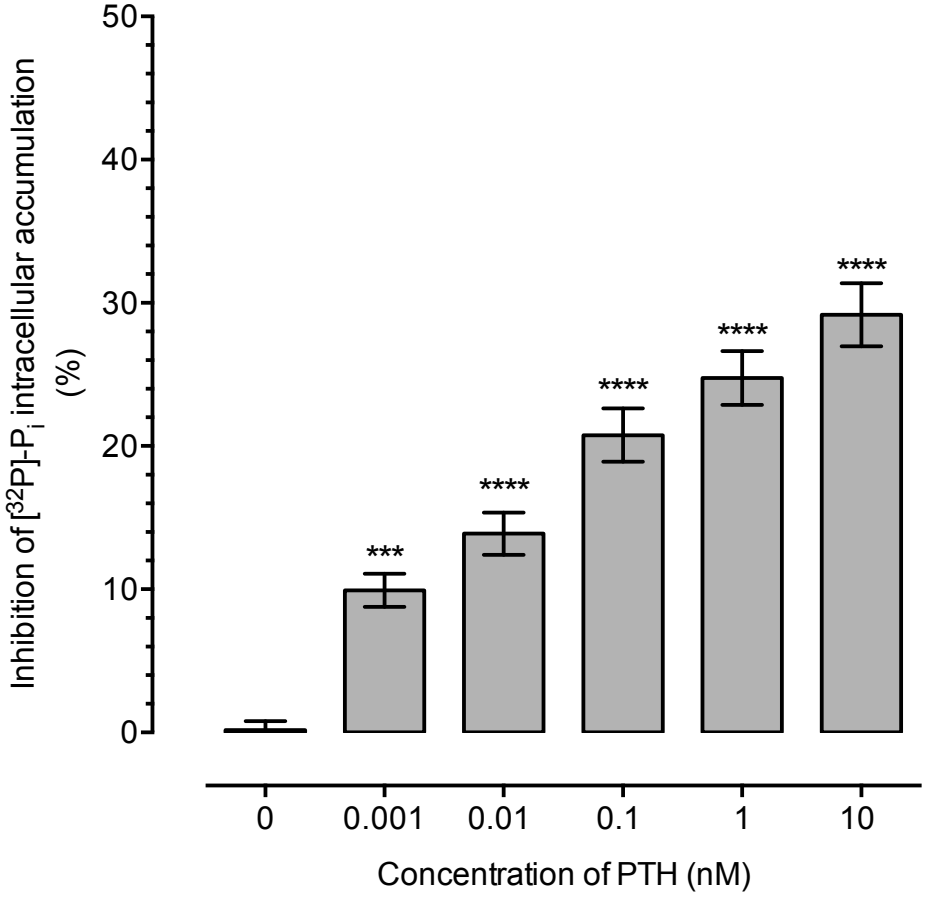

Figure 5.18: The effect of PTH on the renal handling of 100 μM [^{32}P]-P$_i$ by human PTC monolayers.

The uptake of 100 μM [^{32}P]-P$_i$ across the apical membrane of human PTC monolayers was measured in the presence of a range of concentrations of PTH (0 to 10 nM). The presence of PTH significantly inhibited P$_i$ uptake in a concentration dependent manner. The results are expressed as the mean ± SEM from 12 human PTC monolayers derived from 3 individual kidneys. Significance was determined using ANOVA and a Dunnett's post-test.

5.3.9. The effect of FGF-23 and α-klotho upon P_i renal handling by human PTC monolayers.

FGF-23 and serum soluble α-klotho also down regulate proximal tubular cell expression of NaPi-IIa, NaPi-IIc, and PiT2. In order to confirm human PTC cells retain FGF-23 and α-klotho intracellular signalling pathways, the effects of FGF-23 and α-klotho on the rate of P_i uptake were studied in human PTC monolayers. FGFs are heparin-binding proteins. Interactions with cell-surface-associated heparin sulphate proteoglycans have been shown to be essential for FGF signal transduction. Therefore an excess of heparin was included in FGF experiments.

The uptake of 100 μM [^{32}P]-P_i across the apical membrane of human PTC monolayers was measured in the presence 0.89 nM FGF-23 and 0.55 mM heparin at either the apical or basolateral membrane. As shown in Figure 5.19, the presence of FGF-23 and heparin at the basolateral membrane inhibited P_i uptake by 20.33 ± 0.64 %, whereas the presence of FGF-23 and heparin at the apical membrane did not have a significant effect (0.15 ± 0.25 % inhibition) (n = 12, N = 3). These results imply that the FGF receptors were located at the basolateral membrane of the human PTC monolayers, and that membrane-bound α-klotho and the FGF-23 intracellular signalling pathways were retained during culture.

This study was repeated by replacing 0.89 nM FGF-23 with 0.90 nM α-klotho and the results are shown in Figure 5.20. The presence of α-klotho at the basolateral membrane inhibited P_i uptake by 29.04 ± 1.27 %, whilst the presence of α-klotho at the apical membrane did not have a significant effect (5.54 ± 1.50 % inhibition) (n = 12, N = 3). These findings suggest that soluble α-klotho bound to FGF receptor 1 (FGFR1) at the basolateral membrane of human PTC monolayers and caused a decrease in P_i absorption, and the cells retained α-klotho intracellular signalling pathway in culture.

In Figure 5.21, the uptake of 100 μM [^{32}P]-P_i across the apical membrane of human PTC monolayers in the presence of 0.89 nM FGF-23, 0.90 nM α-klotho and 0.55 mM heparin is shown. The presence of FGF-23, heparin and α-klotho at the basolateral membrane inhibited P_i uptake significantly greater than the

presence of each alone (39.18 ± 1.39 % inhibition) suggesting an additive effect (n = 12, N = 3).

The effect of α-klotho concentration on the rate of P_i uptake was also studied in human PTC monolayers. The uptake of 100 μM [^{32}P]-P_i across the apical membrane of human PTC monolayers was measured in the presence of a range of α-klotho concentrations (0.18 to 5.4 nM). Figure 5.22 shows the presence of α-klotho significantly inhibited P_i uptake in a concentration dependent manner (n = 8, N = 2).

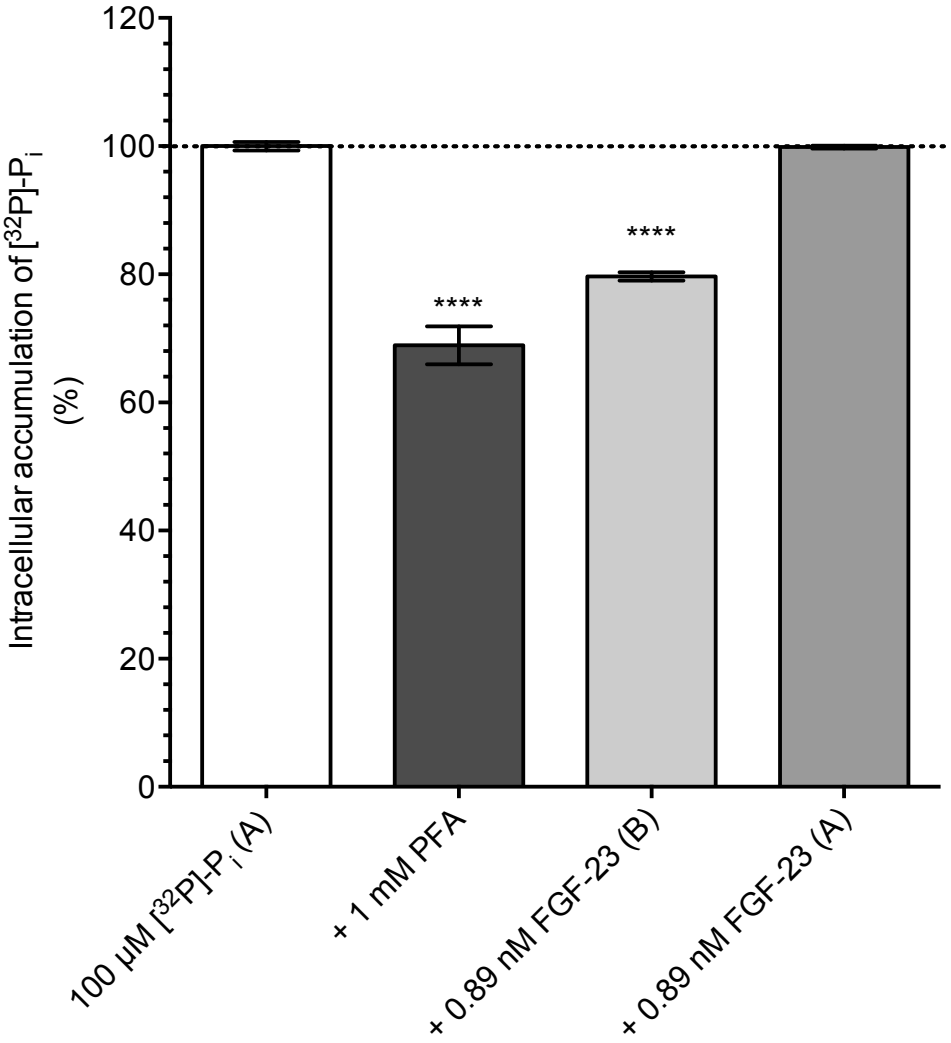

Figure 5.19: The effect of FGF-23 on the renal handling of 100 µM [^{32}P]-P_i by human PTC monolayers.

The uptake of 100 µM [^{32}P]-P_i across the apical membrane of human PTC monolayers was measured in the presence and absence of 0.89 nM FGF-23. 0.55 mM heparin was in all conditions. A positive control of 1 mM PFA was included. The presence of 1 mM PFA inhibited uptake of 100 µM [^{32}P]-P_i across the apical membrane by 31.06 ± 2.96 %. The presence of 0.89 nM FGF-23 at the basolateral membrane inhibited P_i uptake by 20.33 ± 0.64 %, whilst the presence of 0.89 nM FGF-23 at the apical membrane did not have a significant effect (0.15 ± 0.25 % inhibition). The results are expressed as the mean ± SEM from 12 human PTC monolayers derived from 3 individual kidneys. Significance was determined using ANOVA and a Dunnett's post-test.

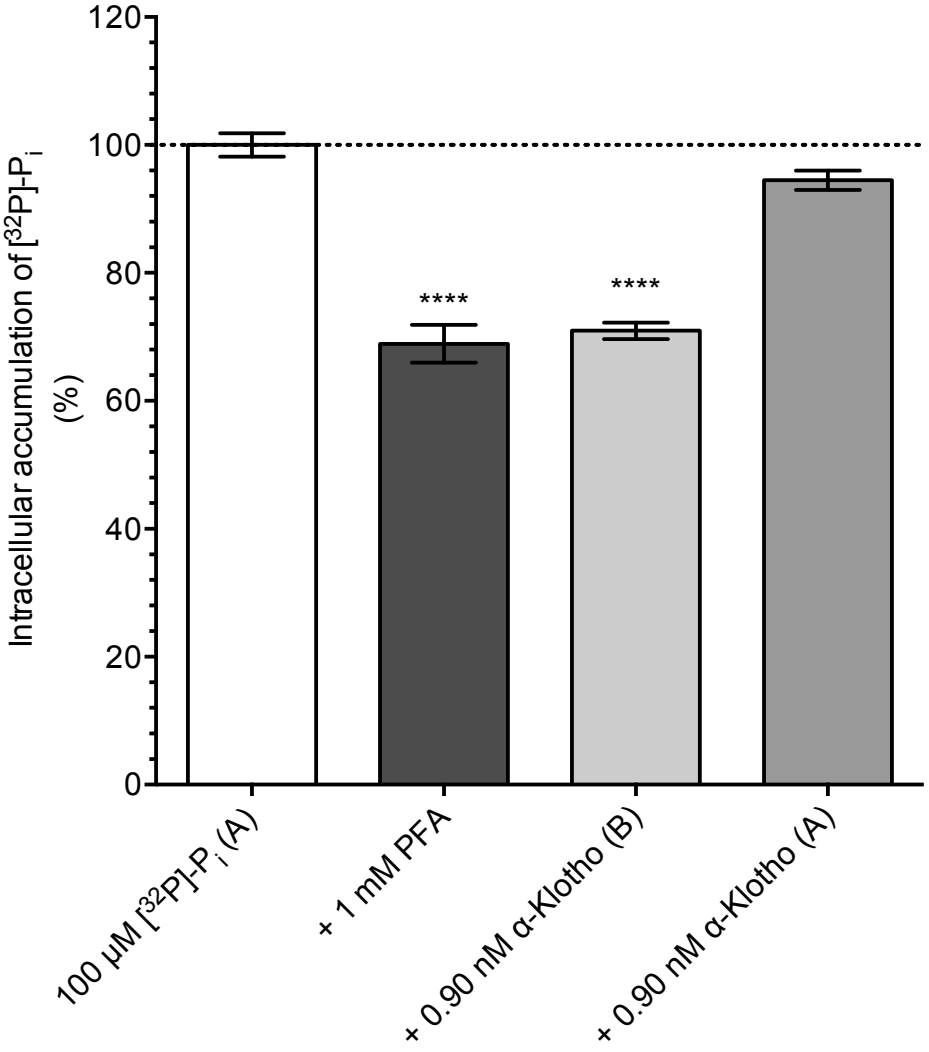

Figure 5.20: The effect of α–klotho on the renal handling of 100 μM [^{32}P]-P$_i$ by human PTC monolayers.

The uptake of 100 μM [^{32}P]-P$_i$ across the apical membrane of human PTC monolayers was measured in the presence and absence of 0.90 nM α-klotho. 0.55 mM heparin was used in all conditions. A positive control of 1 mM PFA was included. The presence of 1 mM PFA inhibited uptake of 100 μM [^{32}P]-P$_i$ across the apical membrane by 31.06 ± 2.96 %. The presence of 0.90 nM α-klotho at the basolateral membrane inhibited P$_i$ uptake by 29.04 ± 1.27 %, whilst the presence of 0.90 nM α-klotho at the apical membrane did not have a significant effect (5.54 ± 1.50 % inhibition). The results are expressed as the mean ± SEM from 12 human PTC monolayers derived from 3 individual kidneys. Significance was determined using ANOVA and a Dunnett's post-test.

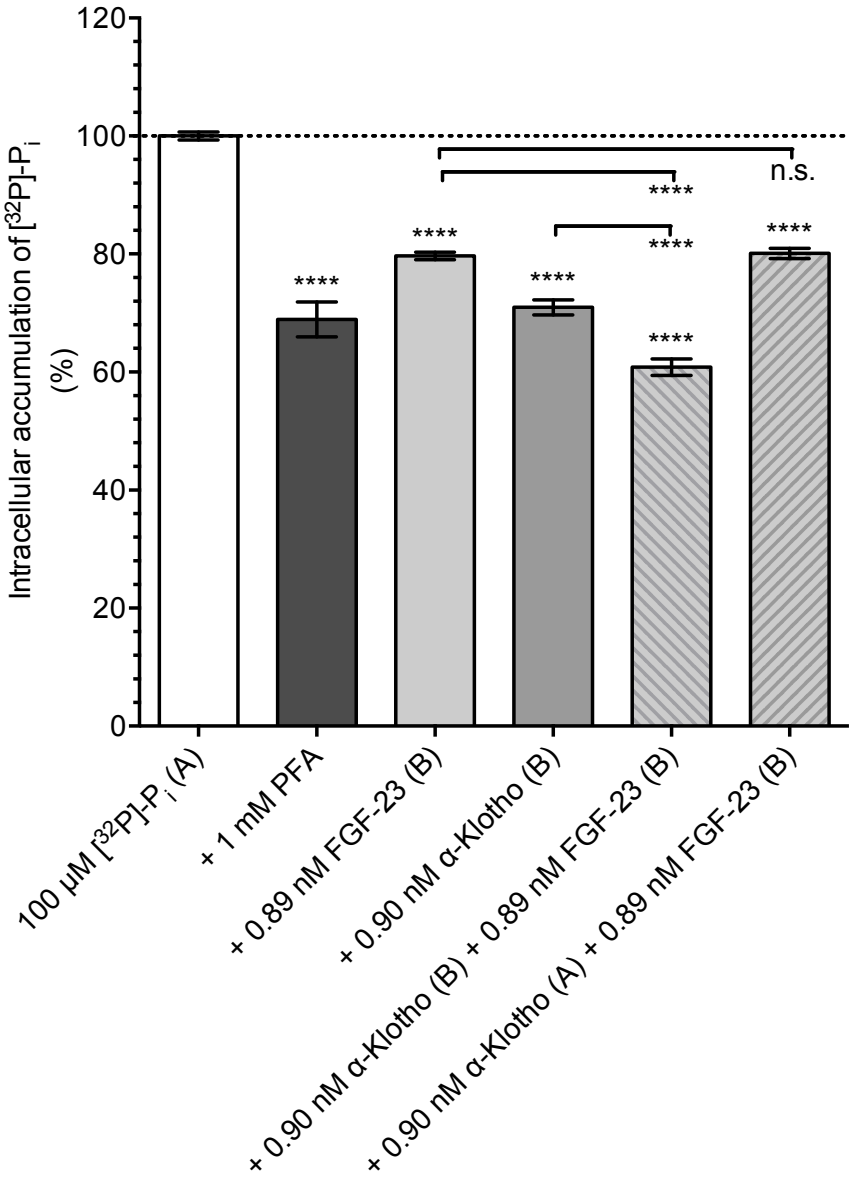

Figure 5.21: The effect of FGF-23 and α–klotho on the renal handling of 100 μM [^{32}P]-P$_i$ by human PTC monolayers.

The uptake of 100 μM [^{32}P]-P$_i$ across the apical membrane of human PTC monolayers was measured in the presence and absence of 1 mM PFA, 0.89 nM FGF-23 and 0.90 nM α-klotho. 0.55 mM heparin was included in all experiments. The presence of 1 mM PFA inhibited uptake of 100 μM [^{32}P]-P$_i$ across the apical membrane by 31.06 ± 2.96 %. The presence of 0.89 nM FGF-23 and 0.55 mM heparin at the basolateral membrane inhibited P$_i$ uptake by 20.33 ± 0.64 %. The presence of 0.90 nM α-klotho and 0.55 mM heparin at the basolateral membrane inhibited P$_i$ uptake by 29.04 ± 1.27 %. The presence of 0.89 nM FGF-23, 0.90 nM α-klotho and 0.55 mM heparin at the basolateral membrane inhibited P$_i$ uptake significantly greater than the presence of each alone (39.18 ± 1.39 % inhibition). The results are expressed as the mean ± SEM from 12 human PTC monolayers derived from 3 individual kidneys. Significance was determined using ANOVA and a Dunnett's post-test.

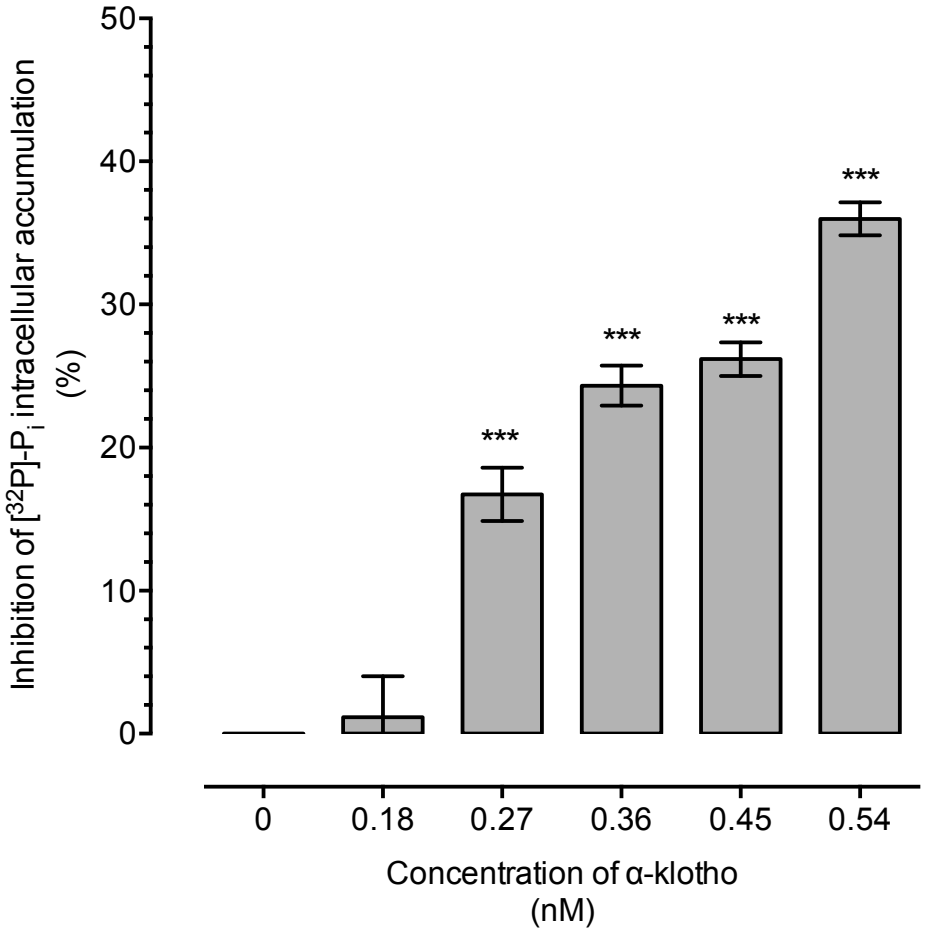

Figure 5.22: The effect of α–klotho on the renal handling of 100 μM [^{32}P]-P$_i$ by human PTC monolayers.

The uptake of 100 μM [^{32}P]-P$_i$ across the apical membrane of human PTC monolayers was measured in the presence of a range of concentrations of α-klotho (0.18 to 0.54 nM). The presence of α-klotho significantly inhibited P$_i$ uptake in a concentration dependent manner. The results are expressed as the mean ± SEM from 8 human PTC monolayers derived from 2 individual kidneys. Significance was determined using ANOVA and a Dunnett's post-test.

5.3.10. The effect of TFV upon P_i renal handling by human PTC monolayers.

The effect of TFV on the rate of P_i uptake was studied in human PTC monolayers. Initially, the uptake of 100 μM [^{32}P]-P_i across the apical membrane of human PTC monolayers was measured in the presence and absence of 10 μM TFV. As shown in Figure 5.23, apical uptake of P_i was 312.40 ± 5.13 pmol / minute /cm^2 in the absence of TFV, and 201.80 ± 3.28 pmol / minute / cm^2 in the presence of 10 μM TFV, which equates to a 35.40 ± 1.05 % decrease in P_i uptake. The kinetics of inhibition were determined by measuring P_i uptake in the presence of a range of TFV concentrations (1 to 500 μM). TFV inhibited P_i uptake in a concentration dependent manner, Figure 5.24. Non-linear regression analysis of the data gave an apparent IC_{50} value of 52.25 ± 4.71 μM TFV.

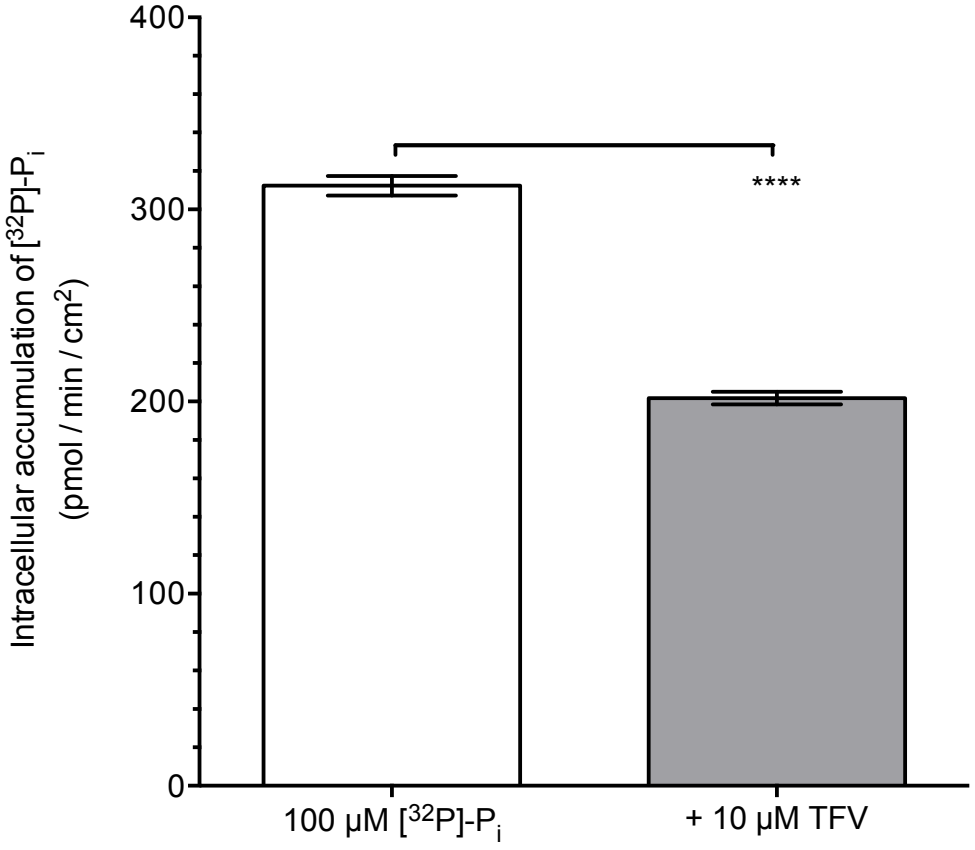

Figure 5.23: The effect of 10 µM TFV on the renal handling of 100 µM [^{32}P]-P_i by human PTC monolayers.

The uptake of 100 µM [^{32}P]-P_i across the apical membrane of human PTC monolayers was measured in the presence and absence of 10 µM TFV. The presence of TFV inhibited uptake of 100 µM [^{32}P]-P_i across the apical membrane by 35.40 ± 1.05 %; apical uptake of P_i was 312.40 ± 5.13 pmol / minute /cm^2 in the absence of TFV, compared to 201.80 ± 3.28 pmol / minute / cm^2 in the presence of 10 µM TFV. The results are expressed as the mean ± SEM from 12 human PTC monolayers derived from 3 individual kidneys. Significance was determined by a Student's t-test.

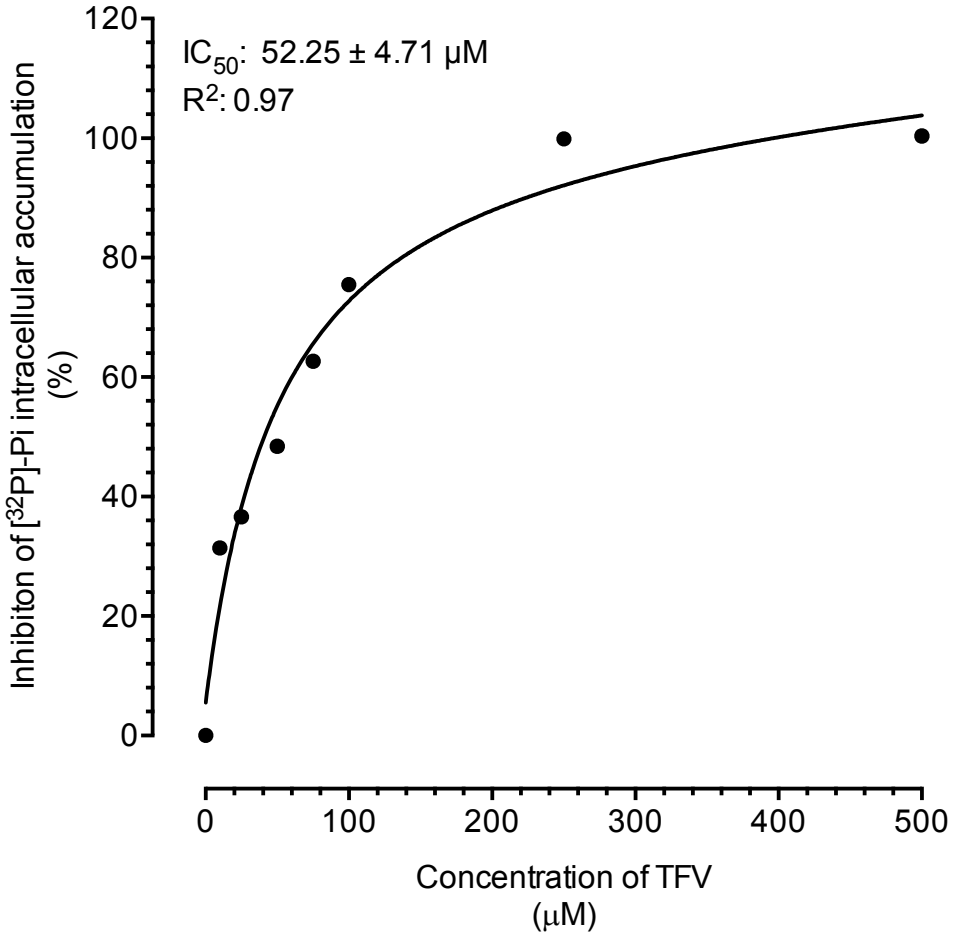

Figure 5.24: The kinetics of TFV inhibition of apical uptake of 100 µM [^{32}P]-P_i across human PTC monolayers.

The uptake of 100 µM [^{32}P]-P_i across the apical membrane of human PTC monolayers was measured in the presence of a range of TFV concentrations. TFV inhibited P_i uptake in a concentration dependent manner. Non-linear regression analysis of the data gave an apparent IC_{50} value of 52.25 ± 4.71 µM TFV. The results are expressed as the mean ± SEM from 12 human PTC monolayers derived from 3 individual kidneys.

5.3.11. Flux and uptake of P_i by rat PTC monolayers over time.

To ensure the renal handling of P_i was measured under initial rate conditions, the rate of P_i unidirectional transepithelial fluxes and uptake over time were studied. The secretory and absorptive fluxes of 100 μM [^{32}P]-P_i across rat PTC monolayers following 20, 40, and 60 min of exposure were measured. Additionally the uptake of 100 μM [^{32}P]-P_i across the apical membrane of rat PTC monolayers was measured at 0, 1, 5, 10, and 20 min of exposure.

Figure 5.25 shows the secretory, absorptive and net fluxes of 100 μM [^{32}P]-P_i increased linearly between the defined time-points (n = 9, N = 3). Correspondingly, the uptake of 100 μM [^{32}P]-P_i increased linearly between 0 and 20 min, with a gradient of 2.86 ± 0.12 pmol / cm^2 / minute (n = 9, N = 3), as shown in Figure 5.26. We can thus deduce that 0 to 60 min lies within the linear rate of P_i transport. Non-specific binding of [^{32}P]-P_i to the Transwell® insert was also found to be 0.19 ± 0.03 pmol / cm^2, which was considered to be negligible.

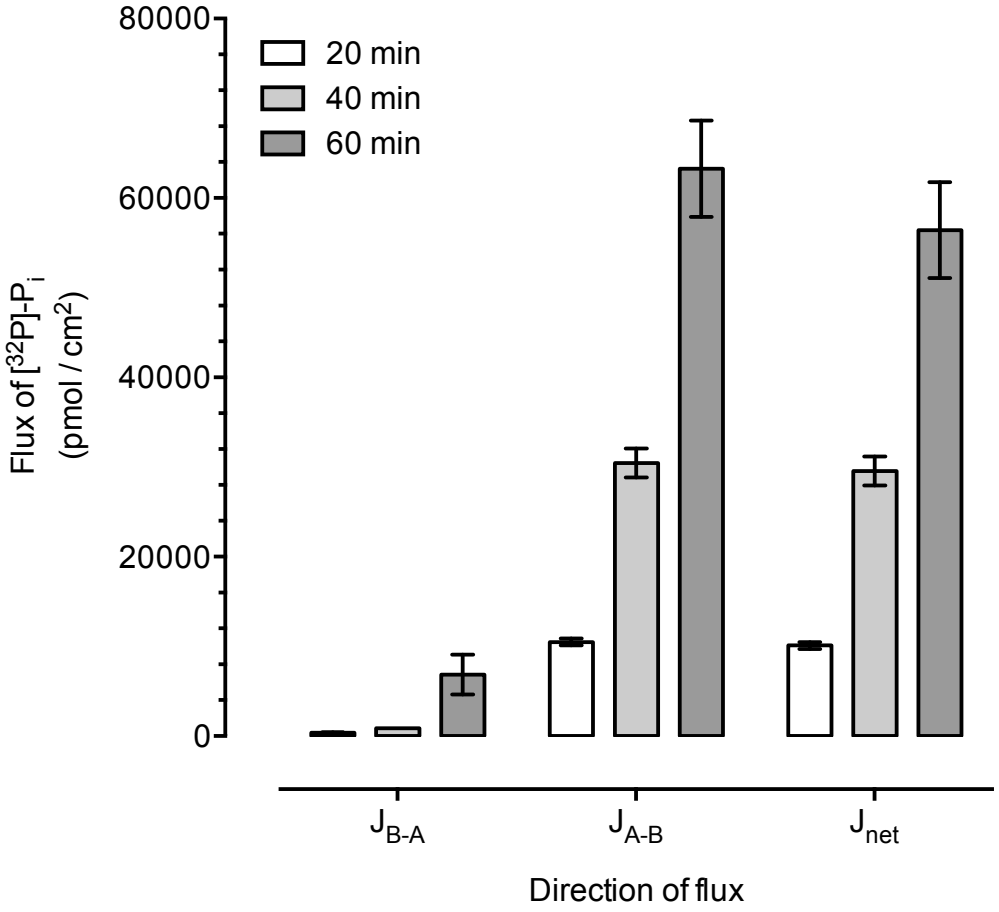

Figure 5.25: Time course of unidirectional fluxes of 100 μM [^{32}P]-P$_i$ across rat PTC monolayers.

The fluxes of 100 μM [^{32}P]-P$_i$ across rat PTC monolayers over the defined periods of time are shown. The fluxes of [^{32}P]-P$_i$ were within the initial rate period between 0 and 60 min as secretory, absorptive and net fluxes were linear over this time period. The results are expressed as the mean ± SEM from 12 rat PTC monolayers derived from 3 individual kidneys.

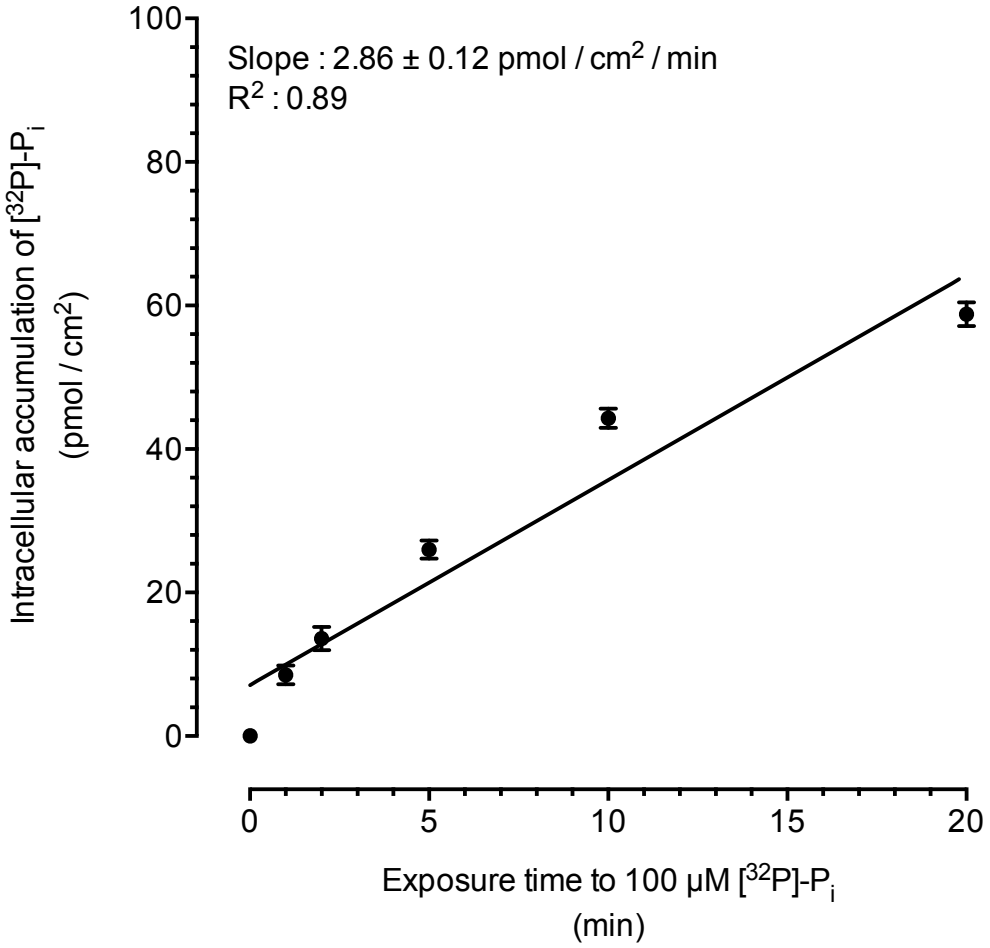

Figure 5.26: Time course of 100 µM [^{32}P]-P$_i$ uptake across the apical membrane of rat PTC monolayers.

The apical membranes of the monolayers were incubated with 100 µM [^{32}P]-P$_i$ for 0, 1, 2, 5, 10 or 20 min. The rate of uptake of [^{32}P]-P$_i$ was linear within the time period investigated. Linear regression analysis of the data gave a slope of 2.86 ± 0.12 pmol / cm^2 / minute (R^2: 0.89). The non-specific binding of [^{32}P]-P$_i$ to the Transwell® insert was 0.19 ± 0.03 pmol / cm^2. The results are expressed as the mean ± SEM from 12 rat PTC monolayers derived from 3 individual kidneys.

5.3.12. Flux of P_i by rat PTC monolayers.

Unidirectional transepithelial fluxes of 100 μM [^{32}P]-P_i over 60 min in both the secretory and absorptive direction were also studied in the rat PTC monolayer model. The findings in Figure 5.27 show a net absorption of P_i (1101.15 ± 24.84 pmol / minute / cm^2) across the rat PTC monolayers. The absorptive and secretory movement of [^{32}P]-P_i was 1129.06 ± 25.01 pmol / minute / cm^2 and 27.91 ± 1.09 pmol / minute / cm^2, respectively (**** $P < 0.0001$, $n = 12$, $N = 3$). These findings suggest the transporters responsible for P_i uptake are predominantly located on the apical membrane of rat PTC monolayers.

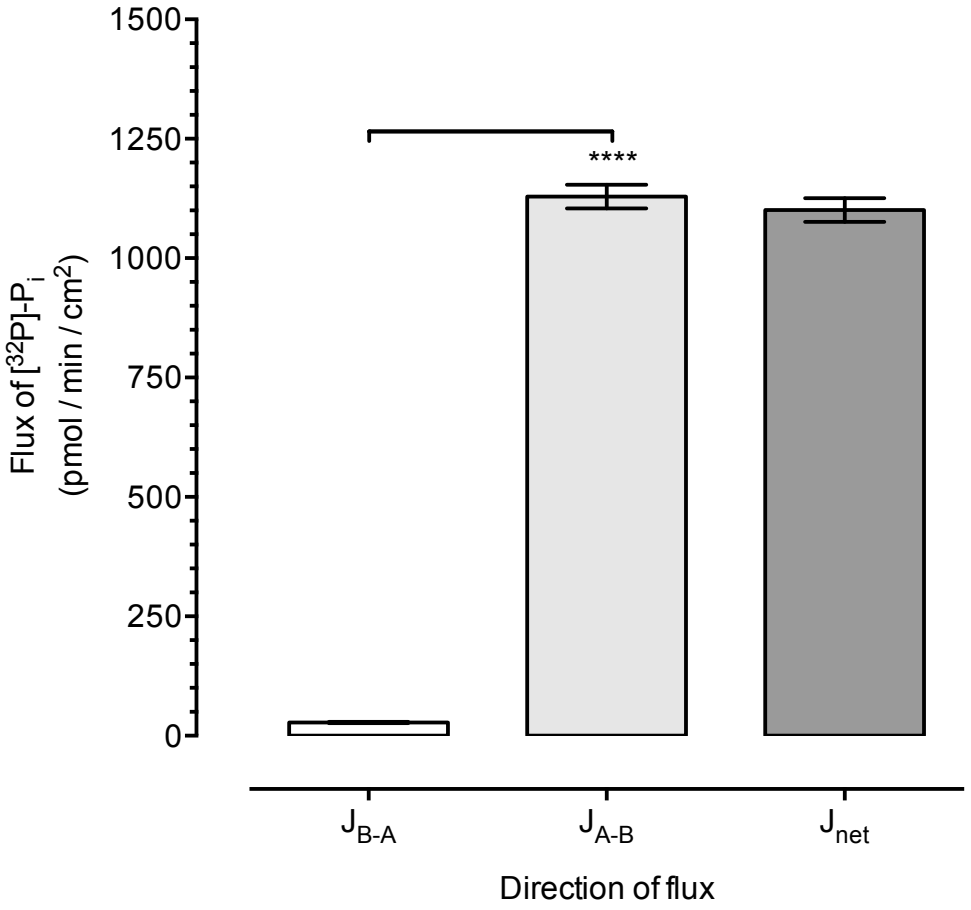

Figure 5.27: Unidirectional fluxes of 100 μM [^{32}P]-P$_i$ by rat PTC monolayers.

*To determine the secretory and absorptive fluxes of P$_i$ by rat PTC monolayers, paired monolayers were incubated with 100 μM [^{32}P]-P$_i$ at either the basolateral or apical chamber. The results show a net absorptive flux (1101.15 ± 24.84 pmol / minute / cm^2). The absorptive movement of [^{32}P]-P$_i$ was 1129.06 ± 25.01 pmol / minute / cm^2, whilst the secretory movement was very small (27.91 ± 1.09 pmol / minute / cm^2) (**** P < 0.0001). The results are expressed as the mean ± SEM from 12 rat PTC monolayers derived from 3 individual kidneys. Significance was determined by a Student's t-test.*

5.3.13. Kinetics of P_i transport by rat PTC monolayers.

The kinetic parameters of P_i transport across the apical membrane of rat PTC monolayers were also investigated.

Rat PTC monolayers were incubated at the apical membrane with a range of [^{32}P]-P_i concentrations (100 to 1000 μM) for 5 min and the intracellular accumulation of [^{32}P]-P_i was measured. Figure 5.28 shows the relationship between [^{32}P]-P_i concentration and uptake of [^{3}H]-TFV across the apical membrane of rat PTC monolayers (n = 9, N = 3). Non-linear regression analysis of the data gave a V_{max} of 433.90 ± 30.42 pmol / minute / cm^2 and an apparent K_m value of 1221.36 ± 133.23 μM.

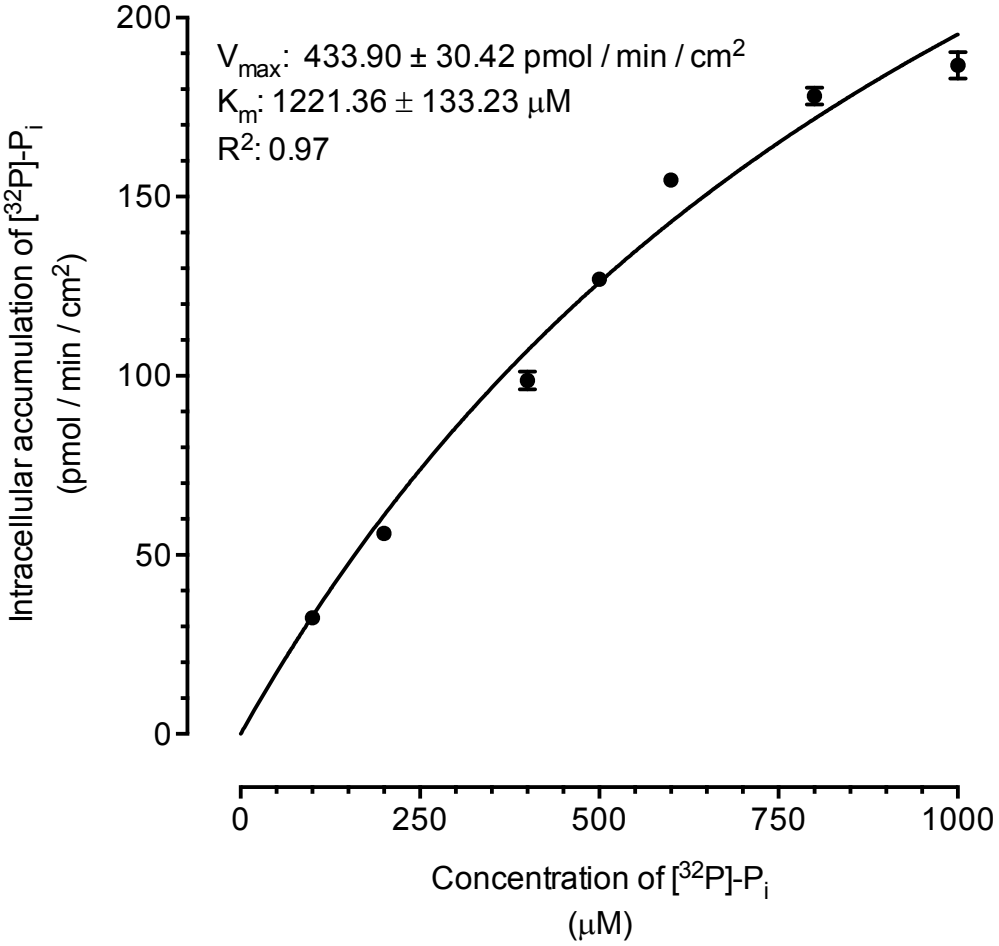

Figure 5.28: Kinetic data on [^{32}P]-P_i uptake across the apical membrane of rat PTC monolayers under initial rate conditions.

In order to obtain kinetic data on P_i uptake under initial rate conditions, the monolayers were incubated with a range of [^{32}P]-P_i concentrations (100 to 1000 μM) for 5 min. Non-linear regression analysis of the data gave a V_{max} of 433.90 ± 30.42 pmol / minute / cm^2 and an apparent K_m value of 1221.36 ± 133.23 μM P_i. The results are expressed as the mean ± SEM from 9 rat PTC monolayers derived from 3 individual kidneys.

5.3.14. The effect of Na^+ concentration upon P_i renal handling by rat PTC monolayers.

The Na^+ dependence of P_i uptake at the apical membrane was investigated using rat PTC monolayers. The uptake of 100 μM [^{32}P]-P_i was measured in the presence and absence of Na^+ over a range of time points. In addition to this the kinetics of apical P_i uptake in the presence of a range of Na^+ concentrations (0 to 137 mM) were also investigated.

Figure 5.29 shows the apical uptake of P_i was significantly reduced in the absence of Na^+ (n = 12, N = 3). Linear regression analysis of the data gave a slope of 2.86 ± 0.12 pmol / cm^2 / minute in the presence of 137 mM Na^+, and 0.64 ± 0.04 pmol / cm^2 / minute with no Na^+. Furthermore, Figure 5.30 shows a strong correlation between Na^+ concentration and apical uptake of 100 μM [^{32}P]-P_i (n = 12, N = 3). The maximum rate of P_i uptake was 25.99 ± 1.24 pmol / minute / cm^2 at 137 mM Na^+. Non-linear regression analysis of the data gave an estimated Hill coefficient of 2.80 ± 0.29, and K_m value of 58.26 ± 2.61 mM Na^+.

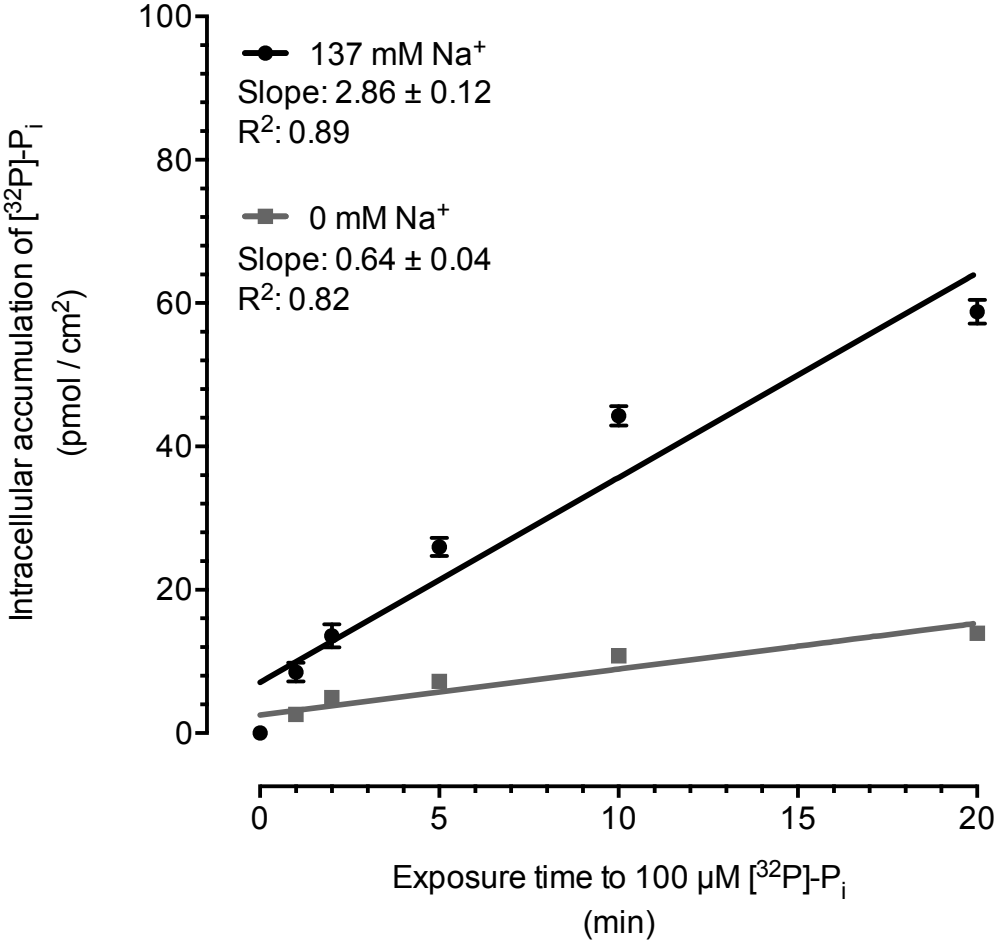

Figure 5.29: The effect of Na^+ upon uptake of 100 μM [^{32}P]-P_i across the apical membrane of rat PTC monolayers.

Uptake of 100 μM [^{32}P]-P_i across the apical membrane of rat PTC monolayers was measured in the presence and absence of Na^+ over several time points (0 to 20 min). The results show uptake of [^{32}P]-P_i across the apical membrane was Na^+ dependent. Linear regression analysis of the data gave a slope of 2.86 $\pm$ 0.12 pmol / cm^2 / minute in the presence of 137 mM Na^+, and 0.64 $\pm$ 0.04 pmol / cm^2 / minute in its absence. The results are expressed as the mean ± SEM from 12 rat PTC monolayers derived from 3 individual kidneys.

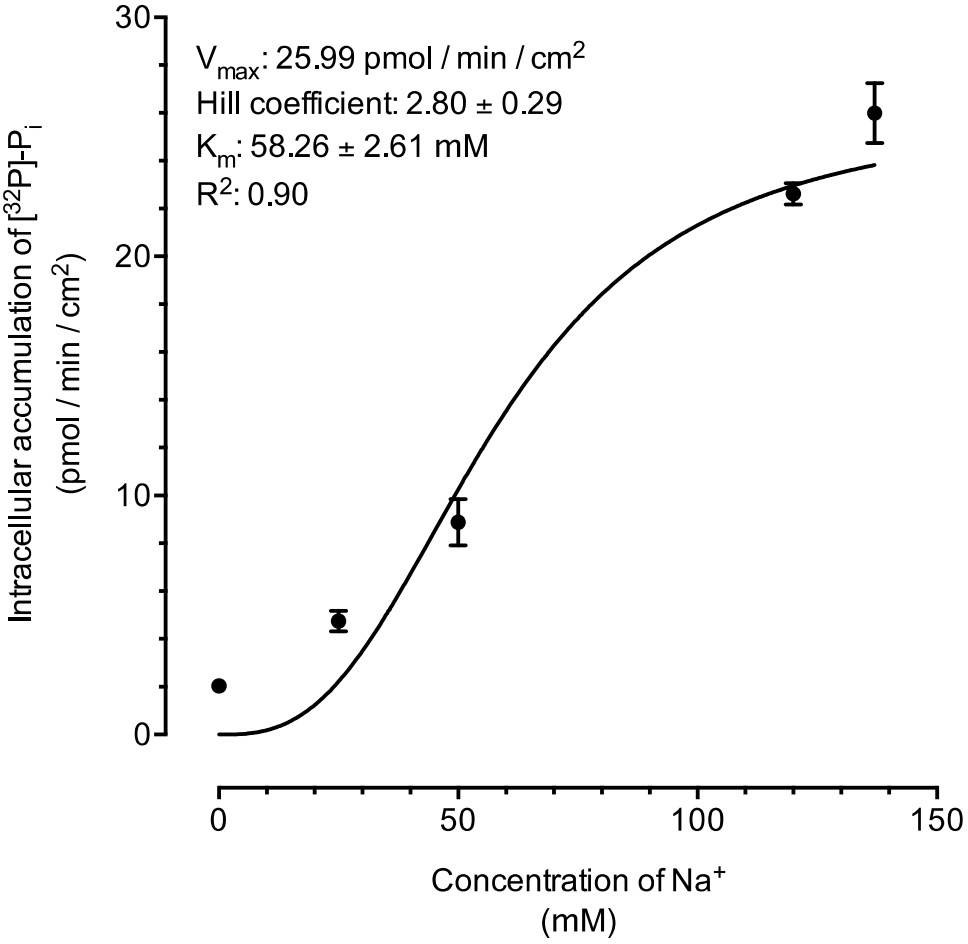

Figure 5.30: The kinetics of Na^+ and uptake of 100 μM [^{32}P]-P_i across the apical membrane of rat PTC monolayers.

Uptake of 100 μM [^{32}P]-P_i across the apical membrane of rat PTC monolayers was measured in a range of concentrations of Na^+ (0 to 137 mM). The results show uptake of [^{32}P]-P_i across the apical membrane was Na^+ dependent. The V_{max} was constrained to 25.99 pmol / min / cm^2 based upon previous findings. Non-linear regression analysis of the data gave an estimated Hill coefficient of 2.80 $\pm$ 0.29, and K_m value of 58.26 ± 2.61 mM Na^+. The results are expressed as the mean ± SEM from 12 rat PTC monolayers derived from 3 individual kidneys.

5.3.15. The effect of pH upon P_i renal handling by rat PTC monolayers.

The effect of pH on the rate of P_i uptake was studied in rat PTC monolayers. The apical uptake of 100 μM [^{32}P]-P_i was measured in experimental buffer of pH 6.0, 6.5, 7.0, 7.5 and 8.0. As shown in Figure 5.31, the rate of P_i uptake was dependent on pH. For instance increasing the pH from 6.0 (12.27 ± 0.48 pmol / minute / cm^2) to 7.5 (27.86 ± 0.54 pmol / minute / cm^2) more than doubled the rate of P_i uptake.

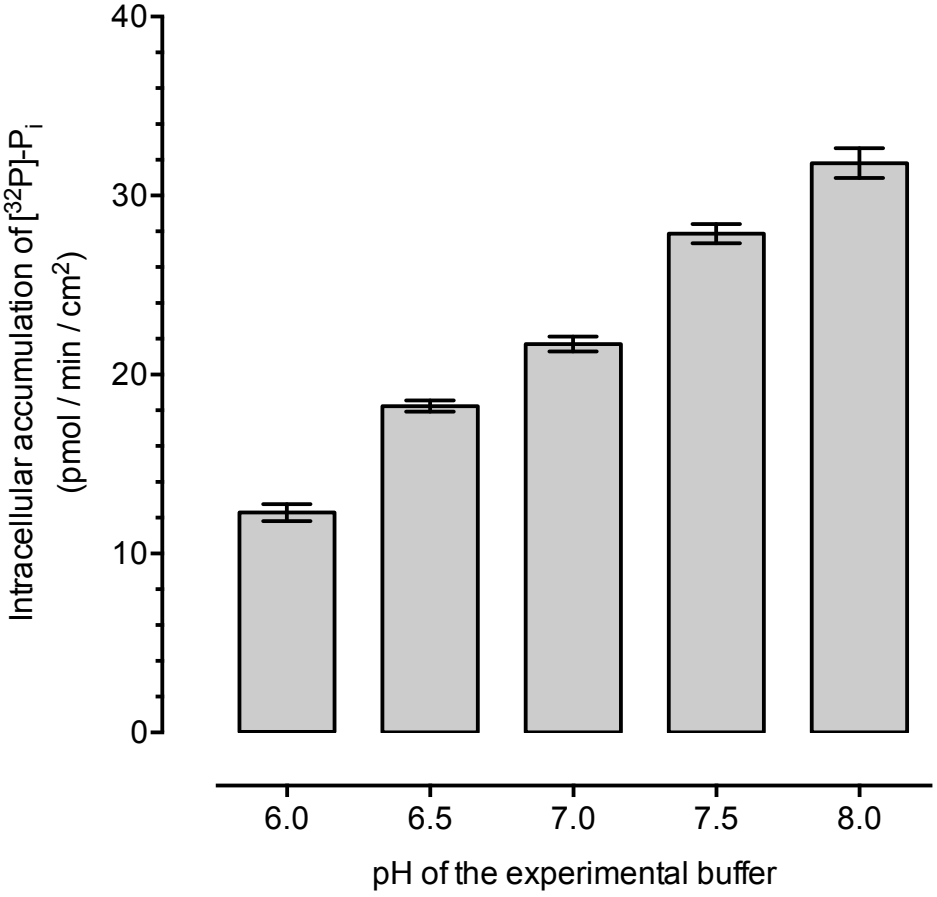

Figure 5.31: The effect of pH upon uptake of 100 μM [^{32}P]-P_i across the apical membrane of rat PTC monolayers.

The uptake of 100 μM [^{32}P]-P_i across the apical membrane of rat PTC monolayers was measured in experimental buffer of pH 6.0, 6.5, 7.0, 7.5 and 8.0. The results show uptake of [^{32}P]-P_i across the apical membrane was pH dependent. Uptake of [^{32}P]-P_i was 12.27 ± 0.48 pmol / minute / cm^2 at pH 6.0, 18.24 ± 0.31 pmol / minute / cm^2 at pH 6.5, 21.71 ± 0.41 pmol / minute / cm^2 at pH 7.0, 27.86 ± 0.54 pmol / minute / cm^2 at pH 7.5, and 31.82 ± 0.83 pmol / minute / cm^2 at pH 8.0. The results are expressed as the mean ± SEM from 12 rat PTC monolayers derived from 3 individual kidneys.

5.3.16. The effect of PFA upon P_i renal handling by rat PTC monolayers.

In order to confirm expression of NaPi-IIa and/or NaPi-IIc, the effect of PFA on the rate of P_i uptake was studied in rat PTC monolayers. Apical uptake of 100 μM [^{32}P]-P_i was measured in the presence of a range of PFA concentrations (100 to 1500 μM). The results in Figure 5.32 show the presence of PFA significantly inhibited P_i uptake (n = 9, N = 3). Non-linear regression analysis of the data gave an apparent IC_{50} value of 1046.08 ± 158.42 μM. This observation confirms rat PTC monolayers expressed NaPi-IIa and/or NaPi-IIc at the functional level.

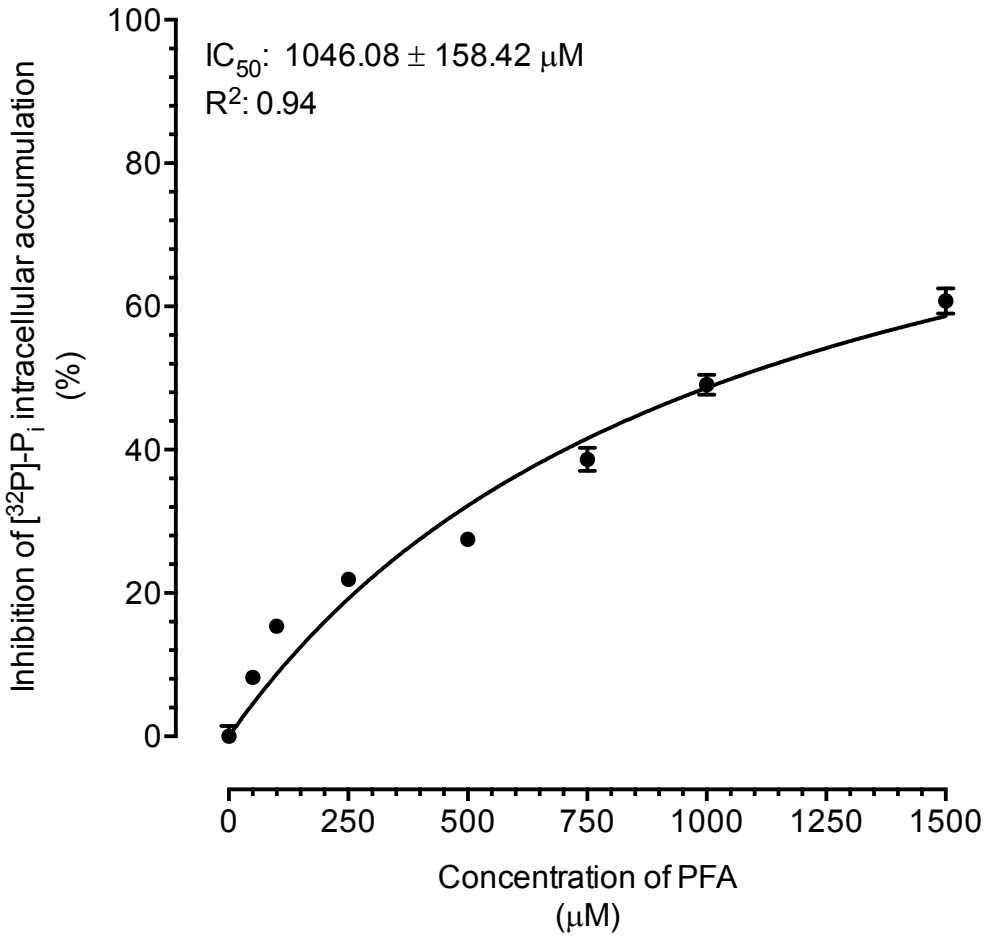

Figure 5.32: The effect of PFA on the renal handling of 100 μM [^{32}P]-P_i by rat PTC monolayers.

The uptake of 100 μM [^{32}P]-P_i across the apical membrane of rat PTC monolayers was measured in the presence of a range of concentrations of PFA (100 to 1500 μM). The presence of PFA significantly inhibited P_i uptake. Non-linear regression analysis of the data gave an apparent IC_{50} value of 1046.08 ± 158.42 μM PFA. The results are expressed as the mean ± SEM from 9 rat PTC monolayers derived from 3 individual kidneys.

5.3.17. The effect of PTH upon P_i renal handling by rat PTC monolayers.

In order ascertain the retention of PTH intracellular signalling pathways in culture rat PTCs, the effect of PTH on the rate of P_i uptake was studied in rat PTC monolayers. The uptake of 100 μM [^{32}P]-P_i across the apical membrane of monolayers was measured in the presence of a range of PTH concentrations (0 to 10 nM). The presence of PTH significantly inhibited P_i uptake in a concentration dependent manner (Figure 5.33, n = 12, N = 3). These findings confirm the PTH intracellular signalling pathways were retained during culture.

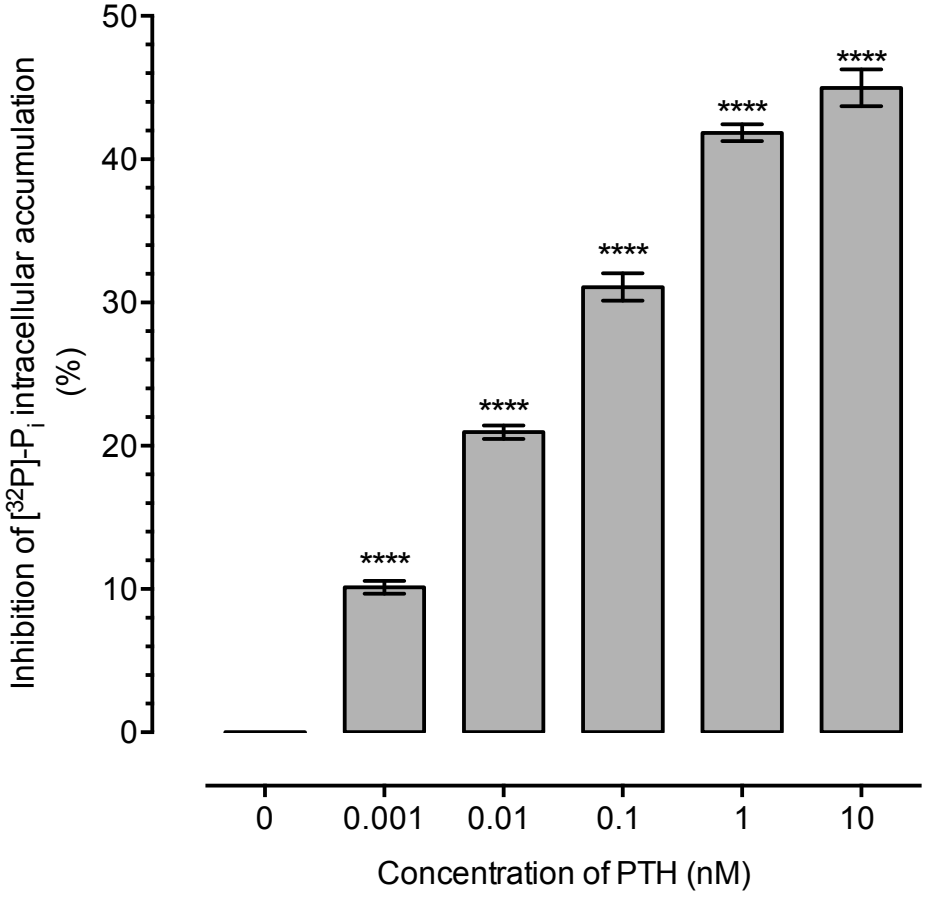

Figure 5.33: The effect of PTH on the renal handling of 100 μM [^{32}P]-Pi by rat PTC monolayers.

The uptake of 100 μM [^{32}P]-P_i across the apical membrane of rat PTC monolayers was measured in the presence of a range of concentrations of PTH (0 to 10 nM). The presence of PTH significantly inhibited P_i uptake in a concentration dependent manner. The results are expressed as the mean ± SEM from 12 rat PTC monolayers derived from 3 individual kidneys. Significance was determined using ANOVA and a Dunnett's post-test.

5.3.18. The effect of FGF-23 and α-klotho upon P_i renal handling by rat PTC monolayers.

In order to confirm FGF-23 and α-klotho intracellular signalling pathways in cultured rat PTCs, the effect of FGF-23 and α-klotho on the rate of P_i uptake was studied in rat PTC monolayers.

The uptake of 100 μM [^{32}P]-P_i across the apical membrane of rat PTC monolayers was measured in the presence of 0.89 nM FGF-23 and 0.55 mM heparin at either the apical or basolateral membrane. As shown in Figure 5.34, the presence of FGF-23 and heparin at the basolateral membrane inhibited P_i uptake by 13.97 ± 1.18 %, whereas the presence of FGF-23 and heparin at the apical membrane did not have a significant effect (2.45 ± 1.19 % inhibition) (n = 12, N = 3). These results imply that the Fgf receptors were located at the basolateral membrane of the rat proximal tubular cells, the monolayers express membrane-bound α-klotho and the FGF-23 intracellular signalling pathways were retained during culture.

This study was repeated by replacing 0.89 nM FGF-23 with 0.90 nM α-klotho and the results are shown in Figure 5.35. The presence of α-klotho at the basolateral membrane inhibited P_i uptake by 20.28 ± 1.64 %, whilst the presence of α-klotho at the apical membrane did not have a significant effect (4.30 ± 1.87 % inhibition) (n = 12, N = 3). These findings suggest that binding of soluble α-klotho to Fgfr1 at the basolateral membrane of rat PTC monolayers caused a decrease in P_i reabsorption. This also implies the cells retained the α-klotho intracellular signalling pathways in culture.

In Figure 5.36, the uptake of 100 μM [^{32}P]-P_i across the apical membrane of rat PTC monolayers in the presence of 0.89 nM FGF-23, 0.90 nM α-klotho and 0.55 mM heparin is shown. The presence of FGF-23, heparin and α-klotho at the basolateral membrane inhibited P_i uptake significantly more than the presence of each alone (38.81 ± 1.23 % inhibition) suggesting an additive effect (n = 12, N = 3).

The effect of different α-klotho concentrations on the rate of P_i uptake was studied in rat PTC monolayers. The uptake of 100 μM [^{32}P]-P_i across the apical

membrane of monolayers was measured in the presence of a range of α-klotho concentrations (0.18 to 5.4 nM). As shown in Figure 5.37, the presence of α-klotho significantly inhibited P_i uptake in a concentration dependent manner (n = 8, N = 2).

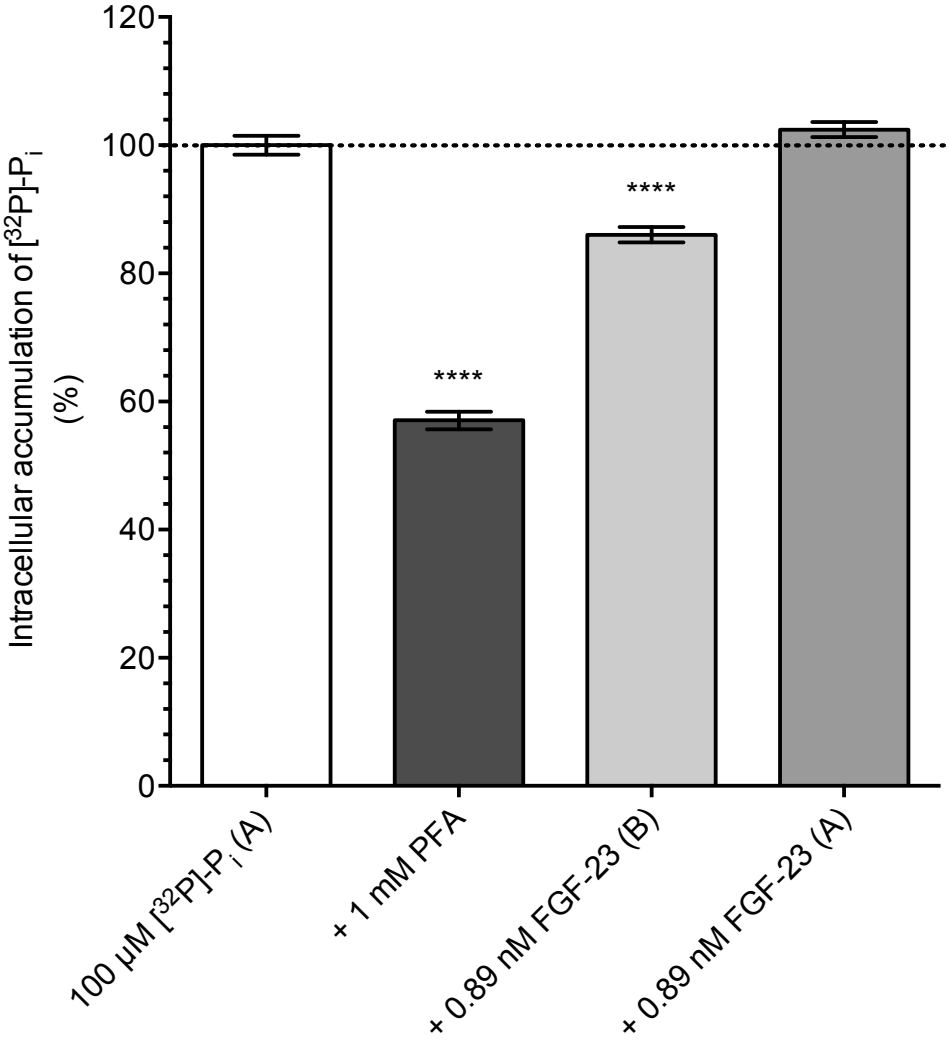

Figure 5.34: The effect of FGF-23 on the renal handling of 100 µM [^{32}P]-P_i by rat PTC monolayers.

The uptake of 100 µM [^{32}P]-P_i across the apical membrane of rat PTC monolayers was measured in the presence and absence of FGF-23. A positive control of 1 mM PFA was included. The presence of 1 mM PFA inhibited uptake of 100 µM [^{32}P]-P_i across the apical membrane by 42.95 ± 1.38 %. The presence of FGF-23 at the basolateral membrane inhibited P_i uptake by 13.97 ± 1.18 %, but the presence of FGF-23 at the apical membrane did not have a significant effect (2.45 ± 1.19 % of inhibition). The results are expressed as the mean ± SEM from 12 rat PTC monolayers derived from 3 individual kidneys. Significance was determined using ANOVA and a Dunnett's post-test.

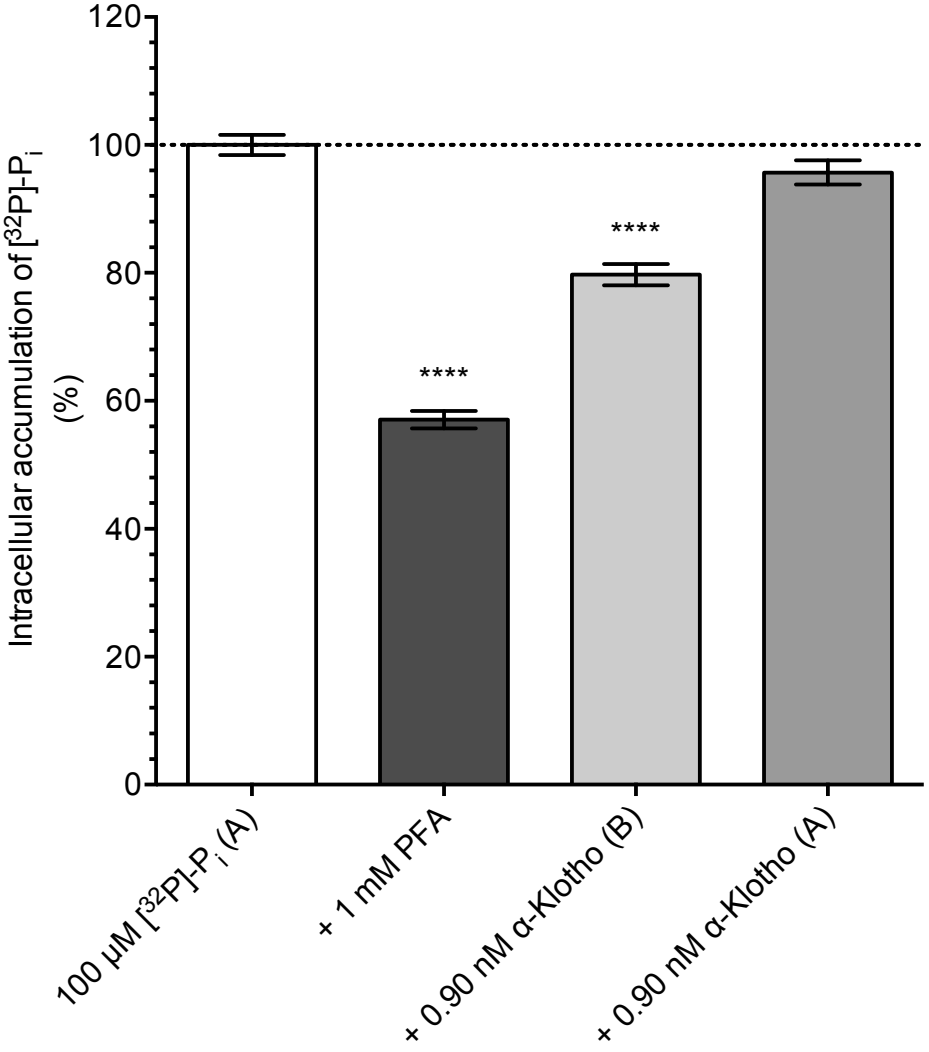

Figure 5.35: The effect of α–klotho on the renal handling of 100 µM [^{32}P]-P_i by rat PTC monolayers.

The uptake of 100 µM [^{32}P]-P_i across the apical membrane of rat PTC monolayers was measured in the presence and absence of α-klotho. A positive control of 1 mM PFA was included. The presence of 1 mM PFA inhibited uptake of 100 µM [^{32}P]-P_i across the apical membrane by 42.95 ± 1.38 %. The presence of α-klotho at the basolateral membrane inhibited P_i uptake by 20.28 ± 1.64 %, whilst the presence of α-klotho at the apical membrane did not have a significant effect (4.30 ± 1.87 % inhibition). The results are expressed as the mean ± SEM from 12 rat PTC monolayers derived from 3 individual kidneys. Significance was determined using ANOVA and a Dunnett's post-test.

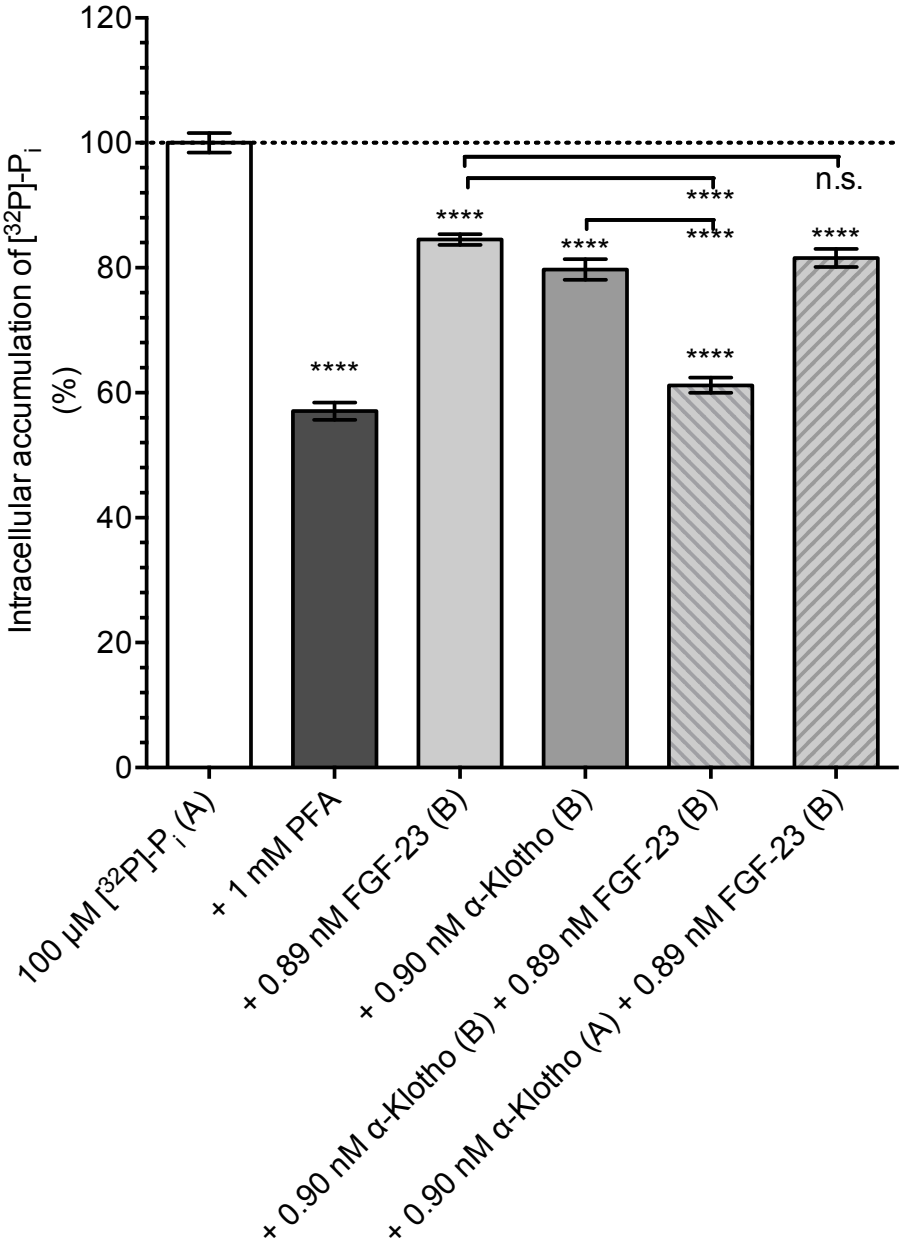

Figure 5.36: The effect of FGF-23 and α–klotho on the renal handling of 100 μM [^{32}P]-P_i by rat PTC monolayers.

The uptake of 100 μM [^{32}P]-P_i across the apical membrane of rat PTC monolayers was measured in the presence and absence of FGF-23 and α-klotho. A positive control of 1 mM PFA was included. The presence of 1 mM PFA inhibited uptake of 100 μM [^{32}P]-P_i across the apical membrane by 42.95 ± 1.38 %. The presence of FGF-23 at the basolateral membrane inhibited P_i uptake by 15.47 ± 0.85 %. The presence of α-klotho at the basolateral membrane inhibited P_i uptake by 20.28 ± 1.64 %. The presence of both FGF-23 and α-klotho at the basolateral membrane inhibited P_i uptake significantly more than the presence of each alone (38.81 ± 1.23 % inhibition). The results are expressed as the mean ± SEM from 12 rat PTC monolayers derived from 3 individual kidneys. Significance was determined using ANOVA and a Dunnett's post-test.

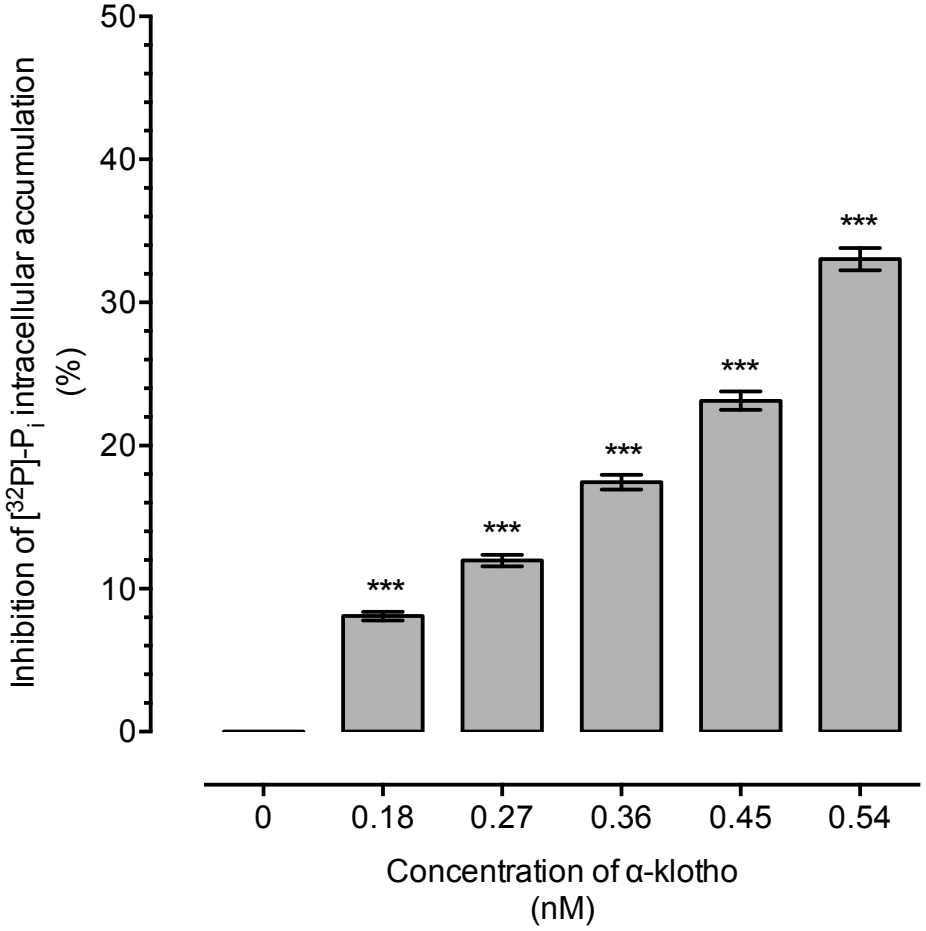

Figure 5.37: The effect of α–klotho on the renal handling of 100 μM [^{32}P]-P$_i$ by rat PTC monolayers.

The uptake of 100 μM [^{32}P]-P$_i$ across the apical membrane of rat PTC monolayers was measured in the presence of a range of concentrations of α-klotho (0.18 to 0.54 nM). α-klotho significantly inhibited P$_i$ uptake in a concentration dependent manner. The results are expressed as the mean ± SEM from 8 rat PTC monolayers derived from 2 individual kidneys. Significance was determined using ANOVA and a Dunnett's post-test.

5.3.19. The effect of TFV upon P_i renal handling by rat PTC monolayers.

The effect of TFV on the rate of P_i uptake was studied in rat PTC monolayers. Initially the uptake of 100 μM [^{32}P]-P_i across the apical membrane of monolayers was measured in the presence and absence of 10 μM TFV. As shown in Figure 5.38, the presence of 10 μM TFV inhibited uptake of 100 μM [^{32}P]-P_i across the apical membrane by 25.05 ± 3.27 %. Apical uptake of P_i was 25.99 ± 1.24 pmol / minute /cm^2 in the absence of TFV, but fell to 19.48 ± 0.85 pmol / minute / cm^2 in the presence of 10 μM TFV. The kinetics of inhibition were determined by measuring uptake in the presence of a range of TFV concentrations (1 to 500 μM). TFV inhibited P_i uptake in a concentration dependent manner, as shown in Figure 5.39. Non-linear regression analysis of the data gave an apparent IC_{50} value of 68.75 ± 5.24 μM TFV.

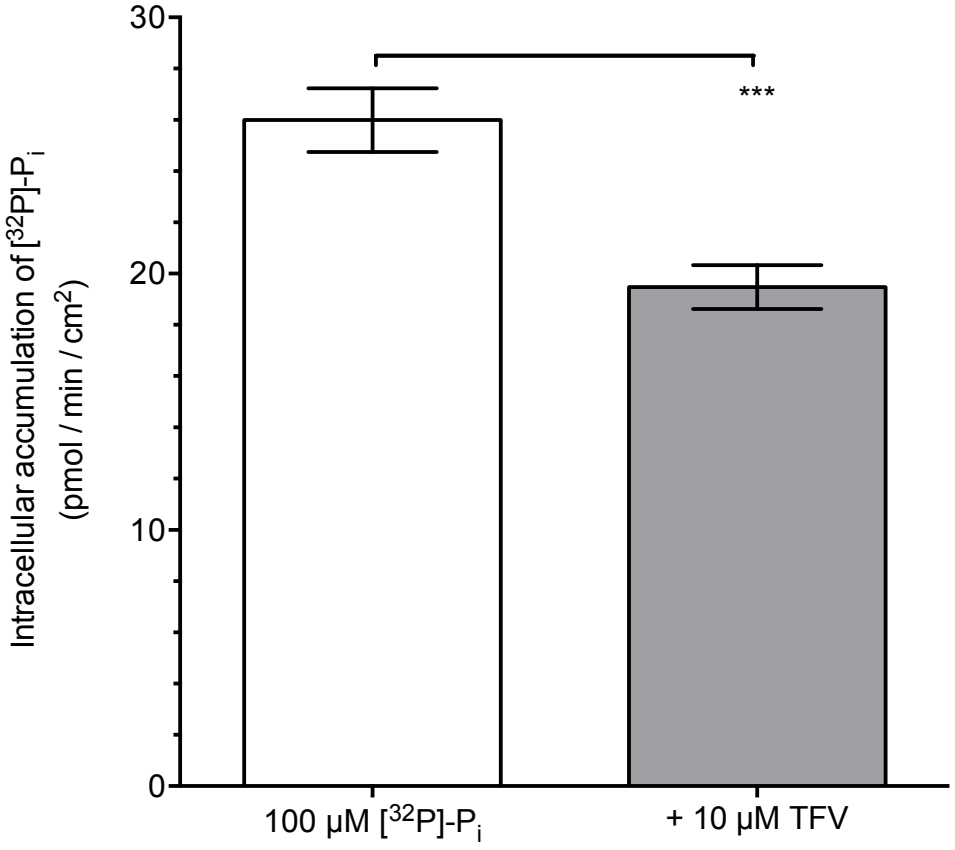

Figure 5.38: The effect of 10 μM TFV on the renal handling of 100 μM [^{32}P]-P_i by rat PTC monolayers.

The uptake of 100 μM [^{32}P]-P_i across the apical membrane of rat PTC monolayers was measured in the presence and absence of 10 μM TFV. The presence of TFV inhibited uptake of 100 μM [^{32}P]-P_i across the apical membrane by 25.05 ± 3.27 %. Apical uptake of P_i was 25.99 ± 1.24 pmol / minute /cm^2 in the absence of TFV, compared to 19.48 ± 0.85 pmol / minute / cm^2 in the presence of 10 μM TFV. The results are expressed as the mean ± SEM from 12 rat PTC monolayers derived from 3 individual kidneys. Significance was determined by a Student's t-test.

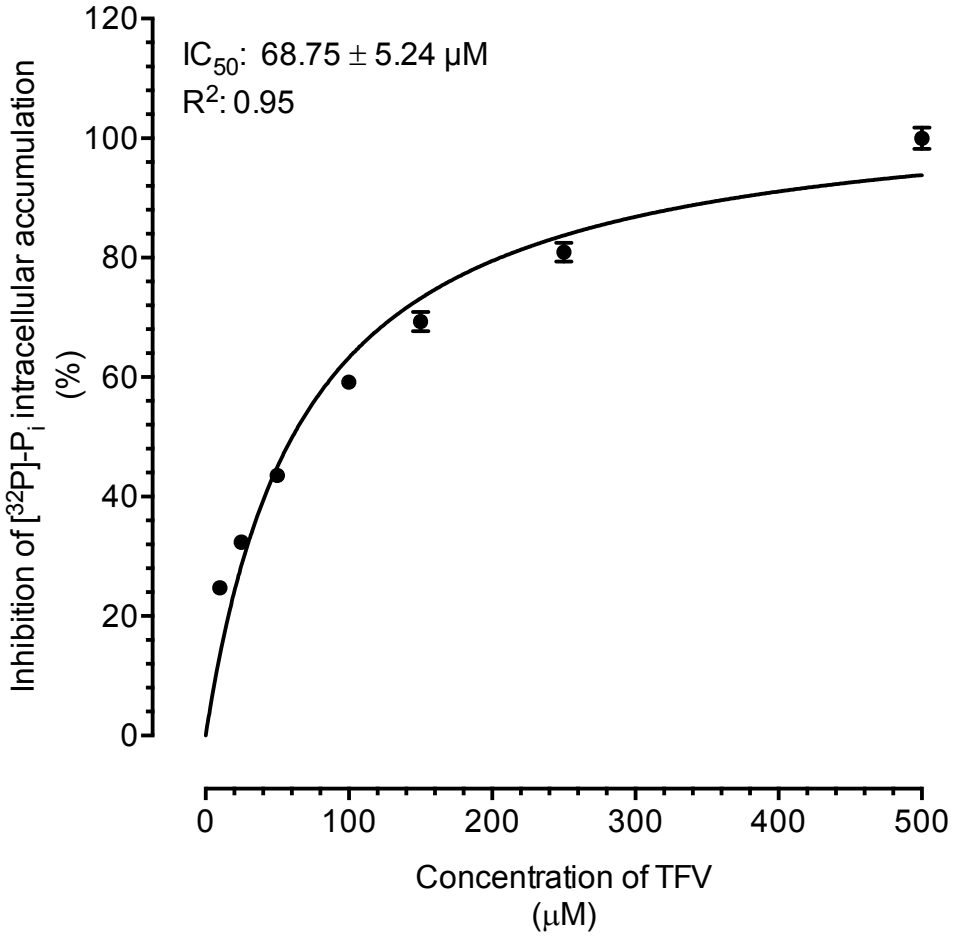

Figure 5.39: The kinetics of TFV inhibition of apical uptake of 100 µM [^{32}P]-P_i across rat PTC monolayers.

The uptake of 100 µM [^{32}P]-P_i across the apical membrane of rat PTC monolayers was measured in the presence of a range of TFV concentrations. TFV inhibited P_i uptake in a concentration dependent manner. Non-linear regression analysis of the data gave an apparent IC_{50} value of 68.75 ± 5.24 µM TFV. The results are expressed as the mean ± SEM from 12 rat PTC monolayers derived from 3 individual kidneys.

5.4. Discussion

Understanding renal P_i handling has been hampered by the lack of a good model of the mammalian proximal tubule. The characteristics of P_i transport across the proximal tubule epithelial cells and the influence of hormones have been studied using below par models; such as OK cells, and other heterologous expression models. However, using a more physiologically relevant *in-vitro* model, like the human and rat PTC monolayers, could reveal more details in the mechanism of P_i transport in the kidney. In this chapter, the handling of P_i by human and rat PTC monolayers was investigated to validate their use as a platform to study renal P_i handling. Alongside this investigation, the impact of TFV on renal P_i transport was explored.

P_i is required for a myriad of cellular functions and skeletal mineralisation. The major source of P_i is the diet, where consumed P_i is absorbed in the small intestine. The main route by which P_i is lost from the body is excretion in the urine. Under regular physiological conditions 80 % of P_i filtered in the kidney is reabsorbed in the proximal tubule and returned to circulation. The proportion that is reabsorbed can be rapidly altered by hormonal and metabolic factors. The prompt response of the P_i transport system in the proximal tubule to changes in the need for P_i means that the kidney plays a major role in the regulation of serum P_i levels.

The apical surface of proximal tubular cells contain multiple microvilli that increase the surface area of the brush border membrane and aid reabsorption. The uptake of P_i across the apical membrane into the proximal tubule cell requires movement against an electrochemical gradient. P_i uptake is coupled with Na^+ uptake to counteract this gradient. The low intracellular Na^+ concentration and the negative electrical potential difference inside the cell create an electrochemical gradient that drives Na^+ entry (Kempson, 1988). Following uptake, P_i is effluxed from the proximal tubule cell into circulation across the basolateral membrane. The molecular identity of the proteins mediating the efflux has not yet been characterised but is thought to be a passive process that follows the electrochemical gradient for P_i. The Na^+-P_i cotransport across the apical membrane is thought to be the rate limiting step in

P_i reabsorption (Hartmann *et al.*, 1996). Therefore this step has been the focus of renal P_i studies.

Two genetically distinct families of secondary active Na^+ coupled co-transporters mediate the uptake of P_i across the apical membrane of proximal tubule cells; SLC34 proteins NaPi-IIa and NaPi-IIc, and the SLC20 protein PiT2. SLC34 proteins are specifically expressed in organs important for P_i homeostasis, whilst SLC20 proteins are expressed ubiquitously in all tissues (Biber *et al.*, 2013; Forster *et al.*, 2013). Any defects in the regulation of these transport proteins or the expression of mutated proteins can lead to severe pathophysiological conditions.

As shown in Figure 5.40, NaPi-IIa and NaPi-IIc preferentially transport divalent P_i (HPO_4^{2-}) (Forster *et al.*, 1999; Bacconi *et al.*, 2005), whereas PiT2 prefers monovalent P_i ($H_2PO_4^-$) (Saliba *et al.*, 2006; Ravera *et al.*, 2007). For SLC34 proteins (NaPi-IIa and NaPi-IIc), transmembrane transport comprises an ordered sequence of binding steps. Two Na^+ ions bind sequentially, followed by divalent P_i, and a third Na^+ ion (Biber *et al.*, 2013; Forster *et al.*, 2013; Fenollar-Ferrer *et al.*, 2015). The carrier protein then re-orientates to release the substrates into the cytosol. NaPi-IIa and NaPi-IIc can be distinguished by their electrogenicity - NaPi-IIa is electrogenic whereas NaPi-IIc is electroneutral. NaPi-IIa has an intrinsic negative charge due to an aspartic acid residue; its transporter rate is a function of membrane potential (Bacconi *et al.*, 2005; Virkki *et al.*, 2005; Ghezzi *et al.*, 2009). It mediates transport with a 3:1 Na^+: HPO_4^{2-} stoichiometry, which results in a net positive charge per transport cycle (Forster *et al.*, 1999). In contrast, NaPi-IIc transport kinetics are independent of membrane potential. The transporter mediate a 2:1 Na^+: HPO_4^{2-} stoichiometry, and a Na^+ ion is not translocated, which results in no net charge (Bacconi *et al.*, 2005; Virkki *et al.*, 2005; Ghezzi *et al.*, 2009). For SLC20 proteins (PiT2) the transport sequence begins with the binding of Na^+ ion, an interaction with a monovalent P_i, and then a second Na^+ ion (Saliba *et al.*, 2006; Ravera *et al.*, 2007). Reorientation of the loaded carrier then results in the release of all the substrates into the cytosol.

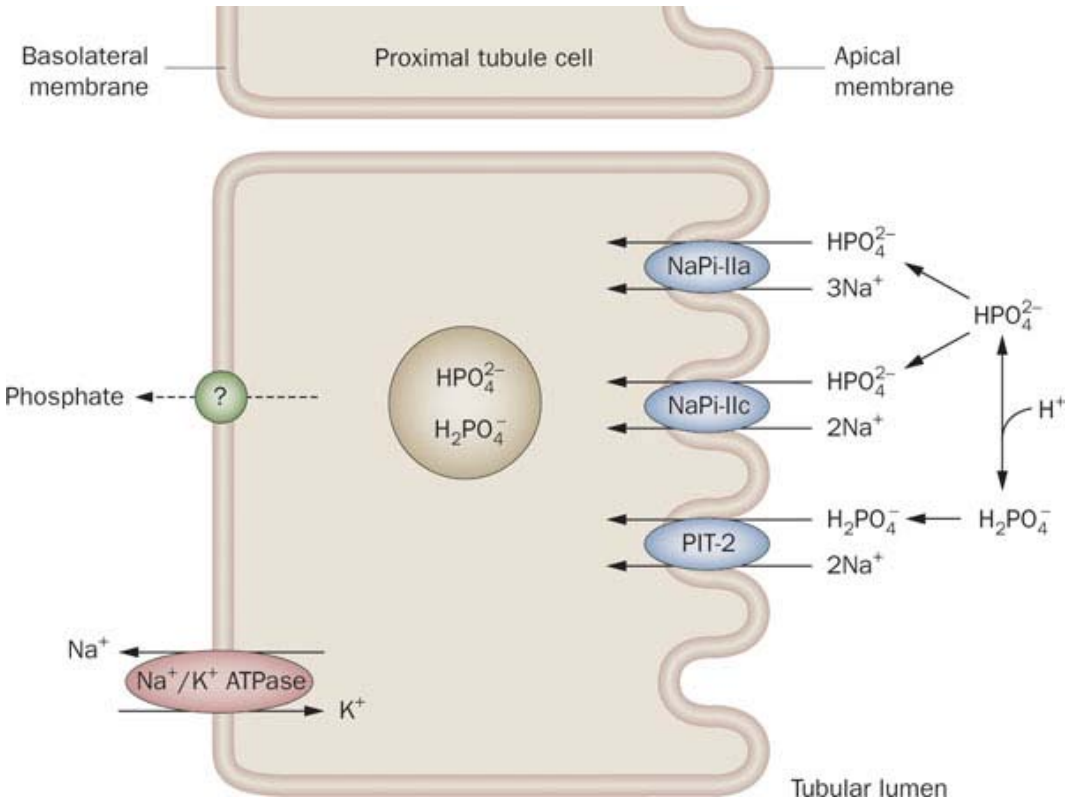

Figure 5.40: Summary of the key renal P_i transporters.

Serum P_i is freely filtered in the glomerulus. Approximately 800 mg P_i per day (80%) is reabsorbed into circulation at the proximal tubule, whilst the rest is excreted in the urine. The uptake of P_i across the apical membrane into the proximal tubule cell requires movement against an electrochemical gradient. Therefore, P_i uptake is coupled with Na^+ uptake. The transmembrane transport of P_i is predominantly mediated by NaPi-IIa and NaPi-IIc, with a minor contribution from PiT2. NaPi-IIa and NaPi-IIc preferentially transport divalent P_i (HPO_4^{2-}), whereas PiT2 prefers monovalent P_i (H_2PO4^-). Within the proximal tubule cell monovalent and divalent P_i may react with water to change their valency. The transport proteins mediating the export of P_i into circulation are not known. Diagram taken from Alizadeh Naderi and Reilly, 2010 (Alizadeh Naderi and Reilly, 2010).

mRNA expression of proximal tubule renal P_i transporters in human PTC monolayers grown on 24-well Transwell® inserts and plastic 24-well plates were measured by qPCR. Table 5.1 shows the percentage of mRNA expression when compared to freshly isolated human PTCs. Human PTC monolayers maintained expression of the key renal P_i transporters, NaPi-IIa, NaPi-IIb and PiT2, under both culture conditions. However, there was a significant fall in the expression of NaPi-IIc, PiT2 and NPT1 when compared with freshly human PTCs. No statistical difference in expression levels was observed between the

two culture conditions. Other putative P_i transporters NPT1, NPT4, NPT5 were identified, but are not thought to be clinically relevant.

Unidirectional transepithelial fluxes of radiolabelled [^{32}P]-P_i (100 µM) in both the secretory and absorptive directions were measured over 1 hr in paired monolayers of human and rat PTCs grown on 24-well Transwell® inserts. A net absorption of P_i (300.94 ± 5.56 pmol / minute / cm^2) across the human PTC monolayers was observed, shown in Figure 5.10. The absorptive and secretory movement of [^{32}P]-P_i was 301.46 ± 5.56 pmol / minute / cm^2 and 0.52 ± 0.02 pmol / minute / cm^2, respectively. Similarly, as shown in Figure 5.27 the rat PTC monolayers the absorptive movement of [^{32}P]-P_i (1129.06 ± 25.01 pmol / minute / cm^2) was significantly greater than the secretory movement (27.91 ± 1.09 pmol / minute / cm^2), resulting in a net reabsorption of 1101.15 ± 24.84 pmol / minute / cm^2. Uptake of [^{32}P]-P_i (100 µM) across the basolateral and apical membrane of human PTCs over 5 min was compared. As shown in Figure 5.11, P_i uptake across the apical membrane (312.36 ± 5.13 pmol / minute / cm^2) was 4.72-times greater than across the basolateral membrane (66.22 ± 1.50 pmol / minute / cm^2). This information suggests both human and rat PTC monolayers exhibit P_i reabsorption in concurrence with the literature.

In order to ensure the flux and uptake of P_i was measured under initial rate conditions the movement of [^{32}P]-P_i (100 µM) across human and rat PTC monolayers over time was studied. The findings in Figure 5.9 and Figure 5.26 suggest P_i transport across human and rat PTC monolayers between 0 and 20 min is within the linear initial rate of uptake P_i transport. Due to the high-energy β emissions from the ^{32}P radionuclide an incubation time of 5 min was selected. This would also ensure the reactions had progressed enough to be measured within the radiation detection instrument's sensitivity and minimise skin and eye dose exposure. The non-specific binding of [^{32}P]-P_i to the human and rat PTC monolayers was found to be 1.62 ± 0.14 pmol / cm^2 and 0.19 ± 0.03 pmol / cm^2, respectively.

The kinetic parameters, V_{max} and K_m of P_i uptake across the apical membrane of both human and rat PTC monolayers were quantified. Human monolayers were incubated with a range of [^{32}P]-P_i concentrations (10 to 500 µM) for 5 min and the intracellular accumulation of [^{32}P]-P_i was measured. Non-linear

regression analysis of the data in Figure 5.12 gave a V_{max} of 562.90 ± 99.18 pmol / minute / cm^2 and an apparent K_m value of 106.05 ± 36.40 µM. This K_m value is within the range of the published values of human P_i transporters, as shown in Table 5.2. In a similar manner rat PTC monolayers were incubated with 100 to 1000 µM [^{32}P]-P_i and non-linear regression analysis of the data in Figure 5.28 gave a V_{max} of 433.90 ± 30.42 pmol / minute / cm^2 and an apparent K_m value of 1221.36 ± 133.23 µM. Unfortunately there are no published K_m values of rat P_i transporters to compare the data against.

Transporter	System	K_m (µM)	Reference
hNaPi-IIa	*X.Laevis* oocytes	140 ± 10	(Bacconi *et al.*, 2005)
hNaPi-IIc	*X.Laevis* oocytes	70	(Segawa *et al.*, 2002)
hPiT2	*X.Laevis* oocytes	160 ± 40	(Bottger *et al.*, 2006)
hNPT1	*X.Laevis* oocytes	290 ± 50	(Miyamoto *et al.*, 1995)

Table 5.2: Published K_m values of P_i transporters.

K_m values were determined by expressing the transporters in Xenopus Laevis oocytes.

The key renal P_i transporters are secondary active Na^+-P_i cotransporters. In order to confirm the P_i transport across human and rat PTC monolayers was Na^+ dependent, P_i transport in the presence and absence of Na^+ was measured over several time periods. In both species the apical uptake of [^{32}P]-P_i (100 µM) was significantly attenuated by the absence of Na^+. Linear regression analysis of the human data in Figure 5.13 gave a slope of 70.18 ± 1.38 pmol / cm^2 / minute in the presence of 137 mM Na^+, but only 0.66 ± 0.11 pmol / cm^2 / minute in absence of Na^+. Similarly, linear regression analysis of the rat data in Figure 5.29 gave a slope of 2.86 ± 0.12 pmol / cm^2 / minute in the presence of 137 mM Na^+, and only 0.64 ± 0.04 pmol / cm^2 / minute in the absence of Na^+.

Furthermore, the kinetics of apical [^{32}P]-P_i (100 µM) uptake in the presence of a range of Na^+ concentrations (0 to 137 mM) was determined in both human and

rat PTC monolayers. A strong correlation between Na^+ concentration and P_i uptake was observed; P_i uptake increased linearly with Na^+ concentration in human PTC monolayers. However, uptake plateaued between 120 and 137 mM Na^+. The maximum rate of P_i uptake in human PTC monolayers was 312.36 ± 5.13 pmol / minute / cm^2 at 137 mM Na^+. Non-linear regression analysis of the human data, shown in Figure 5.15, gave an estimated Hill coefficient of 1.88 ± 0.16, and K_m value of 38.15 ± 1.89 mM Na^+. A Hill coefficient greater than 1 indicates strong positive cooperative interaction, suggesting the apical P_i transporter(s) contain multiple binding sites and once the first Na^+ ion has bound the receptor, it's affinity for other ligand molecules increases (Weiss, 1997). The reported apparent affinities of human NaPi-IIa and NaPi-IIc for Na^+ is 40 mM and the apparent affinity of PiT2 for Na^+ is 50 mM (Biber *et al.*, 2013). A similar Hill coefficient of 1.7 ± 0.2 has previously been reported for human NaPi-IIc (Ghezzi *et al.*, 2009). Comparatively, rat PTC monolayers also exhibited linearity of P_i uptake with Na^+ concentration. The maximum rate of P_i uptake was 25.99 ± 1.24 pmol / minute / cm^2 at 137 mM Na^+. Non-linear regression analysis of the rat data, shown in Figure 5.30, gave an estimated Hill coefficient of 2.80 ± 0.29, and K_m value of 58.26 ± 2.61 mM Na^+. The reported affinity of rat NaPi-II for Na^+ is 63 ± 8 mM, with a Hill coefficient of 3 ± 0.9 (Fucentese *et al.*, 1995).

The pH of the luminal fluid changes markedly, from 7.4 to 6.9, along the length of the proximal tubule. Transport capacity is strongly pH dependent because pH defines the valency of P_i - divalent P_i is common in the proximal tubule lumen ($pK_a \approx 6.8$) (Forster *et al.*, 2000). Therefore the influence of pH on the apical uptake of P_i was measured in human and rat PTC monolayers. The apical uptake of 100 μM [^{32}P]-P_i was measured in experimental buffer of pH 6.0, 6.5, 7.0, 7.5 and 8.0. As shown in Figure 5.16 and Figure 5.31, an increase in pH led to an increased in uptake of P_i. In human and rat PTC monolayers increasing the pH from 6.0 (154.45 ± 12.64 and 12.27 ± 0.48 pmol / minute / cm^2, respectively) to 7.5 (317.09 ± 4.43 and 27.86 ± 0.54 pmol / minute / cm^2, respectively) doubled the rate of P_i uptake. Similar findings in brush border membrane vesicles (BBMVs) of rat and porcine kidney have been reported (Burckhardt *et al.*, 1981; Quamme, 1990; Forster *et al.*, 2000). An increase in P_i uptake with increasing pH suggests a preferential uptake of divalent P_i. This

information in agreement with the published literature, and suggests NaPi-II transporters predominantly mediated the uptake of P_i across the PTC monolayers.

Phosphonocarboxylic acids, originally developed as antiviral agents, are known inhibitors of Na^+-P_i cotransport in rat renal BBMVs (Szczepanska-Konkel *et al.*, 1986). Of this class of molecules, PFA is the most effective inhibitor. This has been attributed to the close structural resemblance between the phosphonoformate ion ($H_2PO_3COO^-$) and P_i (Szczepanska-Konkel *et al.*, 1986; Kempson, 1988). PFA competitively inhibits NaPi-II transporters (Villa-Bellosta and Sorribas, 2008), but is not an inhibitor of PiT2 (Villa-Bellosta *et al.*, 2007). Studies investigating the binding of [^{14}C]-PFA to renal BBMVs show inhibition is saturable and dependent upon time, temperature and the Na^+ concentration (Szczepanska-Konkel *et al.*, 1987), and that PFA may compete with P_i for the binding site on NaPi-II.

PFA inhibition of renal P_i transport was evaluated in human and rat PTC monolayers. The apical uptake of 100 μM [^{32}P]-P_i was measured in the presence of a range of PFA concentrations (0 to 1500 μM). The results in Figure 5.17 and Figure 5.32 show dose-dependent inhibition of P_i uptake by PFA. Non-linear regression analysis of the data gave an apparent IC_{50} value of 570.35 ± 62.50 μM PFA in human PTC monolayers and 1046.08 ± 158.42 μM PFA in rat PTC monolayers. Using the Cheng-Prusoff equation, inhibition constants (K_i) were calculated from these parameters. The calculated K_i values of PFA in human and rat PTC monolayers were 293.55 ± 32.17 and 966.91 ± 146.43 μM, respectively. The relationship between PFA concentration and P_i uptake exhibited in human PTC monolayers was similar to the published literature, which is summarised in Table 5.3. The reported IC_{50} and K_i values for rat PTC monolayers, on the other hand, were higher than expected. From the data in Figure 5.32 it is clear that PFA induced saturation of P_i uptake was not reached. Therefore, to gain more accurate data the experiment should be repeated with higher concentrations of PFA, due to time constraints this was not possible.

System	IC_{50} (μM)	K_i (μM)	Reference
OK cell	320	260	(Villa-Bellosta and Sorribas, 2009)
***X.Laevis* oocytes**	1000	670	(Villa-Bellosta and Sorribas, 2009)
OK cells	_	6000	(Loghman-Adham and Dousa, 1992)
Mouse BBMV	_	310	(Harvey and Tenenhouse, 1992)

Table 5.3: Published IC_{50} and K_i values for PFA inhibition of renal P_i transport.

In rodents and humans, the binding of PTH to PTHR1 at either the basolateral or apical membrane of the proximal tubule initiates a series of intracellular changes that include the generation of cAMP, elevation of the free cytosolic Ca^{2+} level, and the inhibition of P_i reabsorption. Inhibition of P_i reabsorption is induced by the retrieval of NaPi-IIa and NaPi-IIc from the apical membrane (Traebert *et al.*, 2000; Yang *et al.*, 2004; Bacic *et al.*, 2006; Forster *et al.*, 2006). In order to ascertain the retention of PTH intracellular signalling pathways in cultured human and rat PTC monolayers, the effect of PTH on the apical uptake of P_i was investigated. The uptake of 100 μM [^{32}P]-P_i across the apical membrane of human PTC monolayers was measured in the presence of a range of PTH concentrations (0 to 10 nM). The presence of PTH significantly inhibited P_i uptake in a concentration dependent manner in both species as can be seen in Figure 5.18 and Figure 5.33. These findings confirm the PTH intracellular signalling pathways were retained during culture.

FGF-23 is synthesised by osteocytes and osteoblasts (Mirams *et al.*, 2004; Sitara *et al.*, 2004), and released from the bone in response to high dietary P_i intake, hyperphosphatemia, or an increase in serum calcitriol levels (Gupta *et al.*, 2004; Shimada *et al.*, 2004; Ferrari *et al.*, 2005; Kolek *et al.*, 2005; Liu *et al.*, 2006). The regulation of renal P_i transport by FGF-23 is mediated by FGFR1 and 4 (Gattineni *et al.*, 2014). It has been demonstrated that α-klotho and FGFR1 co-localisation converts FGFR1 into a high affinity FGF-23 receptor with a high affinity for FGF-23 (Urakawa *et al.*, 2006). FGF-23 is dependent upon α-klotho to induce FGF-receptor signalling (Kuro-o *et al.*, 1997; Urakawa *et al.*,

2006). FGF-23 binding to the FGF-23 receptor induces phosphaturia and lowers serum P_i levels, by activation of the mitogen-activated protein kinase (MAPK) cascade and phospho-ERK1/2, which results in the retrieval of NaPi-IIa and NaPi-IIc from the apical membrane. (Yamashita *et al.*, 2002; Urakawa *et al.*, 2006; Weinman *et al.*, 2011; Andrukhova *et al.*, 2012). This in turn reduces the amount of P_i reabsorbed from the urine.

α-Klotho is a transmembrane protein that is also found in a serum soluble form after proteolytic cleavage from the membrane. α-Klotho induced phosphaturic effects have also been observed in FGF-23 knock out mice, indicating a direct effect on NaPi-IIa (Vervloet and Larsson, 2011). Klotho has a β-glucuronidase activity (Tohyama *et al.*, 2004). The proposed mechanism of action is that α-klotho deglycosylates NaPi-IIa and NaPi-IIc or a putative regulatory protein, which results in the inhibition of transporter activity and an increased susceptibility to resident proteases. Proteolytic degradation of the transporters then ensue and consequently a reduced surface expression of those transporters (Hu *et al.*, 2010).

In order to validate the abovementioned pathways, FGF-23 and α-klotho effects on P_i uptake rate by human and rat PTC monolayers were studied. As shown in Figure 5.19 and Figure 5.34, the presence of 0.9 nM FGF-23 at the basolateral membrane inhibited P_i uptake in human and rat PTC monolayers by more than 20 % and 13 %, respectively. In contrast, the presence of 0.9 nM FGF-23 and heparin at the apical membrane did not change P_i absorption in either model when compared to the respective controls. These results imply that the FGF receptors were located at the basolateral membrane of the PTC monolayers, they expressed membrane-bound α-klotho, and that the FGF-23 intracellular signalling pathways were retained during culture. Similarly, the presence of soluble 0.9 nM α-klotho at the basolateral membrane inhibited P_i uptake by more than 29 % in human PTC monolayers, and more than 20 % in rat PTC monolayers (Figure 5.20 and Figure 5.35). The presence of α-klotho at the apical membrane did not exhibit significant effects on either models. The data in Figure 5.22 and Figure 5.37 show this is also a concentration dependent effect. These findings suggest that binding of soluble α-klotho at the basolateral membrane of rat PTC monolayers caused a decrease in P_i absorption, and the

cells retained the α-klotho intracellular signalling pathways in culture. In Figure 5.21 and Figure 5.36 human and rat PTC monolayers were exposed to both 0.9 nM FGF-23 and 0.9 nM soluble α-klotho at the basolateral membrane. The presence of both inhibited P_i uptake significantly greater than the presence of each alone (39.18 ± 1.39 % in human and 38.81 ± 1.23 % in rat PTC monolayers), suggesting an additive effect.

Human and rat PTC monolayers were thus demonstrated as capable of P_i transport with sensitivity to PFA, PTH, FGF-23 and α-klotho, typical of the proximal tubule. The impact of TFV on renal P_i transport was then investigated in the human and rat PTC monolayers. Initially the uptake of 100 μM [^{32}P]-P_i across the apical membrane of human and rat PTC monolayers was measured in the presence and absence of 10 μM TFV. As shown in Figure 5.23 and Figure 5.38, the presence of 10 μM TFV inhibited uptake by 35.40 ± 1.05 % in human and 25.05 ± 3.27 % in rat PTC monolayers. The kinetics of inhibition were determined by measuring uptake of 100 μM [^{32}P]-P_i in the presence of a range of TFV concentrations (1 to 500 μM). TFV inhibited P_i uptake in a concentration dependent manner. Non-linear regression analysis of the human data in Figure 5.24 gave an apparent IC_{50} value of 52.25 ± 4.71 μM TFV and K_i value of 26.89 ± 2.42 μM (using the Cheng-Prusoff Equation). Similarly, non-linear regression analysis of the rat data in Figure 5.39 gave an apparent IC_{50} value of 68.75 ± 5.24 μM TFV and K_i value of 63.55 ± 4.84 μM. From the MTS data in Figure 4.20 we know that an hr incubation with 10 μM TFV will not induce proximal tubular toxicity. The findings suggest that TFV induced hypophosphatemia may not arise from TFV-induced proximal tubular damage but from an inhibition of P_i uptake. The reported serum C_{max} of TFV in patients is 0.30 ± 0.09 μg / mL (1.04 ± 0.31 μM, MW 287.213 g / mol) (Kearney *et al.*, 2004). Extrapolation of our data suggests that 1 μM TFV would cause a small inhibition of transporter mediated P_i reabsorption. The consequent increased renal loss of P_i (hyperphosphaturia), would generate decreased serum P_i levels (hypophosphatemia), and P_i loss from bone. If TFV is inhibiting transporter mediated reabsorption of phosphate it may also have an impact upon the absorption of dietary P_i in the small intestine.

In order to confirm if TFV inhibition of P_i reabsorption is the result of a drug substrate interaction a clinical trial has begun under the supervision of Dr David Ashley Price and Dr Brendam Payne in the infectious and tropical medicine service in the Newcastle upon Tyne Hospitals NHS foundation trust. Newly diagnosed HIV patients suitable for TFV combination ART will provide a urine sample before treatment. The concentration of P_i in the urine sample will be measured, and this reading will be considered as the baseline reading. The patients will then take TFV daily and provide a urine sample 24 hrs and 3 months after the therapy was first taken. If TFV inhibition of P_i reabsorption is the result of a drug-substrate interaction, we would expect to see an increase in the urinary P_i concentration within 24 hrs of therapy. Due to the wide spread occurrence of hypophosphatemia in HIV ART-naïve and non-TFV ART patients, it is not believed that TFV alone is the cause of hypophosphatemia but one of many contributing factor in a complex adverse effect.

In addition, this novel finding has led to a new research initiative at Gilead. They have begun investigating the mechanism of TFV interaction with P_i transporters in collaboration with academics at the University of Zurich and Newcastle University. Preliminary radiolabelled [^{32}P]-P_i uptake electrophysiological studies in *Xenopus laevis* oocytes expressing renal NaPi-IIa and intestinal NaPi-IIb have shown inhibition of P_i uptake and suggest TFV binds to the transporters.

The outcomes of this work may have a large translational impact. TFV in combination with other antivirals is a first line therapy for both HIV-1 and HBV infected patients, as recommended by the World Health Organisation (WHO, 2014; WHO, 2015a). In 2014, 36.9 million people were living with HIV and 240 million with HBV globally (WHO, 2015c; WHO, 2015b). Approximately 14.9 million people living with HIV (40.4%) were receiving HIV ART in 2014 (WHO, 2015c). The number of people taking this medication is certain to increase in the future due to the substantial progress in access to HIV-1 treatment and the introduction of ‘pre-exposure prophylaxis’. Furthermore, the validation of human and rat PTC monolayers as platforms to study renal P_i handling will hopefully encourage others to use primary models. The implementation of this more physiologically relevant model may resolve unanswered questions such as the

molecular identity of the basolateral proteins mediating the efflux of P_i into circulation.

5.5. Summary

Understanding renal P_i handling in man has been hampered by the lack of a good model of the human proximal tubule. Therefore in this chapter the renal handling of P_i by human and rat PTC monolayers were characterised to validate their use as platforms to study renal P_i handling. Using qPCR, mRNA expression of the key renal P_i transporters (NaPi-IIa, NaPi-IIc and PiT2) in human PTC monolayers was confirmed. Measurement of radiolabelled 100 μM [^{32}P]-P_i uptake revealed a net reabsorption of P_i across human and rat PTC monolayers. Uptake of P_i across the apical membrane of human and rat PTC monolayers was sodium dependent, saturable and inhibited by PTH, FGF-23 and α-klotho.

TFV is the first-line antiviral therapy for HIV and HBV. It is generally safe but has been associated with hyperphosphaturia, hypophosphatemia and the onset of osteomalacia in around 30% of patients. These adverse effects have been attributed to the renal toxicity of TFV and decline in proximal tubule cell function resulting from cell death. However medically induced renal tubular damage leading to Fanconi syndrome occurs in less than 0.1% of patients on TDF and thus cannot account for the high prevalence of hypophosphatemia.

Uptake of P_i across the apical membrane was inhibited by the addition of TFV in a saturable manner with an apparent K_i value of 52.25 ± 4.71 μM in human PTC monolayers and 68.75 ± 5.24 μM in rat PTC monolayers. This suggesting that the impact of TFV upon renal P_i handling may not arise from TFV-induced proximal tubule damage but rather from an inhibition of transporter mediated P_i uptake. The consequent increased in renal loss of P_i and decrease in plasma levels could then lead to P_i loss from the bones. The data highlight the importance of developing holistic cell based models of the human proximal tubule. The outcomes of this work have initiated a patient clinical trial.

6. Concluding discussion

The kidney plays a key role in the systemic clearance of drugs, with around 32% of the top 200 prescribed drugs in the USA exhibiting significant (>25%) renal elimination (Morrissey *et al.*, 2013). Pre-clinical *in-vivo* screening of NMEs is often poorly predictive of human toxicity (Giacomini *et al.*, 2010). In recognition of this problem regulatory authorities requisitioned the development of alternative *in-vitro* cell based screening assays to reduce and replace current animal testing. It is estimated that nephrotoxicity accounts for 8 % of safety failures in pre-clinical studies and 9 % of safety failures in clinical studies of drug development (Cook *et al.*, 2014). The assays currently offered by contract research organisations are based on human or animal cells transfected to express single or dual human drug transporters on their surfaces. The major limitation of these assays is that they do not accurately reflect *in-vivo*, where there may be more than one transporter involved in the drug handling or competition with other drug molecules. The focus of my PhD project has been the development of rat and human primary proximal tubule cell models as predictive *in-vitro* models of proximal tubule drug handling.

Primary human and rat primary proximal tubule cells (PTCs) were isolated from renal cortex using a combination of enzymatic digestion and density centrifugation. A challenge in the use of primary cells is the acquisition of tissues from which the cells are derived. It is paramount that an efficient isolation protocol is performed to maximise the yield of cells. Therefore the enzymatic digestion phase of the isolation procedure in each species was optimised and detailed in chapter 3.

The difference in cell growth and differentiation is also discussed in chapter 3. For instance, the changes in transporter mRNA expression levels were compared between freshly isolated PTCs with cultured ones. A significant fall in the mRNA expression of most transporters in cultured cells were shown. On average, at day 7 the human PTCs had expression levels around 40 to 50 % of fresh cells and rat PTCs had expression levels around 20 to 30 % of fresh cells.

In stark contrast, immortalised primary proximal tubule cells (RPTEC) showed a profound loss of transporter expression compared with fresh cells; RPTECs at day 7 had expression levels of around 0-5 % of fresh tissue.

While cultured primary cells retained the full array of transporter expression, we also discovered the culture conditions affected expression levels. Human and rat PTCs were cultured on Transwell® inserts and plastic. Cells on Transwell® inserts formed confluent monolayers with low paracellular permeability from day 6 of cell culture. Growth of cells on polycarbonate inserts is reported to improve cell polarisation, transporter expression and viability (Fulcher et al., 2005). Indeed, at day 7 of culture, mRNA expression of key renal drug transporters in human PTCs such as OAT3, OATP4C1, BCRP, MRP1, MRP3 and MRP4, were significantly higher following culture on Transwell® inserts when compared to cells grown on plastic. This suggests that cells grown on Transwell® inserts may be more differentiated than cells grown on plastic. Interestingly, no significance in expression levels was observed between the two culture conditions with rat PTCs.

It is thought that this loss of differentiation in culture is due to the lack of microenvironmental cues that promote kidney histodifferentiation *in-vivo (Jang et al., 2013)*. The apical surface of the epithelium is continuously exposed to shear stress due to the constant flow of the glomerular filtrate. Several research groups have recently developed microfluidic cell culture devices to mimic the *in-vivo* environment. Exposure of mouse proximal tubule cells to shear stress has been shown to alter expression of apical and basolateral transporters. The presence of shear stress led to an increase in protein expression and translocation of Na^+/H^+ antiporter 3 to the apical membrane and Na^+/K^{+-}ATPase to the basolateral membrane (Duan *et al.*, 2010). It has also been shown to improve albumin transport and glucose reabsorption within human primary proximal tubule cells (Jang *et al.*, 2013). Limitations of these models are that the microfluidic devices are very expensive to produce and the number of cells generated is very low, with some only managing approximately 32 000 cells in total. This makes the detection of toxicity biomarkers and substrate concentrations difficult to determine. Within our laboratory we are developing an alternative platform. We have created a prototype of a chain of 3 polycarbonate

inserts with circulating basolateral and apical medium driven by a peristaltic pump. Initial characterisation studies have shown increased mRNA expression and functionality of several ABC and SLC transporters. Advantages of this model are cheaper production costs and higher cell numbers. We have recently recieved proof-of-concept funding to develop this model further into a 24-well plate format in collaboration with the Medical Physics department. A further advantage of these tehnologies is that you could can also link cells from different organs. For example a chip or well containing intesinal (Caco-2) cells could be linked fluidically to hepatocyte (HepG2) cells then renal (primary proximal tubule) cells to mimic the physiological interactions between different organs or to study drug distribution *in-vitro*.

Unlike metabolic enzymes, selective inhibitors or antibodies for most drug transporters have not been identified (Giacomini *et al.*, 2010). Although gene expression data can indicate the presence of different transporters in tissues, this data cannot be used in PKPB modelling because of the poor correlation between mRNA and protein levels (Prasad and Unadkat, 2014). Therefore quantitative information on protein expression of drug transporters, mediating the uptake and efflux of drugs and their metabolites, is crucial for *in-vitro/in-vivo* prediction of drug distribution and clearance. The University of Washington Research Affiliate Program on Transporters (UWRAPT), established by Prof. Jashvant Undakat, have developed a novel muliple reaction monitoring approach to quanitfy transporter expression which links mass spectrometry with liquid chromatography (Prasad and Unadkat, 2014). This technique, which is reliant upon selective quantification of surrogate peptides in a digested protein sample, has shown greater selectivity, speed, and sensitivity than the current semi-quantitative western blotting technique. In order to better understand drug transporter expression in human proximal tubular cells at the protein level, we have been regularly sending samples of human kidney UWRAPT for analysis. Knowledge of transporter expression at the protein level in fresh tissue and models of the proximal tubule will allow creation PK/PB models of drug clearance, using scaling factors.

In chapter 4, the utility of human and rat PTC monolayers as predictive *in-vitro* models of proximal tubular drug handling were demonstrated using radiolabeled

[^{3}H]-TFV. TFV is the first line antiviral therapy given to HIV-1 and HBV patients. Following on from marketing approval, a low rate of nephrotoxicity has been reported with long-term therapy. Retrospective histological and ultrastructural studies conducted in renal biopsies have reported accumulation of TFV within proximal tubular cells results in drug induced-mitochondrial toxicity (Cote *et al.*, 2006; Kohler *et al.*, 2009; Herlitz *et al.*, 2010; Perazella, 2010; Fernandez-Fernandez *et al.*, 2011; Kohler *et al.*, 2011). The renal handling of TFV was therefore characterised using the human and rat PTC models to elucidate the mechanism of drug accumulation.

Human and rat PTC monolayers exhibited a cell-to-media ratio greater than 1, which indicated uptake and accumulation of TFV across the basolateral membrane. The transporters mediating the renal transport of TFV were identified using a cocktail of transporter inhibitors. The basolateral uptake of TFV was mediated by OATP4C1 and OAT1. TFV was found to have low affinities for the apical efflux transporters MRP2, MRP4, MDR1 and BCRP. This could result in poor effux of TFV from the proximal tubular cells and accumulation. Furthermore, from *in-vivo* studies it is known that TFV is cleared by a combination of glomerular filtration and tubular secretion. Thus TFV may also enter the proximal tubule across the apical membrane through OATP1A isoforms and/or P_i transporters. Thereby inhibiting P_i reabsorption from ultrafiltrate and causing hypophosphatemia. A summary of these findings is shown in Figure 6.1.

The novel identification of OATP4C1 as a TFV transporter has led Gilead to develop assays for investigating OATP4C1-mediated DDI, and the FDA to recognise OATP4C1 as a key renal transporter. The life expectancy of HIV-1 and HBV infected patients is now comparable to the general population. Therefore, it is important to be aware of any potential DDIs that may occur with co-medication. Known substrates of OATP4C1 include cardiac glycosides (DX and ouabain), thyroid hormones (T3 and T4), cAMP and methotrexate. These findings also validate the use of human and rat PTC monolayers as a platform for drug transporter and DDI studies.

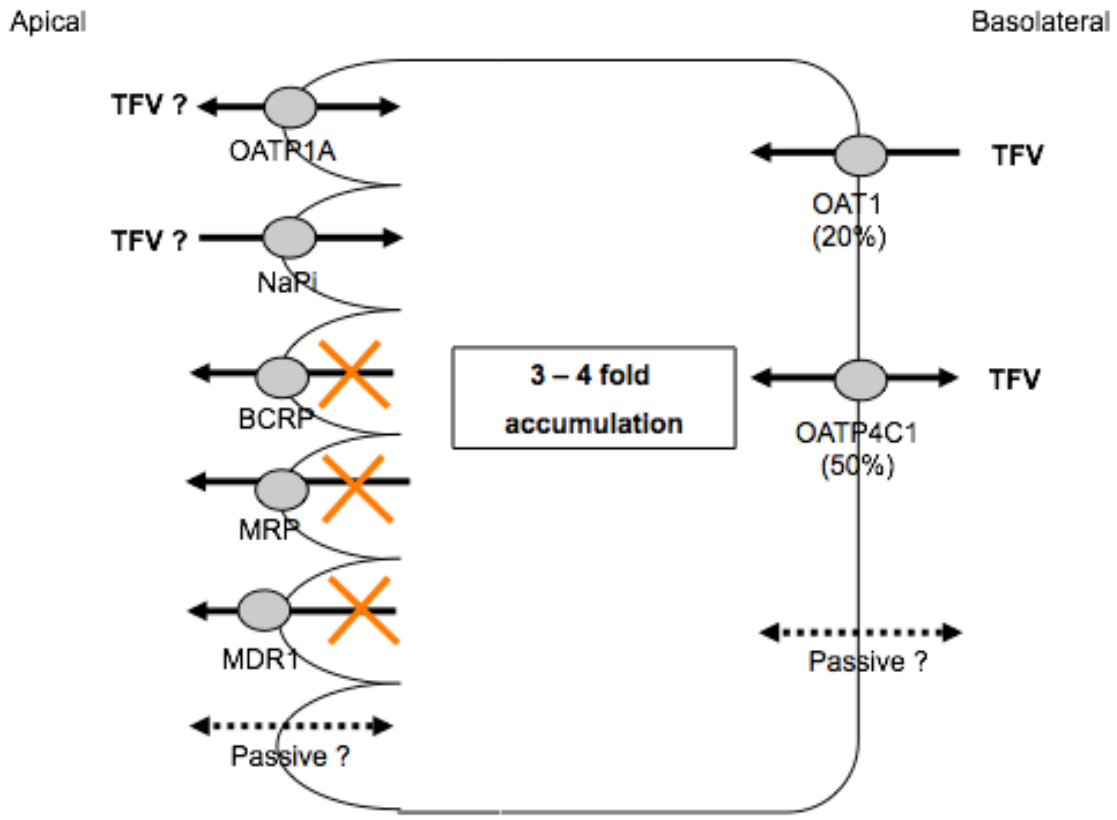

Figure 6.1: An overview of the renal handling of TFV based upon my PhD findings.

The transporters mediating the renal transport of TFV were identified using a cocktail of transporter inhibitors. The basolateral uptake of TFV was mediated by OATP4C1 and OAT1. TFV was found to have low affinities for the apical efflux transporters MRP2, MRP4, MDR1 and BCRP. This could result in poor efflux of TFV from the proximal tubular cells and accumulation. Furthermore, from in-vivo studies it is known that TFV is cleared by a combination of glomerular filtration and tubular secretion. Thus TFV may also enter the proximal tubule across the apical membrane through OATP1A isoforms and/or P_i transporters.

Understanding renal P_i handling has been hampered by the lack of a good model of the mammalian proximal tubule. In chapter 5 the renal handling of [^{32}P]-P_i by human and rat PTC monolayers was characterised to validate their use as platforms to study renal P_i handling. mRNA expression of the key renal P_i transporters (NaPi-IIa, NaPi-IIc and PiT2) in human PTC monolayers was confirmed by qPCR. Measurement of radiolabelled 100 μM [^{32}P]-P_i uptake revealed a net reabsorption of P_i across human and rat PTC monolayers. Uptake of P_i across the apical membrane of human and rat PTC monolayers was found to be sodium dependent, saturable and inhibited by PTH, FGF-23

and α-klotho. The validation of human and rat PTC monolayers as platforms to study renal P_i handling will hopefully encourage others to use primary models. The implementation of this holistic model may resolve unanswered questions such as the molecular identity of the basolateral protein mediating the efflux of P_i into circulation.

TFV has been associated with hyperphosphaturia, hypophosphatemia and the onset of osteomalacia in around 30 % of patients (Badiou et al., 2006; Buchacz et al., 2006). These adverse effects have been attributed to the renal toxicity of TFV and decline in proximal tubule cell function resulting from cell death (Martin et al., 1994; Birkus et al., 2002; Cote et al., 2006; Kohler et al., 2009; Herlitz et al., 2010; Perazella, 2010; Fernandez-Fernandez et al., 2011; Kohler et al., 2011). However, medically induced renal tubular damage leading to Fanconi syndrome occurs in less than 0.1 % of patients on TVF and thus cannot account for the high prevalence of hypophosphatemia (Nelson *et al.*, 2007; Herlitz *et al.*, 2010; Fernandez-Fernandez *et al.*, 2011). In order to determine if there was an alternative explanation, P_i transport in the presence of TFV was investigated using the human and rat PTC models. Uptake of P_i across the apical membrane was inhibited by the addition of TFV in a saturable manner with an apparent K_i value of 26.89 ± 2.42 μM in human PTC monolayers and 63.55 ± 4.84 μM in rat PTC monolayers. This suggests that the impact of TFV upon renal P_i handling may not arise from TFV-induced proximal tubule damage but rather from an inhibition of transporter mediated P_i reabsorption at the apical membrane of proximal tubular cells. The consequent increase in renal loss of phosphate (hyperphosphaturia) due to inhibition of phosphate reabsorption causes decreased plasma levels of phosphate (hypophosphatemia) and phosphate loss from bone (osteomalacia). The data highlight the importance of developing holistic cell based models of the human proximal tubule. If TFV is inhibiting transporter mediated reabsorption of phosphate it may also have an impact upon the absorption of dietary P_i in the small intestine. The outcomes of this work have initiated a patient clinical trial to investigate this hypothesis. The results could have a large translational impact, as over 14.9 million HIV and HBV pateints are pescribed TFV.

Rat and human PTC are not limited to only drug transporter and drug interaction studies. Several studies have confirmed the suitability of rat and human primary proximal tubular cells cultures as an *in-vitro* model to study nephrotoxicity (Cummings and Lash, 2000; Cummings *et al.*, 2000; Lash *et al.*, 2001; Lash *et al.*, 2003; Lash *et al.*, 2005; Lash *et al.*, 2006). However, a limitation to their use in nephrotoxicity studies is the finite lifespan of the human and rat PTCs.

The model can be improved further by identification of biomarkers of proximal tubule damage. Identification of NME induced nephrotoxicity within humans at the pre-clinical *in-vitro* screening stage would decrease drug attrition. Segment specifc biomarkers have been identified to detect and quantify nephrotoxicity better than existing biomarkers. Proximal tubular specific biomarkers include kidney injury molecule 1, α - glutathione-S-transferase, N-acetyl-β-glucosaminidase, Netrin-1, Retinol binding protein, interleukin-18, exosomal feutin A, and L-fatty acid binding protein (Vaidya *et al.*, 2008; Bonventre *et al.*, 2010). As part of my PhD studies I was able to confirm protein expression of kidney injury molecule 1 using an ELISA assay. Further characterisation to idenifty a panel of proximal tubular biomarkers is required. This is because a biomarker of injury might not detect a functional defect or reliably indicate delayed repair. Similarly a biomarker of inflammation may not be sensitive in detecting early toxicity in the absence of inflaamation.

Barriers in the use of tissue for primary cell cultures research studies can be grouped in to the following categories: regulatory, supply, and practical barriers. Regulatory barriers include ethical approval, licenses and regulatory acceptance of data. Supply barriers are the short supply of human tissue, the cost of obtaining human material and inter-individual variability. Practical barriers include the short lifespan of cells, the requirement of specialist equipment, and the shortage of trained technical staff.

Some of the barriers can be addressed. For instance, to provide a reliable source of human cells and limit inter-individual variability, protocols for the differentiation of human embryonic stem cells into renal epithelial cells are currently under development. Indeed, a protocol for the differentiation of human embryonic stem cells into functional proximal tubular cells has been published (Narayanan *et al.*, 2013). The resulting culture of a heterogeneous cell

population expressed characteristic markers of proximal tubular cells, which are comparable to the primary human proximal tubule cells, and generated tubular structures *in-vitro* and *in-vivo*. However, they still showed signs of dedifferentiation, and require further investigation.

Likewise, further investigation is also required in the human and rat PTCs to verify its utility in other aspects of drug development. In this thesis, human and rat PTCs have been validated as physiological relevant models of the proximal tubule in the kidney, and they have been demonstrated as predictive tools of renal drug handling. The robustness of their use is thus presented, and with further validation, for instance in their use in nephrotoxicity prediction, would greatly impact on drug development.

7. References

Ahmed-Belkacem, A., Pozza, A., Munoz-Martinez, F., Bates, S.E., Castanys, S., Gamarro, F., Di Pietro, A. and Perez-Victoria, J.M. (2005) 'Flavonoid structure-activity studies identify 6-prenylchrysin and tectochrysin as potent and specific inhibitors of breast cancer resistance protein ABCG2', *Cancer Res*, 65(11), pp. 4852-60.

Alizadeh Naderi, A.S. and Reilly, R.F. (2010) 'Hereditary disorders of renal phosphate wasting', *Nat Rev Nephrol*, 6(11), pp. 657-65.

Aller, S.G., Yu, J., Ward, A., Weng, Y., Chittaboina, S., Zhuo, R., Harrell, P.M., Trinh, Y.T., Zhang, Q., Urbatsch, I.L. and Chang, G. (2009) 'Structure of P-glycoprotein reveals a molecular basis for poly-specific drug binding', *Science*, 323(5922), pp. 1718-22.

Allikmets, R., Gerrard, B., Hutchinson, A. and Dean, M. (1996) 'Characterization of the human ABC superfamily: isolation and mapping of 21 new genes using the expressed sequence tags database', *Hum Mol Genet*, 5(10), pp. 1649-55.

Andrukhova, O., Zeitz, U., Goetz, R., Mohammadi, M., Lanske, B. and Erben, R.G. (2012) 'FGF23 acts directly on renal proximal tubules to induce phosphaturia through activation of the ERK1/2-SGK1 signaling pathway', *Bone*, 51(3), pp. 621-8.

Anzai, N., Kanai, Y. and Endou, H. (2007) 'New insights into renal transport of urate', *Curr Opin Rheumatol*, 19(2), pp. 151-7.

Aschauer, L., Gruber, L.N., Pfaller, W., Limonciel, A., Athersuch, T.J., Cavill, R., Khan, A., Gstraunthaler, G., Grillari, J., Grillari, R., Hewitt, P., Leonard, M.O., Wilmes, A. and Jennings, P. (2013) 'Delineation of the key aspects in the regulation of epithelial monolayer formation', *Mol Cell Biol*, 33(13), pp. 2535-50.

Atterwill, C.K., Steele, C.E., (1987) *In vitro methods in toxicology*. Cambridge: Cambridge University Press.

Bacconi, A., Virkki, L.V., Biber, J., Murer, H. and Forster, I.C. (2005) 'Renouncing electroneutrality is not free of charge: switching on electrogenicity in a Na+-coupled phosphate cotransporter', *Proc Natl Acad Sci U S A*, 102(35), pp. 12606-11.

Bacic, D., Lehir, M., Biber, J., Kaissling, B., Murer, H. and Wagner, C.A. (2006) 'The renal Na+/phosphate cotransporter NaPi-IIa is internalized via the receptor-mediated endocytic route in response to parathyroid hormone', *Kidney Int*, 69(3), pp. 495-503.

Badagnani, I., Castro, R.A., Taylor, T.R., Brett, C.M., Huang, C.C., Stryke, D., Kawamoto, M., Johns, S.J., Ferrin, T.E., Carlson, E.J., Burchard, E.G. and Giacomini, K.M. (2006) 'Interaction of methotrexate with organic-anion transporting polypeptide 1A2 and its genetic variants', *J Pharmacol Exp Ther*, 318(2), pp. 521-9.

Badagnani I, C.R., Taylor TR, Brett CM, Huang CC, Stryke D, Kawamoto M, Johns SJ, Ferrin TE, Carlson EJ, Burchard EG, Giacomini KM. (2006) 'Interaction of methotrexate with organic-anion transporting polypeptide 1A2 and its genetic variants.', *The journal of pharmacology and experimental therapeutics.*, 2(318), pp. 521-9.

Badiou, S., De Boever, C.M., Terrier, N., Baillat, V., Cristol, J.P. and Reynes, J. (2006) 'Is tenofovir involved in hypophosphatemia and decrease of tubular phosphate reabsorption in HIV-positive adults?', *J Infect*, 52(5), pp. 335-8.

Baer, P.C., Tunn, U.W., Nunez, G., Scherberich, J.E. and Geiger, H. (1999) 'Transdifferentiation of distal but not proximal tubular epithelial cells from human kidney in culture', *Exp Nephrol*, 7(4), pp. 306-13.

Bailey-Dell, K.J., Hassel, B., Doyle, L.A. and Ross, D.D. (2001) 'Promoter characterization and genomic organization of the human breast cancer resistance protein (ATP-binding cassette transporter G2) gene', *Biochim Biophys Acta*, 1520(3), pp. 234-41.

Bakos, E., Evers, R., Szakacs, G., Tusnady, G.E., Welker, E., Szabo, K., de Haas, M., van Deemter, L., Borst, P., Varadi, A. and Sarkadi, B. (1998) 'Functional multidrug resistance protein (MRP1) lacking the N-terminal transmembrane domain', *J Biol Chem*, 273(48), pp. 32167-75.
Bark, H. and Choi, C.H. (2010) 'PSC833, cyclosporine analogue, downregulates MDR1 expression by activating JNK/c-Jun/AP-1 and suppressing NF-kappaB', *Cancer Chemother Pharmacol*, 65(6), pp. 1131-6.
Bass, A.S., Cartwright, M.E., Mahon, C., Morrison, R., Snyder, R., McNamara, P., Bradley, P., Zhou, Y.Y. and Hunter, J. (2009) 'Exploratory drug safety: a discovery strategy to reduce attrition in development', *J Pharmacol Toxicol Methods*, 60(1), pp. 69-78.
Baumann, M., Pontiller, J. and Ernst, W. (2010) 'Structure and basal transcription complex of RNA polymerase II core promoters in the mammalian genome: an overview', *Mol Biotechnol*, 45(3), pp. 241-7.
Bech, A., Van Bentum, P., Nabbe, K., Gisolf, J., Richter, C. and De Boer, H. (2012a) 'Fibroblast growth factor 23 in hypophosphataemic HIV-positive adults on tenofovir', *HIV Med*, 13(9), pp. 558-63.
Bech, A., Van Bentum, P., Telting, D., Gisolf, J., Richter, C. and De Boer, H. (2012b) 'Treatment of calcium and vitamin D deficiency in HIV-positive men on tenofovir-containing antiretroviral therapy', *HIV Clin Trials*, 13(6), pp. 350-6.
Berkhin, E.B. and Humphreys, M.H. (2001) 'Regulation of renal tubular secretion of organic compounds', *Kidney Int*, 59(1), pp. 17-30.
Bi, W., Yan, J., Stankiewicz, P., Park, S.S., Walz, K., Boerkoel, C.F., Potocki, L., Shaffer, L.G., Devriendt, K., Nowaczyk, M.J., Inoue, K. and Lupski, J.R. (2002) 'Genes in a refined Smith-Magenis syndrome critical deletion interval on chromosome 17p11.2 and the syntenic region of the mouse', *Genome Res*, 12(5), pp. 713-28.
Biber, J., Hernando, N. and Forster, I. (2013) 'Phosphate transporters and their function', *Annu Rev Physiol*, 75, pp. 535-50.
Birkus, G., Hajek, M., Kramata, P., Votruba, I., Holy, A. and Otova, B. (2002) 'Tenofovir diphosphate is a poor substrate and a weak inhibitor of rat DNA polymerases alpha, delta, and epsilon*', *Antimicrob Agents Chemother*, 46(5), pp. 1610-3.
Bleasby, K., Castle, J.C., Roberts, C.J., Cheng, C., Bailey, W.J., Sina, J.F., Kulkarni, A.V., Hafey, M.J., Evers, R., Johnson, J.M., Ulrich, R.G. and Slatter, J.G. (2006) 'Expression profiles of 50 xenobiotic transporter genes in humans and pre-clinical species: a resource for investigations into drug disposition', *Xenobiotica*, 36(10-11), pp. 963-88.
Bonventre, J.V., Vaidya, V.S., Schmouder, R., Feig, P. and Dieterle, F. (2010) 'Next-generation biomarkers for detecting kidney toxicity', *Nat Biotechnol*, 28(5), pp. 436-40.
Boogaard, P.J., Nagelkerke, J.F. and Mulder, G.J. (1990) 'Renal proximal tubular cells in suspension or in primary culture as in vitro models to study nephrotoxicity', *Chem Biol Interact*, 76(3), pp. 251-91.
Bossuyt, X., Muller, M. and Meier, P.J. (1996) 'Multispecific amphipathic substrate transport by an organic anion transporter of human liver', *J Hepatol*, 25(5), pp. 733-8.
Bottger, P., Hede, S.E., Grunnet, M., Hoyer, B., Klaerke, D.A. and Pedersen, L. (2006) 'Characterization of transport mechanisms and determinants critical for Na+-dependent Pi symport of the PiT family paralogs human PiT1 and PiT2', *Am J Physiol Cell Physiol*, 291(6), pp. C1377-87.
Brown, C.D., Sayer, R., Windass, A.S., Haslam, I.S., De Broe, M.E., D'Haese, P.C. and Verhulst, A. (2008) 'Characterisation of human tubular cell monolayers as a model of proximal tubular xenobiotic handling', *Toxicol Appl Pharmacol*, 233(3), pp. 428-38.
Buchacz, K., Brooks, J.T., Tong, T., Moorman, A.C., Baker, R.K., Holmberg, S.D. and Greenberg, A. (2006) 'Evaluation of hypophosphataemia in tenofovir disoproxil fumarate (TDF)-exposed and TDF-unexposed HIV-infected out-patients receiving highly active antiretroviral therapy', *HIV Med*, 7(7), pp. 451-6.

Buist, S.C., Cherrington, N.J., Choudhuri, S., Hartley, D.P. and Klaassen, C.D. (2002) 'Gender-specific and developmental influences on the expression of rat organic anion transporters', *J Pharmacol Exp Ther*, 301(1), pp. 145-51.
Burckhardt, G. and Burckhardt, B.C. (2011) 'In vitro and in vivo evidence of the importance of organic anion transporters (OATs) in drug therapy', *Handb Exp Pharmacol*, (201), pp. 29-104.
Burckhardt, G., Stern, H. and Murer, H. (1981) 'The influence of pH on phosphate transport into rat renal brush border membrane vesicles', *Pflugers Arch*, 390(2), pp. 191-7.
Bush JA, L.G. (2002) 'Regulation of the Mdr1 isoforms in a p53-deficient mouse model.', *Carcinogenesis*, 23(10), pp. 1603-7.
Calza, L., Trapani, F., Tedeschi, S., Piergentili, B., Manfredi, R., Colangeli, V. and Viale, P. (2011) 'Tenofovir-induced renal toxicity in 324 HIV-infected, antiretroviral-naive patients', *Scand J Infect Dis*, 43(8), pp. 656-60.
Cha, S.H., Sekine, T., Fukushima, J.I., Kanai, Y., Kobayashi, Y., Goya, T. and Endou, H. (2001) 'Identification and characterization of human organic anion transporter 3 expressing predominantly in the kidney', *Mol Pharmacol*, 59(5), pp. 1277-86.
Chen, Q., Bian, Y. and Zeng, S. (2014) 'Involvement of AP-1 and NF-kappaB in the up-regulation of P-gp in vinblastine resistant Caco-2 cells', *Drug Metab Pharmacokinet*, 29(2), pp. 223-6.
Chen, Y., Teranishi, K., Li, S., Yee, S.W., Hesselson, S., Stryke, D., Johns, S.J., Ferrin, T.E., Kwok, P. and Giacomini, K.M. (2009) 'Genetic variants in multidrug and toxic compound extrusion-1, hMATE1, alter transport function', *Pharmacogenomics J*, 9(2), pp. 127-36.
Cheng X and Klaassen CD (2009) 'Tissue Distribution, Ontogeny, and Hormonal Regulation of Xenobiotic Transporters in Mouse Kidneys', *Drug Metab Dispos*, 37(11), pp. 2178-85.
Cheng, Y., Vapurcuyan, A., Shahidullah, M., Aleksunes, L.M. and Pelis, R.M. (2012) 'Expression of organic anion transporter 2 in the human kidney and its potential role in the tubular secretion of guanine-containing antiviral drugs', *Drug Metab Dispos*, 40(3), pp. 617-24.
Chu, X., Korzekwa, K., Elsby, R., Fenner, K., Galetin, A., Lai, Y., Matsson, P., Moss, A., Nagar, S., Rosania, G.R., Bai, J.P., Polli, J.W., Sugiyama, Y. and Brouwer, K.L. (2013) 'Intracellular drug concentrations and transporters: measurement, modeling, and implications for the liver', *Clin Pharmacol Ther*, 94(1), pp. 126-41.
Cihlar, T. and Ho, E.S. (2000) 'Fluorescence-based assay for the interaction of small molecules with the human renal organic anion transporter 1', *Anal Biochem*, 283(1), pp. 49-55.
Cihlar, T., Ho, E.S., Lin, D.C. and Mulato, A.S. (2001) 'Human renal organic anion transporter 1 (hOAT1) and its role in the nephrotoxicity of antiviral nucleotide analogs', *Nucleosides Nucleotides Nucleic Acids*, 20(4-7), pp. 641-8.
Cihlar, T., Lin, D.C., Pritchard, J.B., Fuller, M.D., Mendel, D.B. and Sweet, D.H. (1999) 'The antiviral nucleotide analogs cidofovir and adefovir are novel substrates for human and rat renal organic anion transporter 1', *Mol Pharmacol*, 56(3), pp. 570-80.
Cihlar, T., Ray, A.S., Laflamme, G., Vela, J.E., Tong, L., Fuller, M.D., Roy, A. and Rhodes, G.R. (2007) 'Molecular assessment of the potential for renal drug interactions between tenofovir and HIV protease inhibitors', *Antivir Ther*, 12(2), pp. 267-72.
Cole, S.P., Bhardwaj, G., Gerlach, J.H., Mackie, J.E., Grant, C.E., Almquist, K.C., Stewart, A.J., Kurz, E.U., Duncan, A.M. and Deeley, R.G. (1992) 'Overexpression of a transporter gene in a multidrug-resistant human lung cancer cell line', *Science*, 258(5088), pp. 1650-4.
Coller, J.K., Barratt, D.T., Dahlen, K., Loennechen, M.H. and Somogyi, A.A. (2006) 'ABCB1 genetic variability and methadone dosage requirements in opioid-dependent individuals', *Clin Pharmacol Ther*, 80(6), pp. 682-90.
Cook, D., Brown, D., Alexander, R., March, R., Morgan, P., Satterthwaite, G. and Pangalos, M.N. (2014) 'Lessons learned from the fate of AstraZeneca's drug pipeline: a five-dimensional framework', *Nat Rev Drug Discov*, 13(6), pp. 419-31.
Cooper, R.D., Wiebe, N., Smith, N., Keiser, P., Naicker, S. and Tonelli, M. (2010) 'Systematic review and meta-analysis: renal safety of tenofovir disoproxil fumarate in HIV-infected patients', *Clin Infect Dis*, 51(5), pp. 496-505.

Cote, H.C., Magil, A.B., Harris, M., Scarth, B.J., Gadawski, I., Wang, N., Yu, E., Yip, B., Zalunardo, N., Werb, R., Hogg, R., Harrigan, P.R. and Montaner, J.S. (2006) 'Exploring mitochondrial nephrotoxicity as a potential mechanism of kidney dysfunction among HIV-infected patients on highly active antiretroviral therapy', *Antivir Ther*, 11(1), pp. 79-86.
Courjault-Gautier, F., Chevalier, J., Abbou, C.C., Chopin, D.K. and Toutain, H.J. (1995) 'Consecutive use of hormonally defined serum-free media to establish highly differentiated human renal proximal tubule cells in primary culture', *J Am Soc Nephrol*, 5(11), pp. 1949-63.
Cui, Y., Konig, J. and Keppler, D. (2001) 'Vectorial transport by double-transfected cells expressing the human uptake transporter SLC21A8 and the apical export pump ABCC2', *Mol Pharmacol*, 60(5), pp. 934-43.
Cummings, B.S. and Lash, L.H. (2000) 'Metabolism and toxicity of trichloroethylene and S-(1,2-dichlorovinyl)-L-cysteine in freshly isolated human proximal tubular cells', *Toxicol Sci*, 53(2), pp. 458-66.
Cummings, B.S., Lasker, J.M. and Lash, L.H. (2000) 'Expression of glutathione-dependent enzymes and cytochrome P450s in freshly isolated and primary cultures of proximal tubular cells from human kidney', *J Pharmacol Exp Ther*, 293(2), pp. 677-85.
Cundy, K.C., Li, Z.H. and Lee, W.A. (1996) 'Effect of probenecid on the distribution, metabolism, and excretion of cidofovir in rabbits', *Drug Metab Dispos*, 24(3), pp. 315-21.
Cundy, K.C., Petty, B.G., Flaherty, J., Fisher, P.E., Polis, M.A., Wachsman, M., Lietman, P.S., Lalezari, J.P., Hitchcock, M.J. and Jaffe, H.S. (1995) 'Clinical pharmacokinetics of cidofovir in human immunodeficiency virus-infected patients', *Antimicrob Agents Chemother*, 39(6), pp. 1247-52.
Cusatis, G., Gregorc, V., Li, J., Spreafico, A., Ingersoll, R.G., Verweij, J., Ludovini, V., Villa, E., Hidalgo, M., Sparreboom, A. and Baker, S.D. (2006) 'Pharmacogenetics of ABCG2 and adverse reactions to gefitinib', *J Natl Cancer Inst*, 98(23), pp. 1739-42.
Daniel, F., Loriot, M.A., Seksik, P., Cosnes, J., Gornet, J.M., Lemann, M., Fein, F., Vernier-Massouille, G., De Vos, M., Boureille, A., Treton, X., Flourie, B., Roblin, X., Louis, E., Zerbib, F., Beaune, P. and Marteau, P. (2007) 'Multidrug resistance gene-1 polymorphisms and resistance to cyclosporine A in patients with steroid resistant ulcerative colitis', *Inflamm Bowel Dis*, 13(1), pp. 19-23.
De Clercq, E. and Holy, A. (2005) 'Acyclic nucleoside phosphonates: a key class of antiviral drugs', *Nat Rev Drug Discov*, 4(11), pp. 928-40.
de Jong, F.A., Marsh, S., Mathijssen, R.H., King, C., Verweij, J., Sparreboom, A. and McLeod, H.L. (2004) 'ABCG2 pharmacogenetics: ethnic differences in allele frequency and assessment of influence on irinotecan disposition', *Clin Cancer Res*, 10(17), pp. 5889-94.
Dorup, J. and Maunsbach, A.B. (1997) 'Three-dimensional organization and segmental ultrastructure of rat proximal tubules', *Exp Nephrol*, 5(4), pp. 305-17.
Doyle LA, Y.W., Abruzzo LV, Krogmann T, Gao Y, Rishi AK, Ross DD. (1998) 'A multidrug resistance transporter from human MCF-7 breast cancer cells.', *Proceedings of the National Academy of Sciences of the United States of America.*, 95(26), pp. 15665-70.
Drescher, S., Schaeffeler, E., Hitzl, M., Hofmann, U., Schwab, M., Brinkmann, U., Eichelbaum, M. and Fromm, M.F. (2002) 'MDR1 gene polymorphisms and disposition of the P-glycoprotein substrate fexofenadine', *Br J Clin Pharmacol*, 53(5), pp. 526-34.
Dresser, M.J., Leabman, M.K. and Giacomini, K.M. (2001) 'Transporters involved in the elimination of drugs in the kidney: organic anion transporters and organic cation transporters', *J Pharm Sci*, 90(4), pp. 397-421.
Duan, Y., Weinstein, A.M., Weinbaum, S. and Wang, T. (2010) 'Shear stress-induced changes of membrane transporter localization and expression in mouse proximal tubule cells', *Proc Natl Acad Sci U S A*, 107(50), pp. 21860-5.
Eguchi, G. and Kodama, R. (1993) 'Transdifferentiation', *Curr Opin Cell Biol*, 5(6), pp. 1023-8.
Eisner, C., Faulhaber-Walter, R., Wang, Y., Leelahavanichkul, A., Yuen, P.S., Mizel, D., Star, R.A., Briggs, J.P., Levine, M. and Schnermann, J. (2010) 'Major contribution of tubular secretion to creatinine clearance in mice', *Kidney Int*, 77(6), pp. 519-26.

Emami Riedmaier, A., Nies, A.T., Schaeffeler, E. and Schwab, M. (2012) 'Organic anion transporters and their implications in pharmacotherapy', *Pharmacol Rev*, 64(3), pp. 421-49.
Endres, C., Hsiao, P., Chung, F. and Unadkat, J. (2006) 'The role of transporters in drug interactions', *European Journal of Pharmaceutical Sciences*, 27(5), pp. 501-517.
Enomoto, A., Kimura, H., Chairoungdua, A., Shigeta, Y., Jutabha, P., Cha, S.H., Hosoyamada, M., Takeda, M., Sekine, T., Igarashi, T., Matsuo, H., Kikuchi, Y., Oda, T., Ichida, K., Hosoya, T., Shimokata, K., Niwa, T., Kanai, Y. and Endou, H. (2002) 'Molecular identification of a renal urate anion exchanger that regulates blood urate levels', *Nature*, 417(6887), pp. 447-52.
Eraly, S.A., Hamilton, B.A. and Nigam, S.K. (2003) 'Organic anion and cation transporters occur in pairs of similar and similarly expressed genes', *Biochem Biophys Res Commun*, 300(2), pp. 333-42.
Eraly, S.A., Vallon, V., Vaughn, D.A., Gangoiti, J.A., Richter, K., Nagle, M., Monte, J.C., Rieg, T., Truong, D.M., Long, J.M., Barshop, B.A., Kaler, G. and Nigam, S.K. (2006) 'Decreased renal organic anion secretion and plasma accumulation of endogenous organic anions in OAT1 knock-out mice', *J Biol Chem*, 281(8), pp. 5072-83.
European Medicines Agency (2012) *Guideline on the investigation of drug interactions*. Available at: http://www.ema.europa.eu/docs/en_GB/document_library/Scientific_guideline/2012/07/WC500129606.pdf (Accessed: 12/09/2015).
Ezinga, M., Wetzels, J.F., Bosch, M.E., van der Ven, A.J. and Burger, D.M. (2014) 'Long-term treatment with tenofovir: prevalence of kidney tubular dysfunction and its association with tenofovir plasma concentration', *Antivir Ther*, 19(8), pp. 765-71.
Fellay, J., Marzolini, C., Meaden, E.R., Back, D.J., Buclin, T., Chave, J.P., Decosterd, L.A., Furrer, H., Opravil, M., Pantaleo, G., Retelska, D., Ruiz, L., Schinkel, A.H., Vernazza, P., Eap, C.B. and Telenti, A. (2002) 'Response to antiretroviral treatment in HIV-1-infected individuals with allelic variants of the multidrug resistance transporter 1: a pharmacogenetics study', *Lancet*, 359(9300), pp. 30-6.
Fenollar-Ferrer, C., Forster, I.C., Patti, M., Knoepfel, T., Werner, A. and Forrest, L.R. (2015) 'Identification of the first sodium binding site of the phosphate cotransporter NaPi-IIa (SLC34A1)', *Biophys J*, 108(10), pp. 2465-80.
Fernandez-Fernandez, B., Montoya-Ferrer, A., Sanz, A.B., Sanchez-Nino, M.D., Izquierdo, M.C., Poveda, J., Sainz-Prestel, V., Ortiz-Martin, N., Parra-Rodriguez, A., Selgas, R., Ruiz-Ortega, M., Egido, J. and Ortiz, A. (2011) 'Tenofovir nephrotoxicity: 2011 update', *AIDS Res Treat*, 2011, p. 354908.
Ferrari, S.L., Bonjour, J.P. and Rizzoli, R. (2005) 'Fibroblast growth factor-23 relationship to dietary phosphate and renal phosphate handling in healthy young men', *J Clin Endocrinol Metab*, 90(3), pp. 1519-24.
Forster, I.C., Biber, J. and Murer, H. (2000) 'Proton-sensitive transitions of renal type II Na(+)-coupled phosphate cotransporter kinetics', *Biophys J*, 79(1), pp. 215-30.
Forster, I.C., Hernando, N., Biber, J. and Murer, H. (2006) 'Proximal tubular handling of phosphate: A molecular perspective', *Kidney Int*, 70(9), pp. 1548-1559.
Forster, I.C., Hernando, N., Biber, J. and Murer, H. (2013) 'Phosphate transporters of the SLC20 and SLC34 families', *Mol Aspects Med*, 34(2-3), pp. 386-95.
Forster, I.C., Loo, D.D. and Eskandari, S. (1999) 'Stoichiometry and Na+ binding cooperativity of rat and flounder renal type II Na+-Pi cotransporters', *Am J Physiol*, 276(4 Pt 2), pp. F644-9.
Fucentese, M., Winterhalter, K., Murer, H. and Biber, J. (1995) 'Functional expression of rat renal Na/Pi-cotransport (NaPi-2) in Sf9 cells by the baculovirus system', *J Membr Biol*, 144(1), pp. 43-8.
Fulcher, M.L., Gabriel, S., Burns, K.A., Yankaskas, J.R. and Randell, S.H. (2005) 'Well-differentiated human airway epithelial cell cultures', *Methods Mol Med*, 107, pp. 183-206.
Garrigues, A., Escargueil, A.E. and Orlowski, S. (2002) 'The multidrug transporter, P-glycoprotein, actively mediates cholesterol redistribution in the cell membrane', *Proc Natl Acad Sci U S A*, 99(16), pp. 10347-52.

Gattineni, J., Alphonse, P., Zhang, Q., Mathews, N., Bates, C.M. and Baum, M. (2014) 'Regulation of renal phosphate transport by FGF23 is mediated by FGFR1 and FGFR4', *Am J Physiol Renal Physiol*, 306(3), pp. F351-8.
Gayet, L., Dayan, G., Barakat, S., Labialle, S., Michaud, M., Cogne, S., Mazane, A., Coleman, A.W., Rigal, D. and Baggetto, L.G. (2005) 'Control of P-glycoprotein activity by membrane cholesterol amounts and their relation to multidrug resistance in human CEM leukemia cells', *Biochemistry*, 44(11), pp. 4499-509.
Ghezzi, C., Murer, H. and Forster, I.C. (2009) 'Substrate interactions of the electroneutral Na+-coupled inorganic phosphate cotransporter (NaPi-IIc)', *J Physiol*, 587(Pt 17), pp. 4293-307.
Giacomet, V., Nannini, P., Vigano, A., Erba, P., Benincaso, A., Bedogni, G., Cattaneo, D., Falvella, F.S. and Zuccotti, G.V. (2015) 'Long-term Renal Effects of Tenofovir-Disoproxil-Fumarate in Vertically HIV-Infected Children, Adolescents, and Young Adults: A 132-Month Follow-Up Study', *Clin Drug Investig*, 35(7), pp. 419-26.
Giacomini, K.M., Huang, S.M., Tweedie, D.J., Benet, L.Z., Brouwer, K.L., Chu, X., Dahlin, A., Evers, R., Fischer, V., Hillgren, K.M., Hoffmaster, K.A., Ishikawa, T., Keppler, D., Kim, R.B., Lee, C.A., Niemi, M., Polli, J.W., Sugiyama, Y., Swaan, P.W., Ware, J.A., Wright, S.H., Yee, S.W., Zamek-Gliszczynski, M.J. and Zhang, L. (2010) 'Membrane transporters in drug development', *Nat Rev Drug Discov*, 9(3), pp. 215-36.
Gilead Sciences, I. (2015) *Drug Information Sheet - Viread* [PDF]. Available at: http://www.gilead.com/~/media/files/pdfs/medicines/hiv/viread/viread_pi.pdf?la=en.
Glavy, J.S., Wu, S.M., Wang, P.J., Orr, G.A. and Wolkoff, A.W. (2000) 'Down-regulation by extracellular ATP of rat hepatocyte organic anion transport is mediated by serine phosphorylation of oatp1', *J Biol Chem*, 275(2), pp. 1479-84.
Goldin, A.L. (1992) 'Maintenance of Xenopus laevis and oocyte injection', *Methods Enzymol*, 207, pp. 266-79.
Goodman, M. (2008) 'Market Watch: Pharma industry performance metrics: 2007-2012E', *Nat Rev Drug Discov*, 7(10), pp. 795-795.
Gorboulev V, U.J., Akhoundova A, Ulzheimer-Teuber I, Karbach U, Quester S, Baumann C, Lang F, Busch AE, Koepsell H. (1997) 'Cloning and characterization of two human polyspecific organic cation transporters.', *DNA and Cell Biology*, 16(7), pp. 971-81.
Gorboulev, V., Ulzheimer, J., Akhoundova, A., Ulzheimer-Teuber, I., Karbach, U., Quester, S., Baumann, C., Lang, F., Busch, A.E. and Koepsell, H. (1997) 'Cloning and characterization of two human polyspecific organic cation transporters', *DNA Cell Biology*, 16(7), pp. 871-81.
Gotoh, Y., Kato, Y., Stieger, B., Meier, P.J. and Sugiyama, Y. (2002) 'Gender difference in the Oatp1-mediated tubular reabsorption of estradiol 17beta-D-glucuronide in rats', *Am J Physiol Endocrinol Metab*, 282(6), pp. E1245-54.
Gründemann D, G.V., Gambaryan S, Veyhl M, Koepsell H. (1994) 'Drug excretion mediated by a new prototype of polyspecific transporter.', *Nature*, 372(6506), pp. 549-52.
Grundemann, D., Schechinger, B., Rappold, G.A. and Schomig, E. (1998) 'Molecular identification of the corticosterone-sensitive extraneuronal catecholamine transporter', *Nat Neurosci*, 1(5), pp. 349-51.
Gstraunthaler, G., Pfaller, W. and Kotanko, P. (1985) 'Lack of fructose-1,6-bisphosphatase activity in LLC-PK1 cells', *Am J Physiol*, 248(1 Pt 1), pp. C181-3.
Guo, G.L. and Klaassen, C.D. (2001) 'Protein kinase C suppresses rat organic anion transporting polypeptide 1- and 2-mediated uptake', *J Pharmacol Exp Ther*, 299(2), pp. 551-7.
Guo, X., Ma, N., Wang, J., Song, J., Bu, X., Cheng, Y., Sun, K., Xiong, H., Jiang, G., Zhang, B., Wu, M. and Wei, L. (2008) 'Increased p38-MAPK is responsible for chemotherapy resistance in human gastric cancer cells', *BMC Cancer*, 8, p. 375.
Gupta, A., Winer, K., Econs, M.J., Marx, S.J. and Collins, M.T. (2004) 'FGF-23 is elevated by chronic hyperphosphatemia', *J Clin Endocrinol Metab*, 89(9), pp. 4489-92.
Gurdon, J.B., Lane, C.D., Woodland, H.R. and Marbaix, G. (1971) 'Use of frog eggs and oocytes for the study of messenger RNA and its translation in living cells', *Nature*, 233(5316), pp. 177-82.

Ha Choi, J., Wah Yee, S., Kim, M.J., Nguyen, L., Ho Lee, J., Kang, J.O., Hesselson, S., Castro, R.A., Stryke, D., Johns, S.J., Kwok, P.Y., Ferrin, T.E., Goo Lee, M., Black, B.L., Ahituv, N. and Giacomini, K.M. (2009) 'Identification and characterization of novel polymorphisms in the basal promoter of the human transporter, MATE1', *Pharmacogenet Genomics*, 19(10), pp. 770-80.
Hagenbuch, B. and Gui, C. (2008) 'Xenobiotic transporters of the human organic anion transporting polypeptides (OATP) family', *Xenobiotica*, 38(7-8), pp. 778-801.
Hagenbuch, B. and Meier, P.J. (2003) 'The superfamily of organic anion transporting polypeptides', *Biochim Biophys Acta*, 1609(1), pp. 1-18.
Hagenbuch B, M.P. (2004) 'Organic anion transporting polypeptides of the OATP/ SLC21 family: phylogenetic classification as OATP/ SLCO superfamily, new nomenclature and molecular/functional properties.', *Pflugers Archiv: European Journal of Physiology*, 447(5), pp. 653-65.
Haley, D.P. and Bulger, R.E. (1983) 'The aging male rat: Structure and function of the kidney', *American Journal of Anatomy*, 167(1), pp. 1-13.
Hall, A.M., Hendry, B.M., Nitsch, D. and Connolly, J.O. (2011) 'Tenofovir-associated kidney toxicity in HIV-infected patients: a review of the evidence', *Am J Kidney Dis*, 57(5), pp. 773-80.
Hartmann, C.M., Hewson, A.S., Kos, C.H., Hilfiker, H., Soumounou, Y., Murer, H. and Tenenhouse, H.S. (1996) 'Structure of murine and human renal type II Na+-phosphate cotransporter genes (Npt2 and NPT2)', *Proc Natl Acad Sci U S A*, 93(14), pp. 7409-14.
Harvey, N. and Tenenhouse, H.S. (1992) 'Renal Na(+)-phosphate cotransport in X-linked Hyp mice responds appropriately to Na+ gradient, membrane potential, and pH', *J Bone Miner Res*, 7(5), pp. 563-71.
Havens, P.L., Kiser, J.J., Stephensen, C.B., Hazra, R., Flynn, P.M., Wilson, C.M., Rutledge, B., Bethel, J., Pan, C.G., Woodhouse, L.R., Van Loan, M.D., Liu, N., Lujan-Zilbermann, J., Baker, A., Kapogiannis, B.G., Gordon, C.M. and Mulligan, K. (2013) 'Association of higher plasma vitamin D binding protein and lower free calcitriol levels with tenofovir disoproxil fumarate use and plasma and intracellular tenofovir pharmacokinetics: cause of a functional vitamin D deficiency?', *Antimicrob Agents Chemother*, 57(11), pp. 5619-28.
Hay, E.D. (1993) 'Extracellular matrix alters epithelial differentiation', *Curr Opin Cell Biol*, 5(6), pp. 1029-35.
He, X., Szewczyk, P., Karyakin, A., Evin, M., Hong, W.X., Zhang, Q. and Chang, G. (2010) 'Structure of a cation-bound multidrug and toxic compound extrusion transporter', *Nature*, 467(7318), pp. 991-4.
Helbert, M.J., Dauwe, S. and De Broe, M.E. (1999) 'Flow cytometric immunodissection of the human nephron in vivo and in vitro', *Exp Nephrol*, 7(5-6), pp. 360-76.
Helbert, M.J., Dauwe, S.E. and De Broe, M.E. (2001) 'Flow cytometric immunodissection of the human distal tubule and cortical collecting duct system', *Kidney Int*, 59(2), pp. 554-64.
Helbert, M.J., Dauwe, S.E., Van der Biest, I., Nouwen, E.J. and De Broe, M.E. (1997) 'Immunodissection of the human proximal nephron: flow sorting of S1S2S3, S1S2 and S3 proximal tubular cells', *Kidney Int*, 52(2), pp. 414-28.
Herlitz, L.C., Mohan, S., Stokes, M.B., Radhakrishnan, J., D'Agati, V.D. and Markowitz, G.S. (2010) 'Tenofovir nephrotoxicity: acute tubular necrosis with distinctive clinical, pathological, and mitochondrial abnormalities', *Kidney Int*, 78(11), pp. 1171-7.
Hilgendorf, C., Ahlin, G., Seithel, A., Artursson, P., Ungell, A.L. and Karlsson, J. (2007) 'Expression of thirty-six drug transporter genes in human intestine, liver, kidney, and organotypic cell lines', *Drug Metab Dispos*, 35(8), pp. 1333-40.
Hinderling, P.H. and Hartmann, D. (1991) 'Pharmacokinetics of digoxin and main metabolites/derivatives in healthy humans', *Ther Drug Monit*, 13(5), pp. 381-401.
Hirano, M., Maeda, K., Shitara, Y. and Sugiyama, Y. (2004) 'Contribution of OATP2 (OATP1B1) and OATP8 (OATP1B3) to the hepatic uptake of pitavastatin in humans', *J Pharmacol Exp Ther*, 311(1), pp. 139-46.
Hitzl, M., Drescher, S., van der Kuip, H., Schaffeler, E., Fischer, J., Schwab, M., Eichelbaum, M. and Fromm, M.F. (2001) 'The C3435T mutation in the human MDR1 gene is associated with

altered efflux of the P-glycoprotein substrate rhodamine 123 from CD56+ natural killer cells', *Pharmacogenetics*, 11(4), pp. 293-8.
Ho, E.S., Lin, D.C., Mendel, D.B. and Cihlar, T. (2000) 'Cytotoxicity of antiviral nucleotides adefovir and cidofovir is induced by the expression of human renal organic anion transporter 1', *J Am Soc Nephrol*, 11(3), pp. 383-93.
Hosoyamada, M., Sekine, T., Kanai, Y. and Endou, H. (1999) 'Molecular cloning and functional expression of a multispecific organic anion transporter from human kidney', *Am J Physiol*, 276(1 Pt 2), pp. F122-8.
Hruska, K.A., Mathew, S., Lund, R., Qiu, P. and Pratt, R. (2008) 'Hyperphosphatemia of chronic kidney disease', *Kidney Int*, 74(2), pp. 148-57.
Hu, M.C., Shi, M., Zhang, J., Pastor, J., Nakatani, T., Lanske, B., Razzaque, M.S., Rosenblatt, K.P., Baum, M.G., Kuro-o, M. and Moe, O.W. (2010) 'Klotho: a novel phosphaturic substance acting as an autocrine enzyme in the renal proximal tubule', *Faseb j*, 24(9), pp. 3438-50.
Huls, M., Brown, C.D., Windass, A.S., Sayer, R., van den Heuvel, J.J., Heemskerk, S., Russel, F.G. and Masereeuw, R. (2008) 'The breast cancer resistance protein transporter ABCG2 is expressed in the human kidney proximal tubule apical membrane', *Kidney Int*, 73(2), pp. 220-5.
Hunt, S.A. (2005) 'ACC/AHA 2005 guideline update for the diagnosis and management of chronic heart failure in the adult: a report of the American College of Cardiology/American Heart Association Task Force on Practice Guidelines (Writing Committee to Update the 2001 Guidelines for the Evaluation and Management of Heart Failure)', *J Am Coll Cardiol*, 46(6), pp. e1-82.
Ieiri, I., Suwannakul, S., Maeda, K., Uchimaru, H., Hashimoto, K., Kimura, M., Fujino, H., Hirano, M., Kusuhara, H., Irie, S., Higuchi, S. and Sugiyama, Y. (2007) 'SLCO1B1 (OATP1B1, an uptake transporter) and ABCG2 (BCRP, an efflux transporter) variant alleles and pharmacokinetics of pitavastatin in healthy volunteers', *Clin Pharmacol Ther*, 82(5), pp. 541-7.
Imaoka, T., Kusuhara, H., Adachi, M., Schuetz, J.D., Takeuchi, K. and Sugiyama, Y. (2007) 'Functional involvement of multidrug resistance-associated protein 4 (MRP4/ABCC4) in the renal elimination of the antiviral drugs adefovir and tenofovir', *Mol Pharmacol*, 71(2), pp. 619-27.
Izzedine, H., Hulot, J.S., Villard, E., Goyenvalle, C., Dominguez, S., Ghosn, J., Valantin, M.A., Lechat, P. and Deray, A.G. (2006) 'Association between ABCC2 gene haplotypes and tenofovir-induced proximal tubulopathy', *J Infect Dis*, 194(11), pp. 1481-91.
Jang, K.J., Mehr, A.P., Hamilton, G.A., McPartlin, L.A., Chung, S., Suh, K.Y. and Ingber, D.E. (2013) 'Human kidney proximal tubule-on-a-chip for drug transport and nephrotoxicity assessment', *Integr Biol (Camb)*, 5(9), pp. 1119-29.
Jansen, J., Schophuizen, C.M., Wilmer, M.J., Lahham, S.H., Mutsaers, H.A., Wetzels, J.F., Bank, R.A., van den Heuvel, L.P., Hoenderop, J.G. and Masereeuw, R. (2014) 'A morphological and functional comparison of proximal tubule cell lines established from human urine and kidney tissue', *Exp Cell Res*, 323(1), pp. 87-99.
Japanese Ministry of Health Labour and Welfare (2014) *Japanese ministry of health, labour and welfare (Draft for public comment)*. Available at: http://www.solvobiotech.com/documents/Japanese_DDI_guideline_(draft)_2014Jan.pdf (Accessed: 12/09/15).
Jenkinson, S.E., Chung, G.W., van Loon, E., Bakar, N.S., Dalzell, A.M. and Brown, C.D. (2012) 'The limitations of renal epithelial cell line HK-2 as a model of drug transporter expression and function in the proximal tubule', *Pflugers Arch*, 464(6), pp. 601-11.
Jones, D.P., Sundby, G.B., Ormstad, K. and Orrenius, S. (1979) 'Use of isolated kidney cells for study of drug metabolism', *Biochem Pharmacol*, 28(6), pp. 929-35.
Jonker, J.W. and Schinkel, A.H. (2004) 'Pharmacological and physiological functions of the polyspecific organic cation transporters: OCT1, 2, and 3 (SLC22A1-3)', *J Pharmacol Exp Ther*, 308(1), pp. 2-9.
Jonker, J.W., Wagenaar, E., Mol, C.A., Buitelaar, M., Koepsell, H., Smit, J.W. and Schinkel, A.H. (2001) 'Reduced hepatic uptake and intestinal excretion of organic cations in mice with a

targeted disruption of the organic cation transporter 1 (Oct1 [Slc22a1]) gene', *Mol Cell Biol*, 21(16), pp. 5471-7.
Jonker, J.W., Wagenaar, E., Van Eijl, S. and Schinkel, A.H. (2003) 'Deficiency in the organic cation transporters 1 and 2 (Oct1/Oct2 [Slc22a1/Slc22a2]) in mice abolishes renal secretion of organic cations', *Mol Cell Biol*, 23(21), pp. 7902-8.
Judd, A., Boyd, K.L., Stohr, W., Dunn, D., Butler, K., Lyall, H., Sharland, M., Shingadia, D., Riordan, A. and Gibb, D.M. (2010) 'Effect of tenofovir disoproxil fumarate on risk of renal abnormality in HIV-1-infected children on antiretroviral therapy: a nested case-control study', *Aids*, 24(4), pp. 525-34.
Kajiwara, M., Terada, T., Asaka, J., Ogasawara, K., Katsura, T., Ogawa, O., Fukatsu, A., Doi, T. and Inui, K. (2007) 'Critical roles of Sp1 in gene expression of human and rat H+/organic cation antiporter MATE1', *Am J Physiol Renal Physiol*, 293(5), pp. F1564-70.
Kajiwara, M., Terada, T., Ogasawara, K., Iwano, J., Katsura, T., Fukatsu, A., Doi, T. and Inui, K. (2009) 'Identification of multidrug and toxin extrusion (MATE1 and MATE2-K) variants with complete loss of transport activity', *J Hum Genet*, 54(1), pp. 40-6.
Karbach, U., Kricke, J., Meyer-Wentrup, F., Gorboulev, V., Volk, C., Loffing-Cueni, D., Kaissling, B., Bachmann, S. and Koepsell, H. (2000) 'Localization of organic cation transporters OCT1 and OCT2 in rat kidney', *Am J Physiol Renal Physiol*, 279(4), pp. F679-87.
Katayama, K., Noguchi, K. and Sugimoto, Y. (2014) 'Regulations of P-Glycoprotein/ABCB1/MDR1 in Human Cancer Cells', *New Journal of Science*, 2014, p. 10.
Kearney, B.P., Flaherty, J.F. and Shah, J. (2004) 'Tenofovir disoproxil fumarate: clinical pharmacology and pharmacokinetics', *Clin Pharmacokinet*, 43(9), pp. 595-612.
Kekuda, R., Prasad, P.D., Wu, X., Wang, H., Fei, Y.J., Leibach, F.H. and Ganapathy, V. (1998) 'Cloning and functional characterization of a potential-sensitive, polyspecific organic cation transporter (OCT3) most abundantly expressed in placenta', *J Biol Chem*, 273(26), pp. 15971-9.
Kempson, S.A. (1988) 'Novel Specific Inhibitors of Epithelial Phosphate Transport', *Physiology*, 3(4), pp. 154-157.
Keogh, J.P. and Kunta, J.R. (2006) 'Development, validation and utility of an in vitro technique for assessment of potential clinical drug-drug interactions involving P-glycoprotein', *Eur J Pharm Sci*, 27(5), pp. 543-54.
Kerb, R., Brinkmann, U., Chatskaia, N., Gorbunov, D., Gorboulev, V., Mornhinweg, E., Keil, A., Eichelbaum, M. and Koepsell, H. (2002) 'Identification of genetic variations of the human organic cation transporter hOCT1 and their functional consequences', *Pharmacogenetics*, 12(8), pp. 591-5.
Keskitalo, J.E., Zolk, O., Fromm, M.F., Kurkinen, K.J., Neuvonen, P.J. and Niemi, M. (2009) 'ABCG2 polymorphism markedly affects the pharmacokinetics of atorvastatin and rosuvastatin', *Clin Pharmacol Ther*, 86(2), pp. 197-203.
Kim, H.S., Sunwoo, Y.E., Ryu, J.Y., Kang, H.J., Jung, H.E., Song, I.S., Kim, E.Y., Shim, J.C., Shon, J.H. and Shin, J.G. (2007) 'The effect of ABCG2 V12M, Q141K and Q126X, known functional variants in vitro, on the disposition of lamivudine', *Br J Clin Pharmacol*, 64(5), pp. 645-54.
Kim, J.S., Hwang, H.Z., Yeo, S.H., Ko, S.W., Song, S.M., Kim, Y.K., Kim, D.J., Oh, H.Y., Choi, H.Y., Kim, M.K., Toru, S., Kohsaka, T., Kim, Y. and Jin, D.K. (2001) 'Morphologic evaluation and integrin expression profile of renal tubular cells cultured from percutaneous renal biopsy specimen', *Ren Fail*, 23(1), pp. 21-9.
Kimura, Y., Morita, S.Y., Matsuo, M. and Ueda, K. (2007) 'Mechanism of multidrug recognition by MDR1/ABCB1', *Cancer Sci*, 98(9), pp. 1303-10.
Kobayashi, Y., Ohbayashi, M., Kohyama, N. and Yamamoto, T. (2005) 'Mouse organic anion transporter 2 and 3 (mOAT2/3[Slc22a7/8]) mediates the renal transport of bumetanide', *Eur J Pharmacol*, 524(1-3), pp. 44-8.
Koepsell, H. and Endou, H. (2004) 'The SLC22 drug transporter family', *Pflügers Archiv*, 447(5), pp. 666-676.

Koepsell, H., Lips, K. and Volk, C. (2007) 'Polyspecific organic cation transporters: structure, function, physiological roles, and biopharmaceutical implications', *Pharm Res*, 24(7), pp. 1227-51.
Kohler, J.J., Hosseini, S.H., Green, E., Abuin, A., Ludaway, T., Russ, R., Santoianni, R. and Lewis, W. (2011) 'Tenofovir renal proximal tubular toxicity is regulated by OAT1 and MRP4 transporters', *Lab Invest*, 91(6), pp. 852-8.
Kohler, J.J., Hosseini, S.H., Hoying-Brandt, A., Green, E., Johnson, D.M., Russ, R., Tran, D., Raper, C.M., Santoianni, R. and Lewis, W. (2009) 'Tenofovir renal toxicity targets mitochondria of renal proximal tubules', *Lab Invest*, 89(5), pp. 513-9.
Kolek, O.I., Hines, E.R., Jones, M.D., LeSueur, L.K., Lipko, M.A., Kiela, P.R., Collins, J.F., Haussler, M.R. and Ghishan, F.K. (2005) '1alpha,25-Dihydroxyvitamin D3 upregulates FGF23 gene expression in bone: the final link in a renal-gastrointestinal-skeletal axis that controls phosphate transport', *Am J Physiol Gastrointest Liver Physiol*, 289(6), pp. G1036-42.
Komatsu, T., Hiasa, M., Miyaji, T., Kanamoto, T., Matsumoto, T., Otsuka, M., Moriyama, Y. and Omote, H. (2011) 'Characterization of the human MATE2 proton-coupled polyspecific organic cation exporter', *Int J Biochem Cell Biol*, 43(6), pp. 913-8.
König J, N.A., Cui Y, Leier I, Keppler D. (1999) 'Conjugate export pumps of the multidrug resistance protein (MRP) family: localization, substrate specificity, and MRP2-mediated drug resistance.', *Biochimica et biophysica acta.*, 1461(2), pp. 377-94.
Konig, J., Nies, A.T., Cui, Y., Leier, I. and Keppler, D. (1999) 'Conjugate export pumps of the multidrug resistance protein (MRP) family: localization, substrate specificity, and MRP2-mediated drug resistance', *Biochim Biophys Acta*, 1461(2), pp. 377-94.
Kool, M., de Haas, M., Scheffer, G.L., Scheper, R.J., van Eijk, M.J., Juijn, J.A., Baas, F. and Borst, P. (1997) 'Analysis of expression of cMOAT (MRP2), MRP3, MRP4, and MRP5, homologues of the multidrug resistance-associated protein gene (MRP1), in human cancer cell lines', *Cancer Res*, 57(16), pp. 3537-47.
Kullak-Ublick GA, H.B., Stieger B, Schteingart CD, Hofmann AF, Wolkoff AW, Meier PJ. (1995) 'Molecular and functional characterization of an organic anion transporting polypeptide cloned from human liver.', *Gastroenterology*, 109(4), pp. 1274-82.
Kuro-o, M., Matsumura, Y., Aizawa, H., Kawaguchi, H., Suga, T., Utsugi, T., Ohyama, Y., Kurabayashi, M., Kaname, T., Kume, E., Iwasaki, H., Iida, A., Shiraki-Iida, T., Nishikawa, S., Nagai, R. and Nabeshima, Y.I. (1997) 'Mutation of the mouse klotho gene leads to a syndrome resembling ageing', *Nature*, 390(6655), pp. 45-51.
Kuro, O.M. (2011) 'Phosphate and Klotho', *Kidney Int Suppl*, (121), pp. S20-3.
Kusuhara, H., Sekine, T., Utsunomiya-Tate, N., Tsuda, M., Kojima, R., Cha, S.H., Sugiyama, Y., Kanai, Y. and Endou, H. (1999) 'Molecular cloning and characterization of a new multispecific organic anion transporter from rat brain', *J Biol Chem*, 274(19), pp. 13675-80.
Kusuhara, H. and Sugiyama, Y. (2009) 'In vitro-in vivo extrapolation of transporter-mediated clearance in the liver and kidney', *Drug Metab Pharmacokinet*, 24(1), pp. 37-52.
Kuteykin-Teplyakov, K., Luna-Tortos, C., Ambroziak, K. and Loscher, W. (2010) 'Differences in the expression of endogenous efflux transporters in MDR1-transfected versus wildtype cell lines affect P-glycoprotein mediated drug transport', *Br J Pharmacol*, 160(6), pp. 1453-63.
Labarga, P., Barreiro, P., Martin-Carbonero, L., Rodriguez-Novoa, S., Solera, C., Medrano, J., Rivas, P., Albalater, M., Blanco, F., Moreno, V., Vispo, E. and Soriano, V. (2009) 'Kidney tubular abnormalities in the absence of impaired glomerular function in HIV patients treated with tenofovir', *Aids*, 23(6), pp. 689-96.
Lacarelle, B., Rahmani, R., de Sousa, G., Durand, A., Placidi, M. and Cano, J.P. (1991) 'Metabolism of digoxin, digoxigenin digitoxosides and digoxigenin in human hepatocytes and liver microsomes', *Fundam Clin Pharmacol*, 5(7), pp. 567-82.
Lacy, S.A., Hitchcock, M.J., Lee, W.A., Tellier, P. and Cundy, K.C. (1998) 'Effect of oral probenecid coadministration on the chronic toxicity and pharmacokinetics of intravenous cidofovir in cynomolgus monkeys', *Toxicol Sci*, 44(2), pp. 97-106.

Lash, L.H., Hueni, S.E. and Putt, D.A. (2001) 'Apoptosis, necrosis, and cell proliferation induced by S-(1,2-dichlorovinyl)-L-cysteine in primary cultures of human proximal tubular cells', *Toxicol Appl Pharmacol*, 177(1), pp. 1-16.
Lash, L.H., Putt, D.A. and Cai, H. (2006) 'Membrane transport function in primary cultures of human proximal tubular cells', *Toxicology*, 228(2-3), pp. 200-18.
Lash, L.H., Putt, D.A., Hueni, S.E. and Horwitz, B.P. (2005) 'Molecular markers of trichloroethylene-induced toxicity in human kidney cells', *Toxicol Appl Pharmacol*, 206(2), pp. 157-68.
Lash, L.H., Putt, D.A., Hueni, S.E., Krause, R.J. and Elfarra, A.A. (2003) 'Roles of necrosis, Apoptosis, and mitochondrial dysfunction in S-(1,2-dichlorovinyl)-L-cysteine sulfoxide-induced cytotoxicity in primary cultures of human renal proximal tubular cells', *J Pharmacol Exp Ther*, 305(3), pp. 1163-72.
Lee, C.G., Tang, K., Cheung, Y.B., Wong, L.P., Tan, C., Shen, H., Zhao, Y., Pavanni, R., Lee, E.J., Wong, M.C., Chong, S.S. and Tan, E.K. (2004) 'MDR1, the blood-brain barrier transporter, is associated with Parkinson's disease in ethnic Chinese', *J Med Genet*, 41(5), p. e60.
Lee, J., Azzaroli, F., Wang, L., Soroka, C.J., Gigliozzi, A., Setchell, K.D., Kramer, W. and Boyer, J.L. (2001) 'Adaptive regulation of bile salt transporters in kidney and liver in obstructive cholestasis in the rat', *Gastroenterology*, 121(6), pp. 1473-84.
Lee, W., Glaeser, H., Smith, L.H., Roberts, R.L., Moeckel, G.W., Gervasini, G., Leake, B.F. and Kim, R.B. (2005) 'Polymorphisms in human organic anion-transporting polypeptide 1A2 (OATP1A2): implications for altered drug disposition and central nervous system drug entry', *J Biol Chem*, 280(10), pp. 9610-7.
Lepist, E.I., Zhang, X., Hao, J., Huang, J., Kosaka, A., Birkus, G., Murray, B.P., Bannister, R., Cihlar, T., Huang, Y. and Ray, A.S. (2014) 'Contribution of the organic anion transporter OAT2 to the renal active tubular secretion of creatinine and mechanism for serum creatinine elevations caused by cobicistat', *Kidney Int*, 86(2), pp. 350-7.
Levey, A.S., Coresh, J., Greene, T., Stevens, L.A., Zhang, Y.L., Hendriksen, S., Kusek, J.W. and Van Lente, F. (2006) 'Using standardized serum creatinine values in the modification of diet in renal disease study equation for estimating glomerular filtration rate', *Annals of internal medicine*, 145(4), pp. 247-254.
Lim, Y., Lyall, H. and Foster, C. (2015) 'Tenofovir-Associated Nephrotoxicity in Children with Perinatally-Acquired HIV Infection: A Single-Centre Cohort Study', *Clin Drug Investig*, 35(5), pp. 327-33.
Liu, M., Aneja, R., Wang, H., Sun, L., Dong, X., Huo, L., Joshi, H. and Zhou, J. (2008) 'Modulation of multidrug resistance in cancer cells by the E3 ubiquitin ligase seven-in-absentia homologue 1', *J Pathol*, 214(4), pp. 508-14.
Liu, S., Tang, W., Zhou, J., Stubbs, J.R., Luo, Q., Pi, M. and Quarles, L.D. (2006) 'Fibroblast growth factor 23 is a counter-regulatory phosphaturic hormone for vitamin D', *J Am Soc Nephrol*, 17(5), pp. 1305-15.
Loghman-Adham, M. and Dousa, T.P. (1992) 'Dual action of phosphonoformic acid on Na(+)-phosphate cotransport in opossum kidney cells', *Am J Physiol*, 263(2 Pt 2), pp. F301-10.
Lohr, J.W., Willsky, G.R. and Acara, M.A. (1998) 'Renal drug metabolism', *Pharmacol Rev*, 50(1), pp. 107-41.
Lu, R., Kanai, N., Bao, Y., Wolkoff, A.W. and Schuster, V.L. (1996) 'Regulation of renal oatp mRNA expression by testosterone', *Am J Physiol*, 270(2 Pt 2), pp. F332-7.
Luo, F.R., Paranjpe, P.V., Guo, A., Rubin, E. and Sinko, P. (2002) 'Intestinal transport of irinotecan in Caco-2 cells and MDCK II cells overexpressing efflux transporters Pgp, cMOAT, and MRP1', *Drug Metab Dispos*, 30(7), pp. 763-70.
Magalhaes-Costa, P., Matos, L., Barreiro, P. and Chagas, C. (2015) 'Fanconi syndrome and chronic renal failure in a chronic hepatitis B monoinfected patient treated with tenofovir', *Rev Esp Enferm Dig*, 107(8), pp. 512-514.
Mandikova, J., Volkova, M., Pavek, P., Cesnek, M., Janeba, Z., Kubicek, V. and Trejtnar, F. (2013) 'Interactions with selected drug renal transporters and transporter-mediated

cytotoxicity in antiviral agents from the group of acyclic nucleoside phosphonates', *Toxicology*, 311(3), pp. 135-46.
Mao, Q. and Unadkat, J.D. (2015) 'Role of the breast cancer resistance protein (BCRP/ABCG2) in drug transport--an update', *Aaps j*, 17(1), pp. 65-82.
Marks, J., Churchill, L.J., Srai, S.K., Biber, J., Murer, H., Jaeger, P., Debnam, E.S. and Unwin, R.J. (2007) 'Intestinal phosphate absorption in a model of chronic renal failure', *Kidney Int*, 72(2), pp. 166-73.
Martin, A., David, V. and Quarles, L.D. (2012) 'Regulation and function of the FGF23/klotho endocrine pathways', *Physiol Rev*, 92(1), pp. 131-55.
Martin, J.L., Brown, C.E., Matthews-Davis, N. and Reardon, J.E. (1994) 'Effects of antiviral nucleoside analogs on human DNA polymerases and mitochondrial DNA synthesis', *Antimicrob Agents Chemother*, 38(12), pp. 2743-9.
Marzolini, C., Paus, E., Buclin, T. and Kim, R.B. (2004) 'Polymorphisms in human MDR1 (P-glycoprotein): recent advances and clinical relevance', *Clin Pharmacol Ther*, 75(1), pp. 13-33.
Masuda, S., Terada, T., Yonezawa, A., Tanihara, Y., Kishimoto, K., Katsura, T., Ogawa, O. and Inui, K. (2006) 'Identification and functional characterization of a new human kidney-specific H+/organic cation antiporter, kidney-specific multidrug and toxin extrusion 2', *J Am Soc Nephrol*, 17(8), pp. 2127-35.
McArdle, W.D., Katch, F.I. and Katch, V.L. (2010) *Exercise Physiology: Nutrition, Energy, and Human Performance*. Lippincott Williams & Wilkins.
McDevitt, C.A., Collins, R.F., Conway, M., Modok, S., Storm, J., Kerr, I.D., Ford, R.C. and Callaghan, R. (2006) 'Purification and 3D structural analysis of oligomeric human multidrug transporter ABCG2', *Structure*, 14(11), pp. 1623-32.
Merta, A., Votruba, I., Jindrich, J., Holy, A., Cihlar, T., Rosenberg, I., Otmar, M. and Herve, T.Y. (1992) 'Phosphorylation of 9-(2-phosphonomethoxyethyl)adenine and 9-(S)-(3-hydroxy-2-phosphonomethoxypropyl)adenine by AMP(dAMP) kinase from L1210 cells', *Biochem Pharmacol*, 44(10), pp. 2067-77.
Mikkaichi T, S.T., Onogawa T, Tanemoto M, Mizutamari H, Okada M, Chaki T, Masuda S, Tokui T, Eto N, Abe M, Satoh F, Unno M, Hishinuma T, Inui K, Ito S, Goto J, Abe T. (2004) 'Isolation and characterization of a digoxin transporter and its rat homologue expressed in the kidney.', *Proceedings of the National Academy of Sciences of the United States of America.*, 101(10), pp. 3569-74.
Mikkaichi, T., Suzuki, T., Onogawa, T., Tanemoto, M., Mizutamari, H., Okada, M., Chaki, T., Masuda, S., Tokui, T., Eto, N., Abe, M., Satoh, F., Unno, M., Hishinuma, T., Inui, K., Ito, S., Goto, J. and Abe, T. (2004) 'Isolation and characterization of a digoxin transporter and its rat homologue expressed in the kidney', *Proc Natl Acad Sci U S A*, 101(10), pp. 3569-74.
Mirams, M., Robinson, B.G., Mason, R.S. and Nelson, A.E. (2004) 'Bone as a source of FGF23: regulation by phosphate?', *Bone*, 35(5), pp. 1192-9.
Miyamoto, K., Tatsumi, S., Sonoda, T., Yamamoto, H., Minami, H., Taketani, Y. and Takeda, E. (1995) 'Cloning and functional expression of a Na(+)-dependent phosphate co-transporter from human kidney: cDNA cloning and functional expression', *Biochem J*, 305 (Pt 1), pp. 81-5.
Morita, Y., Kataoka, A., Shiota, S., Mizushima, T. and Tsuchiya, T. (2000) 'NorM of vibrio parahaemolyticus is an Na(+)-driven multidrug efflux pump', *J Bacteriol*, 182(23), pp. 6694-7.
Morrissey, K.M., Stocker, S.L., Wittwer, M.B., Xu, L. and Giacomini, K.M. (2013) 'Renal transporters in drug development', *Annu Rev Pharmacol Toxicol*, 53, pp. 503-29.
Moss, D.M., Kwan, W.S., Liptrott, N.J., Smith, D.L., Siccardi, M., Khoo, S.H., Back, D.J. and Owen, A. (2011) 'Raltegravir is a substrate for SLC22A6: a putative mechanism for the interaction between raltegravir and tenofovir', *Antimicrob Agents Chemother*, 55(2), pp. 879-87.
Muller, P.Y. and Milton, M.N. (2012) 'The determination and interpretation of the therapeutic index in drug development', *Nat Rev Drug Discov*, 11(10), pp. 751-761.
Mutoh, K., Tsukahara, S., Mitsuhashi, J., Katayama, K. and Sugimoto, Y. (2006) 'Estrogen-mediated post transcriptional down-regulation of P-glycoprotein in MDR1-transduced human breast cancer cells', *Cancer Sci*, 97(11), pp. 1198-204.

Nakanishi, T., Fukushi, A., Sato, M., Yoshifuji, M., Gose, T., Shirasaka, Y., Ohe, K., Kobayashi, M., Kawai, K. and Tamai, I. (2011) 'Functional characterization of apical transporters expressed in rat proximal tubular cells (PTCs) in primary culture', *Mol Pharm*, 8(6), pp. 2142-50.
Narayanan, K., Schumacher, K.M., Tasnim, F., Kandasamy, K., Schumacher, A., Ni, M., Gao, S., Gopalan, B., Zink, D. and Ying, J.Y. (2013) 'Human embryonic stem cells differentiate into functional renal proximal tubular-like cells', *Kidney Int*, 83(4), pp. 593-603.
Natarajan, K., Xie, Y., Baer, M.R. and Ross, D.D. (2012) 'Role of breast cancer resistance protein (BCRP/ABCG2) in cancer drug resistance', *Biochem Pharmacol*, 83(8), pp. 1084-103.
Nelson, J.A., Santos, G. and Herbert, B.H. (1984) 'Mechanisms for the renal secretion of cisplatin', *Cancer Treat Rep*, 68(6), pp. 849-53.
Nelson, M.R., Katlama, C., Montaner, J.S., Cooper, D.A., Gazzard, B., Clotet, B., Lazzarin, A., Schewe, K., Lange, J., Wyatt, C., Curtis, S., Chen, S.S., Smith, S., Bischofberger, N. and Rooney, J.F. (2007) 'The safety of tenofovir disoproxil fumarate for the treatment of HIV infection in adults: the first 4 years', *Aids*, 21(10), pp. 1273-81.
Ni, Z., Bikadi, Z., Rosenberg, M.F. and Mao, Q. (2010) 'Structure and function of the human breast cancer resistance protein (BCRP/ABCG2)', *Curr Drug Metab*, 11(7), pp. 603-17.
Nicolle, E., Boumendjel, A., Macalou, S., Genoux, E., Ahmed-Belkacem, A., Carrupt, P.A. and Di Pietro, A. (2009) 'QSAR analysis and molecular modeling of ABCG2-specific inhibitors', *Adv Drug Deliv Rev*, 61(1), pp. 34-46.
Nies, A.T. and Keppler, D. (2007) 'The apical conjugate efflux pump ABCC2 (MRP2)', *Pflugers Arch*, 453(5), pp. 643-59.
Nyengaard, J.R. and Bendtsen, T.F. (1992) 'Glomerular number and size in relation to age, kidney weight, and body surface in normal man', *The Anatomical Record*, 232(2), pp. 194-201.
Ohtomo, T., Saito, H., Inotsume, N., Yasuhara, M. and Inui, K.I. (1996) 'Transport of levofloxacin in a kidney epithelial cell line, LLC-PK1: interaction with organic cation transporters in apical and basolateral membranes', *J Pharmacol Exp Ther*, 276(3), pp. 1143-8.
Okuda, M., Saito, H., Urakami, Y., Takano, M. and Inui, K. (1996) 'cDNA cloning and functional expression of a novel rat kidney organic cation transporter, OCT2', *Biochem Biophys Res Commun*, 224(2), pp. 500-7.
Otsuka, M., Matsumoto, T., Morimoto, R., Arioka, S., Omote, H. and Moriyama, Y. (2005) 'A human transporter protein that mediates the final excretion step for toxic organic cations', *Proc Natl Acad Sci U S A*, 102(50), pp. 17923-8.
Paccou, J., Viget, N., Legrout-Gerot, I., Yazdanpanah, Y. and Cortet, B. (2009) 'Bone loss in patients with HIV infection', *Joint Bone Spine*, 76(6), pp. 637-41.
Paul, S.M., Mytelka, D.S., Dunwiddie, C.T., Persinger, C.C., Munos, B.H., Lindborg, S.R. and Schacht, A.L. (2010) 'How to improve R&D productivity: the pharmaceutical industry's grand challenge', *Nat Rev Drug Discov*, 9(3), pp. 203-214.
Perazella, M.A. (2010) 'Tenofovir-induced kidney disease: an acquired renal tubular mitochondriopathy', *Kidney Int*, 78(11), pp. 1060-3.
Pfaller, W. and Gstraunthaler, G. (1998) 'Nephrotoxicity testing in vitro--what we know and what we need to know', *Environ Health Perspect*, 106 Suppl 2, pp. 559-69.
Prasad, B. and Unadkat, J.D. (2014) 'Optimized approaches for quantification of drug transporters in tissues and cells by MRM proteomics', *Aaps j*, 16(4), pp. 634-48.
Prie, D., Urena Torres, P. and Friedlander, G. (2009) 'Latest findings in phosphate homeostasis', *Kidney Int*, 75(9), pp. 882-9.
Quamme, G.A. (1990) 'Effect of pH on Na(+)-dependent phosphate transport in renal outer cortical and outer medullary BBMV', *Am J Physiol*, 258(2 Pt 2), pp. F356-63.
Racusen, L.C., Monteil, C., Sgrignoli, A., Lucskay, M., Marouillat, S., Rhim, J.G. and Morin, J.P. (1997) 'Cell lines with extended in vitro growth potential from human renal proximal tubule: characterization, response to inducers, and comparison with established cell lines', *J Lab Clin Med*, 129(3), pp. 318-29.
Rasmussen, F. (1983) 'Renal clearance: species differences and similarities.', *Veterinary research communications.*, 7(1-4), pp. 301-6.

Ravera, S., Virkki, L.V., Murer, H. and Forster, I.C. (2007) 'Deciphering PiT transport kinetics and substrate specificity using electrophysiology and flux measurements', *Am J Physiol Cell Physiol*, 293(2), pp. C606-20.
Reid, G., Wielinga, P., Zelcer, N., De Haas, M., Van Deemter, L., Wijnholds, J., Balzarini, J. and Borst, P. (2003) 'Characterization of the transport of nucleoside analog drugs by the human multidrug resistance proteins MRP4 and MRP5', *Mol Pharmacol*, 63(5), pp. 1094-103.
Riches, Z., Cameron, G., Hawksworth, G. (2010) 'Uptake and efflux of abacavir and Tenofovir by human renal transporters: a mechanism for drug-drug interactions?', *BPS Winter Meeting 2010*. 134P Queen Elizabeth II Conference Centre London. pA2 online. Available at: http://www.pa2online.org/abstracts/vol8issue1abst134p.pdf.
Rifkin, B.S. and Perazella, M.A. (2004) 'Tenofovir-associated nephrotoxicity: Fanconi syndrome and renal failure', *Am J Med*, 117(4), pp. 282-4.
Ritter, C.S., Armbrecht, H.J., Slatopolsky, E. and Brown, A.J. (2006) '25-Hydroxyvitamin D(3) suppresses PTH synthesis and secretion by bovine parathyroid cells', *Kidney Int*, 70(4), pp. 654-9.
Rizwan, A.N. and Burckhardt, G. (2007) 'Organic anion transporters of the SLC22 family: biopharmaceutical, physiological, and pathological roles', *Pharm Res*, 24(3), pp. 450-70.
Robbins, B.L., Srinivas, R.V., Kim, C., Bischofberger, N. and Fridland, A. (1998) 'Anti-human immunodeficiency virus activity and cellular metabolism of a potential prodrug of the acyclic nucleoside phosphonate 9-R-(2-phosphonomethoxypropyl)adenine (PMPA), Bis(isopropyloxymethylcarbonyl)PMPA', *Antimicrob Agents Chemother*, 42(3), pp. 612-7.
Roth, M., Obaidat, A. and Hagenbuch, B. (2012) 'OATPs, OATs and OCTs: the organic anion and cation transporters of the SLCO and SLC22A gene superfamilies', *Br J Pharmacol*, 165(5), pp. 1260-87.
Rothnie, A., Theron, D., Soceneantu, L., Martin, C., Traikia, M., Berridge, G., Higgins, C.F., Devaux, P.F. and Callaghan, R. (2001) 'The importance of cholesterol in maintenance of P-glycoprotein activity and its membrane perturbing influence', *Eur Biophys J*, 30(6), pp. 430-42.
Ryan, M.J., Johnson, G., Kirk, J., Fuerstenberg, S.M., Zager, R.A. and Torok-Storb, B. (1994) 'HK-2: an immortalized proximal tubule epithelial cell line from normal adult human kidney', *Kidney Int*, 45(1), pp. 48-57.
Saidenberg-Kermanac'h, N., Souabni, L., Prendki, V., Prie, D. and Boissier, M.C. (2011) 'Normal plasma FGF23 levels kinetic in tenofovir-related hypophosphatemic osteomalacia in an HIV-infected patient with von Recklinghausen disease', *Joint Bone Spine*, 78(3), pp. 306-8.
Saito, H., Hirano, H., Nakagawa, H., Fukami, T., Oosumi, K., Murakami, K., Kimura, H., Kouchi, T., Konomi, M., Tao, E., Tsujikawa, N., Tarui, S., Nagakura, M., Osumi, M. and Ishikawa, T. (2006) 'A new strategy of high-speed screening and quantitative structure-activity relationship analysis to evaluate human ATP-binding cassette transporter ABCG2-drug interactions', *J Pharmacol Exp Ther*, 317(3), pp. 1114-24.
Sakata, T., Anzai, N., Kimura, T., Miura, D., Fukutomi, T., Takeda, M., Sakurai, H. and Endou, H. (2010) 'Functional analysis of human organic cation transporter OCT3 (SLC22A3) polymorphisms', *J Pharmacol Sci*, 113(3), pp. 263-6.
Saliba, K.J., Martin, R.E., Broer, A., Henry, R.I., McCarthy, C.S., Downie, M.J., Allen, R.J., Mullin, K.A., McFadden, G.I., Broer, S. and Kirk, K. (2006) 'Sodium-dependent uptake of inorganic phosphate by the intracellular malaria parasite', *Nature*, 443(7111), pp. 582-5.
Sasaki, M., Suzuki, H., Ito, K., Abe, T. and Sugiyama, Y. (2002) 'Transcellular transport of organic anions across a double-transfected Madin-Darby canine kidney II cell monolayer expressing both human organic anion-transporting polypeptide (OATP2/SLC21A6) and Multidrug resistance-associated protein 2 (MRP2/ABCC2)', *J Biol Chem*, 277(8), pp. 6497-503.
Schaich, M., Kestel, L., Pfirrmann, M., Robel, K., Illmer, T., Kramer, M., Dill, C., Ehninger, G., Schackert, G. and Krex, D. (2009) 'A MDR1 (ABCB1) gene single nucleotide polymorphism predicts outcome of temozolomide treatment in glioblastoma patients', *Ann Oncol*, 20(1), pp. 175-81.

Schaub, T.P., Kartenbeck, J., Konig, J., Vogel, O., Witzgall, R., Kriz, W. and Keppler, D. (1997) 'Expression of the conjugate export pump encoded by the mrp2 gene in the apical membrane of kidney proximal tubules', *J Am Soc Nephrol*, 8(8), pp. 1213-21.
Schuetz, J.D., Connelly, M.C., Sun, D., Paibir, S.G., Flynn, P.M., Srinivas, R.V., Kumar, A. and Fridland, A. (1999) 'MRP4: A previously unidentified factor in resistance to nucleoside-based antiviral drugs', *Nat Med*, 5(9), pp. 1048-51.
Segawa, H., Kaneko, I., Takahashi, A., Kuwahata, M., Ito, M., Ohkido, I., Tatsumi, S. and Miyamoto, K. (2002) 'Growth-related renal type II Na/Pi cotransporter', *J Biol Chem*, 277(22), pp. 19665-72.
Sekine, T., Cha, S.H., Tsuda, M., Apiwattanakul, N., Nakajima, N., Kanai, Y. and Endou, H. (1998) 'Identification of multispecific organic anion transporter 2 expressed predominantly in the liver', *FEBS Lett*, 429(2), pp. 179-82.
Sekine, T., Watanabe, N., Hosoyamada, M., Kanai, Y. and Endou, H. (1997) 'Expression cloning and characterization of a novel multispecific organic anion transporter', *J Biol Chem*, 272(30), pp. 18526-9.
Shapiro, A.B., Fox, K., Lam, P. and Ling, V. (1999) 'Stimulation of P-glycoprotein-mediated drug transport by prazosin and progesterone. Evidence for a third drug-binding site', *Eur J Biochem*, 259(3), pp. 841-50.
Shaw, J.P., Sueoko, C.M., Oliyai, R., Lee, W.A., Arimilli, M.N., Kim, C.U. and Cundy, K.C. (1997) 'Metabolism and pharmacokinetics of novel oral prodrugs of 9-[(R)-2-(phosphonomethoxy)propyl]adenine (PMPA) in dogs', *Pharm Res*, 14(12), pp. 1824-9.
Shen, H., Liu, T., Morse, B.L., Zhao, Y., Zhang, Y., Qiu, X., Chen, C., Lewin, A.C., Wang, X.T., Liu, G., Christopher, L.J., Marathe, P. and Lai, Y. (2015) 'Characterization of Organic Anion Transporter 2 (SLC22A7): A Highly Efficient Transporter for Creatinine and Species-Dependent Renal Tubular Expression', *Drug Metab Dispos*, 43(7), pp. 984-93.
Shimada, T., Hasegawa, H., Yamazaki, Y., Muto, T., Hino, R., Takeuchi, Y., Fujita, T., Nakahara, K., Fukumoto, S. and Yamashita, T. (2004) 'FGF-23 is a potent regulator of vitamin D metabolism and phosphate homeostasis', *J Bone Miner Res*, 19(3), pp. 429-35.
Shin, H.J., Lee, C.H., Lee, S.S., Song, I.S. and Shin, J.G. (2010) 'Identification of genetic polymorphisms of human OAT1 and OAT2 genes and their relationship to hOAT2 expression in human liver', *Clin Chim Acta*, 411(1-2), pp. 99-105.
Shu, Y., Bello, C.L., Mangravite, L.M., Feng, B. and Giacomini, K.M. (2001) 'Functional characteristics and steroid hormone-mediated regulation of an organic cation transporter in Madin-Darby canine kidney cells', *J Pharmacol Exp Ther*, 299(1), pp. 392-8.
Simonson, G.D., Vincent, A.C., Roberg, K.J., Huang, Y. and Iwanij, V. (1994) 'Molecular cloning and characterization of a novel liver-specific transport protein', *J Cell Sci*, 107 (Pt 4), pp. 1065-72.
Sitara, D., Razzaque, M.S., Hesse, M., Yoganathan, S., Taguchi, T., Erben, R.G., Juppner, H. and Lanske, B. (2004) 'Homozygous ablation of fibroblast growth factor-23 results in hyperphosphatemia and impaired skeletogenesis, and reverses hypophosphatemia in Phex-deficient mice', *Matrix Biol*, 23(7), pp. 421-32.
Slager, R.E., Newton, T.L., Vlangos, C.N., Finucane, B. and Elsea, S.H. (2003) 'Mutations in RAI1 associated with Smith-Magenis syndrome', *Nat Genet*, 33(4), pp. 466-8.
Smith, D.A., Di, L. and Kerns, E.H. (2010) 'The effect of plasma protein binding on in vivo efficacy: misconceptions in drug discovery', *Nat Rev Drug Discov*, 9(12), pp. 929-939.
Song, I.S., Shin, H.J., Shim, E.J., Jung, I.S., Kim, W.Y., Shon, J.H. and Shin, J.G. (2008) 'Genetic variants of the organic cation transporter 2 influence the disposition of metformin', *Clin Pharmacol Ther*, 84(5), pp. 559-62.
Sparreboom, A., Loos, W.J., Burger, H., Sissung, T.M., Verweij, J., Figg, W.D., Nooter, K. and Gelderblom, H. (2005) 'Effect of ABCG2 genotype on the oral bioavailability of topotecan', *Cancer Biol Ther*, 4(6), pp. 650-8.

Sweet, D.H., Wolff, N.A. and Pritchard, J.B. (1997) 'Expression cloning and characterization of ROAT1. The basolateral organic anion transporter in rat kidney', *J Biol Chem*, 272(48), pp. 30088-95.
Swift, B., Pfeifer, N.D. and Brouwer, K.L. (2010) 'Sandwich-cultured hepatocytes: an in vitro model to evaluate hepatobiliary transporter-based drug interactions and hepatotoxicity', *Drug Metab Rev*, 42(3), pp. 446-71.
Szczepanska-Konkel, M., Yusufi, A.N. and Dousa, T.P. (1987) 'Interactions of [14C]phosphonoformic acid with renal cortical brush-border membranes. Relationship to the Na+-phosphate co-transporter', *J Biol Chem*, 262(17), pp. 8000-10.
Szczepanska-Konkel, M., Yusufi, A.N., VanScoy, M., Webster, S.K. and Dousa, T.P. (1986) 'Phosphonocarboxylic acids as specific inhibitors of Na+-dependent transport of phosphate across renal brush border membrane', *J Biol Chem*, 261(14), pp. 6375-83.
Tahara, H., Kusuhara, H., Endou, H., Koepsell, H., Imaoka, T., Fuse, E. and Sugiyama, Y. (2005) 'A species difference in the transport activities of H2 receptor antagonists by rat and human renal organic anion and cation transporters', *J Pharmacol Exp Ther*, 315(1), pp. 337-45.
Takeuchi, A., Masuda, S., Saito, H., Abe, T. and Inui, K. (2001) 'Multispecific substrate recognition of kidney-specific organic anion transporters OAT-K1 and OAT-K2', *J Pharmacol Exp Ther*, 299(1), pp. 261-7.
Takeuchi A, M.S., Saito H, Abe T, Inui K. (2001) 'Multispecific substrate recognition of kidney-specific organic anion transporters OAT-K1 and OAT-K2.', *The journal of pharmacology and experimental therapeutics.*, 299(1), pp. 261-7.
Tan, E.K., Chan, D.K., Ng, P.W., Woo, J., Teo, Y.Y., Tang, K., Wong, L.P., Chong, S.S., Tan, C., Shen, H., Zhao, Y. and Lee, C.G. (2005) 'Effect of MDR1 haplotype on risk of Parkinson disease', *Arch Neurol*, 62(3), pp. 460-4.
Tan, E.K., Drozdzik, M., Bialecka, M., Honczarenko, K., Klodowska-Duda, G., Teo, Y.Y., Tang, K., Wong, L.P., Chong, S.S., Tan, C., Yew, K., Zhao, Y. and Lee, C.G. (2004) 'Analysis of MDR1 haplotypes in Parkinson's disease in a white population', *Neurosci Lett*, 372(3), pp. 240-4.
Tanihara, Y., Masuda, S., Sato, T., Katsura, T., Ogawa, O. and Inui, K. (2007) 'Substrate specificity of MATE1 and MATE2-K, human multidrug and toxin extrusions/H(+)-organic cation antiporters', *Biochem Pharmacol*, 74(2), pp. 359-71.
Taub, M.L., Yang, I.S. and Wang, Y. (1989) 'Primary rabbit kidney proximal tubule cell cultures maintain differentiated functions when cultured in a hormonally defined serum-free medium', *In Vitro Cell Dev Biol*, 25(9), pp. 770-5.
Terada, T., Masuda, S., Asaka, J., Tsuda, M., Katsura, T. and Inui, K. (2006) 'Molecular cloning, functional characterization and tissue distribution of rat H+/organic cation antiporter MATE1', *Pharm Res*, 23(8), pp. 1696-701.
To, K.K., Zhan, Z. and Bates, S.E. (2006) 'Aberrant promoter methylation of the ABCG2 gene in renal carcinoma', *Mol Cell Biol*, 26(22), pp. 8572-85.
Tohyama, O., Imura, A., Iwano, A., Freund, J.N., Henrissat, B., Fujimori, T. and Nabeshima, Y. (2004) 'Klotho is a novel beta-glucuronidase capable of hydrolyzing steroid beta-glucuronides', *J Biol Chem*, 279(11), pp. 9777-84.
Torres, P.A. and De Brauwere, D.P. (2011) 'Three feedback loops precisely regulating serum phosphate concentration', *Kidney Int*, 80(5), pp. 443-5.
Toyama, K., Yonezawa, A., Tsuda, M., Masuda, S., Yano, I., Terada, T., Osawa, R., Katsura, T., Hosokawa, M., Fujimoto, S., Inagaki, N. and Inui, K. (2010) 'Heterozygous variants of multidrug and toxin extrusions (MATE1 and MATE2-K) have little influence on the disposition of metformin in diabetic patients', *Pharmacogenet Genomics*, 20(2), pp. 135-8.
Toyoda, Y., Hagiya, Y., Adachi, T., Hoshijima, K., Kuo, M.T. and Ishikawa, T. (2008) 'MRP class of human ATP binding cassette (ABC) transporters: historical background and new research directions', *Xenobiotica*, 38(7-8), pp. 833-62.
Traebert, M., Roth, J., Biber, J., Murer, H. and Kaissling, B. (2000) 'Internalization of proximal tubular type II Na-P(i) cotransporter by PTH: immunogold electron microscopy', *Am J Physiol Renal Physiol*, 278(1), pp. F148-54.

Tramonti, G., Romiti, N., Norpoth, M. and Chieli, E. (2001) 'P-glycoprotein in HK-2 proximal tubule cell line', *Ren Fail*, 23(3-4), pp. 331-7.
Trifillis, A.L., Regec, A.L. and Trump, B.F. (1985) 'Isolation, culture and characterization of human renal tubular cells', *J Urol*, 133(2), pp. 324-9.
Tsuda, M., Terada, T., Mizuno, T., Katsura, T., Shimakura, J. and Inui, K. (2009) 'Targeted disruption of the multidrug and toxin extrusion 1 (mate1) gene in mice reduces renal secretion of metformin', *Mol Pharmacol*, 75(6), pp. 1280-6.
Tufts Center for the Study of Drug Development (2014) *Cost to Develop and Win Marketing Approval for a New Drug Is $2.6 Billion*. Available at: http://csdd.tufts.edu/news/complete_story/cost_study_press_event_webcast (Accessed: 21/09/2015).
Ueda, K., Clark, D.P., Chen, C.J., Roninson, I.B., Gottesman, M.M. and Pastan, I. (1987) 'The human multidrug resistance (mdr1) gene. cDNA cloning and transcription initiation', *J Biol Chem*, 262(2), pp. 505-8.
Urakami, Y., Okuda, M., Masuda, S., Saito, H. and Inui, K.I. (1998) 'Functional characteristics and membrane localization of rat multispecific organic cation transporters, OCT1 and OCT2, mediating tubular secretion of cationic drugs', *J Pharmacol Exp Ther*, 287(2), pp. 800-5.
Urakawa, I., Yamazaki, Y., Shimada, T., Iijima, K., Hasegawa, H., Okawa, K., Fujita, T., Fukumoto, S. and Yamashita, T. (2006) 'Klotho converts canonical FGF receptor into a specific receptor for FGF23', *Nature*, 444(7120), pp. 770-4.
Urquhart, B.L., Ware, J.A., Tirona, R.G., Ho, R.H., Leake, B.F., Schwarz, U.I., Zaher, H., Palandra, J., Gregor, J.C., Dresser, G.K. and Kim, R.B. (2008) 'Breast cancer resistance protein (ABCG2) and drug disposition: intestinal expression, polymorphisms and sulfasalazine as an in vivo probe', *Pharmacogenet Genomics*, 18(5), pp. 439-48.
Uwai, Y., Ida, H., Tsuji, Y., Katsura, T. and Inui, K. (2007) 'Renal transport of adefovir, cidofovir, and tenofovir by SLC22A family members (hOAT1, hOAT3, and hOCT2)', *Pharm Res*, 24(4), pp. 811-5.
Vaidya, V.S., Ferguson, M.A. and Bonventre, J.V. (2008) 'Biomarkers of acute kidney injury', *Annu Rev Pharmacol Toxicol*, 48, pp. 463-93.
Vallon, V., Rieg, T., Ahn, S.Y., Wu, W., Eraly, S.A. and Nigam, S.K. (2008) 'Overlapping in vitro and in vivo specificities of the organic anion transporters OAT1 and OAT3 for loop and thiazide diuretics', *Am J Physiol Renal Physiol*, 294(4), pp. F867-73.
van Aubel, R.A., Smeets, P.H., Peters, J.G., Bindels, R.J. and Russel, F.G. (2002) 'The MRP4/ABCC4 gene encodes a novel apical organic anion transporter in human kidney proximal tubules: putative efflux pump for urinary cAMP and cGMP', *J Am Soc Nephrol*, 13(3), pp. 595-603.
Van der Biest, I., Nouwen, E.J., Van Dromme, S.A. and De Broe, M.E. (1994) 'Characterization of pure proximal and heterogeneous distal human tubular cells in culture', *Kidney Int*, 45(1), pp. 85-94.
van Gelder, J., Deferme, S., Naesens, L., De Clercq, E., van den Mooter, G., Kinget, R. and Augustijns, P. (2002) 'Intestinal absorption enhancement of the ester prodrug tenofovir disoproxil fumarate through modulation of the biochemical barrier by defined ester mixtures', *Drug Metab Dispos*, 30(8), pp. 924-30.
VanWert, A.L., Gionfriddo, M.R. and Sweet, D.H. (2010) 'Organic anion transporters: discovery, pharmacology, regulation and roles in pathophysiology', *Biopharm Drug Dispos*, 31(1), pp. 1-71.
Verhulst, A., Asselman, M., Persy, V.P., Schepers, M.S., Helbert, M.F., Verkoelen, C.F. and De Broe, M.E. (2003) 'Crystal retention capacity of cells in the human nephron: involvement of CD44 and its ligands hyaluronic acid and osteopontin in the transition of a crystal binding- into a nonadherent epithelium', *J Am Soc Nephrol*, 14(1), pp. 107-15.
Verhulst, A., D'Haese, P.C. and De Broe, M.E. (2004) 'Inhibitors of HMG-CoA reductase reduce receptor-mediated endocytosis in human kidney proximal tubular cells', *J Am Soc Nephrol*, 15(9), pp. 2249-57.

Verhulst, A., Sayer, R., De Broe, M.E., D'Haese, P.C. and Brown, C.D. (2008) 'Human proximal tubular epithelium actively secretes but does not retain rosuvastatin', *Mol Pharmacol*, 74(4), pp. 1084-91.
Vervloet, M.G. and Larsson, T.E. (2011) 'Fibroblast growth factor-23 and Klotho in chronic kidney disease', *Kidney inter., Suppl.*, 1(4), pp. 130-135.
Vethanayagam, R.R., Wang, H., Gupta, A., Zhang, Y., Lewis, F., Unadkat, J.D. and Mao, Q. (2005) 'Functional analysis of the human variants of breast cancer resistance protein: I206L, N590Y, and D620N', *Drug Metab Dispos*, 33(6), pp. 697-705.
Villa-Bellosta, R., Bogaert, Y.E., Levi, M. and Sorribas, V. (2007) 'Characterization of phosphate transport in rat vascular smooth muscle cells: implications for vascular calcification', *Arterioscler Thromb Vasc Biol*, 27(5), pp. 1030-6.
Villa-Bellosta, R. and Sorribas, V. (2008) 'Role of rat sodium/phosphate cotransporters in the cell membrane transport of arsenate', *Toxicol Appl Pharmacol*, 232(1), pp. 125-34.
Villa-Bellosta, R. and Sorribas, V. (2009) 'Different effects of arsenate and phosphonoformate on P(i) transport adaptation in opossum kidney cells', *Am J Physiol Cell Physiol*, 297(3), pp. C516-25.
Virkki, L.V., Forster, I.C., Bacconi, A., Biber, J. and Murer, H. (2005) 'Functionally important residues in the predicted 3(rd) transmembrane domain of the type IIa sodium-phosphate co-transporter (NaPi-IIa)', *J Membr Biol*, 206(3), pp. 227-38.
Wainwright, E., Sherrard, J., Duncan, S., Shine, B. and Dorrell, L. (2013) 'Hypophosphataemia with non-tenofovir-containing antiretroviral therapy', *Int J STD AIDS*, 24(7), pp. 579-81.
Walker, C. (2008) 'Genetic and electrophysiological analyses of Stg-1 and Sol-1 evolutionarily conserved accessory subunits of C. Elegans Glutamate receptor.'. p. 110.
Walling, M.W. (1977) 'Intestinal Ca and phosphate transport: differential responses to vitamin D3 metabolites', *Am J Physiol*, 233(6), pp. E488-94.
Wang, R.B., Kuo, C.L., Lien, L.L. and Lien, E.J. (2003) 'Structure-activity relationship: analyses of p-glycoprotein substrates and inhibitors', *J Clin Pharm Ther*, 28(3), pp. 203-28.
Wang, Z.J., Yin, O.Q., Tomlinson, B. and Chow, M.S. (2008) 'OCT2 polymorphisms and in-vivo renal functional consequence: studies with metformin and cimetidine', *Pharmacogenet Genomics*, 18(7), pp. 637-45.
Warren, R.B., Smith, R.L., Campalani, E., Eyre, S., Smith, C.H., Barker, J.N., Worthington, J. and Griffiths, C.E. (2008) 'Genetic variation in efflux transporters influences outcome to methotrexate therapy in patients with psoriasis', *J Invest Dermatol*, 128(8), pp. 1925-9.
Weinman, E.J., Steplock, D., Shenolikar, S. and Biswas, R. (2011) 'Fibroblast growth factor-23-mediated inhibition of renal phosphate transport in mice requires sodium-hydrogen exchanger regulatory factor-1 (NHERF-1) and synergizes with parathyroid hormone', *J Biol Chem*, 286(43), pp. 37216-21.
Weiss, J., Rose, J., Storch, C.H., Ketabi-Kiyanvash, N., Sauer, A., Haefeli, W.E. and Efferth, T. (2007) 'Modulation of human BCRP (ABCG2) activity by anti-HIV drugs', *J Antimicrob Chemother*, 59(2), pp. 238-45.
Weiss, J.N. (1997) 'The Hill equation revisited: uses and misuses', *Faseb j*, 11(11), pp. 835-41.
WHO (2014) *Global update on the health sector response to HIV, 2014.* Available at: http://www.who.int/hiv/pub/progressreports/update2014-executive-summary/en/.
WHO (2015a) *Guidelines for the prevention, care and treatment of persons with chronic hepatitis B infection.* Available at: http://www.who.int/hepatitis/publications/hepatitis-b-guidelines/en/.
WHO (2015b) 'Hepatitis B Fact Sheet No. 204'.
WHO (2015c) *HIV/AIDS Fact Sheet No. 360*. Available at: http://www.who.int/mediacentre/factsheets/fs360/en/.
Wieser, M., Stadler, G., Jennings, P., Streubel, B., Pfaller, W., Ambros, P., Riedl, C., Katinger, H., Grillari, J. and Grillari-Voglauer, R. (2008) 'hTERT alone immortalizes epithelial cells of renal proximal tubules without changing their functional characteristics', *Am J Physiol Renal Physiol*, 295(5), pp. F1365-75.

Windass, A.S., Lowes, S., Wang, Y. and Brown, C.D. (2007) 'The contribution of organic anion transporters OAT1 and OAT3 to the renal uptake of rosuvastatin', *J Pharmacol Exp Ther*, 322(3), pp. 1221-7.
Woodland, C., Ito, S. and Koren, G. (1998) 'A model for the prediction of digoxin-drug interactions at the renal tubular cell level', *Ther Drug Monit*, 20(2), pp. 134-8.
Wright, S.H. (2005) 'Role of organic cation transporters in the renal handling of therapeutic agents and xenobiotics', *Toxicol Appl Pharmacol*, 204(3), pp. 309-19.
Wright SH and Dantzler WH (2004) 'Molecular and Cellular Physiology of Renal Organic Cation and Anion Transport', *Physiological Reviews*, 84(3), pp. 987-1049.
Wu, X., Kekuda, R., Huang, W., Fei, Y.J., Leibach, F.H., Chen, J., Conway, S.J. and Ganapathy, V. (1998) 'Identity of the organic cation transporter OCT3 as the extraneuronal monoamine transporter (uptake2) and evidence for the expression of the transporter in the brain', *J Biol Chem*, 273(49), pp. 32776-86.
Xie, Y., Xu, K., Linn, D.E., Yang, X., Guo, Z., Shimelis, H., Nakanishi, T., Ross, D.D., Chen, H., Fazli, L., Gleave, M.E. and Qiu, Y. (2008) 'The 44-kDa Pim-1 kinase phosphorylates BCRP/ABCG2 and thereby promotes its multimerization and drug-resistant activity in human prostate cancer cells', *J Biol Chem*, 283(6), pp. 3349-56.
Xu, J., Liu, Y., Yang, Y., Bates, S. and Zhang, J.T. (2004) 'Characterization of oligomeric human half-ABC transporter ATP-binding cassette G2', *J Biol Chem*, 279(19), pp. 19781-9.
Xu, J.J., Henstock, P.V., Dunn, M.C., Smith, A.R., Chabot, J.R. and de Graaf, D. (2008) 'Cellular imaging predictions of clinical drug-induced liver injury', *Toxicol Sci*, 105(1), pp. 97-105.
Yamaguchi, H., Sugie, M., Okada, M., Mikkaichi, T., Toyohara, T., Abe, T., Goto, J., Hishinuma, T., Shimada, M. and Mano, N. (2010) 'Transport of estrone 3-sulfate mediated by organic anion transporter OATP4C1: estrone 3-sulfate binds to the different recognition site for digoxin in OATP4C1', *Drug Metab Pharmacokinet*, 25(3), pp. 314-7.
Yamakawa, Y., Hamada, A., Shuto, T., Yuki, M., Uchida, T., Kai, H., Kawaguchi, T. and Saito, H. (2011) 'Pharmacokinetic impact of SLCO1A2 polymorphisms on imatinib disposition in patients with chronic myeloid leukemia', *Clin Pharmacol Ther*, 90(1), pp. 157-63.
Yamashita, T., Konishi, M., Miyake, A., Inui, K. and Itoh, N. (2002) 'Fibroblast growth factor (FGF)-23 inhibits renal phosphate reabsorption by activation of the mitogen-activated protein kinase pathway', *J Biol Chem*, 277(31), pp. 28265-70.
Yamauchi, A., Ieiri, I., Kataoka, Y., Tanabe, M., Nishizaki, T., Oishi, R., Higuchi, S., Otsubo, K. and Sugimachi, K. (2002) 'Neurotoxicity induced by tacrolimus after liver transplantation: relation to genetic polymorphisms of the ABCB1 (MDR1) gene', *Transplantation*, 74(4), pp. 571-2.
Yang, L.E., Maunsbach, A.B., Leong, P.K. and McDonough, A.A. (2004) 'Differential traffic of proximal tubule Na+ transporters during hypertension or PTH: NHE3 to base of microvilli vs. NaPi2 to endosomes', *Am J Physiol Renal Physiol*, 287(5), pp. F896-906.
Yang, Y., Chen, Q. and Zhang, J.T. (2002) 'Structural and functional consequences of mutating cysteine residues in the amino terminus of human multidrug resistance-associated protein 1', *J Biol Chem*, 277(46), pp. 44268-77.
Yi, S.Y., Hong, K.S., Lim, H.S., Chung, J.Y., Oh, D.S., Kim, J.R., Jung, H.R., Cho, J.Y., Yu, K.S., Jang, I.J. and Shin, S.G. (2004) 'A variant 2677A allele of the MDR1 gene affects fexofenadine disposition', *Clin Pharmacol Ther*, 76(5), pp. 418-27.
Yonezawa, A. and Inui, K. (2011) 'Importance of the multidrug and toxin extrusion MATE/SLC47A family to pharmacokinetics, pharmacodynamics/toxicodynamics and pharmacogenomics', *Br J Pharmacol*, 164(7), pp. 1817-25.
Zhang, L., Dresser, M.J., Chun, J.K., Babbitt, P.C. and Giacomini, K.M. (1997) 'Cloning and functional characterization of a rat renal organic cation transporter isoform (rOCT1A)', *J Biol Chem*, 272(26), pp. 16548-54.
Zhang, Y.T., Yang, L.P., Shao, H., Li, K.X., Sun, C.H. and Shi, L.W. (2008) 'ABCB1 polymorphisms may have a minor effect on ciclosporin blood concentrations in myasthenia gravis patients', *Br J Clin Pharmacol*, 66(2), pp. 240-6.

Zhou, Q., Sparreboom, A., Tan, E.H., Cheung, Y.B., Lee, A., Poon, D., Lee, E.J. and Chowbay, B. (2005) 'Pharmacogenetic profiling across the irinotecan pathway in Asian patients with cancer', *Br J Clin Pharmacol*, 59(4), pp. 415-24.
Zwart, R., Verhaagh, S., Buitelaar, M., Popp-Snijders, C. and Barlow, D.P. (2001) 'Impaired activity of the extraneuronal monoamine transporter system known as uptake-2 in Orct3/Slc22a3-deficient mice', *Mol Cell Biol*, 21(13), pp. 4188-96.